

University of Bath



PHD

Pulse position modulation for optical fiber local area networks

Hausien, H. H.

Award date:
1991

Awarding institution:
University of Bath

[Link to publication](#)

General rights

Copyright and moral rights for the publications made accessible in the public portal are retained by the authors and/or other copyright owners and it is a condition of accessing publications that users recognise and abide by the legal requirements associated with these rights.

- Users may download and print one copy of any publication from the public portal for the purpose of private study or research.
- You may not further distribute the material or use it for any profit-making activity or commercial gain
- You may freely distribute the URL identifying the publication in the public portal ?

Take down policy

If you believe that this document breaches copyright please contact us providing details, and we will remove access to the work immediately and investigate your claim.

Download date: 13. May. 2019


PULSE POSITION MODULATION FOR OPTICAL FIBER LOCAL AREA NETWORKS

Submitted by H. H. Hausien
for the degree of Ph.D. of the
University of Bath
1991

COPYRIGHT

Attention is drawn to the fact that copyright of this thesis rests with its author. This copy of the thesis has been supplied on condition that anyone who consults it is understood to recognise that its copyright rests with its author and that no quotation from the thesis and no information derived from it may be published without the prior written consent of the author.

This thesis may be made available for consultation within the University Library and may be photocopied or lent to other libraries for the purposes of consultation.


H. H. Hausien

UMI Number: U034093

All rights reserved

INFORMATION TO ALL USERS

The quality of this reproduction is dependent upon the quality of the copy submitted.

In the unlikely event that the author did not send a complete manuscript and there are missing pages, these will be noted. Also, if material had to be removed, a note will indicate the deletion.



UMI U034093

Published by ProQuest LLC 2013. Copyright in the Dissertation held by the Author.
Microform Edition © ProQuest LLC.

All rights reserved. This work is protected against
unauthorized copying under Title 17, United States Code.



ProQuest LLC
789 East Eisenhower Parkway
P.O. Box 1346
Ann Arbor, MI 48106-1346

UNIVERSITY OF TORONTO	
LIBRARY	
33	61 MAR 1992
Ph.D.	

5058544

ACKNOWLEDGMENTS

I would like to express my deep gratitude to Mr. J. D. Martin for his continuous guidance, support, encouragement, help, invaluable contribution and supervision. Also, I wish to thank Mr. R. Norcross for his help in some of the hardware in this project and Professor J. F. Eastham for permission to study in the school of Electrical Engineering. I should also like to thank the technical staff in the department for their co-operation.

SUMMARY

In a passive fiber-optic local area network the limited power budget of each optical fiber link sharply limits the number of stations in the network. Any improvement in receiver sensitivity means that the number of stations or tap points can be increased, and this was the aim of the investigation presented in this thesis. Digital pulse-position-modulation (PPM) exploits the large bandwidth of optical fiber to offer a greater receiver sensitivity than PCM. Application of the PPM principle to LAN parameters is studied in the thesis, and design criteria confirmed by the construction of a model system. The number of extra tapping points or stations is calculated for a certain value of improvement in receiver sensitivity, for both passive bus and star networks.

The analysis in this work assumes that PCM signalling exists in a given LAN, and then seeks to discover the conditions under which a conversion to PPM will give similar performance, and the conditions under which PPM gives an advantage over PCM. The predicted advantage of PPM depends critically on achieving a high peak/mean power ratio at the transmitting source, which is ideally provided by an optical source. The practical characteristics of some laser diodes and edge-emitting light-emitting diodes were measured, and their suitability for PPM was confirmed.

Practical PPM and PCM systems were built and their characteristics measured to verify the theory discussed and analysed in this work.

The sensitivity and error rate characteristics of an experimental PPM system have been measured for different numbers of time slots M , and modulation depth m . Practical results are shown to correlate well with theoretical results.

TABLE OF CONTENTS

Acknowledgements

Summary	(i)
Table of contents	(ii)

Chapter -1- Introduction

1.1-Data networks and local area networks	1
1.2-Optical fiber local area networks	4
1.3-Pulse position modulation	6
1.4-Organisation of the thesis	7
1.5-References	8

Chapter -2- Optical networks

2.1-Introduction	10
2.2-Local area network configurations	10
2.2.1-Switched star network	11
2.2.2-Ring network	12
2.2.3-Bus network	12
2.2.4-The ETHERNET	14
2.3-Fiber optics	15
2.4-Fiber bandwidth	17
2.4.1-Laser-based systems	18
2.4.2-LED-based systems	19
2.5-Transmission link analysis	22
2.5.1-Optical power budget	22
2.5.2-Rise time budget	22
2.6-Fiber optic local area networks	23
2.7-Passive fiber optic components for LANs	26
2.7.1-Connectors	26
2.7.2-Couplers	27
2.7.3-Splices	29
2.7.4-Switches	29

2.8-Summary	31
2.9-References	31
Chapter -3- Digital Pulse Position Modulation	
3.1-Introduction	41
3.2-DPPM signal detection	43
3.3-PPM error types and frame size	45
3.4-Error performance of DPPM system	47
3.4.1-Slot erasure error	49
3.4.2-Slot false-alarm error	50
3.4.2.1-In adjacent slots	50
3.4.2.2-In other than adjacent slots	51
3.4.3-Frame errors	51
3.4.3.1-Probability of no detection error	51
3.4.3.2-Probability of an undetected error	51
3.4.3.3-Probability of detected error	52
3.4.4-Comparison of analytical methods	53
3.5-Error probability of PCM system	54
3.6-PPM versus PCM	55
3.7-Summary	56
3.8-References	57
Chapter -4- Optical sources for PPM system	
4.1-Introduction	65
4.2-The laser diode	66
4.2.1-Limit to laser diode output power	67
4.2.2-Maximum optical power as a function of pulse width	71
4.2.3-Determination of laser diode temperature	73
4.2.4-Practical measurements	74
4.2.4.1-Temperature control	74
4.2.4.2-Thermal rise time of laser diode	76
4.2.4.3-Dynamic thermal conditions in the laser diode	79

4.2.5-Laser diode test	82
4.2.6-Summary	82
4.3-The light emitting diode	83
4.3.1-Introduction	83
4.3.2-Output power limitations and temperature effect	84
4.3.3-Practical results (ELED 44-62)	86
4.3.4-Summary	87
4.4-LD versus LED	88
4.5-Refernces	89
Chapter -5- Clock synchronization in PPM system	
5.1-Introduction	106
5.2-PPM signal pre-processing	107
5.2.1-Spectrum of fixed pulse position	108
5.2.2-Processed pulse	108
5.3-Phase-locked loop	112
5.3.1-Introduction	112
5.3.2-Noise processing by the PLL	113
5.3.3-VCO drift	115
5.4-PLL lock indicator	119
5.5-Frequency synthesis using PLL	120
5.6-Summary	121
5.7-References	121
Chapter -6- The optical PPM transmitter	
6.1-Introduction	128
6.2-PPM coder	129
6.3-Frequency synthesis	130
6.4-Packet generation	132
6.5-Optical source driver	133
6.6-Summary	134
6.7-References	135

Chapter -7- The optical PPM receiver

7.1-Introduction 141

7.2-Optical receiver theory 142

 7.2.1-Photo-detectors 142

 7.2.2-The pre-amplifier 144

 7.2.3-Noise considerations in optical receiver
 design 145

 7.2.4-Receiver sensitivity 147

7.3-The practical design 148

 7.3.1-The optical receiver 149

 7.3.2-Data regeneration 149

 7.3.3-Clock recovery 151

 7.3.3.1-Pre-processing 151

 7.3.3.2-The PLL 153

 7.3.3.3-The lock indicator 155

 7.3.4-Frame synchronization 156

 7.3.5-PPM decoder 157

7.4-Summary 158

7.5-References 159

Chapter -8- Practical PPM system

8.1-Introduction 170

8.2-Clock recovery circuit performance 171

8.3-Setting-up the PPM system 172

8.4-Error-rate characteristics of the PPM system 173

8.5-Effect of varying m on the BER 174

8.6-Error rate characteristics of the PCM system 175

8.7-PPM versus PCM 176

8.8-Summary 177

8.9-References 178

Chapter -9- Application of PPM to LANs

9.1-Introduction 189

9.2-PPM versus PCM 190

9.3-PPM system design	191
9.3.1-Single-mode fiber	194
9.3.2-Graded-index fiber	195
9.4-Passive bus LAN	197
9.5-Passive star LAN	198
9.6-Summary	199
9.7-References	200
Chapter -10- Conclusions and future work	
10.1-Conclusions	203
10.2-Future work	210

CHAPTER - 1 -

INTRODUCTION

1.1-DATA NETWORKS AND LOCAL AREA NETWORKS

Thousands of data communication networks are used worldwide to enhance the ability of data users to communicate with one another. These systems range from small networks interconnecting data terminals and computers within a single building or campus-like complex, to large geographically distributed networks covering entire countries or, in some cases , spanning the globe.

Some networks use packet-switched technology, in which blocks of data called packets are transmitted from a source to a destination. In these networks, packets from multiple users share the same distribution and transmission facilities. Other networks are of the circuit-switched type, which generally transmit voice or data, and where a private transmission path is established between any pair or group of users attempting to communicate and is held as long as transmission is required. A network consists essentially of network switches, or nodes, interconnected by transmission links. These links can be wire, cable, radio, satellite, or fiber optic facilities. A network can accommodate a large number of users, up to the limit that the switch can handle.

Networks interconnecting locations within a city (Metropolitan Area Network) or connecting cities within a country are considered long-haul networks, where the distances between implements (networks) are greater than 10 km and less than 100 km. Networks connecting countries (Wide Area Network) are considered as interconnected long-haul networks [SCHWARTZ, WILLSON].

Local Area Networks, are small networks and are becoming the preferred method for efficient distribution of data within a business or organisation. A local network is a communication network that provides

interconnection of a variety of data communicating devices, (computers, terminals, telephones, television, peripheral devices, and sensors), within a small area (0.1-10km) [STALLING].

These networks serve as conduits for the flow of information. They can increase a group's productivity by enabling its members to share expensive peripherals (such as laser printers and hard disks), to share information and programs and to communicate more easily. LANs can provide services such as file transfer, graphics applications, word processing, electronic mail, distributed data bases, interconnections to other LANs, digital telephony, and some kind of video service. Moreover, LANs can support a wide variety of data devices: computers, video terminals, mass storage devices, printers, plotters, facsimile printers, and gateways to other networks.

The rapid growth of interest in LANs has been caused by falling costs of intelligent work-stations with considerable computing potential, and by a growth in consumer demand for communication services. Such trends have accelerated the growth of information technology.

LANs have been developed with many different formats. LANs can basically be classified by network topology and access procedure, the choice of which is determined by the type of information to be transmitted. Common LAN topologies are the ring, the star, and the bus, which will be discussed in section 2.2. In the past few years, many different proposals for LAN architectures have appeared in the literature using combinations of the above basic topologies, and a variety of different protocols has been proposed for the transmission of data packets over these networks [STALLING, NASSEHI], (see section 2.2). The purpose of the protocol is to establish a virtual connection between two stations [BAKER]; that is, the devices communicate as though individually wired point-to-point, but in reality they share a common path.

Most of today's LANs are based on coaxial cable or twisted pair wires and typically operate at data rates of up to 10 Mbit/s over distances of up to a kilometre. In these copper systems, the bandwidth is affected

by the cable capacitance, signal, and ground paths in the cable. Twisted wire pair is a common transmission medium for both analog and digital data, and can be used for point-to-point and multi-point applications at data rates of up to 4 Mbit/s. For digital signals, repeaters are required every 2 or 3 km at 1-2 Mbit/s. Compared to other guided media, twisted pair is limited in distance, bandwidth, and data rate. Coaxial cable is the most versatile transmission medium for LANs, where the 50 ohm coaxial cable is used mainly for digital transmission, and data rates of 10 Mbit/s can be achieved. Coaxial cable is applicable to point-to-point and to multi-point configurations. Maximum distances in a typical baseband cable, which has an attenuation of 50 to 200 dB/km, are limited to a few kilometres. For example, Ethernet uses baseband coaxial cable at 10 Mbit/s over a maximum end-to-end length of 2.5 km [STALLING, SCHMIDT, SOUTHARD, BAKER].

Metallic-cable LANs however, are restricted with respect to transmission capacity, transmission losses, tapping, and immunity against electromagnetic interference and protection against signal leakage. So the big increase in computer processing power and usage over the past few years has made these lower speed local networks the weak link among devices needing huge transfer of data. High data rates are required to keep up with the work, which typically involves the transfer of large blocks of data. For example, current hard disks can record data at rates up to 24 Mbit/s; future hard and optical disks will operate at twice this rate. Other applications, including video transmission for teleconferencing and graphics work-stations, are further pushing the capacity of modern LANs. High-speed devices need expensive buffering, or memory storage, for co-ordinating the transmission of output onto a low-speed data channel. Getting away from the buffering mode and into direct transmission will demand higher-speed data networks.

1.2-OPTICAL FIBER LOCAL AREA NETWORKS

The relatively low data rates for coaxial cables and twisted pair transmission lines are not adequate to meet the requirements of many modern information processing systems [TAYLER]. Optical fiber communication systems are the obvious solution for overcoming the current bandwidth limitations of coaxial links [SOUTHARD, MURPHY]. Optical cables have orders of magnitude more bandwidth, occupy smaller volumes, display lower attenuation, neither generate nor are susceptible to electrical noise, and have excellent security because it is nearly impossible to wiretap without detection [TANENBAUM]. For example, optical fibers are at least an order of magnitude smaller in diameter than metallic cables for comparable data transmission capacity, and their bandwidth is 100 times as great as that of coaxial cables. In general the greater the bandwidth of the physical medium, the larger the LAN that can be built and the greater the volume of the messages that can be exchanged [SUH, OLIVER].

Since fiber optics is suitable for carrying either low- or high-speed signals, it offers considerable flexibility for designing networks and for wiring installations in buildings. In many cases, the capacity of fiber optic media can be upgraded by simply changing the emitters, detectors, and connectors at the ends of the fiber optic links. This contrasts with the total rewiring of facilities required for copper media.

Fiber optics has not been considered a suitable medium for LANs primarily due to its relatively high cost compared to metallic-based media, but rapid advances in fiber optic components and sub-systems as well as standardization efforts, are changing the criteria for using fiber optics in LANs [SUH]. Fiber optic LANs can run at bit rates of hundreds and even thousands of Mbit/s.

The basic optical LAN topologies are the bus, the ring, and the star, and can be classified as active networks or passive networks. The passive

networks give high reliability because no active repeaters are required; the source terminal transmits its data on the passive network and the data is received by all terminals. The number of stations that can be put on an optical fiber data bus is usually limited by the total allowable attenuation between transmitter and receiver. The transmission loss is made up mostly of branching and tapping losses [MARTIN]. In bus and ring networks, the transmission losses are an important problem because the losses are accumulative along the data bus, so in these networks the number of nodes is restricted to 10 to 15 because of the optical losses associated with the use of passive couplers [MOSTAKAS]. By using a passive star network the number of nodes can be increased to 64 or more, although the main problems are firstly the lack of a collision detection method that operates effectively over the wide optical dynamic range which is present, and secondly that they require more cable [LYMPANY]. Because fiber optic data links in passive networks have a limited available power budget compared to electronic data links, they can only support a limited number of stations. The active star has several advantages over the passive star, it can support more devices over a greater distance, but the central switch can be complex and expensive. The central switch limits the network speed, and it is an obvious source of catastrophic failure which makes these networks unreliable. These networks also require more cable. Active ring networks are mostly used, where the transmission between active nodes is essentially point-to-point. A failure at one node can interrupt transmission unless a redundant path of a by-pass switch is incorporated at each node, although at increased cost. For example, FDDI employs a redundant ring topology and operates at 100 Mbit/s [BURR]. However active ring networks are not convenient for some applications and use a lot of fiber, and the cost and reliability of active networks may limit their use at high speed [GERLA]. It is clear that passive networks, are more reliable than active networks, and these will be considered

in this work. In a passive network any improvement in receiver sensitivity means that the number of nodes or tap points could be increased, and this will be the aim of the investigation presented in this thesis.

1.3-PULSE POSITION MODULATION

The limited power budget of an optical link, together with the unavoidable loss of branching and tapping, sharply limits the number of nodes in a passive fiber optic LAN. The very low attenuation of optical fiber more than compensates for the limited power budget, and explains why the initial fiber optic applications have been mostly in long distance telecommunication links. For a given transmission power and receiver sensitivity, a low loss optical fiber enables a longer transmission distance to be achieved for a given error performance. The availability of a wider bandwidth may be used to achieve higher information capacity, but it too can be exploited by using suitable modulation methods, to achieve longer transmission distance. Assuming that an already existing system is using PCM signalling, then a suitable modulation method could be used to improve system performance.

In a passive LAN, improvement in receiver sensitivity implies that the number of network tapping points may be increased [MARTIN]. Various authors [LESH, GAGLIARDI, GARRETT, CALVERT, PIRES] have shown that PPM, (see chapter 3 for the advantages of PPM over PCM), can in principle be used to effect a trade-off between the large transmission bandwidth provided by optical waveguides and an increased transmission distance. For example [GARRETT] has predicted a 10-12 dB improvement in receiver sensitivity for DPPM over binary PCM for certain optical fiber systems. [CALVERT] has got practically a 4.2 dB improvement in receiver sensitivity for DPPM over an equivalent binary PCM when the fiber bandwidth was several times that required by PCM. The excess bandwidth of the fiber can be exploited using DPPM to improve receiver sensitivity, but to get an improvement in receiver sensitivity the PPM transmitted mean power

should be comparable to that produced by a "CW" laser or LED in a binary PCM system.

In other words, the predicted advantage of PPM depends very much on peak/mean power characteristics of the optical source [KATZ]. This thesis discusses the possibility of using DPPM to increase the allowable system loss, and hence to increase number of tapping points (nodes) in passive fiber optic LANs by using PPM. Application of the principle to LAN parameters is studied, and design criteria investigated by construction of a model system. Conclusions are drawn.

1.4-ORGANISATION OF THE THESIS

The main characteristics of LANs, LAN topologies, optical fibers, fiber bandwidth, optical fiber LANs, and the fiber optic components for LANs are discussed briefly in chapter 2, which gives the theoretical background of LANs, and fiber optic applications to LANs. The next chapter, chapter 3, begins with a review of the characteristics of digital pulse position modulation, frame size, and error types, followed by an analysis of the probability of the error in DPPM signal detection. The results of the analysis are compared with the characteristics of an existing PCM system. Chapter 4 discusses the optical sources, laser diodes and light emitting diodes, and gives practical results for the possibility of using them for PPM. When the emitter of the optical source (LD or LED) is driven hard, various factors limit its peak power, and these are discussed in this chapter. The practical results obtained are used in PPM transmitter design in chapter 6.

In chapter 5 clock synchronization is dealt with, which is very important in PPM, and a PLL is used for this purpose. This chapter gives the theoretical background for timing synchronization circuit design used in the receiver circuit in chapter 7. The design and implementation of Optical DPPM transmitter and receiver are examined in chapters 6 and 7 respectively, including the theoretical and practical results. The PPM

transmitter designed in chapter 6 includes the PPM coder, block generator, and the driving circuit for the optical source. The PPM receiver given in chapter 7 includes the receiver, the decision circuit, timing recovery circuit, frame synchronizer, and the PPM decoder. The results of the overall DPPM system performance are given in chapter 8, and are found to be quite satisfactory. Chapter 9 discusses the application of PPM to LANs in general, and chapter 10 gives some conclusions and suggestions for future work.

1.5-REFERENCES

BAKER, D. G., "Local Area Networks with fiber optic applications," Prentice-Hall, New Jersey, 1986, Chapter 5.

BURR, W. E., "The FDDI Optical Data Link," IEEE Commun. Magazine, Vol. 24, No. 5, May 1986, pp. 18-23.

CALVERT, N. M., SIBLEY, M. J., and UNWIN, R. T., "Experimental optical fiber digital PPM system," Electronics Letters, Vol. 24, No. 2, Jan. 1988, pp. 129-131.

GAGLIARDI, R. M., and KARP, S., "M-ary poisson detection and optical communications," IEEE-Trans. on commun., Vol. COM-17, 1969, pp. 208-16.

GARRETT, I., "Pulse position modulation for transmission over optical fiber with direct or heterodyne detection," IEEE Trans. on commun., Vol. COM-31, No. 4, April 1983, pp. 518-27.

GERLA, M., RODRIGUES, P., and YEH, C. W., "Token-based protocols for high-speed optical-fiber networks," J. Of Light Wave Technology, Vol. LT-3, No. 3, June 1985, pp. 449-465.

KATZ, J., "Average power constraints in AlGaAs semiconductor lasers under pulse position modulation conditions," Optics Communications, Vol. 56, No. 5, Jan. 1986.

LESH, J., "Capacity limit of the noiseless, energy-efficient optical PPM channel," IEEE Trans. on commun., Vol. COM-31, April 1983, pp. 546-8.

LYMPANY, S. S., "Fiber optic components for local area networks," IEEE 1985 military commun. Conference MILCOM 85, Boston MA USA 20-23 Oct. 1985, pp. 82-8.

MARTIN, J. D., "PPM for Local Area Networks," Proceedings "Fiber Optics 89", SPIE, Vol. 1120, London, Apr. 1989, pp. 14-24.

MOUSTAKAS, S., "The standardization of IEEE 802.3 compatible fiber optic CSMA/CD LANs," IEEE commun. Magazine, Vol. 25, Feb. 1987, pp. 22-29.

MURPHY, K. W., "Design standards for Local Area Networks," Photonics spectra, November 1985, pp. 79-87.

NASSEHI, M. M., TOBAGI, F. A., and MARHIC, M. E., "Fiber optic configurations for Local Area Networks," IEEE J. On selected areas in commun., Vol. SAC-3, No. 6, November 1985.

OLIVER, J., "Light speed communications," Electrical Equipment (UK), Sept. 1987, pp. 26-30.

PIRES, J. J., and DA ROCHA, J. R., "Digital pulse position modulation over optical fibers with avalanche photodiode receivers," IEE proceedings, Vol. 133, pt. J, No. 5, Oct. 1986, pp. 309-13.

SCHMIDT, R. V., RAWSON, E. G., NORTON, R. E., JACKSON, S. B., and BAILEY, M. D., "Fibernet II: A Fiber Optic Ethernet," IEEE J. On selected areas in commun., Vol. SAC-1, No. 5, November 1983.

SCHWARTZ, M., "Telecommunication networks," Addison-Wesly, N. Y., 1987, Chapter 1.

SOUTHARD, R. K., "Fiber optics: A winning technology for LANs," Electronics, Feb. 4, 1988, pp. 111-114.

STALLING, W., "Local Networks , an introduction," Macmillan, NY, 1987.

SUH, S. Y., GRANLUND, S. W., and HEGDE, S. S., "Fiber optic local area network topology," IEEE commun. Magazine, Vol. 24, No. 8, August 1986, pp. 26-31.

TANENBAUM, A. S., "Computer networks," Prentice-Hall, NY, 1988, chapter 3.

WILSON, R. G., and SQUIBB, N., "Broadband data communications and local area networks," Collins, 1986, chapter 1.

CHAPTER -2-
OPTICAL NETWORKS

2.1-INTRODUCTION

The development of low loss optical fibers has resulted in an explosion of the use of optical communication, which offers many desirable properties over conventional metallic media. The number of useful applications of optical fiber systems has increased rapidly because of the excellent characteristics of optical fibers. Fiber optic local area networks (FO-LAN) that make use of the excellent features of optical fibers, are expected to become the fundamental large-scale LANs, capable of accommodating a much larger number of terminals and higher speed transmission over a wider geographical area than metallic-cable LANs. Optical LAN systems may be segregated into two categories, active and passive. Passive FO-LANs are more reliable than active ones.

A key issue when selecting a viable network is whether it will transfer the data at an adequate rate, the maximum number of network nodes required and the maximum distance between nodes. No single LAN meets all the criteria, but one of them may provide the best performance. Another factor that must be considered is the maximum length of the network, which affects frame size, token hold time, CSMA/CD transmission timeout, packet service time, and so on.

In this chapter we will focus our attention on the characteristics of optical fibers, LANs, fiber optic LANs, and optical components required by FO-LANs.

2.2-LOCAL AREA NETWORK CONFIGURATIONS

A LAN is a resource-sharing data communications network, which is limited in geographic scope to the range of 0.1-10 km, provides high bandwidth communication (above 1 Mbit/s) over inexpensive transmission

media, and is usually privately owned. Its primary purpose is to provide connectivity and switching functions for information equipment (such as terminals, work-stations, personal computers, and shared resources like disk storage and high-speed printers), thus allowing users to efficiently accomplish required tasks. Such tasks include accessing databases or application software residing in a mainframe computer, distributing files, mailing messages, and most importantly, communicating with other devices [TSAO, KUMMERLE]. LANs have the following general characteristics:

- a- A geographic extent of 1 to 10 km at most.
- b- Moderate to high data rate (1 to 100 Mbit/s).
- c- Low error rate (10^{-8} to 10^{-11})
- d- Transmits bits serially rather than in parallel.
- e- Switches packets or frames of data rather than holding transmission bandwidth for the duration of a communication session.
- f- Can have a wide variety of devices attached (e. g. Sensors, thermo-stats, security alarms, process control devices, low speed data terminals, voice, facsimile, computer high speed I/O, video) offering multiple services.

There are three main media in use in LANs, twisted pair cable, coaxial cable, and fiber optic cable. For general networking the most common transmission media are twisted pair cable and coaxial cable. The third medium is optical fibers, which will be discussed in section 2.3.

Common LAN topologies are the ring, the star, and the bus. These three common topologies are described briefly below, followed by an example of CSMA/CD coaxial data bus, the Ethernet.

2.2.1-SWITCHED-STAR NETWORK

The simple star diagram of Fig. 2.1 illustrates the star topology, each station is connected by a point-to-point link to a common central hub; the hub contains a switch that is shared among all stations. The

switch provides a path between any two devices wishing to communicate. For a station to transmit data, it must first send a request to the central switch, asking for a connection to some destination station. Once the circuit is set up, data may be exchanged between the two stations as if they were connected by a dedicated point-to-point link. The main advantages of a star network are that access to the network is under central switch control. The central switches can be complex and expensive, speeds are generally limited and central switch is an obvious source of catastrophic failure.

2.2.2-RING NETWORK

As shown in Fig. 2.2, a ring network consists of a set of active repeaters joined by point-to-point links in a closed loop. The repeater is a simple device, and is responsible for passing on each fragment of the data, which is sent in packets, and within each station there is a controller responsible for recognising packets sent to the station, i.e. addressed to that station, and for controlling access to the ring, i.e. deciding when it is clear to start transmitting. The principal disadvantage of a ring is that every station is involved in the transfer of data, and thus one failure of a repeater brings the whole network to a halt. The second disadvantage lies in the ring control mechanisms required; to start up the ring, determine that the packets are not corrupt, and prevent the same packet from going around the ring for ever because of a station fault. The two most popular ring-based schemes are the token passing rings and slotted rings [RORABAUGH].

2.2.3-BUS NETWORK

Bus networks are the most common LANs. In this topology the communications network is simply the transmission medium, there are no switches, no repeaters, but simply a common medium. As shown in Fig.

2.3, each station is attached directly to the transmission medium through appropriate hardware (a tap), which must be capable of delivering the signal to all the stations on the bus. Because all the nodes share a common transmission link, only one device can transmit at a time. The data are sent in packets, and each station hears all the transmissions, picking up those addressed to it. Some form of access control is required to determine which station may transmit next, and the two most common technologies are contention and token-passing. Most bus networks have the advantage of being passive, i.e. all of the active components are in the stations, and a failure affects only that one station. The most significant bus network is Ethernet [ROWLANDS, STALLINGS]. The tree topology is a generalisation of the bus topology, in that the cable can be made to branch down many side shoots by the use of a cable splitting device (Fig. 2.4). Tree topologies are significant in broadband networks.

In the past few years, many different proposals for LAN architectures have appeared in the literature using combinations of the above basic topologies, and a variety of different protocols have been proposed for the transmission of data packets over these networks [ROWLANDS]. The access control method of a LAN is the means whereby the flow of data to and from stations is controlled. The most commonly used medium access control technique for bus topology is carrier sense multiple access with collision detection (CSMA/CD), and will be discussed in section 2.2.4. The token passing technique is applicable to both ring and bus topologies, although the token bus technique is more complex than CSMA/CD [MOUSTAKAS]. For this technique the stations on the bus form a logical ring. Each station knows the identity of the stations preceding and following it. A control frame (token) regulates the right of access, and contains a destination address. The station receiving the token is granted control of the medium for a specified time. The greatest positive feature of the token bus is its excellent throughput performance, which increases as the data rate increases. In networks with a ring topology,

token passing is a popular technique for access control of the transmission medium. An idle token is circulated from node to node around the ring, and when it is received by a node which has data to be transmitted, the node changes it into a busy token before relaying it on to the next node, followed immediately by a packet containing data. As it circles about the ring, it is ignored by every other node except the one marked as its destination. Once it returns to its origin, the packet is cancelled and the token is passed along the ring again. The principal disadvantage of token ring is the requirement for token maintenance [RORABAUGH]. The other most common techniques for controlling access to the ring are slotted ring and register insertion [STALLINGS].

2.2.4-THE ETHERNET

Ethernet is a baseband bus system in which the signal is directly modulated on to the transmission medium. It uses a tapped passive coaxial cable, commonly called its Ether, to distribute variable length 10 Mbit/s digital packets among geographically dispersed stations. These stations typically are computer work-stations, storage devices, printers, and gateways to other networks. An Ethernet is built up from segments of cable, each of which must be terminated in its characteristic impedance at both ends, Fig. 2.5. Each segment may have a maximum of 100 stations and be up to 500 m in length [SCHMIDT, ROWLANDS, STALLINGS, CURRIE]. Stations attach to the cable by means of a tap, with the distance between any two taps being a multiple of 2.5 m; this is to ensure that reflections from adjacent taps do not add in phase [STALLINGS]. All stations should have equal access to the network when averaged over time. Digital data packets are coupled to and from the coaxial cable by the transceivers which serve as cable taps, and the transceivers detect the presence of data collisions on the cable. Ethernet has no central controller but rather uses the distributed channel access discipline CSMA/CD. If a station requires to use the

network it must first determine whether the Ethernet is in use. Should the network be busy, then the station must wait until the network is clear before attempting transmission. Because of finite propagation delays through the network, it is possible for two stations to begin transmission almost simultaneously, and in this case the two data packets collide and become garbled. The transceivers determine the presence of such a collision by monitoring the average signal level on the cable. After a collision, each station wishing to transmit retries after a random delay. To ensure that a collision will be detected, each packet must be large enough to occupy the whole length of the bus. The packet size is then a function of the speed of transmission: basically the higher the speed the larger the minimum packet, or the shorter the bus.

2.3-FIBER OPTICS

An optical fiber is a dielectric waveguide. It consists of a core with refractive index n_1 surrounded by a cladding with lower refractive index n_2 . In low and medium loss fibers the core material is generally glass, which is surrounded by either glass or a plastic cladding. Higher-loss plastic core fibers with plastic claddings are also widely in use for distances of the order of 10-100 m. Light can be propagated down an optical fiber cable by either reflection or refraction, depending on the mode of propagation and the index profile of the fiber. There are three types of optical fiber configurations: single mode step index, multimode step index, and multimode graded index (Fig. 2.6).

When choosing an optical waveguide fiber, three major performance criteria must be considered; signal losses (attenuation), ease of light coupling and interconnection, and bandwidth.

In a power limited system, fiber attenuation is more critical than pulse spreading. The numerical aperture (NA), which is a measure of the angle over which light is accepted, is directly related to the source-coupling efficiency, so it is important in a power-limited system. For long

high-rate links, the pulse spreading may be the chief concern, and losses may be secondary in importance.

The fiber is not a perfect conductor of light and important intrinsic material properties as well as extrinsic effects can cause the signal to be attenuated. The three mechanisms causing the attenuation are; absorption, scattering, and waveguide effect. Such effects are discussed in detail in a variety of references [MILLER, MIDWINTER, SENIOR]. The degree of attenuation depends on the wave-length of light transmitted, as shown in Fig. 2.7. We need concern ourselves only with fiber losses in a range of wavelengths from about 500 to 1600 nm. This is the range within which fiber communications is most practical.

The choice between single mode and multimode depends on the type of light source used, the amount of dispersion that can be tolerated, and the desired transmission distance. The maximum data rate is determined partly by the fiber, but mostly by the type of transmitting device in use.

Single mode fibers have core diameters about four-six times the wavelength of light, and the light is propagated in a single mode down the fiber. The difficulty of coupling light into such a small core led to the development of multimode fiber, where core diameters are on the order of 50 to 100 μm . These fibers support more than one propagating mode, the number of modes that can propagate in a fiber depending on the fiber numerical aperture and core diameter, as well as the wavelength. For a step index multimode fiber, the number of such modes N is defined by [HECHT]:

$$N = \frac{[D \cdot NA \cdot \frac{\pi}{\lambda}]^2}{2} \quad (2.1)$$

where λ is the wavelength and D is the core diameter. For example, $D = 50 \mu\text{m}$, $NA = 0.2$, $\lambda = 0.85 \mu\text{m}$, then $N = 2732$.

A major difference between multimode and single mode fibers, aside from the difference in core diameter, is that nearly all the power in multimode

fibers travels within the core whereas in single mode fibers a large fraction of power propagates through the cladding near the core region. In spite of the advantages that single mode fibers can potentially offer in regard to signal transmission characteristics, multimode fibers with their significantly larger diameters remain superior to monomode fibers for low to medium speed applications, because a greater source power can be coupled to the fiber.

The information capacity of an optical fiber is usually specified by the bandwidth-distance product in MHz.km, which approximately equal to: 20 MHz.km for step index multimode fiber, 0.5-2.5 GHz.km for graded index multimode fiber, and greater than 100 GHz.km for single mode fiber [SENIOR].

2.4-FIBER BANDWIDTH

Fiber bandwidth (electrical) is defined as the value of modulation frequency at which the received optical power has fallen by 3 dB of its constant value. It limits the maximum rate at which information can be transmitted over a fiber because it introduces a form of signal degradation that causes light pulses to spread in time [REFI 87, GOWAR, SENIOR, SINGH]. The amount of pulse broadening is dependent upon the distance the pulse travels within the fiber, and hence for a given fiber link the restriction on usable bandwidth is dictated by the distance between repeaters. Thus the dispersive property of a particular fiber is usually stated as the pulse broadening in time over a unit length of the fiber. Waveguide dispersion, multimode dispersion, and material dispersion are the main causes of pulse broadening in fibers. Waveguide dispersion is a result of wave-guiding effects close to the mode cutoff, and so is important in single mode fibers, while for multimode fibers it can be neglected since it affects only lossy high-order modes of little relevance for long lengths of fiber. Pulse broadening due to material dispersion results from the different group velocities of the

various spectral components launched into the fiber from the optical source. The sum of material and waveguide dispersion is called chromatic or intramodal dispersion. Chromatic dispersion arises in both multimode and single mode fibers because most optical sources emit light at several wavelengths, and because different wavelengths travel at different speeds in the fiber. The chromatic dispersion in single-mode step index fibers is plotted in Fig. 2.8 [HECHT]. Dispersion due to multimode effects (intermodal) dominates the dispersion characteristics in fibers supporting more than one mode, and is caused by the difference in group velocity between the various propagating modes and the wavelength dependence of group delay for each mode. A dramatic improvement in multimode fiber bandwidth is achieved by grading the fiber index in a parabolic fashion. The reason is that a nearly parabolic index tends to equalize the modes group velocities and in turn it theoretically reduces the pulse dispersion [GOWAR]. Practical pulse broadening values for graded index fibers lie in the range 0.2-1 ns/km.

Fiber manufacturers measure the bandwidth of multimode fiber using laser sources having wavelength at 825 nm (or 850 nm) and/or 1300 nm. The performance of a lightwave transmission system depends on the final exit bandwidth of the installed and spliced fiber-section when measured with the system source not the fiber manufacturers source [REFI 87, 86]. To calculate the installed fiber bandwidth we should distinguish between laser-based and LED-based systems:

2.4.1- Laser-based systems:

If we designate the section bandwidth when measured with a laser as $BW_{s_{laser}}$, when the operating wavelength of the system laser is similar to that used by the fiber manufacturer, section laser bandwidth can be correlated to the manufacturers spooled-fiber bandwidth by [REFI 87]:

$$BW_{s_{laser}} = BW_f \cdot L_s^{-\alpha_{laser}} \quad (2.2)$$

where:

$BW_{S_{laser}}$: section bandwidth in (MHz) measured with a laser,

BW_f :spooled-fiber bandwidth in (MHz.km) measured with a similar laser,

γ_{laser} :laser bandwidth concatenation length scaling factor ($0.5 \leq \gamma_{laser} \leq 1$), and

L_s : installed section length in km.

γ_{laser} value depends on the system operating wavelength and how the fibers were designed, manufactured, and spliced. Its value is equal to one if the system operating wavelength differs substantially from the wavelength at which the fiber has its highest bandwidth. If the system wavelength coincides with the fiber highest bandwidth wavelength then its value is equal to 0.5.

2.4.2- LED-based system:

Because LEDs have wide spectral widths, a fiber bandwidth when measured with a LED can be significantly different from that measured with a laser. When the multimode fiber is used with a LED source both modal and chromatic effects must be considered: i.e. $BW_{S_{LED}}$ consists of the laser bandwidth and chromatic bandwidth [REFI 87]:

$$\frac{1}{BW_{LED}^2} = \frac{1}{BW_{chr}^2} + \frac{1}{BW_{S_{laser}}^2} \quad (2.3)$$

where:

$BW_{S_{LED}}$: LED bandwidth in MHz,

$BW_{S_{chr}}$: chromatic bandwidth in MHz, and

$BW_{S_{laser}}$: laser bandwidth in MHz, calculated in Eq. 2.2.

Because both chromatic and laser bandwidths comprise the total bandwidth of a section measured with a LED, the chromatic bandwidth calculated with the Eqs. 2.4 and 2.5, below, must be combined with the laser bandwidth calculated using Eq. 2.2.

1- short wavelengths (near 870 nm) :

$$BWs_{chr} = \frac{[k \cdot \lambda_c^3 \cdot L_s^{-\gamma_{chr}}]}{[a_1 \cdot \lambda_c^4 - a_2] \lambda_w} \quad (2.4)$$

2- long wavelengths (near 1300 nm) :

$$BWs_{chr} = \frac{L_s^{-\gamma_{chr}}}{\sqrt{\lambda_w [b_1 + b_2] \lambda_c - b_3}} \quad (2.5)$$

where:

λ_c : center wavelength of the LED in nm,

γ_{chr} : chromatic bandwidth length scaling factor,

λ_w : full width half maximum spectral width of LED in nm,

L_s : section length in km, and

k, a_i , and b_i : constants that depend on wavelength and fiber

type.

The chromatic bandwidth calculated with the Eqs. 2.4 and 2.5 must be combined with the laser bandwidth calculated using Eq. 2.2 to calculate BWs_{LED} in Eq. 2.3. For example, Fig. 2.9 shows the application of this theory to graded-index multimode fiber (with core diameter=62.5 μm , and NA=0.29). The figure shows exit LED bandwidth versus exit laser bandwidth for a LED having $\lambda_c = 1320$ nm and $\lambda_w = 150$ nm. BWs_{LED} depends strongly on BWs_{laser} at short section lengths, but this dependence decreases as section length increases. If the fiber is used with a LED having $\lambda_c = 870$ nm, and $\lambda_w = 50$ nm then section LED bandwidth will decrease [REFI87]. Overall however, BWs_{LED} is more sensitive to BWs_{laser} at long wavelength than at short.

The word bandwidth is a frequency domain term and is inversely proportional to its time domain counterpart pulse spreading. As bandwidth decreases, pulse spreading increases. If we consider that the light pulses at the output of an optical channel to have a Gaussian shape, Fig. 2.10, with an rms width of σ , and 1/e width t_e , (where $t_e = \sigma\sqrt{2}$) then

for no overlapping of light pulses down an optical fiber link the digital bit rate B_T , in bit/s, is given approximately by [SENIOR, GOWER]:

$$B_T(\text{max}) = \frac{0.2}{\sigma} \quad (2.6)$$

This equation can be derived from the optical output power with time (Fig. 2.10) which may be described as:

$$P_o(t) = \frac{1}{\sigma\sqrt{2\pi}} \exp\left[\frac{-t^2}{2\sigma^2}\right] \quad (2.7)$$

The Fourier transform of Eq. 2.7 is given by:

$$P(\omega) = \frac{1}{\sqrt{2\pi}} \exp\left[\frac{-\omega^2\sigma^2}{2}\right] \quad (2.8)$$

The 3-dB optical bandwidth (B_{opt}) is defined as the modulation frequency at which the received optical power has fallen to one half of its constant value. From Eq. 2.8:

$$B_{opt} = \frac{0.187}{\sigma} \quad (2.9)$$

The 3-dB electrical bandwidth (B_{elec}) occurs when the received optical power has dropped to 0.707 of the constant value giving:

$$B_{elec} = \frac{0.133}{\sigma} \quad (2.10)$$

The conversion of bit rate to bandwidth in Hertz depends on the digital coding format used. For non-return to zero (NRZ) the maximum bandwidth (B_{opt}) is one half the maximum data rate of Eq. 2.6, or $B_T(\text{max}) = 2 \cdot B_{opt}$. For return to zero (RZ) $B_T(\text{max}) = B_{opt}$.

The bandwidth calculated can be related to rms pulse width or 1/e width using the equations above. It is clear from Fig. 2.9 that for multimode fiber the pulse broadening has no effect or very little effect on system performance for distances up to 4 km, and data rates of up to 120 Mbit/s if the section is used with a LED with longer wavelengths.

2.5-TRANSMISSION LINK ANALYSIS

To ensure that the system performance requirements are met, two separate analyses must be performed. These are (a) the optical power budget analysis and (b) the system rise time budget analysis.

2.5.1- Optical power budget:

The first task in designing a fiber optic system is to make sure enough power reaches the receiver after all internal losses considered. The analysis determines the power margin between the optical transmitter output and the minimum receiver sensitivity required for a specified bit-error-rate (BER). The difference between transmitter output P_t and receiver input P_r , in dB equals the sum of system losses P_l and margin P_m , or:

$$P_t - P_r = P_l + P_m \quad (2.11)$$

All losses everywhere in the system must be considered. These losses include: light source to fiber coupling loss, connector loss, splice loss, coupler loss, fiber loss, and fiber to receiver coupling loss. System margin is a safety factor to allow for aging of components and system modifications and repairs. Typical values are 3-10 dB. The power budget is easily handled by writing the power levels in dBm. From the loss budget, one may determine whether to use light emitting diode or laser diode transmitter. Also, the detector type may be selected, either a PIN or APD type.

Transmission over short distances, for example in a building, can be dominated by connector losses if there are several connectors in the system. For longer distances system losses dominated by attenuation of the fiber. In a multi-terminal network, coupling losses are the largest.

2.5.2- Rise time budget:

The system rise time budget analysis allows us to determine the dispersion limitation of an optical fiber link. System speed is typically limited by the transmitter rise time, fiber response time, and the receiver rise time. The total rise time of a digital system is given by the following formula [KEISER]:

$$t_{rs} = \sqrt{\sum_{i=1}^N t_i^2} \quad (2.12)$$

Generally, the total transition time degradation of a digital link should not exceed 70 percent of an NRZ bit period, where one bit period is defined as the reciprocal of the data rate [CORKE].

Connectors, splices, and couplers do not affect time response significantly. Fiber response time is the square root of the squares of the modal and chromatic dispersion (see section 2.4). The transmitter rise time is attributable primarily to the light source and its circuitry, while the receiver rise time results from the photodetector response and the 3-dB electric bandwidth of the receiver front end. If B_{rx} is the 3 dB electric bandwidth of the receiver in MHz, then the receiver front end rise time t_{rx} in nanoseconds is given by the standard empirical formula [KEISER]:

$$t_{rx} = \frac{350}{B_{rx}} \quad (2.13)$$

For short-distance transmission, the prime limitation on transmission speed is receiver response time. The relative importance of receiver, transmitter, and fiber response depends on the system design.

2.6-FIBER OPTIC LOCAL AREA NETWORKS

As discussed earlier in chapter 1, LANs using metallic cables are not adequate to meet the requirements of many modern information processing systems, so fiber optic transmission technology has been applied

to LANs to meet these requirements. The reasons behind the application were the need to go further in distance, to connect more stations to the network, to run at high data rates, to offer electrical isolation, and to provide signal security.

The basic optical LAN topologies are the bus, the ring, and the star, and can be classified as active networks and passive networks. By using a passive star coupler, Fig. 2.11, the network can support a few tens of devices at a radial distance of up to about 1 kilometre, the limitations on number of devices and distances are imposed by the losses in the network. Fig. 2.12 shows the tradeoff between distance and number of devices for a typical system [STALLINGS]. Since the star is passive, it is an inherently reliable device and eliminates the concern of a central node failure with traditional active star networks. The main problem in passive star networks is the lack of a collision detection method that operates effectively over the 25 to 30 dB optical dynamic range present in such networks. The active star networks can support more devices over a greater distance and they are suitable for implementing fiber optic CSMA/CD LANs. The disadvantage of the active star is that it is more expensive due to the active components in the central node, which may limit the speed of the network, and is an obvious source of catastrophic failure. Star connected networks also suffer from a rather clumsy topology and higher cabling costs than other topologies. A ring topology uses active elements at each node and transmission between nodes is essentially point-to-point. A failure at any one node can interrupt transmission unless a redundant path of a by-pass switch is used at each node. The number of nodes in a ring is defined by system constraints due to the low loss of optical fibers, and the unrepeated distance between nodes can be very large [LYMPANY]. The cost and reliability of active ring networks, in spite of some fail-safe node proposals, may set a limit to their use at high speed. Furthermore, special procedures are needed to recover from token loss or duplication and to avoid non-recognized packets circulating endlessly in the ring.

It is clear that the cost and reliability of active networks may limit their use. A data buss could be active or passive. Data buses with passive taps, Fig. 2.13, are of particular interest in LAN applications due to the simplicity and reliability of the tap itself. The taps extracts a portion of the optical energy from the bus for reception and it injects optical energy directly into the medium for transmission. However, passive tapping of an optical fiber has a high insertion loss. Because of the loss characteristics of these couplers, the maximum number of nodes is restricted to 10 to 15. Fig. 2.14 plots performance limits for a tapped bus with a head end repeater [SUH]. The number of stations that can be put on an optical fiber data bus is usually limited by the total allowable attenuation between transmitter and receiver. Less optical power may be lunched into a fiber than electrical power lunched into metallic cable, but the lower limit on optical receiver sensitivity requires more input power than that required by metallic cable receivers, and the optical splitters and couplers have high insertion loss. For these reasons the maximum number of nodes that can be put on an optical fiber data bus is limited and less than that can be put on metallic cable [RHODES]. The most commonly used medium access control technique for bus topology is CSMA/CD. Token-bus technique is also used, but it is more complex than CSMA/CD.

There are clearly trade-offs to be made in the design process. For example, by choosing an active ring configuration, the problem of coupler or tap losses essentially disappears; one has the point-to-point link. However, one also has the problem of complexity with the medium-access method and the critical question of providing fault-tolerance mechanisms such as by-pass switching. At this point one may decide to throw out the active network idea and try a passive network which gives more a reliable and cost-effective network.

The first commercially available fiber optic component for LAN was the passive star coupler which was used in Fibernet [RAWSON]. Fibernet II, Fig. 2.15, is a fiber optic Ethernet which uses an active star coupler

It can extend an existing coaxial cable Ethernet installation or can serve as a stand alone Ethernet replacing coaxial cable with fiber cable. Fiber Distributed Data Interface (FDDI) is a high performance fiber optic token ring LAN running at 100 Mbit/s over distances up to 200 km with up to 1000 stations connected [HECHT]. FDDI-II is the successor to FDDI, modified to handle synchronous circuit switched PCM data for voice or ISDN traffic, in addition to ordinary data [TANENBAUM]. FDDI uses multimode fiber and LEDs. Several additional systems are described in [HECHT, STALLINGS, and TANENBAUM]. As we mentioned before, these networks are very expensive, they have problem of reliability, and they are not suitable for some applications. Passive optical networks are still potentially attractive.

2.7-PASSIVE FIBER OPTIC COMPONENTS FOR LANS

For optical fiber technology to make a large impact in LANS, there is a requirement for readily available low cost, high quality components. The required components include optical couplers, star couplers, optical switches and connectors, which are discussed briefly in this section. The specific requirements for individual components depend heavily on the particular application and operating conditions.

2.7.1- Connectors:

Connectors are used for connecting the fiber cable to terminal and line equipment, to access fiber paths for testing, making temporary connection among equipments, and for network rearrangements. They must guarantee mechanical compatibility between the various system components, and they must be able to withstand repeated mating without significant degradation of performance. Connector loss is measured for a mated pair of connectors. Their loss is the sum of losses caused by several factors, which are easier to isolate in theory than in practice.

All these factors stem from the way light is guided in fibers. The major ones are: overlap of fiber cores, alignment of fiber axes, fiber numerical aperture, fiber spacing, and reflection at fiber ends. These factors interact to some degree. Connectors for single mode fibers have to meet more stringent alignment accuracies, and alignment errors of less than 200 nm have been obtained. The resulting connector loss for single mode fiber is less than 0.5 dB, which is comparable to that for multimode fibers. Fiber connectors are specified for lifetimes of a few hundred matings, but most can be torn from cable ends by a sharp tug.

2.7.2- Couplers:

A coupler links two or more fibers together providing two or more paths for the transmission signal. A coupler may be passive or active. A passive coupler is used either to tap off a portion of the optical power from the bus or to distribute optical power from an input fiber among several output fibers. These functions are inherently directional, depending on which way the signal is being transmitted. Optical couplers are multiport devices and thus have at least two optical ports at which light waves can be coupled in and out. They can be divided into two groups according to the number of ports, the first group comprising three and four port couplers, the second group containing mixers with a large fiber count (star couplers), [ZEITLER].

A directional coupler, an example of four port coupler, forms the basis of many distribution networks. To describe the characteristics of the coupler we will assume that power P_1 is incident on port 1 of the coupler, Fig. 2.16. This power will divide between ports 2 and 3 according to the desired splitting ratio. Ideally, no power will reach port 4, the isolated port. We then define two parameters that used in system design; the splitting ratio [PALAIS]:

$$C_r = \frac{P_2}{P_3} \quad (2.14)$$

and the excess loss (in dB):

$$L_E = -10 \log \left[\frac{P_2 + P_3}{P_1} \right] \quad (2.15)$$

The excess loss includes radiation, scattering, absorption, and coupling to the isolated port. Some excess loss is inevitable in passive couplers, but it can be as small as 0.05 dB in small directional couplers, and couplers with losses below 0.5 dB can be produced routinely. Couplers are often described by their tap loss; which specifies the transmission loss between the input and the tap (port 3).

$$L_{TAP} = -10 \log \frac{P_3}{P_1} \quad (2.16)$$

The other important parameter of the directional coupler is the throughput loss; which specifies the amount of transmission loss between the input port and the favoured port (port 2):

$$L_{THP} = -10 \log \frac{P_2}{P_1} \quad (2.17)$$

The star coupler has more than four ports. It has $2N$ ports. Light is mixed in a central mixing element and the output light emerges from that element into fibers. The star coupler distributes power equally to each of the receiver ports from any one of the transmitter ports, as illustrated in Fig. 2.17. The transmission efficiency for each port is then $1/N$ and the corresponding insertion loss (in dB) is:

$$L_{in} = -10 \log \frac{1}{N} \quad (2.18)$$

If we include connector loss (L_c) and the star excess loss (L_E), the total distribution loss associated with the star coupler is [PALAIS]:

$$L = -10 \log \frac{1}{N} + L_E + 2L_c \quad (2.19)$$

Over 95% of the multimode and single mode fibers couplers used are fabricated using the fused biconical taper technology [CORKE]. Star couplers can be made by fusing many fibers to create a mixing region.

2.7.3- Splices:

Splices are low-loss, permanent connections between fiber ends. The major problem for splicing is to obtain and maintain accurate alignment of the fibers to be joined. Proper alignment must be maintained in three dimensions: the separation between the fibers, the angle between the fiber axis, and the offset perpendicular to the fibers. There are three principal concerns in splicing: the attenuation of the finished splice, its physical durability, and ease of splicing. Basic splicing techniques include fusing the two fibers or bonding them together in an alignment structure. The bond may be provided by an adhesive, by mechanical pressure, or by a combination of the two [PALAIS, HECHT]. The average loss of fusion splices is usually under 0.1 dB when fibers with identical specifications are spliced together. However, losses of individual splices can be higher [HECHT].

2.7.4- Switches:

The routing of signals is an important feature in a communications network, and switches normally perform this task. There are two types of fiber optic switch that are in common use; these are the two position and bypass switch. Fig. 2.18 shows a two position switch. An input at port 1 can be switched to either port 2 or 3. For the following definitions, assume the switch is set for coupling to port 2. The insertion loss (in dB) is:

$$L_{IL} = -10 \log \frac{P_2}{P_1} \quad (2.20)$$

where P_1 is the power going into port 1 and P_2 is the power emerging from port 2. Insertion loss depends on fiber alignment. Losses of less than 1.5 dB can be obtained with good mechanical switches. Crosstalk

is a measure of how well the uncoupled port is isolated. It is given by:

$$L_{CT} = -10 \log \frac{P_3}{P_1} \quad (2.21)$$

where P_3 is the power emerging from port 3. Crosstalk depends on the particular design of the switch, but values of 40 to 60 dB are typical. Switching speed is a crucial factor in some applications. Switching can be done electromechanically. Fig. 2.19 shows the function of a bypass switch. In the bypass state, ports 1 and 4 are coupled. Ports 2 and 3 are isolated. In the branch state, ports 1 and 2 are coupled and ports 3 and 4 are coupled. The bypass switch can be incorporated into a ring network by attaching it to the data bus, Fig. 2.20, [PALAIS].

Fig. 2.21a shows an example of simple bus network with 4 terminals, which contains some of the components discussed in this section. Each terminal contains a transmitter and a receiver. A trunk fiber carries the information between taps. Taps are provided by tee couplers. The tee coupler shown in Fig. 2.21b permits bidirectional information flow in the bus fiber. In Fig. 2.21b, two directional couplers constitute the tee coupler. Terminals 1 and 4 are connected to the bus by a single directional coupler.

Consider the total loss between terminals 1 and 4, assuming that the directional couplers that attach to the bus fiber each have throughput loss L_{THP} , tap loss L_{TAP} , and excess loss L_E . The signal must pass through 3 directional couplers before reaching the coupler at the receiver. The receiver connects to the tap port of this coupler. Each coupler input and output port requires a connector, so there are 2x4 connectors in the path between terminals 1 and 4. A loss of L_c dB per connector adds a loss of $8L_c$ to the path loss. At least two splices required for each coupler, so there are 2x4 splices in the path between terminals 1 and 4. A loss of L_s dB per splice adds a loss of $8L_s$ to the path loss. If

the path length is 1 km, and the fiber loss is α dB/km then, the total distribution loss is now:

$$L = 3L_{THP} + 4L_E + L_{TAP} + 8L_c + 8L_s + l\alpha$$

For example, for the splitting ratio 3:1, if $L_{TAP} = 6$ dB, $L_{THP} = 1.25$ dB, $L_E = 1$ dB, $L_c = 1$ dB, $L_s = 0.2$ dB, $l = 1$ km, and $\alpha = 0.2$ dB/km, then $L = 25.35$ dB.

2.8-SUMMARY

In this chapter we have examined the suitability of fiber-optic components to LANs, and the advantages we get from using fiber-optic LANs over metallic-cable LANs. Passive fiber optic LANs are more reliable and cost effective than active networks.

Fiber attenuation is not significant in a networks with a diameter of less than 1 km. The pulse broadening (dispersion) has no effect or very little effect on system performance for distances of up to 4 km, and data rates of up to 120 Mbit/sec if the section is used with a LED with longer wavelengths (1300 nm), and with multimode graded index fiber. If we want to go further in distance or higher in frequency we should use a laser diode or single-mode fiber or both.

2.9-REFERENCES

CORKE, M., SWEENEY, K., PRATER, R., MUHS, J., and SCHMIDT, K., "Fiber optic components for communication application", Proceedings of the 37th electronic components, Conf. Cat. No 87CH2448-9, Boston MA, USA, 11-13 May 1987.

CURRIE, W. S., "LANs explained", John Wiley & Sons, 1988.

GOWAR, J., "Optical communication systems", Prentice-Hall, Chapter 2, 1984.

HECHT, J., "Understanding fiber optics", Howard W. Sams & Company, USA,

1987, Chapter 4.

KEISER, G., "Optical fiber communications", McGraw-Hill, 1985.

KUMMERLE, K., and REISER, M., "Local area communication networks- an overview", J. Telcommun. Networks, Vol. 1, No. 4, 1982, pp. 349-370.

LYMPANY, S., "Fiber optic components for local area networks", IEEE 1985 Military communication conference, MILCOM 85 conference record (CAT 85CH22020), Boston, MA, USA, 20-23 Oct. 1985.

MIDWINTER, J. E., "Optical for transmission", John Wiley and Son, New York, 1979, pp. 410.

MILLER, S. E., and CHYNOWETH, A. G., "Optical fiber telecommunications", Academic press, Inc., New York, 1979, pp. 905.

MOUSTAKAS, S., "The standardization of IEEE 802.3 compatible fiber optic CSMA/CD LANs", IEEE Commun. Magazine, Vol. 25, Feb. 1987, pp. 22-29.

PALAIS, J. C., "Fiber optic communications", Prentice Hall, N Y, 1988, chapter 9.

RAWSON, E., and METCALFE, R., "Fibernet: multimode optical fibers for local computer networks", IEEE trans. on Commun., Vol. COM-26, No. 6, July 1978.

REFI 87, J. J., "Fiber bandwidth and its relation to system design", J. of Optical Sensors, Vol. 2, 1987, pp. 89-105.

REFI 86, J. J., "LED bandwidth of multimode fibers as a function of laser bandwidth and LED spectral characteristics", J. Lightwave Technology, Vol. LT-4, No. 3, March 1986, pp. 265-272.

RHODES, N., "Interaction of network design and fiber optic component design in local area networks", IEEE J. on selected areas in Commun., Vol. SAC-1, No. 3, April 1983.

RORABAUGH, B., "Data communications and local area networking handbook", TAB books, 1985, Chapter 13.

ROWLANDS, M. G., "Local area networks", British Telecommun. Eng., Vol. 2, April 1983, pp. 6-11.

SCHMIDT, R. V., RAWSON, E. G., NORTON, R. E., JACKSON, S. B., and BAILEY, M. D., "Fibernet II: A Fiber Optic Ethernet", IEEE J. On selected areas

in Commun., Vol. SAC-1, No. 5, November 1983.

SENIOR, J., "Optical fiber communications: principles and practice", Prentice Hall, London, 1985, Chapter 2.

SINGH, A., and RAINA, J. P., "Dispersion in optical fibers-measurement methods and state of the art", IETE Tech. Rev. (India), Vol. 2, No. 8, Aug. 1985, pp. 257-69.

STALLING, W., "Local Networks, an introduction", Macmillan, NY, 1987.

SUH, S. Y., GRANLUND, S. W., and HEGDE, S. S., "Fiber optic local area network topology", IEEE Commun. Magazine, Vol. 24, No. 8, August 1986, pp. 26-31.

TANENBAUM, A. S., "Computer networks", Prentice-Hall, NY, 1988, chapter 3.

TSAO, C. D., "A local area network architecture overview", IEEE Commun. Magazine, Vol. 22, No. 8, Aug. 1984, pp. 7-11.

ZEITLER, B., "Optical communications ", Telecom. report, Vol. 6, 1983.

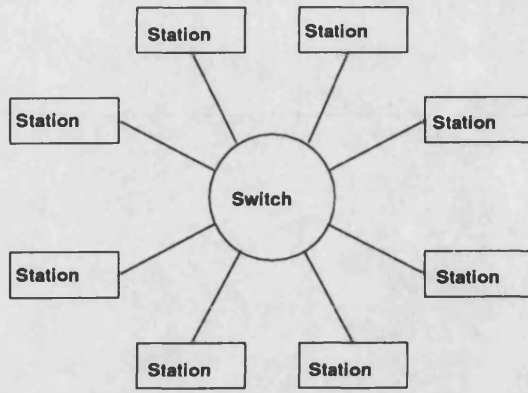


Figure 2.1 Star topology

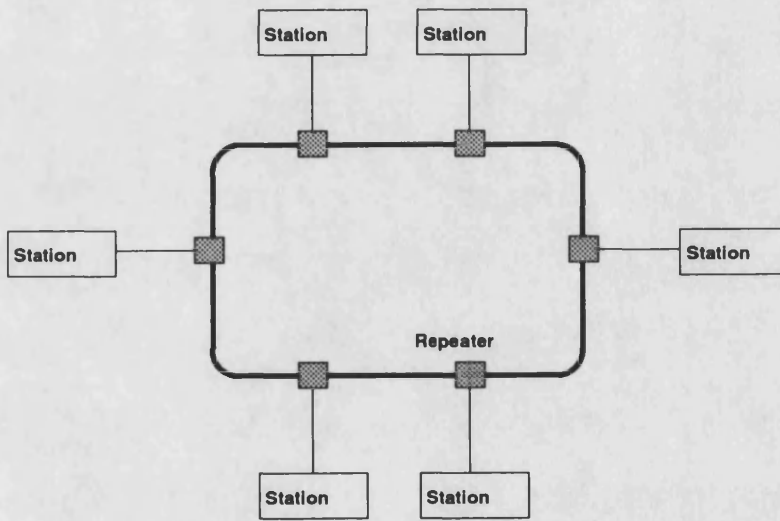


Figure 2.2 Ring topology

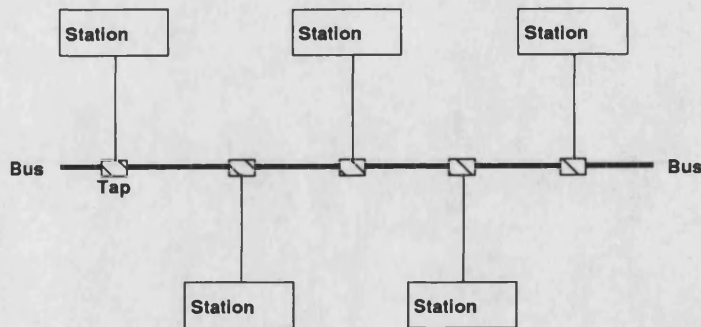


Figure 2.3 Bus topology

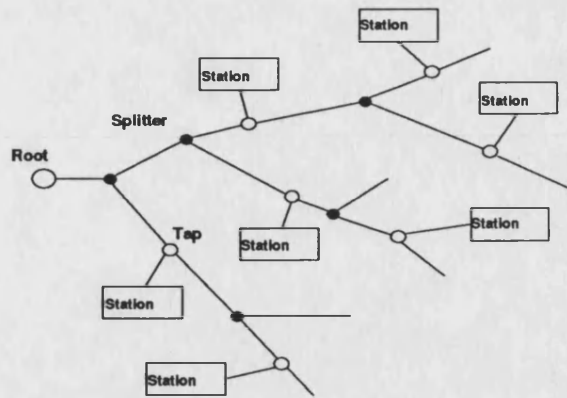


Figure 2.4 Tree topology

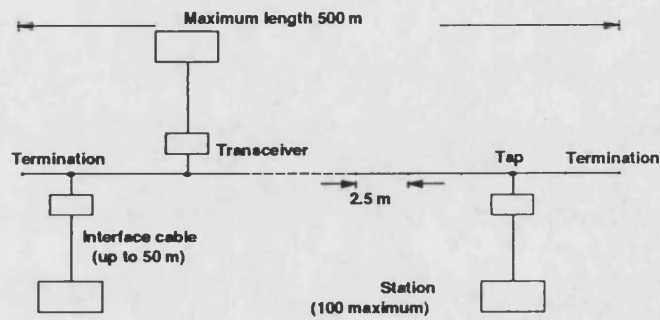


Figure 2.5 A single segment Ethernet configuration

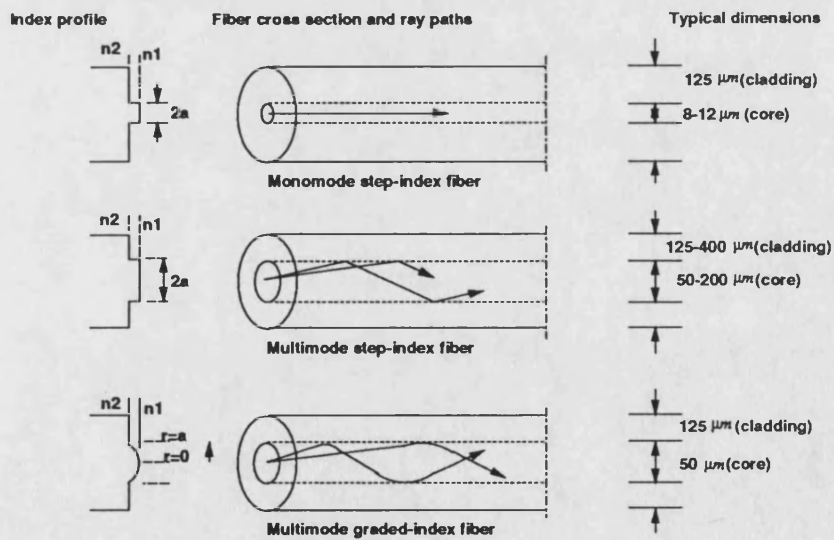


Figure 2.6 Comparison of single-mode and multimode step-index and graded-index optical fibers

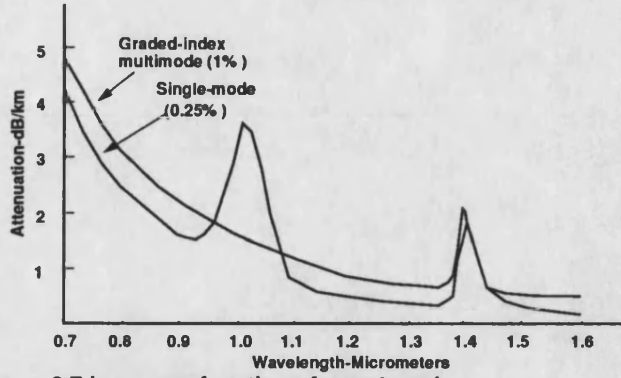


Figure 2.7 Loss as a function of wavelength

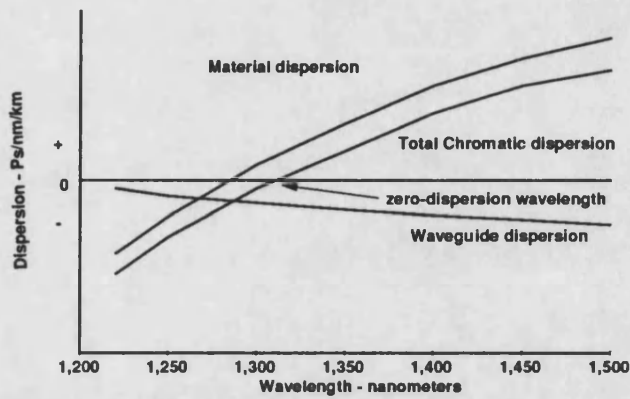


Figure 2.8 Chromatic Dispersion in Single-mode step-index fiber

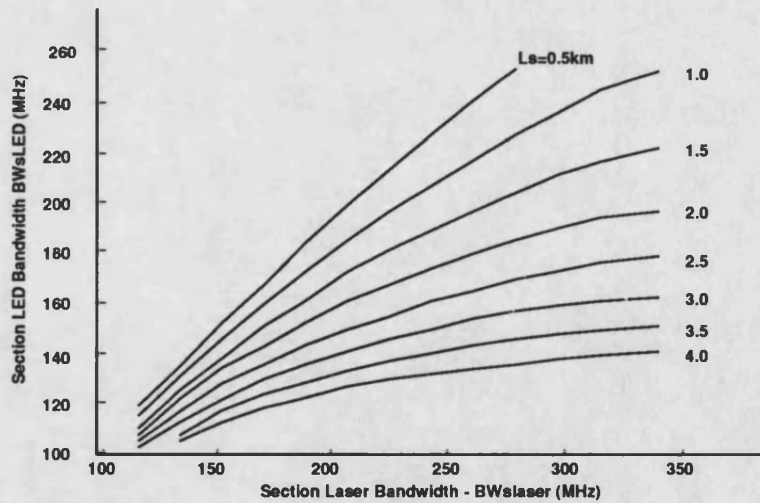


Figure 2.9 Section LED bandwidth for 62.5µm fiber versus section laser bandwidth for various section lengths

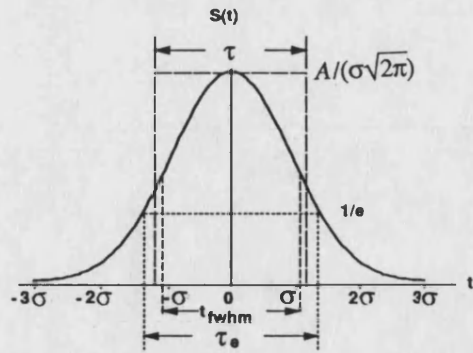


Figure 2.10 Gaussian pulse

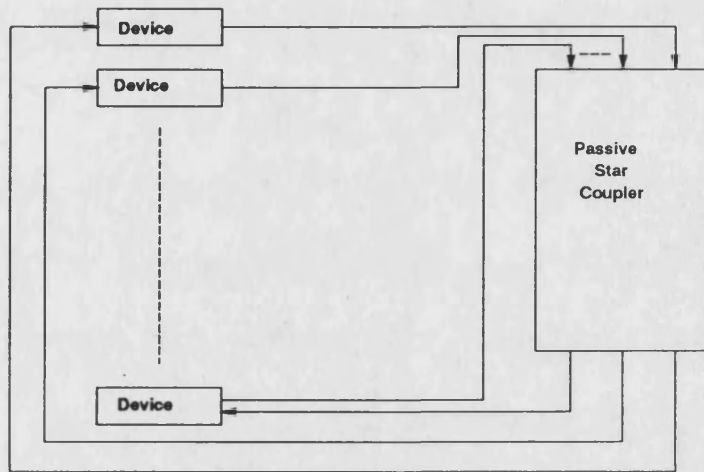


Figure 2.11 Optical Fiber Passive Star Configuration

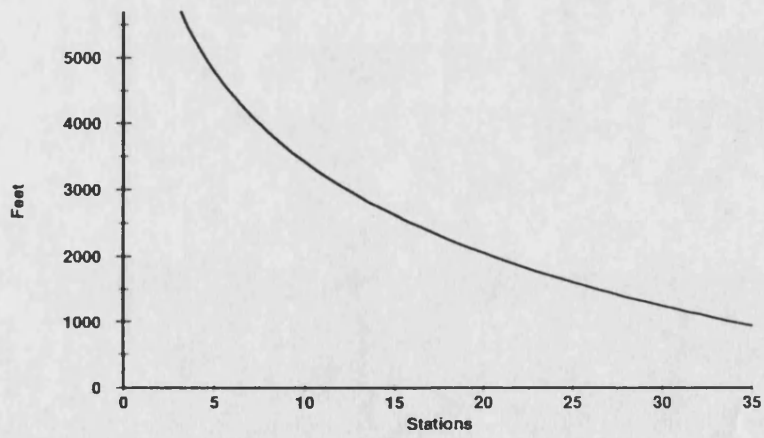


Figure 2.12 Passive Star Performance

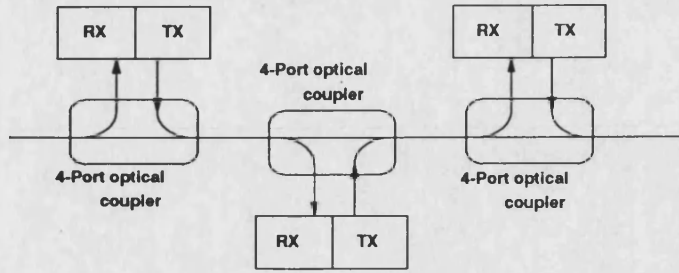


Figure 2.13 In-Line topology with 4-port passive couplers

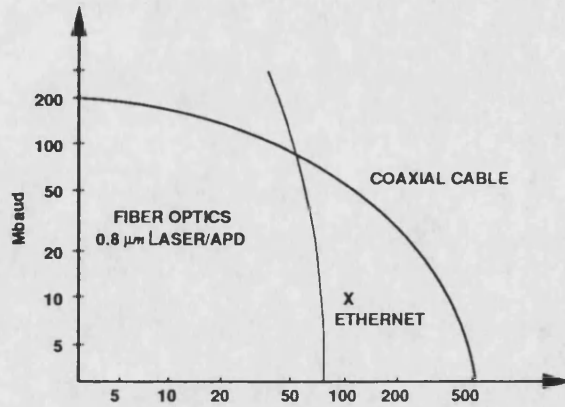


Figure 2.14 Representative bit rate vs. number of node limitations for coaxial cable and fiber-optic tapped buses.

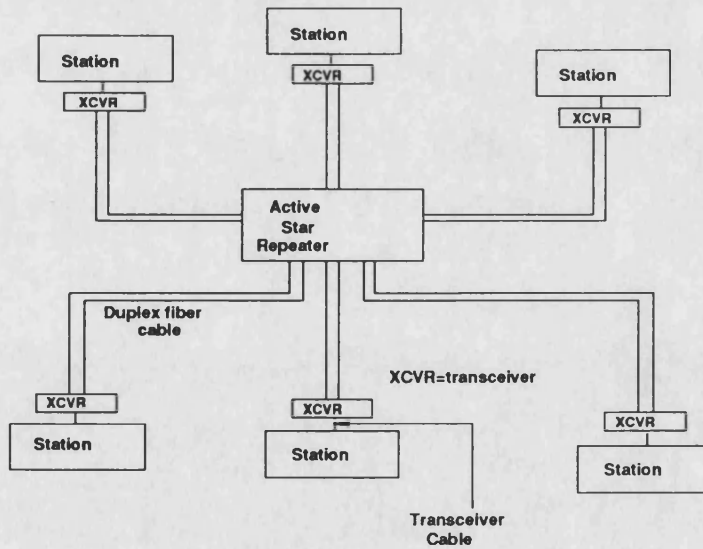


Figure 2.15 Fibernet II Active Star Configuration

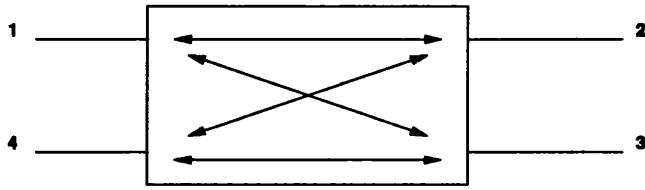


Figure 2.16 Four port directional coupler

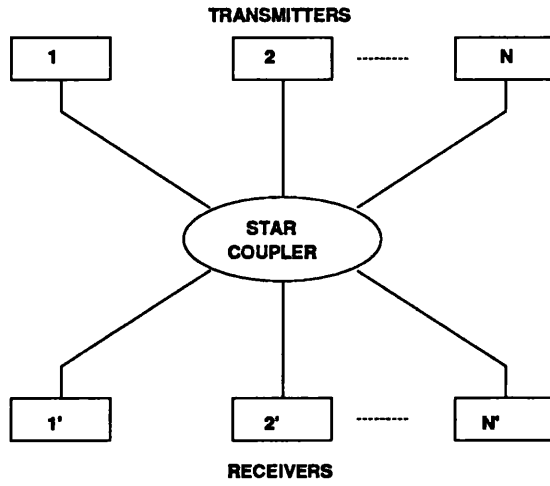


Figure 2.17 Star network

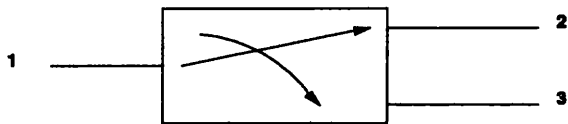


Figure 2.18 Two position switch

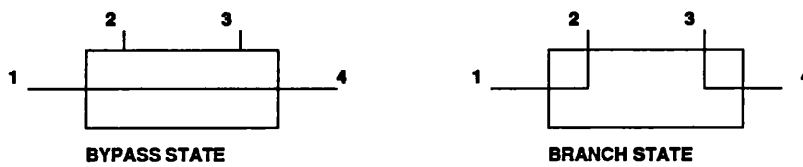


Figure 2.19 Bypass switch

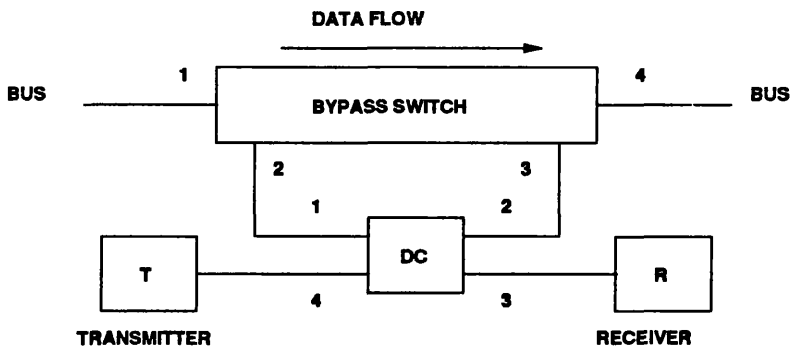
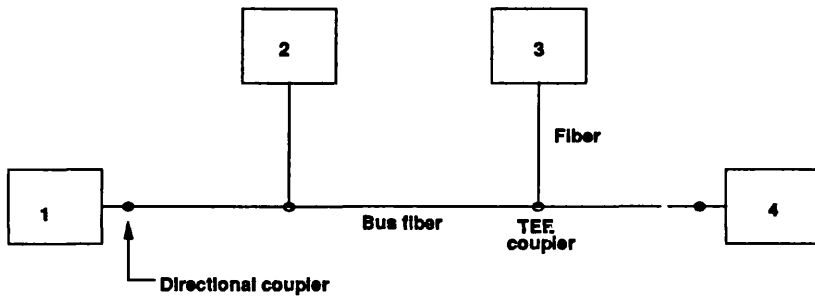
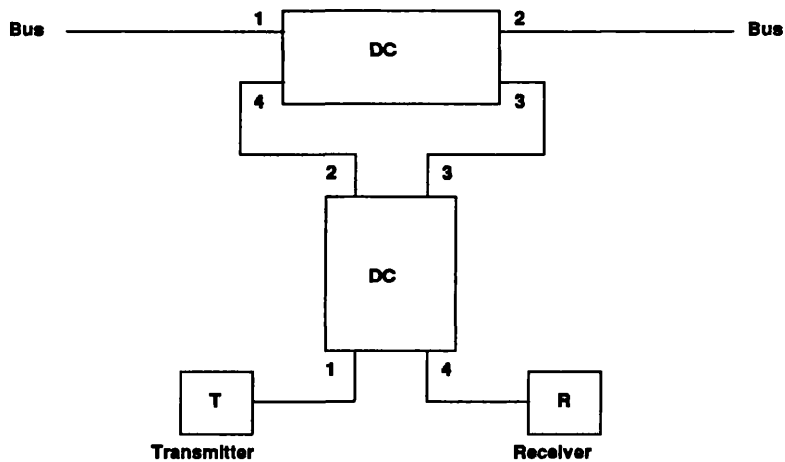


Figure 2.20 Bypass switch incorporated into a tap for a tee (or ring) network



(a) Tee network interconnecting 4 terminals



(b) Tee coupler using two directional couplers

Figure 2.21

CHAPTER -3-

DIGITAL PULSE POSITION MODULATION

3.1-INTRODUCTION

Digital pulse position modulation has been shown in principle, to be a very effective modulation format for optical communications. It is an attractive technique for fully utilizing the wide bandwidth characteristics of optical fiber communication systems, and can in principle be used to effect a trade-off between the large transmission bandwidth provided by optical fibers and an increased transmission distance (or signal to noise ratio) [GARRETT].

Digital information may be transmitted using PPM by dividing each data frame (T_f) into M time slots, and allowing the location of a pulse in just one of these time slots/frame to indicate the data. Every T_f seconds, an optical pulse is placed in one and only one of the M slots, and during the other $(M-1)$ slot times, the transmitter is turned off. For example, the PPM signalling format is illustrated in Fig. 3.1a, for $M=8$ time slots per frame. The pulse which is placed in one of M time slots, conveys $\log_2 M$ bits of information, and its duty-cycle is equal to $1/M$. For a time slot width T_s , the data rate R (in bits/sec), is given by:

$$R = \frac{\log_2 M}{M \cdot T_s} \quad (3.1)$$

If the modulation index m is less than 1, then:

$$M \cdot T_s = m \cdot T_f \quad (3.2)$$

or:

$$m = \frac{M \cdot T_s}{T_f} \quad (3.3)$$

and the guard interval, G , is equal to:

$$G = (1-m)T_f = T_f - M \cdot T_s \quad (3.4)$$

We leave a guard interval, $(1-m)T_f$, at the end of each frame to prevent pulses spreading into the adjoining frame as a result of dispersion in the fiber. As the frame and the slot sizes do not change in a PPM signal, the two clock signals (for the slot and the frame) are not independent. Practically, it is much easier to relate the two signals if the slot frequency is a multiple of the frame frequency. What this implies is that the modulation index should not be arbitrarily selected between 0 and 1 but with the constraints:

$$\frac{mT_f}{T_s} = M \quad (3.5)$$

and:

$$\frac{(1-m)T_f}{T_s} = i \quad ; \quad i \in \{0, 1, 2, 3, \dots\} \quad (3.6)$$

Which means that the m can only take the discrete values given by:

$$m = \frac{M}{M+i} \quad (3.7)$$

Fig. 3.1b, is an example for $M=8$, and $m=0.8$. The best choice of m is also affected by the accuracy with which the source laser can be pulsed (see chapter 4). The more time slots we allocate per frame, the higher the information rate we can achieve for a given rate. On the other hand, as we increase the number of time slots, synchronization becomes more critical (see chapter 5).

In this chapter, we compare a binary PCM system operating at an information rate of B bits/sec, and a PPM system operating with M time slots per frame as mentioned above. For the two systems to have the same information throughput, so that the PPM system is balanced by the corresponding PCM signal stream at B bauds, then:

$$BT_s = \frac{m \cdot \log_2 M}{M} \quad (3.8)$$

To analyse the performance of a PPM system and compare its characteristics with an existing PCM system, we assume that the same fiber transmission network is to be used by both PPM and PCM; so for the PCM case, we may

use a wide-band assumption (since for LANs we use short links), and any bandwidth restriction imposed by the fiber will influence the PPM signal more than the PCM transmission.

3.2-DPPM SIGNAL DETECTION

The function of the optical transmitter is to convert the electric signal to an optical signal. The electric current can be used to modulate directly an optical source. In order to obtain maximum peak power from an optical transmitting device, it is necessary to make the pulses extremely short so that the device does not heat up under the pulse (see chapter 4). In the limiting case of maximum amplitude, the generated pulse is therefore not rectangular.

If the pulse travels along a fiber having infinitely high bandwidth, the width and the shape of the received pulse will be the same as the input pulse, but if the pulse travels over a fiber having finite bandwidth, the received pulse will spread in time due to the dispersion. We assume that the fiber has finite bandwidth, then the generated pulse after transmission tends to a Gaussian shape because of fiber dispersion [SENIOR]. The received Gaussian pulse at the receiver input may be represented by [MARTIN]:

$$x(t) = A \cdot \exp\left[-2\left(\frac{t}{t_w}\right)^2\right] \quad (3.9)$$

where:

t_w ; is the rms full-width, and,

A ; is the received electrical pulse amplitude, and equal to: βA_p ,

where:

β ; is related to the photo-diode responsivity, and

A_p ; is the peak optical amplitude.

The frequency spectrum of this pulse is obtained by taking the Fourier Transform of both sides of Eq. 3.9,

$$X(f) = \left(A t_w \sqrt{\frac{\pi}{2}} \right) \cdot \exp \left[- \left(\frac{\pi t_w f}{\sqrt{2}} \right)^2 \right] \quad (3.10)$$

The direct detection PPM system, which were used in this work, is shown in Fig. 3.2. The received pulse is fed to a Gaussian filter which is matched to the Gaussian received pulse. A matched filter is known to be the optimum linear detector in white noise [CLARKE]. Such a filter having a one-sided rms bandwidth of W Hz, is described by:

$$H(f) = \exp \left[- \left(\frac{f}{W\sqrt{2}} \right)^2 \right] \quad (3.11)$$

And its impulse response is :

$$h(t) = W\sqrt{2\pi} \cdot \exp[-(\pi t W\sqrt{2})^2] \quad (3.12)$$

Since the response of a Gaussian filter to a Gaussian wave-form is in turn Gaussian, it is easily shown that the filtered received pulse can be written as:

$$y(t) = A \frac{t_w}{t_y} \cdot \exp \left[- \left(\frac{t\sqrt{2}}{t_y} \right)^2 \right] \quad (3.13)$$

And:

$$Y(f) = \left(A t_w \sqrt{\frac{\pi}{2}} \right) \cdot \exp \left[- \left(\frac{f}{W_y\sqrt{2}} \right)^2 \right] \quad (3.14)$$

where:

t_y : is a measure of the output pulse rms full-width given by:

$$t_y = \frac{1}{\pi W_y} \quad (3.15)$$

and W_y : is the output pulse rms bandwidth given by:

$$W_y^2 = \frac{W^2}{1 + (\pi t_w W)^2} \quad (3.16)$$

For the special case of a matched filter, when $W = \frac{1}{\pi t_w}$, then:

$$W_s = \frac{W}{\sqrt{2}} \quad (3.17a)$$

$$t_s = t_w \sqrt{2} \quad (3.17b)$$

From the Eqs. 3.17 and 3.13, the output signal at the output of a matched Gaussian filter is equal to:

$$y(t) = \frac{A}{\sqrt{2}} \cdot \exp\left[-\left(\frac{t}{t_w}\right)^2\right] \quad (3.18)$$

Noise of spectral density $\frac{N_o}{2}$ ($\frac{V^2}{Hz}$) of the white Gaussian noise is added to the incoming group of pulses at the receiver (for a PIN photo-diode detector and transimpedance amplifier, the noise sources can be assumed Gaussian in statistics and flat in spectrum; or white noise). The noise power N , at the detector can be calculated from the equivalent noise bandwidth of the filter, which is the ideal filter bandwidth that gives the same noise power as the actual system [STREMLER]. Hence:

$$N = \frac{N_o}{t_w \sqrt{2\pi}} \quad (3.19)$$

For a matched filter, the signal to noise ratio depends upon signal energy, and that is the maximum that can be obtained for white noise and is independent of the shape of the signal. [CLAPKE].

When a pulse is transmitted in a given time slot, most of the pulse energy will arrive in the corresponding time slot at the receiver, as shown in Fig. 3.3. However, because of pulse spreading induced by the fiber, some of the transmitted energy will progressively spread into neighbouring time slots as the pulse propagates along the fiber (see section 3.4).

3.3-PPM ERROR TYPES AND FRAME SIZE

Noise is added to the incoming group of pulses in the receiver, and after filtering, there is a possibility that the noise will cause an error in the decoding of the signal. An error will occur if noise

in the absence of a signal happens to have an instantaneous amplitude comparable to that of a pulse when present or if noise in the presence of a signal has a large enough negative amplitude to destroy the pulse. So the presence of noise forces the detector to make a wrong decision on some occasions. In general, three types of error can occur in PPM signal detection, and they are:

a- Wrong position error: in which the assumed signal slot is different from that in which the original pulse was sent.

b- Multi-detection error: when more than one slot appears to contain a signal pulse in a single PPM frame.

c- Erasure error: when no signal slot is found in a frame.

Wrong position error can be distinguished further into two cases, namely false alarm error and wrong slot error [GARRETT]. A false alarm error is the result of receiver noise alone crossing the threshold when there is no signal pulse present. A wrong slot error can occur when noise added to the finite slope leading or trailing edge of a signal pulse due to limited bandwidth of the transmission channel, causes the sum of signal plus noise to exceed the threshold in its adjacent slot.

The size of a PPM frame is of importance to the system performance. Increasing the number of slots in each frame will increase the amount of information per pulse, which tends to reduce the average power per bit. But at the same time the chance of getting a wrong position error (false alarm error) in a frame increases with M (see section 3.4). To keep the error rate constant, a higher threshold is needed and this increases the required signal power if erasure errors are not to become dominant. An optimum value of M exists for a given bandwidth condition [GARRETT]. He showed that if the fiber bandwidth is 100 times the data rate, the optimum M appears to be around 32, as is shown in Fig. 3.4. It is also seen that the optima are rather broad. Fig. 3.5 gives the relationship between the fiber bandwidth and the optimum M , suggesting that optimum slot number is not too critically dependent on the bandwidth assumption.

These results obtained by GARRETT may differ from our results (see section 3.4) because these are obtained under different conditions. GARRETT in his analysis used a very complicated method for the special type of PIN-FET receiver using a whitening filter, over a slightly dispersive channel. The detector operates on the first zero crossing in the frame, and hence ignores any subsequent pulse detection, and the optimum filter for this condition, generates a long tail to the pulse before it is detected. In his second paper, GARRETT derived an optimum filter for the channel with additive stationary noise by considering the effect of erasure errors and minimizing the channel equivocation. This complicated filter is difficult to realize in practice, and the results are difficult to apply directly to the broad comparative study of PPM in Local Area Networks that is presented here.

In our analysis we will follow slightly different and simpler method to calculate the error performance of a PPM system. For a band-limited fiber we assume a Gaussian received pulse, and the detector filter will be a matched filter followed by a sampler and comparator (Fig. 3.2). This type of detector is used because it is simple to realise in practice. The effective error performance is calculated on the frame basis, for the following three cases; error free, un-detected error, and detected error. The definitions and the analyses of different types of error used in this work are covered in the next section.

3.4-ERROR PERFORMANCE OF DPPM SYSTEM

This section begins with the definitions of different types of error for the slot and the frame, and is then followed by their analysis. A PPM pulse in a frame is subjected to two types of error, they are:

- a- Erasure error:** Failing to detect a transmitted pulse because the signalling pulse is eradicated by noise.
- b- False-alarm error:** Due to detecting pulse in an empty slot. This can be sub-divided into two cases:

b-1- In adjacent slots: Due to pulse spreading, slots adjacent to the signaling pulse slot are much more likely to produce a false-alarm, than other slots.

b-2- In other than adjacent slots: An apparent signalling pulse is produced in a vacant slot.

From the two types of error defined above, if we consider the frame as a whole then we can define three major conditions:

1- Probability of no detection error: When no error is detected in the frame (error free case), this measures the throughput of the system.

2- Probability of an undetected error: Occurs when the proper pulse not detected, but one false-alarm pulse is detected.

3- Probability of detected error: Which can be calculated by adding the following three cases:

3-a- When the proper pulse is detected, but at least one false-alarm pulse is also detected.

3-b- When the proper pulse is not detected, and there are no false-alarm pulses.

3-c- When the proper pulse is not detected, but more than one false-alarm pulse are detected.

To analyse the error performance of a PPM system from the definitions above, we start first with the slot errors, and then the error types for the frame as a whole are analysed. We assume that the noise is Gaussian in form, of power $N(=\sigma^2)$ at the detector. The probability density function of the input when there is no signal present, (noise alone), is:

$$P_0(v) = \frac{1}{\sigma\sqrt{2\pi}} \cdot \exp\left[-\frac{v^2}{2\sigma^2}\right] \quad (3.20)$$

The probability density of the input when the signal $y(t)$ is present is also Gaussian but with a mean value equal to Y (Fig. 3.6):

$$P_1(v) = \frac{1}{\sigma\sqrt{2\pi}} \cdot \exp\left[-\frac{(v-Y)^2}{2\sigma^2}\right] \quad (3.21)$$

The correct sampling instant within each received slot is determined by some external means. As we mentioned before, the PPM pulse in a frame is subjected to erasure and false-alarm errors, (Fig. 3.7); which we analyse separately.

3.4.1- Slot erasure error: failing to detect a transmitted pulse. When a pulse is transmitted the probability density function for the signal is Gaussian with a mean value equal to Y_1 . The presence of the noise brings uncertainty to the actual value of the sample. The threshold is set at v_{th} (Fig. 3.8a), so any sample value which falls below v_{th} is going to be interpreted as a "0", and an erasure error will have occurred. The probability of an erasure error, designated here by P_m is given by the shaded area in Fig. 3.8a:

$$P_m = \frac{1}{\sigma\sqrt{2\pi}} \int_{-\infty}^{v_{th}} \exp\left[-\frac{(v-Y_1)^2}{2\sigma^2}\right] dv \quad (3.22)$$

where σ^2 is the variance which equal to $\frac{N_o}{t_w\sqrt{2\pi}}$.

Now in order to evaluate the integral, we make use of error functions to get:

$$P_m = \frac{1}{2} \left[1 - \operatorname{erf}\left(\frac{v_{th}-Y_1}{\sigma\sqrt{2}}\right) \right] \quad (3.23)$$

Noisy signals are commonly described by their signal to noise ratio (SNR). At the output of the matched filter, the SNR depends only on pulse energy and noise power spectral density. Eq. 3.23 can be written in terms of signal to noise ratio using the Eqs. 3.18 and 3.19, and assuming that v_{th} is equal to $\frac{\alpha A}{\sqrt{2}}$, where A is PPM pulse amplitude (defined in Eq. 3.9). From Eq. 3.18, assuming that the sample timing is exact, the sample value in the true slot is given by:

$$y(0) = \frac{A}{\sqrt{2}} \quad (3.24)$$

From the Eqs. 3.19 and 3.24, the signal to noise ratio is equal to:

$$SNR = \frac{A^2 t_w \sqrt{\pi}}{N_o \sqrt{2}} \quad (3.25)$$

This represents the SNR for an ideal matched filter. Substituting Eq. 3.25 into 3.23 gives:

$$P_m = \frac{1}{2} \left[1 - \operatorname{erf} \left\{ (\alpha - 1) \sqrt{\frac{\text{SNR}}{2}} \right\} \right] \quad (3.26)$$

3.4.2- Slot false-alarm error: due to detecting pulse in an empty slot.

This can be resolved into two cases:

3.4.2.1- In adjacent slots: when the noise is added to the finite slope leading (or falling) edges of a signal pulse, it causes the sum of the signal plus noise to exceed the threshold in its adjacent slots. This is highest in two slots adjacent to the transmitted pulse. The probability designated here by P_{fa} , is given by the shaded area in Fig. 3.8b:

$$P_{fa} = \frac{1}{2} \left[1 - \operatorname{erf} \left(\frac{v_{th} - Y_2}{\sigma\sqrt{2}} \right) \right] \quad (3.27)$$

For the signal alone the value of Y_2 can be found from the output of the Gaussian filter when the detector samples the wave-form (Eq. 3.18) at interval T_s , i.e. the sample in the adjacent slot, which is given by:

$$Y_2 = y(T_s) = \frac{A}{\sqrt{2}} \cdot \exp \left[-\left(\frac{T_s}{t_w} \right)^2 \right] \quad (3.28)$$

Substituting Eq. 3.28 into 3.27 gives:

$$P_{fa} = \frac{1}{2} \operatorname{erfc} \left[\frac{v_{th} - \frac{A}{\sqrt{2}} \exp \left(-\left(\frac{T_s}{t_w} \right)^2 \right)}{\sigma\sqrt{2}} \right] \quad (3.29)$$

Or:

$$P_{fa} = \frac{1}{2} \operatorname{erfc} \left[\left\{ \alpha - \exp \left(-\left(\frac{T_s}{t_w} \right)^2 \right) \right\} \sqrt{\frac{\text{SNR}}{2}} \right] \quad (3.30)$$

As discussed in section 3.1, since the reference PCM rate is fixed at B bauds, the slot width T_s is not independent of the pulse width t_w . The optical receiver filter is band-limited to W Hz, and $t_w = \frac{1}{\pi W}$, so from Eq. 3.8, we get:

$$\frac{T_s}{t_w} = \frac{W \pi m \cdot \log_2 M}{B M} \quad (3.31)$$

$\frac{T_s}{T_w}$, from Eq. 3.31, can be substituted into Eq. 3.30 to find the value of $\frac{T_s}{T_w}$.

3.4.2.2- In other than adjacent slots: in the other slots (other than adjacent slots to the pulse slot), the probability designated here by P_{fb} , is given by the shaded area in Fig. 3.8c:

$$P_{fb} = \frac{1}{\sigma\sqrt{2\pi}} \int_{v_{th}}^{\infty} \exp\left(-\frac{v^2}{2\sigma^2}\right) dv \quad (3.32)$$

Solving Eq. 3.32, we have:

$$P_{fb} = \frac{1}{2} \left[1 - \operatorname{erf}\left(\frac{v_{th}}{\sigma\sqrt{2}}\right) \right] \quad (3.33)$$

Or:

$$P_{fb} = \frac{1}{2} \operatorname{erfc}\left[\alpha\sqrt{\frac{\operatorname{SNR}}{2}}\right] \quad (3.34)$$

3.4.3- Frame errors:

From the three types of error discussed above (P_m, P_{fa}, P_{fb}), if we consider the frame of $M+i$ slots as a whole then:

3.4.3.1- Probability of no detection error: P_1 , (error free case), is given by:

$$P_1 = (1 - P_m)(1 - P_{fa})^2(1 - P_{fb})^{k-3} \quad (3.35)$$

where $k=M+i$, and i is given in Eq. 3.6. For $M=16$, and $m=0.8$, P_1 versus SNR for different values of threshold voltage level, $\frac{\alpha}{\sqrt{2}}$, is shown in Fig. 3.9. Fig. 3.9a, is for $T_s = T_w$ (or $W/B=1.6$), and Fig. 3.9b is for $\frac{T_s}{T_w} = 2\pi$, (or $W/B=10$). It is clear from these graphs that the throughput of the system increases with the signal to noise ratio, the threshold level, and the bandwidth of the system. An optimum value of α for higher throughput is equal to 0.5, even when $\alpha=0.6$ we get higher throughput but the probability of an undetected error will be low.

3.4.3.2- Probability of an un-detected error: P_2 occurs when the proper pulse not detected, but one false-alarm pulse is detected:

$$P_2 = P_m [2P_{fa}(1 - P_{fa})(1 - P_{fb})^{k-3} + (k-3)P_{fb}(1 - P_{fa})^2(1 - P_{fb})^{k-4}] \quad (3.36)$$

P_2 versus SNR for different values of threshold voltage level is shown in Fig. 3.10, for $M=16$, and $m=0.8$. Fig. 3.10a is for $W/B=1.6$, while Fig. 3.10b is for $W/B=10$. It is clear from these graphs that, in a band-limited system, the probability of an undetected error increases with α because the probability of missing the pulse (or erasure error) increases, while for lower values of α the probability of false alarm increases. In wideband system, increasing the threshold level (for $\alpha > 0.3$) has very little effect on the probability of error because the dispersion is very low.

The probability of undetected error versus signal to noise ratio for different values of M is shown in Fig. 3.11. It is clear from Fig. 3.11 that the probability of an undetected error changes slightly with M , (around 0.5 dB for $SNR > 12$ dB).

Fig. 3.12 shows the probability of an undetected error versus signal to noise ratio for different values of the modulation index m . It is clear from the figure that the probability of an undetected error decreases when the value of m increases (around 1 dB for $\Delta m = 0.2$).

3.4.3.3- Probability of detected error: can be calculated by adding the following three cases;

1- When proper pulse detected, but at least one false-alarm pulse is detected:

$$P_3 = (1 - P_m) [1 - (1 - P_{fa})^2 (1 - P_{fb})^{k-3}] \quad (3.37)$$

2- When proper pulse not detected, and no false-alarm pulses are detected:

$$P_4 = P_m (1 - P_{fa})^2 (1 - P_{fb})^{k-3} \quad (3.38)$$

3- When proper pulse not detected, but more than one false-alarm pulse is detected:

$$P_5 = P_m [1 - (1 - P_{fa})^2 (1 - P_{fb})^{k-3}] \quad (3.39)$$

Then the probability of detected error P_6 is equal to:

$$P_6 = P_3 + P_4 + P_5 \quad (3.40)$$

The probability of the detected error P_e versus SNR for $M=16$, and $m=0.8$, is shown in Fig. 3.13, for different values of threshold voltage level. Fig. 3.13a is for $W/B=1.6$, while Fig. 3.13b is for $W/B=10$, (or $\frac{T_s}{T_c}=2\pi$). These graphs shows that the probability of detected error decreases with α , SNR and, the system bandwidth.

3.4.4- Comparison of analytical methods:

Next we compare the analysis done in this section to calculate the probability of error, with the already existing methods to analyze the performance of the PPM systems. We used in our analysis a very simple method on the frame basis for general PPM system, by examining each slot alone then considering the frame as a whole, to get broad feel for performance in network. The type of the detector chosen is a matched filter followed by a sampler and a comparator which is simple to realise in practice. GARRETT used a very complicated analysis for the special type of PIN-FET receiver using a whitened matched filter, over a slightly dispersive optical fiber channel. He derived analytical expressions for the receiver sensitivity of an optimised system limited by wrong slot errors and threshold violations (false-alarm errors). In his second paper, he derived an optimum filter (which is a combination of a whitened matched filter with a proportional derivative and delay network) for a channel with additive stationary noise by considering the effect of erasure errors. This complicated filter is difficult to realize in practice. [CALVERT] used this type of optimum receiver filter in an experimental PPM system and got an improvement of 4.2 dB over an equivalent binary PCM system.

Sensitivity improvement resulting from use of APD receivers in digital optical fiber PPM systems has been investigated by [PIRES].

According to our analysis; the advantages we can get in PPM systems over the conventional PCM systems is dependent on how much peak power we can get from the optical source at the transmitter. These results are similar to those obtained by [GARRETT] (see Figs. 3.10 to 3.13).

3.5-ERROR PROBABILITY OF PCM SYSTEM

To compare the error probabilities of PPM with the existing PCM systems we should calculate the error probabilities of PCM systems at the same conditions as calculated in section 3.4 for PPM system. We assume that the PCM receiver is similar to the one used for PPM signal, but with smaller bandwidth.

For PCM wave-form assume that the binary levels at the receiver are 0 and βA_c , where β is related to the responsivity of the photo-diode, and A_c is the peak optical amplitude in the receiver input. The received wave-form $x(t)$ at the receiver also contains additive noise $n(t)$. For equi-probable zeros and ones, the net probability of error, P_e , of PCM system is given by [STREMLER]:

$$P_e = \frac{1}{2}(P_{e0} + P_{e1}) \quad (3.41)$$

where P_{e0} is the probability of false-alarm when the receiver decides that the signal is present even though it is absent, and P_{e1} is the probability of false dismissal when the receiver decides that the signal is absent even though it is present (the probability density function P_v is similar to Fig. 3.8). The sum of these two areas (P_{e0} and P_{e1}) will be minimum if $v_{th} = \frac{\beta A_c}{2}$. By symmetry we can write:

$$P_e = \frac{1}{\sigma\sqrt{2\pi}} \int_{v_{th}}^{\infty} \exp\left(-\frac{v^2}{2\sigma^2}\right) dv \quad (3.42)$$

Solving of Eq. 3.42, yields:

$$P_e = \frac{1}{2} \left[1 - \operatorname{erf}\left(\frac{\beta A_c}{2\sigma\sqrt{2}}\right) \right] \quad (3.43)$$

To describe Eq. 3.43 as a function of signal to noise ratio, we assume that PCM system is operating under the same condition as PPM system described in section 3.4, so the signal to noise ratio of PCM system (SNR_c) (in (energy/bit)/(noise-power/Hz)) operating at a signalling rate

of B bauds and white noise spectral density of $\frac{N_o}{2}$ and bandwidth W, is given by [MARTIN]:

$$SNR_c = \frac{2\beta^2 A_c^2}{BN_o} \quad (3.44)$$

If the two systems, PPM and PCM, have the same signal to noise ratio at the detector, then from the Eqs. 3.25 and 3.44, we can write the ratio of the peak powers, for $\frac{T_s}{T_c} > 2$, as:

$$\left(\frac{A_p}{A_c}\right)^2 = \frac{W}{B} \cdot 2\sqrt{2\pi} \quad (3.45)$$

This condition approximately sets the two systems to have equivalent performance (see Fig. 3.10)

Comparing Eqs. 3.25 and 3.43, we can write Eq. 3.43 as follows:

$$P_e = \frac{1}{2} \left[1 - \operatorname{erf} \left(\frac{1}{2} \sqrt{SNR} \right) \right] \quad (3.46)$$

where SNR is the signal to noise ratio of PPM system. These assumptions are done to get right basis for comparison. The probability of error versus SNR for PCM system is shown in Fig. 3.10.

3.6-PPM VERSUS PCM

The probability of an un-detected error versus signal to noise ratio for PPM and PCM are shown in Figs. 3.10 and 3.11 respectively. These relations are derived for equal signal to noise ratio. We assumed in the analysis that the receivers are similar for PPM and PCM systems, but with different bandwidths. For band-limited filter ($W/B=1.6$) there is around 1 to 2 dB difference in SNR between them to give the same probability of error. In a fiber with higher bandwidth, $W/B=10$, this difference will be very small (less than 0.5 dB). It is clear from Fig. 3.10, that as α , the threshold level, increases beyond (0.3) the probability of an un-detected error decreases sharply for $SNR > 12$ dB. So any increase in PPM system transmitted peak power means increase in signal to noise ratio, or decrease in the error probability, and getting

an advantages over the PCM systems. The relation between the peak and the average power of the optical device, will be discussed in chapter 4.

3.7-SUMMARY

The characteristics of a PPM system are analysed and compared with the characteristics of an existing PCM system. A simplified analysis has been made to calculate the error performance of a PPM system, so that broad systems calculations may be made.

Choosing the threshold level (α) is important in the bandlimited system because of pulse dispersion. As the threshold level increases the probability of an un-detected error increases because the probability of missing the pulses increases. In the wideband system the threshold level variation has very little effect on the probability of an un-detected error because the dispersion in the pulse is very low.

The optimum value of α for a given W/B is determined by the probability of an undetected error and the throughput of the system. $\alpha=0.5$ is the optimum value for the bandlimited and the wideband systems analysed.

The modulation index variation has a little effect on the error performance of the system.

For $M=16$, $W/B=10$, and $P_2=10^{-9}$, the ratio of $\frac{A_2}{A_c}=5.35$, so to get an advantage of using PPM over PCM the ratio of the peak powers should be more than this value. At larger values of W/B, PPM peak power is proportional to W/B because the fiber dispersion is very low. When a wideband fiber is used and the received pulse is rectangular, under these conditions the adjacent-slot errors have no special preference, and the ratio $\left(\frac{A_2}{A_c}\right)^2$ is equal to $\frac{1}{T_B}$, in this case $\frac{A_2}{A_c}=5$ (for $T_p=50$ ns and, $B=4$ MHz, these data are obtained from chapter 8).

W/B is a better parameter to use in the analysis because most of the system parameters depends on the fiber bandwidth and the data rate and they are known to the designer.

It is clear from the analysis that, an improvement in receiver sensitivity is only possible if the PPM transmitter can work with the same mean power as for PCM. Real improvements are therefore possible, provided that the optical transmitter can deliver a greater peak power than in the PCM case.

3.8-REFERENCES

CALVERT, N. M., SIBLEY, M. J., and UNWIN, R. T., "Experimental optical fiber digital PPM system", Electronics letters, Vol. 24, No. 2, January 1988.

CLARKE, A. P., "Principles of digital data transmission", Pentech-Press 1976, Chapter 12.

GARRETT, I., "Pulse position modulation for transmission over optical fiber with direct or heterodyne detection," IEEE Trans. on Commun., Vol. COM-31, No. 4, April 1983, pp. 518-27.

MARTIN, J. D., "PPM for Local Area Networks", Proceedings "Fiber-Optics 89", SPIE, Vol. 1120, London, Apr. 1989, pp. 14-24.

MARTIN 89, J. D., "PPM compared with PCM", A draft paper.

PIRES, J. J., and DA ROCHA, J. R., "Digital PPM over optical fibers with avalanche photodiode receivers", IEE Proceedings, Vol. 133, Pt. J, No. 5, October 1986, pp. 309-13.

SENIOR, J., "Optical Fiber Communications: Principles and Practice", Prentice-Hall, 1985, pp. 544.

STREMLER, G. S., "Introduction to communication systems", Addison-Wesley Publishing Company, 1982, chapter 4.

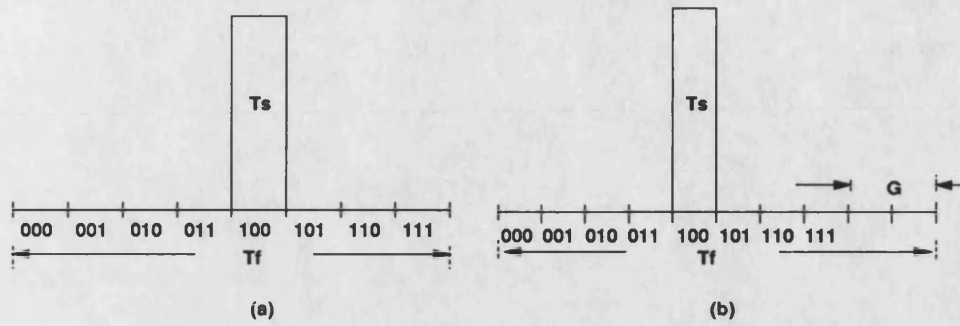


Figure 3.1 PPM signalling format

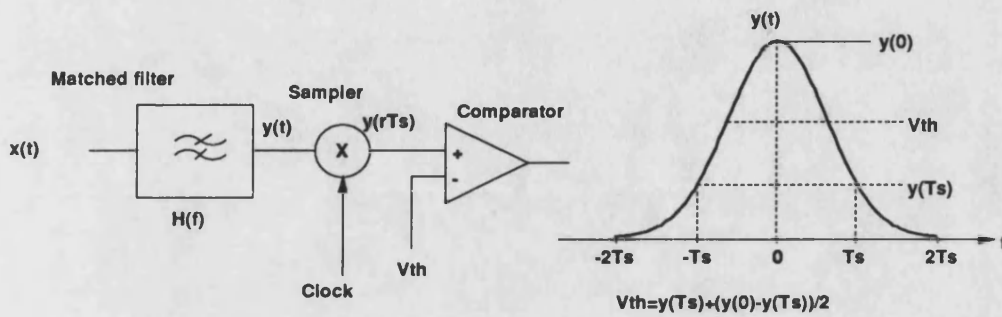


Figure 3.2 Matched-filter detector

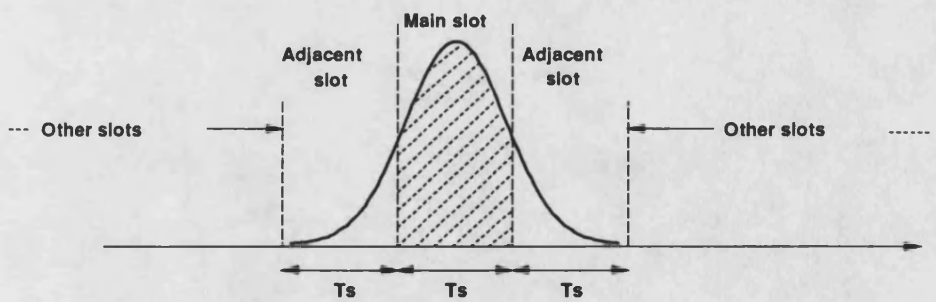


Figure 3.3 PPM pulse spreading

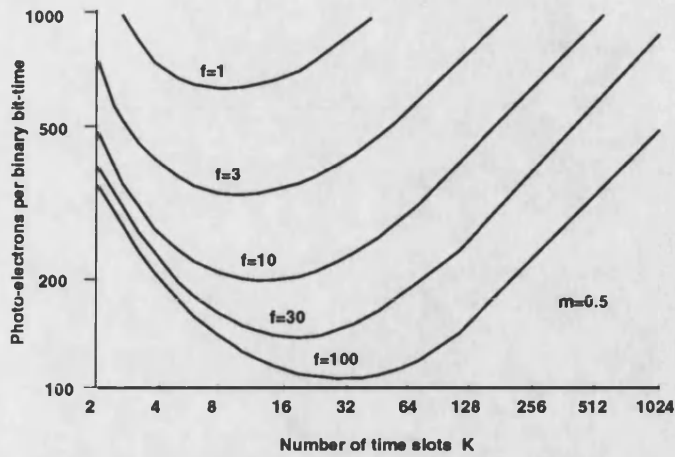


Figure 3.4 Optimum number of slots in a PPM frame [GARRETT]

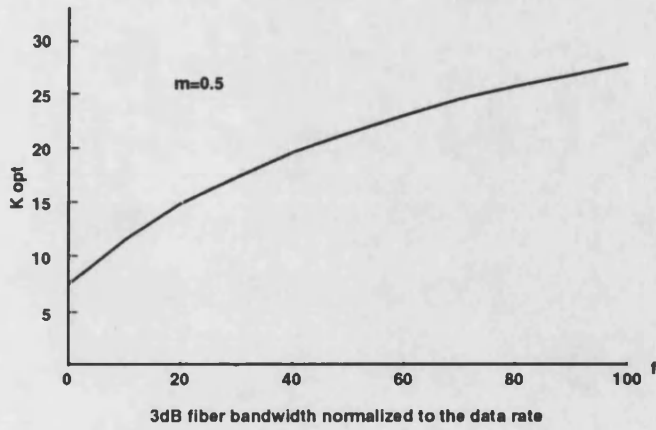


Figure 3.5 Relationship between optimum frame size and fiber bandwidth [GARRETT]

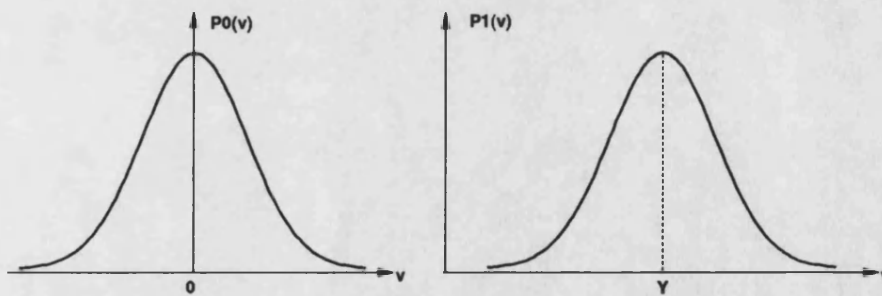


Figure 3.6 The Probability density function of the input signal

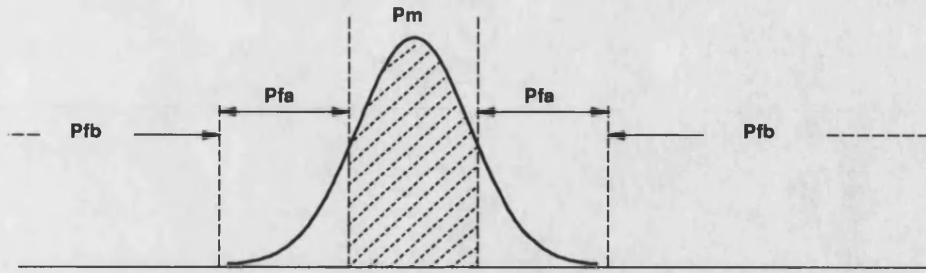


Figure 3.7 Error types in a PPM pulse

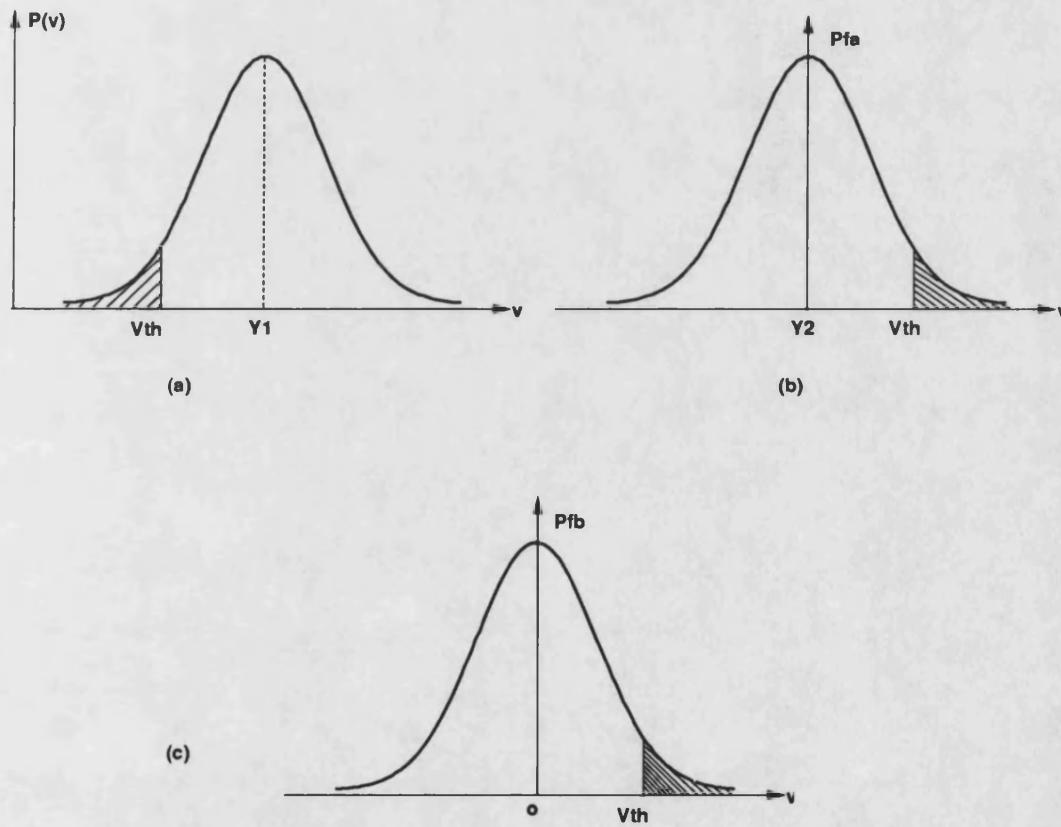


Figure 3.8 Probability density function of PPM error types

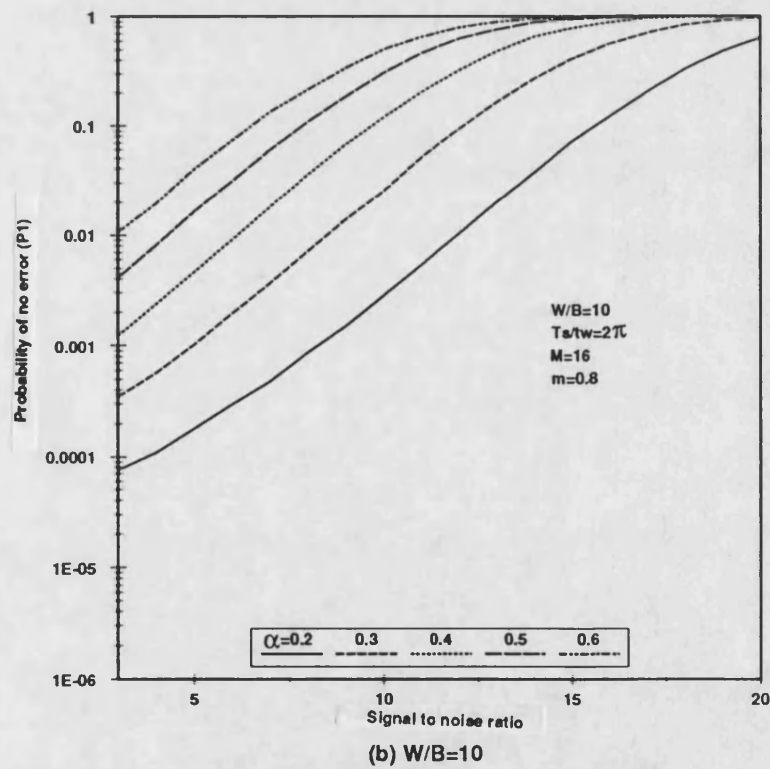
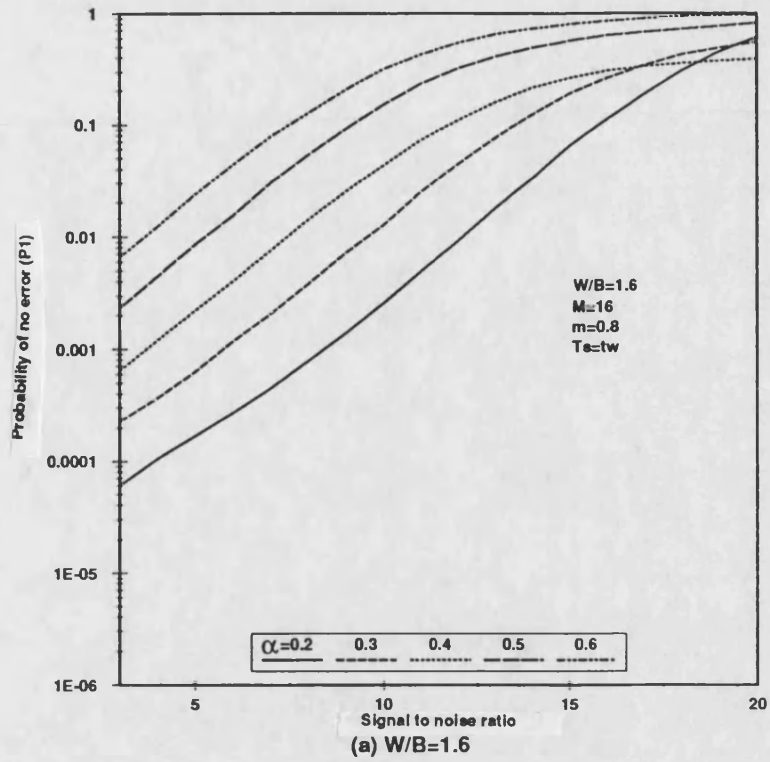


Figure 3.9 Probability of no error versus SNR

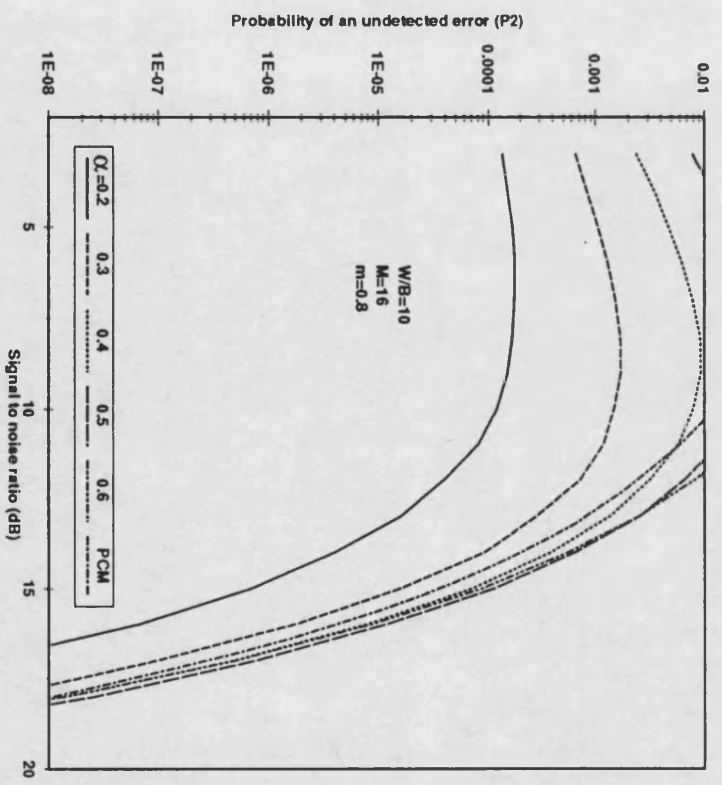
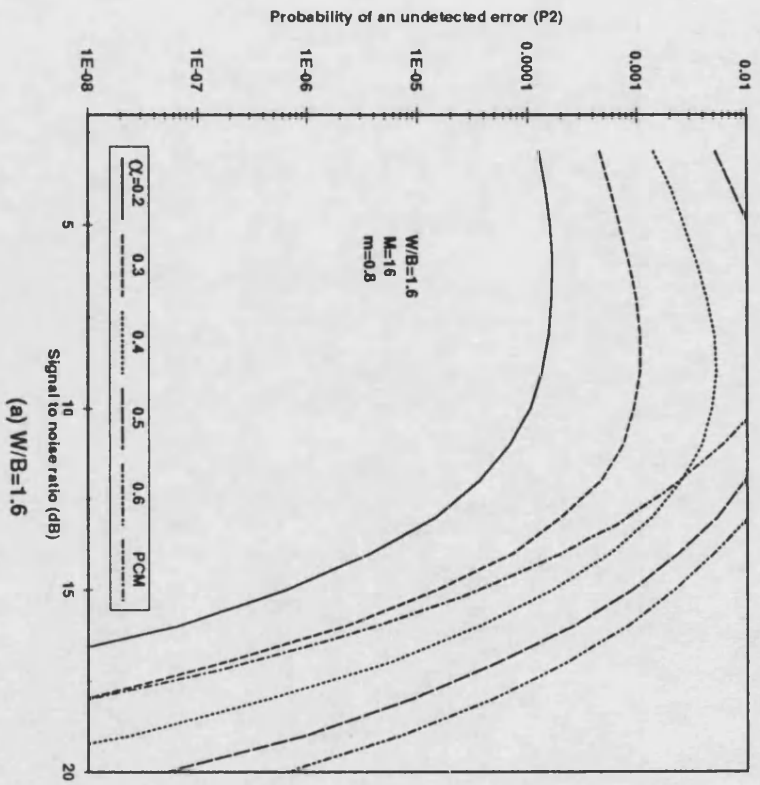


Figure 3.10 Probability of an undetected error versus SNR

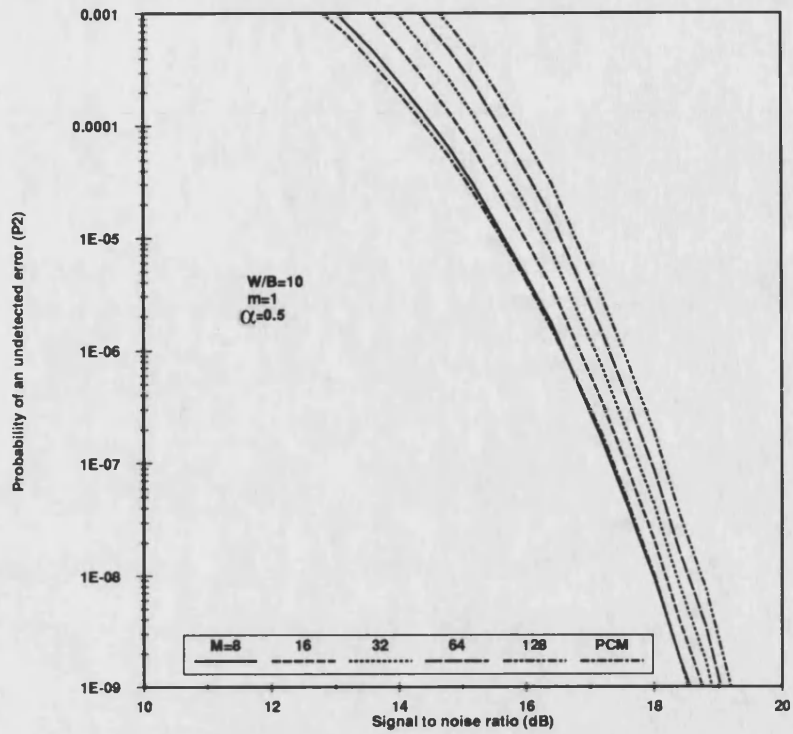


Figure 3.11 Probability of an undetected error versus SNR

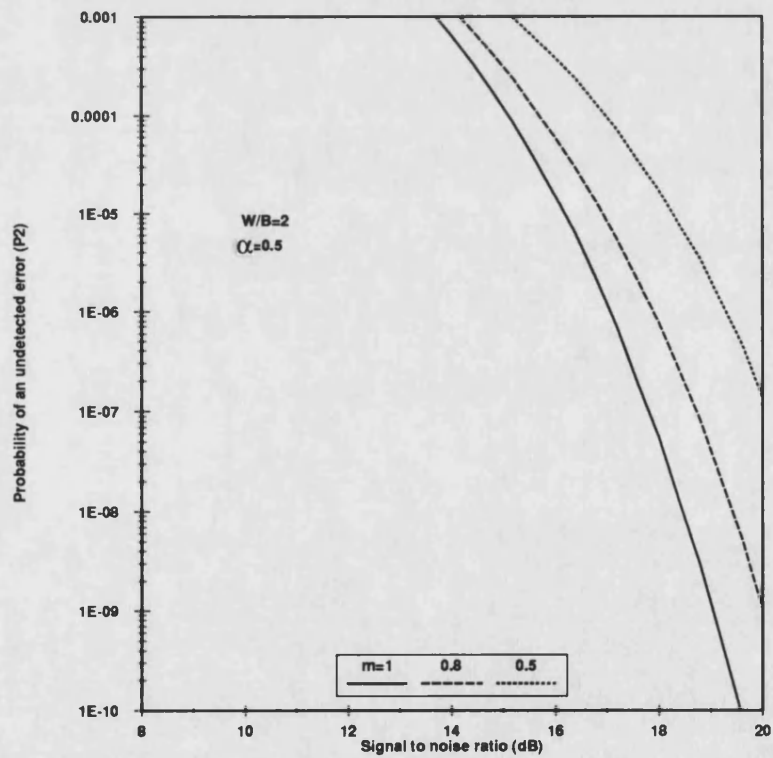
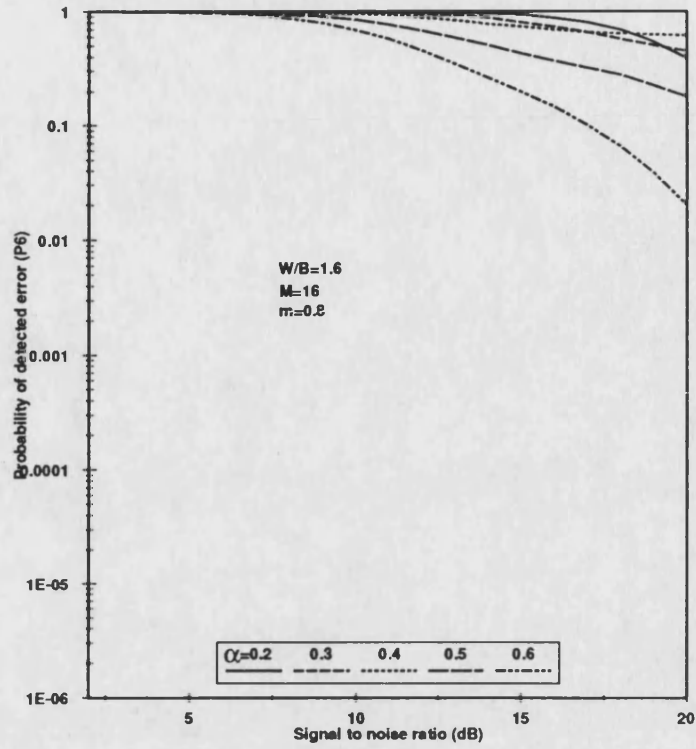
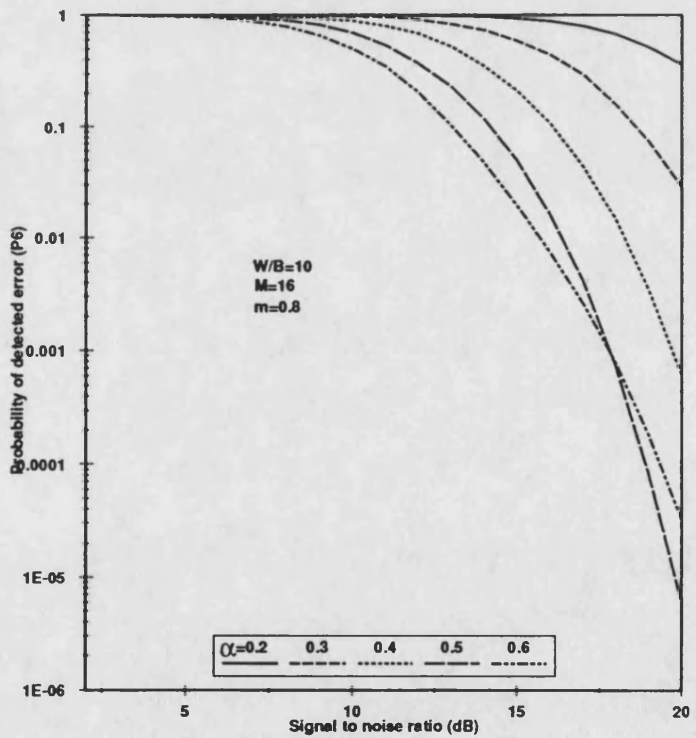


Figure 3.12 Probability of an undetected error versus SNR



(a) W/B=1.6



(b) W/B=10

Figure 3.13 Probability of detected error versus SNR

CHAPTER -4-

OPTICAL SOURCES FOR PPM SYSTEM

4.1-INTRODUCTION

An optical source is the direct link between the electrical and optical portions of the communication system input, providing the optical signal power to the fiber by modulation of its input current. Light emitting diodes and laser diodes form the sources for optical communication systems, their small size is compatible with the small diameter of a fiber, and their solid structure and low power requirements are compatible with modern solid-state electronics. Both devices have advantages and disadvantages and selection of one device over the other is determined by system requirements.

From the communication theoretical aspects, the advantage of PPM is enhanced by choosing a larger number of slots per frame, M . Thus, one of the main features of M -slot PPM is the requirement for higher peak to average power ratios of the transmitted light, which is attractive for fiber optic communications as the optical energy source (LD or LED) can be operated at a low duty-cycle, thus increasing the life time of the device. It may also be possible to overdrive the emitter for short periods, which will increase the power launched into the fiber, giving PPM an advantage over an existing PCM system and enabling greater distances between the repeaters.

This chapter will be in two parts. The first part will discuss the characteristics of a laser diode and its application to a PPM system, with practical results. In the second part LED characteristics are discussed, and practical results when measuring the characteristics of an ELED are given. In the last section of this chapter a comparison between LD and LED characteristics is given.

4.2-THE LASER DIODE

A laser diode is a small, rugged, coherent optical radiation source of high intensity which requires only a low supply voltage and which can be modulated directly at high speed. Literature concerning all aspects of laser diodes is available [SENIOR, KEISER, BARNOSKI], and this review is limited to the practical characteristics of a laser diode when used in an optical communication system, especially a PPM system.

The performance of a semiconductor laser is characterized by its static, dynamic, and spectral characteristics. Under operation an important role is played by the light-current (L-I) characteristic which describes the variation of the light output with the current applied to the semiconductor laser. The relationship between optical output power and drive current is shown in Fig. 4.1a. At low diode currents only spontaneous radiation is emitted, and both the spectral range and the lateral beam width of this emission are broad. A dramatic and sharply defined increase in power occurs at the lasing threshold. As this transition point is approached, the spectral range and the beam width both narrow with increasing drive current, the final spectral width of approximately 1 nm and the fully narrowed lateral beam width of nominally 5 to 10° being reached just past the threshold point. The threshold current is conventionally defined by extrapolation of the lasing region of the power-versus current curve. At high power outputs the slope of the curve decreases because of junction heating (see section 4.2.1).

The optical output power level is strongly dependent on temperature. The threshold current increases with the temperature in all types of semiconductor lasers because of various complex temperature-dependent factors [KEISER]. The temperature variation of the threshold current I_r can be approximated by the empirical expression [KEISER]:

$$I_r(T) = I_{r0} \exp \frac{T}{T_0} \quad (4.1)$$

where T_0 is a measure of the relative temperature insensitivity and I_{r0} is a constant. Fig. 4.1b shows, as an example, the L-I curves at different temperatures for a AlGaAs laser [BAKER]. From Eq. 4.1:

$$\ln I_r = \frac{T}{T_0} + \ln I_{r0} \quad (4.2)$$

By drawing a relation between $\ln I_r$ and T a straight line will be obtained, and from the slope of this line T_0 can be determined. The value of the threshold current at any temperature corresponding to a certain shift in T can then be predicted.

The laser diode is operated in one of three ways:

- (1) Continuously at some output power above threshold (CW).
- (2) Direct current biased to some value (usually near threshold) and then current modulated above that point.
- (3) Current modulation without bias (on/off modulation).

CW operation is the most severe condition for degradation experiments. Higher peak power values are attainable from a diode in pulsed operation, but the power-current curve is duty-cycle dependent because the increasing junction temperature changes the threshold current and differential quantum efficiency.

Laser reliability problems can be divided into two major parts: gradual degradation processes (relevant to normal CW operation) and catastrophic degradation processes (occurring at the high current limit of pulsed operation) [MONEMAR].

4.2.1-LIMITS TO LASER DIODE OUTPUT POWER

The maximum available optical power from a semiconductor laser is limited by catastrophic optical damage of the end mirror facets, which will reduce the facet reflectivity and thus increase the threshold current and reduce the differential quantum efficiency [ETTENBERG]. High optical power densities (several milliwatts per micrometer of emitting facet width) may damage the facets mechanically after a short

operating time. Power densities at the facets, in GaAlAs/GaAs lasers, can reach levels of 10^7 (W/cm^2) before failure occurs [HENRY].

The basic origin of catastrophic facet degradation process is uncertain, but it is known to be a function of the optical power density and of the pulse length. The power level at which catastrophic damage occurs in a given laser has been found to decrease with the square root of the pulse length under about 1 μs [KRESSEL, ELISEEV]. For substantially longer pulse lengths, CW operation may be assumed in so far as this damage process is concerned.

A detailed study of catastrophic degradation in double-hetrostructure (DH) laser material has been carried out by [HENRY], from which two conclusions are reached; First local melting occurs due to intense non-radiative recombination of minority carriers at a cleaved surface or at a defect, and the minority carriers are generated by absorbed superradiant light. Second, the dark line associated with catastrophic damage results from propagation of a molten zone confined to the active layer. [HENRY] added that catastrophic degradation is a process of thermal runaway, in which the surface is heated to the melting point by absorbed light, incident on the surface. Runaway can take place provided that the following conditions are met:

- (1) A substantial fraction of the incident light is absorbed and dissipated as heat at the surface, such that the surface is heated to melting point during the duration of the pulse.
- (2) The surface is sufficiently non-radiative that electron-hole recombination can take place fast enough to heat the surface to melting point.
- (3) Initially, the surface layer is sufficiently absorbing and the increase in superradiant light absorption with increasing temperature is sufficiently rapid, that the surface is able to switch from a weakly absorbing to a highly absorbing state in a time small compared with the pulse duration.

Most investigators find that the degradation rate increases with temperature, and the maximum power of a laser is restricted by saturation due to the increase of the junction temperature.

Continuous wave (CW) operation is the most severe condition for degradation experiments, and most experimental data are derived from CW life tests. A great deal of effort has been directed toward the development of high power emission of semiconductor lasers. GaAs-GaAlAs DH lasers are usually operated at a power density of around 0.5 mW/ μm , which corresponds to 5 mW per facet for stripe lasers with 10-15 μm stripe width [HARTMAN]. [CHINONE] has shown that the rate of degradation due to facet damage increases with the increase of power density. [NAMIZAKI] developed a new method of laser facet passivation, which operates at 4 mW/ μm power density (CW). 60 mW from the front facet of an AlGaAs/GaAs SBH laser is obtained in CW operation at room temperature in a junction-up configuration [TAKAHASHI]. [BOTEZ81] presented and discussed results of CDH AlGaAs diode lasers to record-high ambient temperatures for both CW and pulsed operation of lasers, and found that this laser can operate CW to 170 ° C and pulsed to 280 ° C. In $\text{Ga}_{1-x}\text{Al}_x\text{As}$ lasers, available optical output powers are restricted due to the catastrophic optical damage on the facet, or due to optical output saturation resulting from local heating [TODOROKI]. In this type of laser, the temperature rise will form the dark region, which is very nonradiative so that the electron-hole recombination in that region produces heat rather than light. [KAPPELER] has shown that in GaAlAs/GaAs oxide stripe lasers under high-pulsed-power conditions at a pulse width of 10 ns, the best samples delivered optical powers of more than 2 W per facet. The maximum available power was found to vary less than the inverse square root of the pulse width between 20 ns and 1 μs . [KIM] reported the highest peak power low-threshold DH AlGaAs/GaAs stripe laser diodes grown on Si substrates, which showed peak powers of up to 184 mW per facet, for room-temperature pulsed threshold currents as low as 150 mA. A summary of the principles which govern the operation of

major types of high power (CW) GaAlAs/GaAs and GaInAs/InP single mode lasers is provided by [FIGUEROA]. He discussed the concepts for high CW power operation and various methods for increasing the catastrophic intensity. He added that two factors contribute to a temperature rise in the active layer; conversion of a portion of the injected current in the active layer to heat and, ohmic heating in the top cladding and contact layers.

[TEMKIN] has studied catastrophic degradation in InGaAsP/InP DH material under intense optical excitation. The threshold power for catastrophic damage is about an order of magnitude larger in InGaAsP DH material than in AlGaAs DH material. [UEDA] has reported the observation of catastrophic degradation of InGaAsP lasers following a large current pulse. Generally, no facet degradation characteristic of melting at the active region (similar to AlGaAs lasers) is observed. This may be partly due to smaller surface recombination rate in InGaAsP compared to that of AlGaAs. In cases where facet degradation is seen, it extended from the top contact to the p-InP cladding layer, implying that heating was caused by a large amount of current passing near the facet. They suggest catastrophic degradation may be caused by local degradation of some internal region, which can result in large localized leakage current and subsequent melting. Pulsed output power of over 100 mW has been obtained from an InGaAsP SBH laser with active layer strip widths of 5 μm [NELSON], and output powers as high as 500 mW are observed without catastrophic damage. Total pulsed power of 1.4 W at 658 nm is obtained from AlGaInP graded-index separate confinement heterostructure visible laser [BOUR]. [KOBAYASHI] reported that for single-longitudinal-mode InGaAsP/InP DFB laser diodes, continuous operation is possible up to 140 ° C. High output power (103 mW CW) emission and high-temperature operation with a stable single longitudinal mode can be achieved as a result of asymmetrical facet reflection.

The characteristics of some of the diodes discussed above are summarized in table 4.1. From the results discussed above we conclude that the

laser diodes originally designed for CW operation is also well suited for applications where high peak power is required, as PPM. Up to 20 times of AlGaAs diodes rated power and, up to 50 times of InGaAsP rated power can be obtained without catastrophic optical damage if the pulse width is very small (less than 20 ns).

Laser type	λ (nm)	Max. CW power (mW)	Max. peak power (mW)	Author
InGaP/InAlP	649-651	27.5	105	ISHIKAWA
AlGaInP	658	--	1400	BOUR
(GaAl)As/GaAs	880	5	100	WOLF
AlGaAs	820-860	30	240	KRESSEL
GaAlAs/GaAs	880	--	2100	KAPPELER
GaAlAs/GaAs	880	25	400	BOTH
AlGaAs	870	40	100	BOTEZ
GaAs-GaAlAs	887-890	10	60	NAMIZAKI
AlGaAs/GaAs	--	--	184	KIM
AlGaAs	820	10	14	ETTENBERG
GaAlAs	830	20	--	TODOROKI
InGaAsP	1300	10	500	NELSON
InAsP/InP	1300	103	--	KOBAYASHI

Table 4.1 Laser diode characteristics

4.2.2-MAXIMUM OPTICAL POWER AS A FUNCTION OF PULSE WIDTH

As discussed in section 4.2.1, the power level at which catastrophic damage occurs in a given laser has been found to decrease with the square root of the pulse length for pulse lengths under about 1 μ s. The basic mechanisms responsible for catastrophic degradation are local heating caused by absorption of radiation near the surface and

non-radiative recombination of carriers at the facets. On the basis of these mechanisms a model has been developed by [KAPPELER] which relates the maximum optical power to the pulse width. The results of an experimental and theoretical investigation of GaAlAs/GaAs oxide stripe lasers under high-pulsed power conditions are given. Central to the theoretical model is the assumption that there is a critical temperature at which a facet is destroyed. The results of an experimental investigation by [KAPPELER] for pulse durations ranging between 10 ns and 1 μ s at a constant duty factor of 0.2% , are shown in Fig. 4.2. Fig. 4.3 shows the direct comparison between the experimental and theoretical results. The laser diode used in the experiment has CW optical power of 10 mW/facet.

In another experiment, [BOTH], studied catastrophic optical damage of mounted GaAlAs/GaAs DH laser diodes by measuring structure parameter influence. The study include the mirror protection measurement and an estimation considering the dependence of the laser characteristics on structure parameters. Damage power was measured against current pulse length for different wafers (Fig. 4.4). In single pulse experiments the output power obtained was 90 mW when the pulse length was 450 ns, and the power was 1 W for the pulse length of 23 ns. He added that the inner temperature rise leads to a decrease in optical power because of the threshold rise, but the damage power is the same.

From various experimental results, [KATZ], derived an approximate empirical formula for the upper limit on the peak available powers from semiconductor lasers set by the catastrophic degradation. The relationships between peak power (P_{PK}), pulse duration (T), and the CW power (P_{CW}) of AlGaAs lasers, according to [KATZ], are given as:

$$P_{PK} = \frac{A}{T^b} \quad , \quad T < T_{CW} \quad (4.3a)$$

$$= P_{CW} \quad , \quad T \geq T_{CW} \quad (4.3b)$$

where A is a proportionality constant, T_{CW} is a (constant) pulse duration beyond which the peak power limitation is basically the same as for CW operation, and (b) is a constant. Typical values derived from experimental results are $T_{CW} = 0.5$ to $5 \mu s$, and $b=0.5$.

At $T=T_{CW}$ we have:

$$P_{CW} = \frac{A}{T_{CW}^b} \quad (4.4)$$

Thus:

$$P_{PK} = P_{CW} \left(\frac{T_{CW}}{T} \right)^b, \quad T \leq T_{CW} \quad (4.5)$$

For a PPM signal with frame size M, [KATZ] defined a derating factor (B) as:

$$B = (T_{CW} R)^b (\log_2 M)^b M^{b-1}, \quad T \leq T_{CW} \quad (4.6a)$$

$$= \frac{1}{M}, \quad T > T_{CW} \quad (4.6b)$$

where R is the bit rate. The critical value of B is 1 for if $B > 1$, which is the area above the curve in Fig. 4.5, the laser does not impose any restrictions to the PPM signalling.

A fact also mentioned by [KATZ] is that InGaAsP lasers are not susceptible to catastrophic degradation phenomena so that they should be more suitable to PPM. Also their longer wave-lengths ($1.3-1.55 \mu m$) make them more attractive for optical fibers.

From the analysis done by KAPPELLER, BOTH and, KATZ, it seems that the application of AlGaAs laser diodes to digital PPM is possible up to $M=16$, and pulse width up to 50 ns, and the application of InGaAsP diodes is possible for higher values of M (~ 32), and pulse width up to 20 ns.

4.2.3-DETERMINATION OF LASER DIODE TEMPERATURE

In view of the theoretical work above, it is important to know the internal temperature of a laser diode under pulse conditions, to make sure that it is safe when currents are high. The performance of a

laser diode is influenced by a temperature rise within it which affects its properties. This effect is specially important during a pulse operation when relatively rapid temperature increase takes place. Thermal properties of a semiconductor laser are associated with the threshold current, the available output power, and the wavelength of oscillating modes, as well as the device reliability. The temperature rise inside the laser diode will increase the threshold current, hence, affecting strongly the operating characteristics and life time of the device. Measurement of this temperature cannot be carried out, so it must be estimated indirectly. To do this we need to know the static and dynamic thermal characteristics of the laser diode. In dynamic response we need to find the thermal step response, which can be obtained by measuring optical pulse droop caused by a shift of threshold current with increasing temperature (see Eq. 4.1). Hence, the shift of threshold current with temperature must first be measured, and the thermal rise time of the laser diode found from L-I characteristics at a fixed operating temperatures. The thermal resistance between the laser diode and the mounting block can be found from L-I characteristics when the diode is driven by a current pulse of amplitude more than the threshold current. These measurements will be carried out in the following sections.

4.2.4-PRACTICAL MEASUREMENTS

4.2.4.1-TEMPERATURE CONTROL

In this section the practical results of measuring the characteristics of the LD ML 4102 are examined in order to verify the theory above, and to see what performance can be obtained from an ordinary commercial laser diode. This diode, which is AlGaAs, emits light at around 780 nm wavelength, at a power of about 3 mW/facet with an operating current 10 mA in excess of the threshold current. The diode can operate, under CW or pulse conditions according to input current, at case temperature up to 60 °C. The overall block diagram of the experimental set up is

shown in Fig. 4.6. The diode is fixed in a copper block, and has a good thermal contact with it. To operate the diode at constant temperature, in order to achieve a constant radiant power, an active heat transfer is applied using a thermoelectric heat pump, utilising the Peltier effect. The rate at which heat is pumped is approximately proportional to the current applied [ABDELKADIR], and is reversible, thus allowing the temperature to be controlled both above and below ambient. The block diagram of the control circuit is also shown in Fig. 4.6, the temperature controller keeping the laser diode at constant temperature by monitoring the block temperature with a monolithic sensor.

The laser diode driving circuit (Fig. 4.7) drives the laser diode with flat-top current pulses which are produced by pulses at ECL levels, at the input of laser driving circuit. The value of the current pulse amplitude is measured using a current probe.

A lens collimates the laser beam on to the sensitive area of a photodetector, and the receiver used to measure the optical wave-form is shown in Fig. 4.8. It is calibrated so that (1) mV received waveform amplitude at the detector correspond to 43 μ W transmitted power.

If a current passes in the laser diode its temperature rises above the ambient temperature T_a , then the heat is transferred to the copper block by conduction and from the copper block to the air by radiation. Because of the heat capacity and thermal resistance of the copper block its temperature rises exponentially above the ambient till reaching the steady state [ABDELKADIR]:

$$T(t) = T_a + T_m [1 - \exp(-t/\tau)] \quad (4.7)$$

where $T(t)$ is the temperature of the copper block at time (t), T_m is the rise in temperature from ambient to steady state and, τ is the time constant of the copper block which depends on its thermal resistance and its heat capacity. If the input power to the block, P is known, then its thermal resistance, θ in $^{\circ}$ C/watt, can be determined:

$$\theta = \frac{T_m}{P} \quad (4.8)$$

To determine the rate of temperature rise of the laser diode ML 4102, and the thermal resistance and the thermal time constant of the copper block practically, the diode is driven with current near to the threshold ($I_r=38$ mA at 20°C , and its junction voltage drop $V=1.755$ V). When driven with current pulses of width 140 ns and duty cycle 27.4% just above threshold, the power dissipation in the laser diode is equal to $P=0.274 \times 1.755 \times 0.038=18.22$ mW. The duty cycle is then changed to be 23.3% and 18.9% which are equivalent to power dissipation of 15.5 mW and 12.6 mW respectively, in each case the rise in the temperature of the copper block has been recorded with time (Fig. 4.9). The figure indicates a rate of rise in temperature of up to $0.25^\circ\text{C}/\text{min}$, while the thermal resistance of the copper block to ambient, from Eq. 4.8, is equal to $165^\circ\text{C}/\text{W}$, and the thermal time constant, from Eq. 4.7, is ≥ 500 sec, (the real value for the time constant may be bigger than the measured one because we did not go far enough to the steady state). This long thermal time constant indicates that the rate of rise in the copper block temperature is very slow.

4.2.4.2-THERMAL RISE TIME OF LASER DIODE

The L-I characteristic of the diode at a certain temperature, has been measured by pulsing the diode with current pulses of width 140 ns and period 200 μs . The amplitude of the pulse and its corresponding optical response have been measured. This step has been repeated by changing the amplitude of the driving current pulses, and in each case the optical receiver pulse amplitude has been measured at the leading edge and the trailing edge of the pulse [ABDELKADIR]. This experiment has been carried out at block temperatures 18, 20, 22, 24, 26, 28, 30, and 32°C . In each case the average temperature of the laser diode has been kept constant during the measurement by the temperature controller.

Fig. 4.10 shows the L-I characteristics drawn at the leading edge of the pulse. The derived threshold currents are tabulated in table 4.2, where I_{tr} and I'_{tr} represent the values of threshold currents measured from the L-I characteristics at the leading and the trailing edges of the optical pulse respectively.

	Pulse period 200 μ m	
Temperature ($^{\circ}$ C)	I_{tr} (mA)	I'_{tr} (mA)
18	34.2	36.4
20	34.55	36.8
22	34.85	37.1
24	35.05	37.4
26	35.3	37.75
28	35.7	38.1
30	35.9	38.85

Table 4.2 The threshold currents measured from Fig. 4.10

From table 4.2 it is seen that I_{tr} and I'_{tr} increase with temperature. Also, $I'_{tr} > I_{tr}$ at the same operating temperature which indicates a shift in the threshold current value due to the increase in temperature of the laser chip with time during the pulse. To predict the threshold current at any temperature or the temperature rise correspond to a shift in the threshold current, Fig. 4.11 has been drawn from the results obtained in table 4.2, which represents the relation between $\log I_{tr}$ and temperature T (Eq. 4.2). The relation is straight line with slope equal to $1.69 \times 10^{-3} [^{\circ}\text{C}]^{-1}$, and from the slope T_0 can be determined which equals 256° C.

The average rise in temperature during the pulse duration of 140 ns is found to be $\Delta T = 16^{\circ}$ C. This rise in temperature is in the laser diode chip itself, since the monitoring block has a much greater time constant than the length of one pulse. The diode temperature reaches to within 5% of its final value in a time of 100 ns.

The thermal rise time of the laser diode can be found from L-I characteristics at an average operating temperature T . If the diode is driven by a current pulse of amplitude I , where $I > I_r$, heat is generated because of the increase of the current and the laser chip rises in temperature until reaching a steady-state, as a result the threshold current will increase and the optical pulse amplitude will decrease. If (L) is the maximum amplitude of the received optical pulse which corresponds to the lowest temperature of the laser diode during the pulse time at instant of time (t) , then after an interval of time Δt the temperature of the laser diode increases by ΔT and the received optical pulse amplitude decreases by ΔL . From Fig. 4.12 the slope efficiency of the stimulated emission part of the L-I characteristics is:

$$\eta = \frac{\Delta L}{\Delta I_r} \quad (4.9)$$

And:

$$\Delta T = T_s \log \left[1 + \frac{\Delta I_r}{I_r} \right] \quad (4.10)$$

By measuring η and ΔL the shift in the threshold current ΔI_r can be determined. Knowing $\log(I_r + \Delta I_r)$ and using Fig. 4.11, the rise in temperature ΔT which causes the shift in the threshold current can be determined. Similarly by determining ΔT at different instants of time, where Δt equals 20, 40, 60, 80, 100, 120 and 140 ns, a curve showing the rise in temperature of the laser diode versus time can be drawn from the data calculated (table 4.3). From Eq. 4.7:

$$t = -\tau \ln \left[1 - \frac{T(t) - T_s}{T_m} \right] \quad (4.11)$$

From table 4.3, a relation is drawn between t and $-\ln \left[1 - \frac{T(t) - T_s}{T_m} \right]$, (where T_m is equal to 16.3 °C) the resultant graph is the straight line shown in Fig. 4.13. The straight line confirms that thermal step response is exponential, and from the slope of this line the thermal rise time of the laser diode is $\tau = 34$ ns.

Time (ns)	ΔL (mV)	ΔI_r (mA)	$\log(\Delta I_r + I_r)$	Rise in Temp. ° C
20	5	0.8665	1.549	6.7
40	9	1.559	1.557	11.3
60	11	1.906	1.561	13.6
80	11.8	2.04	1.563	14.7
100	12.4	2.149	1.564	15.7
120	13	2.253	1.565	16.3
140	13	2.253	1.569	16.3

$I=38$ mA, Pulse width=140 ns, Pulse period=200 μ s
 $I_r=34.55$ mA, $\eta=13/2.25=5.77$ mV/mA, $T_s=20$ ° C

Table 4.3 The shift in threshold current values due to rise in temperature at different instants of time along the pulse

4.2.4.3-DYNAMIC THERMAL CONDITIONS IN THE LASER DIODE

To find the internal temperature of a laser diode under pulse conditions, its dynamic thermal characteristics need to be known. A model has been derived from the practical results for the temperature rise inside the LD chip. From the model the temperature of the device can be calculated for a given driving current and pulse duty-cycle. The model is analysed and applied practically. The laser diode is fixed in the copper block as shown in Fig. 4.14a. We assume that the laser diode temperature increases exponentially when the pulse is applied, and decreases when there is no pulse (Fig. 4.14b) but experimental evidence shows that the time constants are different. We assume that:

Laser diode mount (block) temperature = T_s , ° C.

Laser diode thermal rise time constant = τ , sec.

Power input to the laser $P=V.I$ (watt).

Laser diode to block thermal resistance $=\theta_1$ ° C/W.

Block to ambient thermal resistance $=\theta_2$ ° C/W.

Laser diode thermal fall time $=\tau_f$ sec.

Pulse width $=T_f$, Pulse period $=T_f$, and $T_f=MT_f$, i.e. PPM case with M-slots.

Assume that the block stays at constant temperature T_b , and that the diode commences one pulse cycle at temperature T_1 , rises to a maximum temperature of T_2 , and completes with temperature T_3 , then:

$$T_2 = T_1 + P\theta_1 \left[1 - \exp\left(-\frac{T_f}{\tau_f}\right) \right] \quad (4.12)$$

$$T_3 = (T_2 - T_b) \left[\exp\left(-\frac{(T_f - T_f)}{\tau_f}\right) \right] + T_b \quad (4.13)$$

Combining and writing $T_f=MT_f$, when $T_3=T_1$ for repeated pulses we get:

$$\frac{T_1 - T_b}{P\theta_1} = \frac{1 - \exp(-u_1)}{\exp(M-1)u_2 - 1} \quad (4.14)$$

And:

$$\begin{aligned} \frac{T_2 - T_b}{P\theta_1} &= \frac{(1 - \exp(-u_1))}{(\exp(M-1)u_2 - 1)} \exp(M-1)U_2 \\ &\approx 1 - \exp(-u_1) \quad M-1 > 10 \end{aligned} \quad (4.15)$$

where $u_1 = T_f/\tau_f$, and $u_2 = T_f/\tau_f$.

But the temperature of the mount is affected by the mean power input (P/M) to the laser diode, so the rise in T_b is:

$$\Delta T_b = \frac{P}{M} \theta_2 \quad (4.16)$$

The block temperature will become $(T_b + \Delta T_b)$. By using a cooling system we can control the block temperature.

In the measurements, we assumed that the observed reduction in the optical power because of temperature rise is due to T_1 and not T_2 , even in the practical measurements we got the same amount of reduction in the output power due to T_1 and T_2 .

In the analysis we assumed that the rising temperature time constant

is different than the time constant for falling temperature, because the thermal paths are different.

From section 4.2.4, the values of the assumed constants are; $\theta_2=0.16^\circ$ C/mW, $\theta_1=0.24^\circ$ C/mW, and $\tau_r=34$ ns. τ_r can be calculated using Eq. 4.14 as follows: for $M=5$, $T_r=10$ μ s, $T_i=20$ ns, $I=60$ mA, and $V=1.755$ V, $P=V.I.\theta_1=25.3^\circ$ C, and the reduction in the output power due to temperature rise is 7.2 mV (1mV reduction in the output power is equivalent to 1° C increase in the temperature), then from Eq. 4.14, $\tau_r=85$ ns. We assume that its value is constant even though it appears to change slightly with temperature.

Substituting for the values of the constants mentioned above in the Eqs. 4.14 and 4.15, the temperature rise of the laser diode can be calculated at any driving current and pulse duty-cycle. Fig. 4.15 shows the calculated results from the relation between T_2-T_i and M for constant values of the driving current and the pulse width. It is clear from the graph that when M is more than 15 the temperature rise is very low.

Fig. 4.16 shows the calculated results from the relation between T_1-T_i and M for constant values of the driving current and the pulse width, which indicates that at higher values of the pulse width the temperature rise is low, because τ_r will be comparable with T_r and τ_r when the pulse width is small. Fig. 4.17 shows the relation between ΔT_b and M for constant values of the driving current. The temperature of the block (the heat sink) decreases when M increases or the driving current decreases.

We conclude from the calculated results that the temperature rise of the laser diode increases with the driving current and the pulse width. To keep the temperature rise of the diode very low M should be more than 15, and the pulse width should be less than 20 ns.

Finally, two practical tests were conducted to verify this theory. For a constant value of the driving current (60 mA), Fig. 4.18 shows the relation between the measured received pulse amplitude (in mV) and M, for constant values of the mount temperature. This figure shows the

effect of varying the duty-cycle on the output power of the diode, and the reduction in the output power is due to the increase of the diode temperature during the application of the pulse. It is clear from the graph that for $M > 15$ the temperature effect on the output power is very small. The relation between the measured received output signal amplitude (in mV) and the pulse period, T_p , for constant values of pulse width and driving current, is shown in Fig. 4.19. It is clear from the figure that the temperature effect on the output power increases with the pulse width.

From Eq. 4.14, the reduction in the optical output signal due to temperature rise can be calculated for given values of M , and I . For example, when $M=5$, $I=100$ mA, and $T_p=20$ ns, the temperature rise $T_1 - T_b$ is equal to 11.9° C, which is equal to the value measured practically (see Fig. 4.19).

4.2.5-LASER DIODE TEST

Narrow pulse width, low duty-cycle L-I measurements were made on the device (pulse width was 20 ns, and pulse period was 200 μ s). The device was subjected to extremely large drive currents (up to 247 mA), and the power increase compared to the device rated level was 10 dB. Fig. 4.20 shows typical L-I measurement at different temperatures. The kink in the characteristics is due to this particular diode internal characteristics which we can not control. Fig. 4.21 shows the photograph of the optical output of the laser diode at 150 mA drive current and 25° C (the equivalent power is equal to 8.9 mW).

The temperatures T_1 and T_2 calculated for above operating condition; $I=247$ mA, $M=10000$, is $T_1 \approx T_b$, and $T_2 = T_b + 46.3$. For the same operating condition if we assume $M=16$, then $T_1 = T_b + 1.4$, and $T_2 = T_b + 47.7$. We conclude that for $M > 15$, the temperature effect is very low.

4.2.6-SUMMARY

The characteristics of the LD have been measured and analysed, especially when the device is driven with short current pulses, and low duty-cycle. It is clear from the results that it is possible to overdrive the device and to achieve high peak output power provided that the transmitted pulse width is short compared with the thermal time constant of the device. With drive currents of approximately 247 mA, more than 10 dB increase in the peak power over the device rated power was observed. The results indicate that this diode can be used for PPM in LANs. The temperature rise is negligible for $M > 15$, and about 8.2 dB increase in the diode peak power over the diode rated power. Many other devices of the same kind were tested and they gave similar results.

4.3-THE LIGHT EMITTING DIODE (LED)

4.3.1-INTRODUCTION

Light emitting diodes, are the most common fiber optic light sources, the two basic configurations being surface emitters and edge emitters. For the surface emitter, the light is emitted perpendicular to the grown layer. A well is etched into the substrate so that the fiber is positioned close to the light emitting region for maximum capture of the light by the fiber, and the emission from such a diode is essentially isotropic. The edge-emitting structure, in which the light is emitted along the plane of the epitaxially grown layer, is very similar to that of a laser, and so it emits a more directional light pattern than does a surface emitting LED, coupling light more efficiently into a fiber. The lasing action is generally suppressed by using a short cavity or by destroying the mirror facets using anti-reflection coatings or chemical etching [DIXON]. Surface-emitting and edge-emitting LEDs both emit several milliwatts of power at current densities in excess of 1000 A/cm^2 , with the maximum

current being limited by junction heating. Surface emitters generally radiate more power into air (2.5-3 times) than edge emitters since the emitted light is less affected by reabsorption and interfacial recombination. Comparisons [BOTEZ 79] have shown that edge emitters couple more optical power into low NA fibers (less than 0.3) than surface emitters (3.5-6 times), whereas the opposite is true for large NA fibers (greater than 0.3). Edge emitting LEDs are superior to surface emitting LEDs for optical data rates >20 Mbit/sec, while surface LEDs are preferable for short optical links with high NA fiber and data rates less than 20 Mbit/sec.

Optical fiber-systems using LED sources can provide reliable, inexpensive alternatives to laser-based systems. LEDs utilize relatively simple driving circuits without need for feedback to control output power, and they are capable of operating over a wide range of temperatures with projected device lifetimes one to two orders of magnitude longer than those of laser diodes made of the same material [MILLER].

LEDs operating in the region 0.8 to 0.9 μm (GaAlAs) generally have spectral widths of 20 to 50 nm, while LEDs emitting in the longer-wavelength region (InGaAsP emits near 1300 nm) have spectral widths of 50 to 100 nm. The increased spectral width of a longer wavelength emitter is compensated by the markedly reduced material dispersion in this region (see chapter 2).

In the next section the practical characteristics of LEDs when they are used for optical communication systems (specially for PPM) are discussed. The practical results of measuring the characteristics of ELED LH44-62 are then given.

4.3.2-OUTPUT POWER LIMITATIONS AND TEMPERATURE EFFECT

The output power of an LED increases linearly at first with the current, then saturates gradually. Several mechanisms have been proposed to explain this phenomena [SAUL, MILLER]. First the internal quantum

efficiency of a p-n junction LED device decreases exponentially with increasing temperature. Second, the internal conductivity of semiconductor compounds is an exponentially decreasing function of increasing temperature. Thus the maximum output is set by the junction temperature regardless of the size of the junction, but the temperature rise due to resistive heating from the driving current is very much dependent upon the structure. Another mechanism known as in-plane superluminescence which results from stimulated emission in the junction plane at high injection levels, has been postulated to account for the observed excessive radiance saturation of the surface emission. On the basis of this mechanism alone, saturation is expected to be strongly temperature dependent.

Another factor limiting the power output was revealed by the measurement of the diode current and carrier lifetimes as a function of injection level, which indicated that at high current density the nonradiative component increases with the square of injection level. At present it is not clear which mechanism dominates, and it is likely that more than one mechanism may be acting, the dominant ones being dependent on the details of the device structure and excitation conditions. However, in these devices optical gain (single pass gain) may be sufficient to compensate for the nonradiative losses resulting in a linear or super-linear behaviour of output power versus drive current [MILLER]. Fig. 4.22 depicts the relative output power versus current observed for typical surface emitters and edge emitters exhibiting various amounts of gain. Fig. 4.23 shows the reduction in output power with increased temperature for the devices depicted in Fig 4.22 [SAUL]. The output power of a surface emitter is quite stable, decreasing only about 1.5 dB as the device temperature is increased from room temperature to 75 ° C. For an edge emitter, the temperature sensitivity increases with the amount of gain but, in general, it is substantially less than for a laser (Fig. 4.23). Overall, an LED is expected to be less dependent on temperature than a LD.

4.3.3-PRACTICAL RESULTS (ELED 44-62)

ELED LH44-62 is an edge-emitting LED with single-mode fiber pigtail and is an unclassified manufacturer's sample device. Its peak spectral wavelength is 1295 nm, its rated CW power is 3 mW, and its typical spectral width is 90 nm. The driving circuit used for this ELED is shown in Fig. 4.24, which is simply an emitter follower circuit, enabling the driving current to be increased up to 1.6 A, with very low rise and fall times. The device is driven with very low duty-cycle pulses and the output optical power is measured using a Plessey P35-6661-0120, transimpedance opto-receiver with a bandwidth of 140 Mbit/s.

Narrow pulse width, low duty-cycle, high current, L-I measurements were made on the device, and a typical high current L-I characteristic is shown in Fig. 4.25. When the device is driven at ~500 mA, the increase in the peak power was approximately 10.5 dB compared with the 100 mA values (CW rate current for the device). When subjected to extremely large drive currents (up to 1.6 A), the increase in the peak power was approximately 17.9 dB compared to 100 mA level.

As mentioned in section 4.3.2, during application of a high current pulse to such a device, the junction temperature of the chip rises until it reaches a steady-state. The junction temperature of the device is minimised by keeping the drive current pulses as short as possible and by using a low duty-cycle pulse. The differential output between the leading and trailing edges of a pulse was measured for the device at a duty-cycle of 1:20 in order to observe the effect of an internal temperature rise. At a drive current of 200 mA, there was no change in output until the pulse width became greater than about 800 ns (Fig. 4.26), when the differential increased as expected. Fig. 4.27 shows how the relative change in light intensity varies with increasing drive currents for a 300 ns pulse. Investigations into the maximum duty-cycle of the pulse showed that at pulse widths of ~50 ns, the duty-cycle could be increased to 1:2 at drive currents of 200 mA and to 1:10 at 800 mA

before there was any significant differential output. Fig. 4.28 shows the relation between the received output power amplitude and the pulse duty-cycle for a 50 ns pulse.

From Figs. 4.26 and 4.27, it appears that the temperature differential for this particular device, is numerically dependent on the electrical pulse energy. The pulse energy ($\propto(I^2T_p)$) is constant, ($\approx 3.2 \times 10^{-5} \text{ (A}^2 \cdot \text{s)}$), for each case where the temperature differential just becomes discernible. If this criteria is applied to Fig. 4.25 where $T_p=40 \text{ ns}$, then the temperature rise inside the laser diode will be very low up to $\approx 900 \text{ mA}$.

It is clear from the results that it is possible to overdrive the device with low duty cycle pulses and to achieve high peak power without degradation.

4.3.4-SUMMARY

It is clear from the results that it is possible to overdrive the ELED device and achieve high peak output power provided the ELED is driven with short current pulses ($\sim 50 \text{ ns}$) at low duty cycle ($M > 8$). With a drive current of approximately 1.6 A, a 17.9 dB increase over the 100 mA CW output power has been observed. The temperature effect to the device is very low provided that the pulse width is kept short (20-50 ns) up to about 900 mA. The results indicate that the diode seems ideal for use in an optical LAN operating in a PPM mode, for example with a slot width of 30 ns and a frame width of 16 slots, the diode can be overdriven by an easily attainable drive current of 500-700 mA and produce a 12 dB enhancement of the system sensitivity. Many other ELEDs of the same kind with different powers were tested and they show the same results.

4.4-LD VERSUS LED

Fiber optic systems using LED sources provide reliable a less expensive alternative to laser-based systems. LEDs have certain advantages over injection laser diodes. LEDs traditionally have had a cost advantage over laser diodes, utilise relatively simple drive circuits and operate over a wide temperature range, especially in long wavelength devices where the laser threshold current increases rapidly with temperature. Drive currents are not similar; lasers require bias currents and large peak currents as compared to LEDs, which are the source of choice provided that adequate performance can be achieved. LEDs require the minimum of control circuitry, unlike laser diodes which require complicated feedback circuits.

One of the greatest advantages a laser has over an LED is at least one order of magnitude greater bandwidth, and the rise times of a good laser diode run between 0.1 and 1 ns. The disadvantages of LEDs are a broader spectral linewidth, and a smaller modulation bandwidth. Traditionally, LEDs have had a much smaller power output and lower fiber-coupling efficiency than lasers, however recent advances in high-radiance edge-emitting and superluminescent diodes have reduced these disadvantages.

The lifetime of ELEDs is longer than that of lasers, by about an order of magnitude since the operating conditions are less severe, and Lasers exhibit more effects that will cause failure. LEDs are not generally affected by catastrophic degradation mechanisms which severely affect lasers. However, they do exhibit gradual degradation which may take the form of a rapid degradation mode or a slow degradation mode, although is slower than for lasers [FUKUDA]. In system applications, the performance level of edge-emitting LEDs is between that of surface emitting LEDs and lasers.

It is possible to overdrive the LD and the LED and achieve high optical peak output power provided that the transmitted pulse width is short.

More than 10 dB increase in the LD ML 4102 peak power was observed practically. When the ELED LH44-62 was tested, the increase in its peak power was 17.9 dB over its rated power. The experiments showed that using the ELED is simpler than using the LD.

4.5-REFERENCES

- ABDELKADIR, H. I., "Electronic control of semiconductor laser for an optical fiber packet LAN", Ph.D. thesis, Elect. Eng. Dept., University of Bath, 1988.
- BAKER, D. G., "Fiber-optic design and applications", Prentice-Hall, Reston, 1985, chapter 3.
- BOTEZ 81, D., CONNOLLY, J. G., and GILBERT, D. B., "High-temp. CW and pulsed operation in constricted double heterojunction AlGaAs diode lasers", J. Appl. Phys. Letters, Vol. 39, July 1981, pp. 3-6.
- BOTEZ 79, D., and ETTENBURG, M., "Comparison of surface and edge emitting LEDs for use in fiber-optical communications", IEEE Trans. Electron. Devices, ED-26(3), 1979, pp. 1230-38.
- BOTH, W., ERBERT, G., KLEHR, A., RIMPLER, R., STADERMANN, G., and ZEIMER, U., "Catastrophic optical damage in GaAlAs/GaAs laser diodes", IEE Proc., Vol. 134, Part J, February 1987, pp. 95-103.
- BOUR, D. P., and SHEALY, J. R., "High-power (1.4 W) AlGaInP graded-index separate confinement heterostructure visible ($\lambda=658nm$) laser", Appl. Phys. Letters, Vol. 51, November 1987, pp. 1658-60.
- CHINONE N., NAKASHIMA, H., and ITO, R., "Long-term degradation of GaAs-Ga_{1-x}Al_xAs DH lasers due to facet erosion" J. Appl. Phys., Vol. 48, 1977, pp. 1160.
- DIXON, W., and DUTTA, N. K., "Lightwave device technology", AT&T Technical Journal, Vol. 66, Issue 1, January/February 1987, pp. 73-83.
- ELISEEV, P. G., "Semiconductor light emitters and detectors", A. Frova, Ed., Amsterdam: North-Holland, J. Luminescence, Vol. 7, 1973, pp. 338-356.

ETTENBERG, M., and KRESSEL, H., "The reliability of (AlGa)As CW laser diodes", IEEE J. of Quantum Elect., Vol. QE-16, Feb. 1980, pp. 186-195.

FIGUEROA, L., "High power semiconductor lasers", Proc. SPIE Int. Soc. Opt. Eng. (USA), Vol. 723, 1987, pp. 2-24.

FUKUDA, M., "Laser and LED reliability update", J. Lightwave Tech., Vol. LWT-6, No. 10, October 1988, pp. 1488-95.

HARTMAN, R. L., SCHUMAKER, N. E., and DIXON, R. W., "Continuously operated (Al,Ga)As DH lasers with 70 °C lifetimes as long as two years", Apply Physics Letters, Vol. 31, 1977, pp. 756.

HENRY, C. H., PETROFF, P. M., LOGAN, R. A., and MERRITT, F. R., "Catastrophic damage of $Al_xGa_{1-x}As$ double heterostructure material", J. Appl. Phys., Vol. 50, May 1979, pp. 3722-3732.

KAPPELER, F., METTLER, K., and ZSCHAUER, K., "Pulsed-power performance and stability of 880 nm GaAlAs/GaAs oxide-stripe lasers", IEE Proc., Vol. 129, Pt. I., Dec. 1982, pp. 256-261.

KATZ, J., "Average power constraints in AlGaAs semiconductor lasers under PPM conditions", Optics Communications, Vol. 56, No. 5, January 1986, pp. 330-333.

KEISER, G., "Optical fiber communications", McGraw-Hill, 1985, pp. 94.

KIM J., NOUHI, A., RADHAKRISHNAN, G., LIU, J., LANG, R., and KATZ, J., "High-peak-power low threshold AlGaAs/GaAs stripe laser diodes on Si substrates grown by migration-enhanced molecular beam epitaxy", Appl. Phys. Letters, Vol. 53, No. 14, October 1988, pp. 1248-1250.

KOBAYASHI, K., and MITO, I., "High output-power single longitudinal-mode semiconductor laser diodes", IEEE J. Lightwave Tech., Vol. LT-3, Dec. 1985, pp. 1202-10.

KRESSEL, H. LADANY, I., ETTENBERG, M., and LOCKWOOD, H. F., "Reliable semiconductor light sources for fiber optical communications", in Tech. Dig. Int. Electron. Devices Meeting, Washington DC, December 1975, pp. 477-479.

MILLER, S. E., and KAMINOW, I. P., "Optical fiber telecommunications II", Academic Press, 1988, Chapter 12.

MONEMAR, B., "Degradation processes in semiconductor lasers", *Physica Scripta*. (SWEDEN), Vol. 24, Aug. 1981, pp. 367-74.

NAMIZAKI, H., TAKAMIYA, S., ISHII, M., and SUSAKI, W., "High-power density single-mode operation of GaAs-GaAlAs TJS lasers utilizing Si_3N_4 plasma deposition for facet coating", *J. Appl. Phys.*, Vol. 50, May 1979, pp. 3743-45.

NELSON, R. J., WRIGHT, P. D., BARNES, P. A., BROWN, R. L., CELLA, T., and SOBERS, R. G., "High output power InGaAsP ($\lambda=1.3\mu m$) strip-buried heterostructure lasers", *J. Appl. Phys. Letters*, Vol. 36, March 1980, pp. 358-360.

SAUL, R. H., "Recent advances in the performance and reliability of InGaAsP LEDs for lightwave communication systems", *IEEE Trans. on Electron Devices*, Vol. ED-30, No. 4, April 1983, pp. 285-295.

SENIOR, J. M., "Optical fiber communications: principles and practice", Prentice-Hall 1985, Chapter 7.

TAKAHASHI, K., IKEDA, K., OSHSAWA, J., and SUSAKI, W., "High efficiency and high power AlGaAs/GaAs laser", *IEE J. Quantum Electronics*, Vol. QE-19, June 1983, pp. 1002-8.

TEMKIN, H., MAHAJAN, S., DIGIUSEPPE, M., and DENTAI, A., "Optically induced catastrophic degradation in InGaAsP/InP layers", *Appl. Phys. Lett.*, Vol. 40, April 1982, pp. 562-5,

UEDA, O., IMAI, H., YAMAGUCHI, A., KOMIYA, S., UMEBU, I., and KOTANI, T., "Mechanism of catastrophic degradation in 1.3 μm V-grooved substrate buried-heterostructure lasers with the application of large pulsed currents", *J. Appl. Phys.*, Vol. 55, February 1984, pp. 665-9.

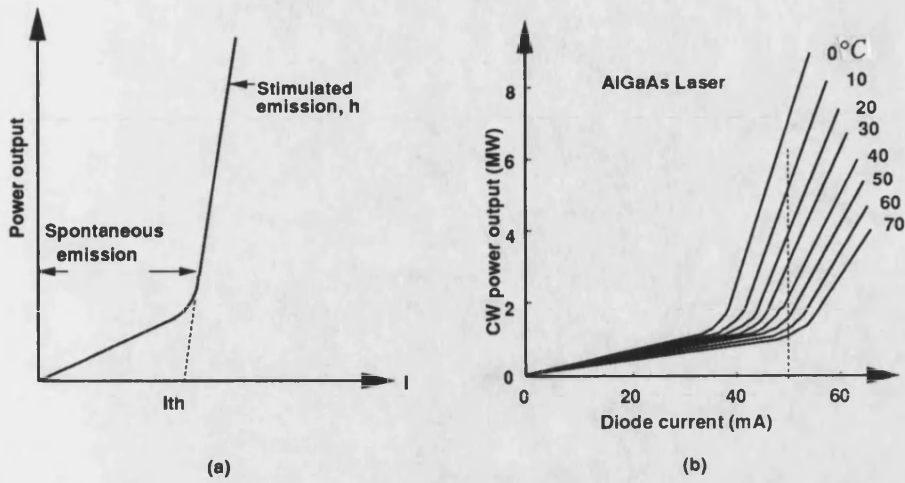


Figure 4.1 (a) laser diode characteristics,
 (b) temperature effect [BAKER]

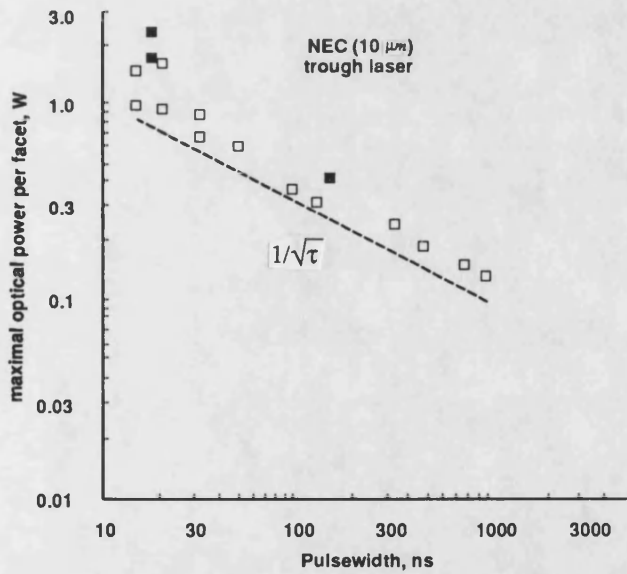


Figure 4.2 Maximum optical power against pulsewidth
 for oxide-stripe lasers. Duty factor=0.2%, $T_{case}=25^\circ\text{C}$
 [KAPPELER] Limits of catastrophic degradation for

- best lasers
- average lasers

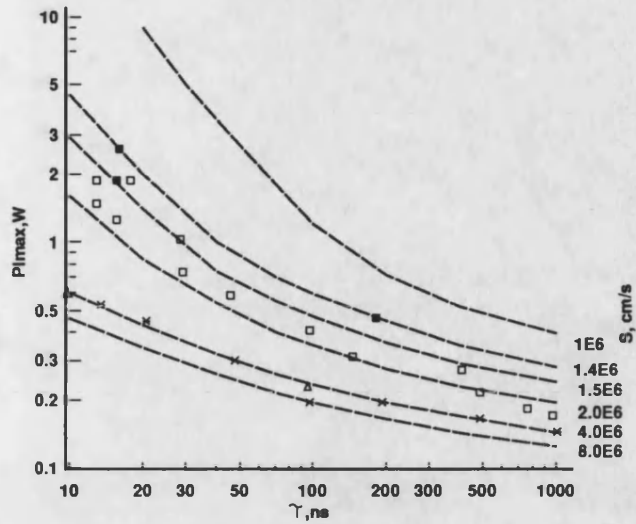


Figure 4.3 Measured and calculated optical power P_{max} against pulsewidth for lasers with differently prepared mirrors [KAPPELER]

- best
- average lasers, 300 V-sputtered, AL₂O₃ coated
- × lasers with 1 kV-sputtered mirrors
- △ uncoated lasers
- calculated with $B=0.12 \text{ cm}^3/\text{Ws}$, $C=3.1\text{E-}7 \text{ cm}^2/\text{W}$

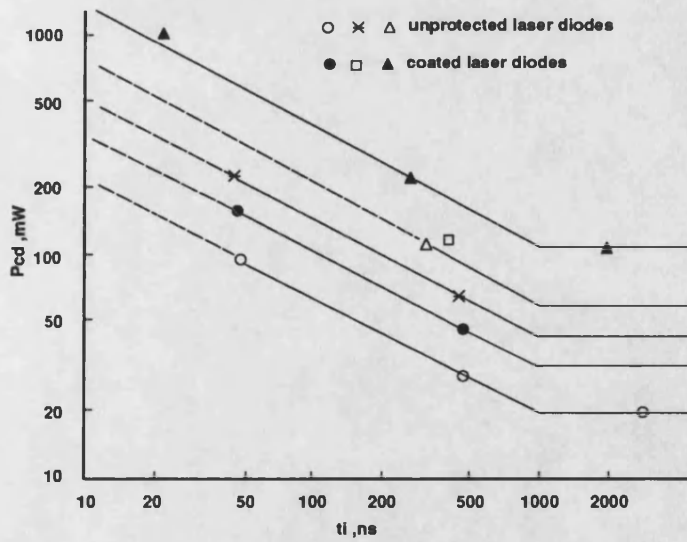


Figure 4.4 Measured damage power against current pulse length of different wafers [BOTH]

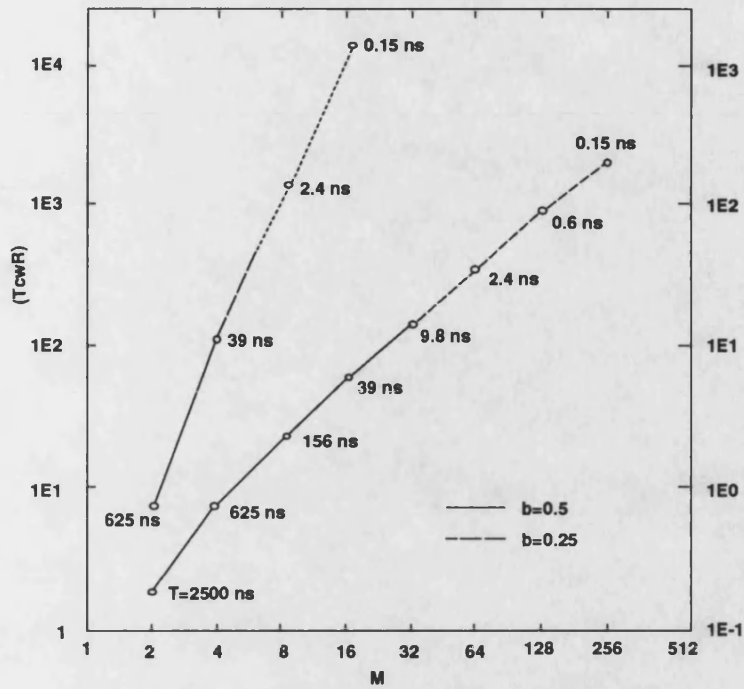


Figure 4.5 Data-rate versus M for B(M)-1. (B(M)=1 means that no degradation in the average power occurs) [KATZ].

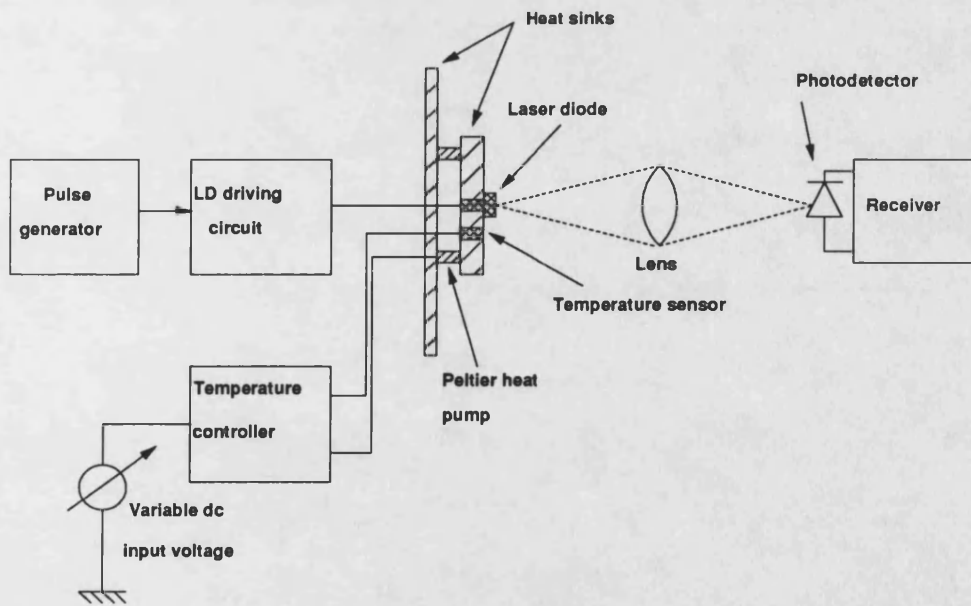


Figure 4.6 Practical measurement set-up for laser diode

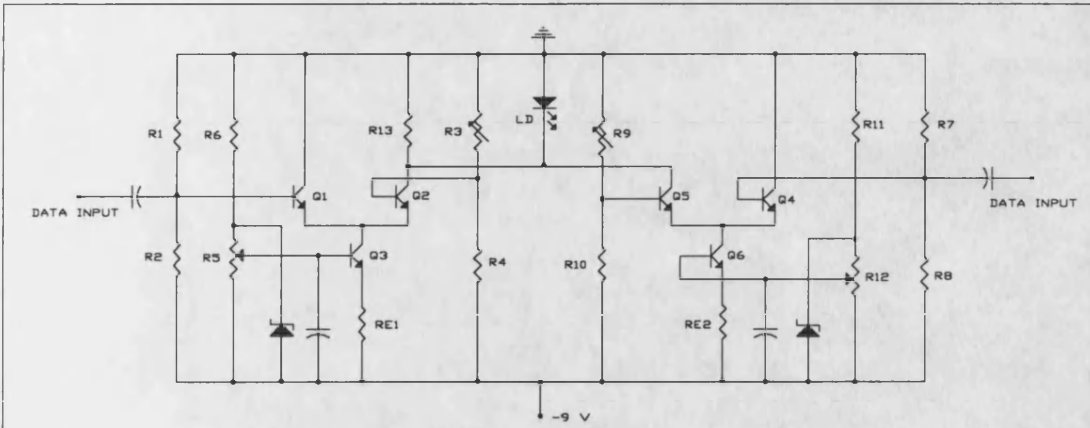


Figure 4.7 Laser diode drive circuit

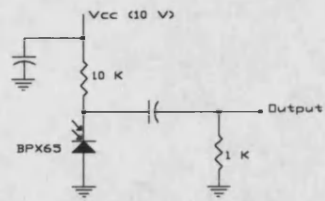


Figure 4.8 Receiver circuit diagram

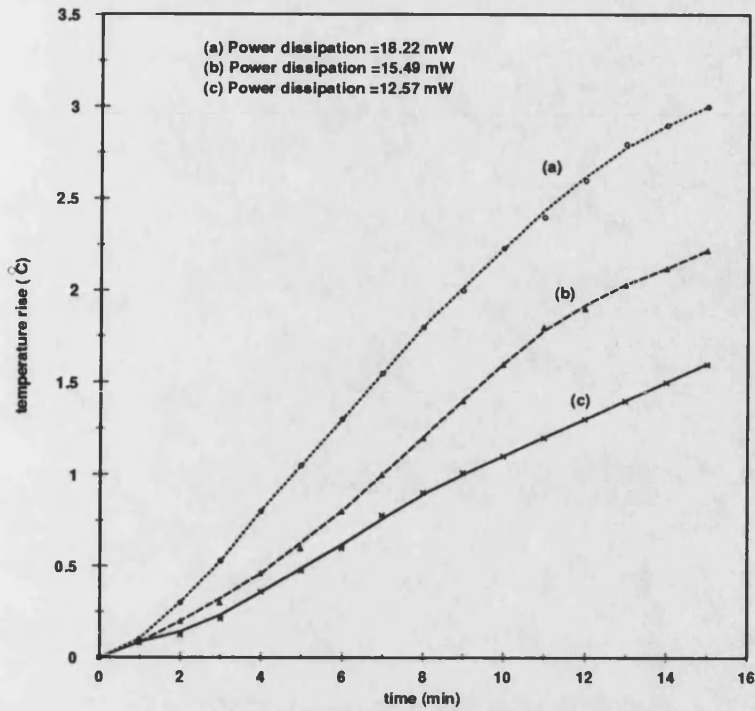


Figure 4.9 Relation between the time and the rise in temperature

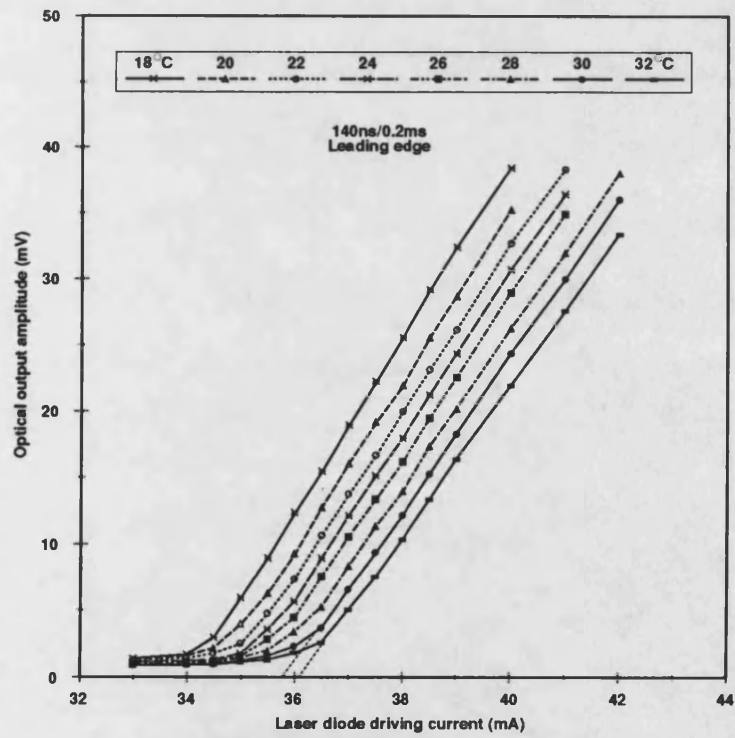


Figure 4.10 Laser diode characteristics

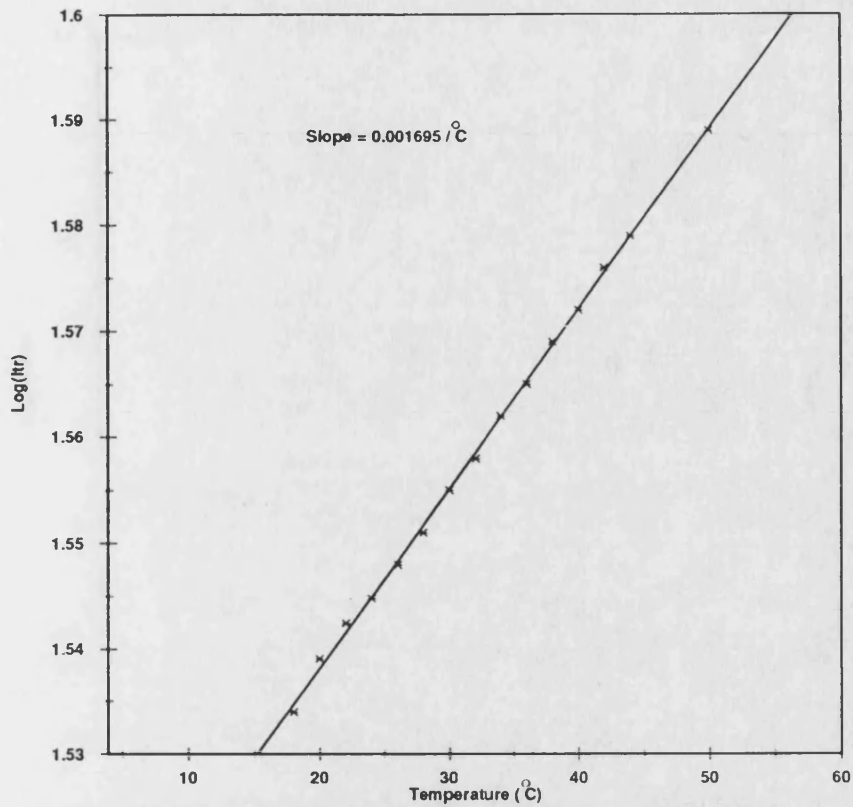


Figure 4.11 The relation between $\log(I_{tr})$ and temperature

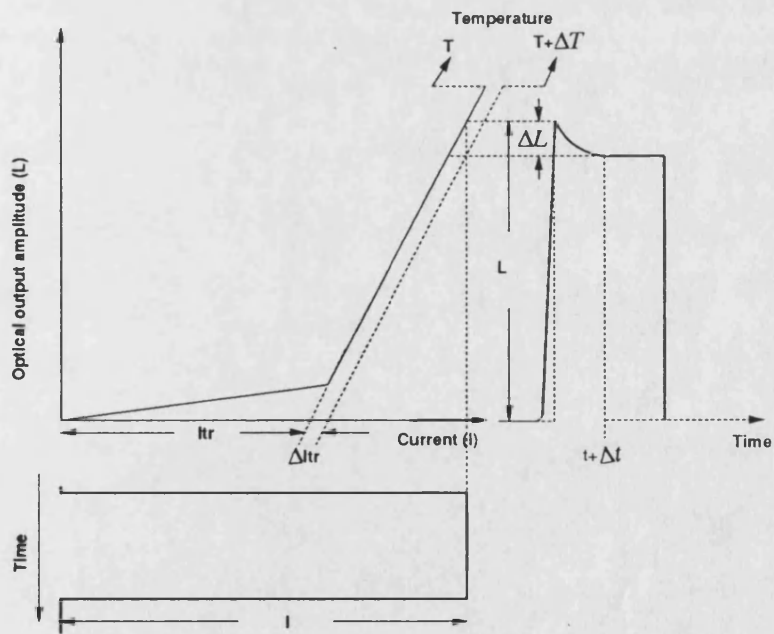


Figure 4.12 Threshold current variation with temperature

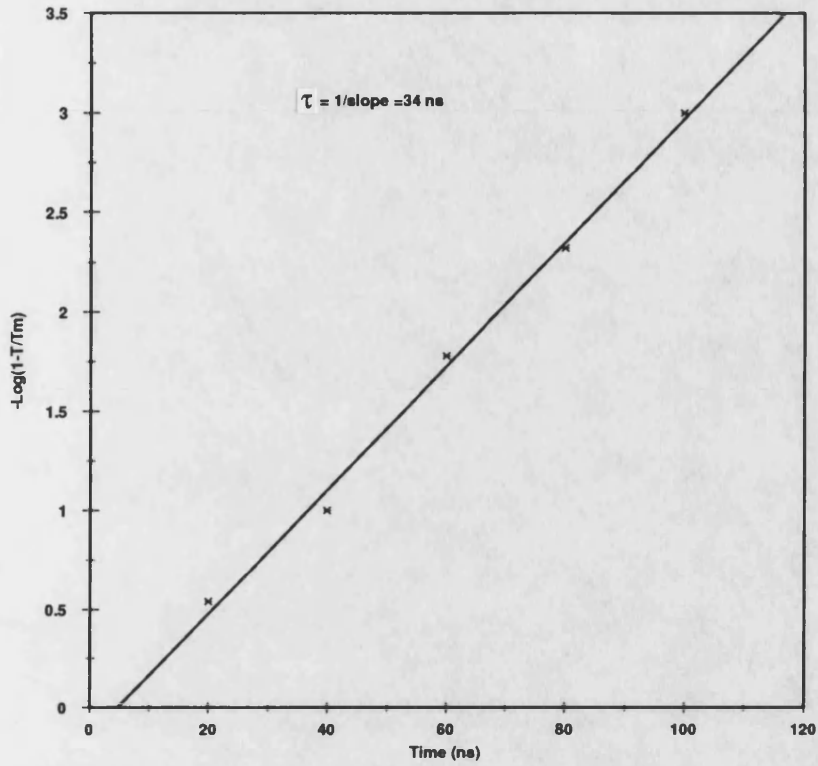


Figure 4.13 The relation between the time and $-\log[1-T/T_m]$

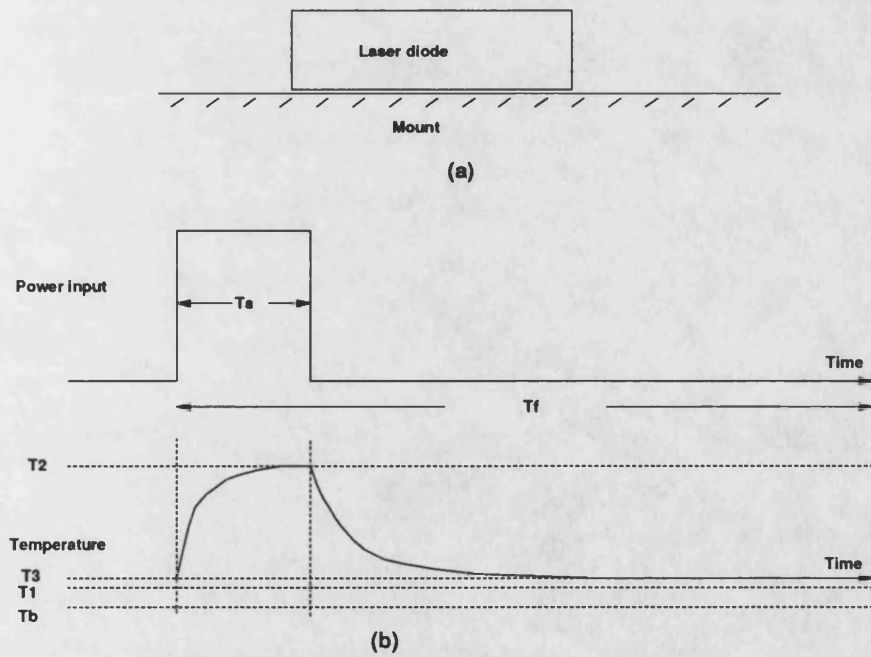


Figure 4.14 Laser diode temperature increase

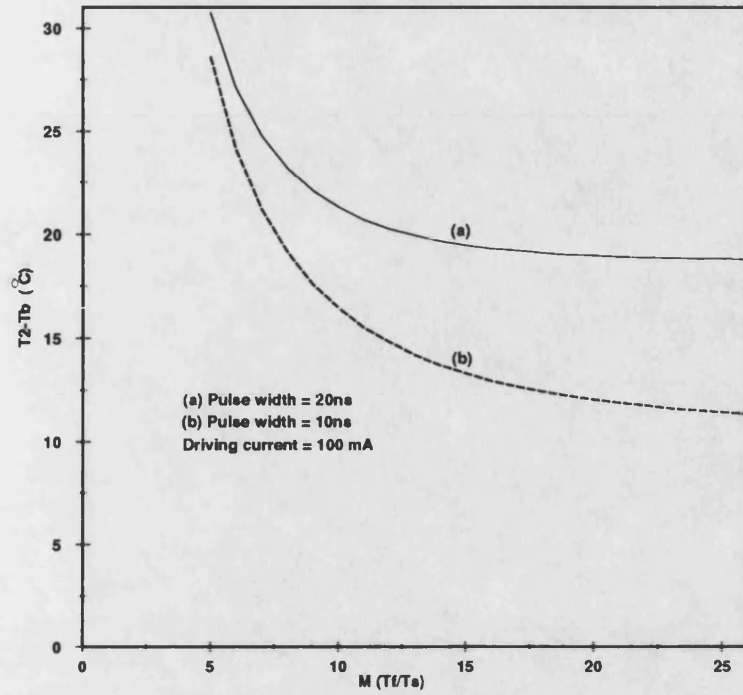


Figure 4.15 The temperature rise of the laser diode versus M

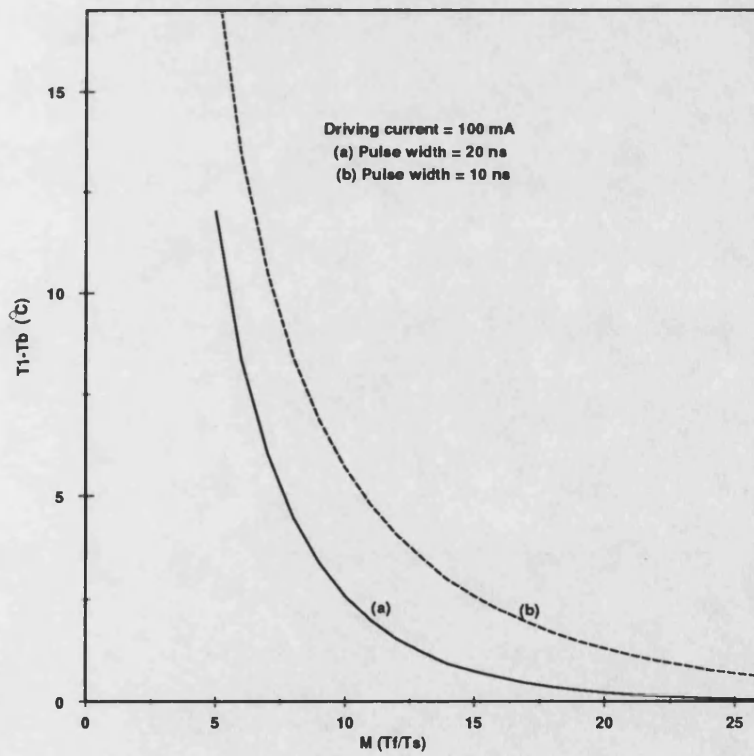


Figure 4.16 The temperature rise of the laser diode versus M

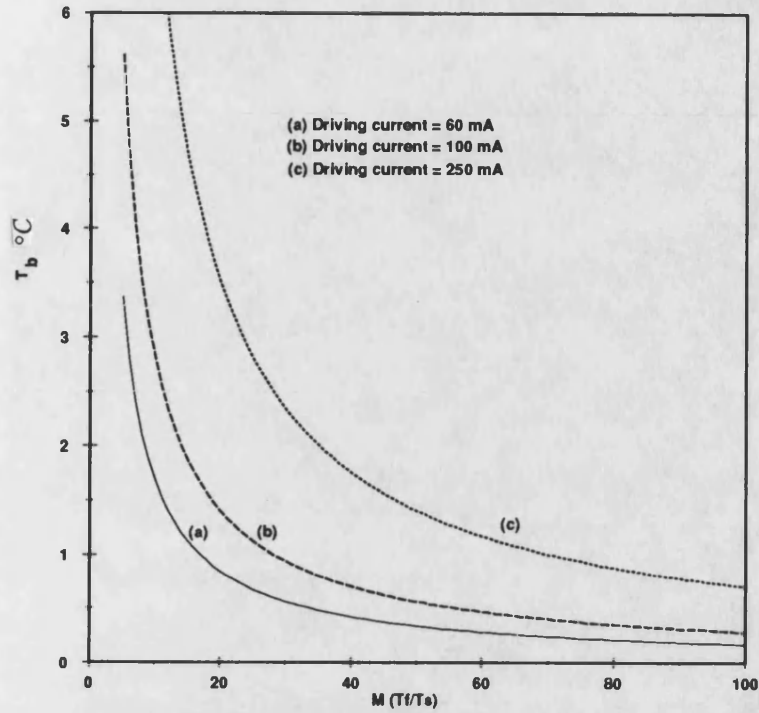


Figure 4.17 Block temperature rise

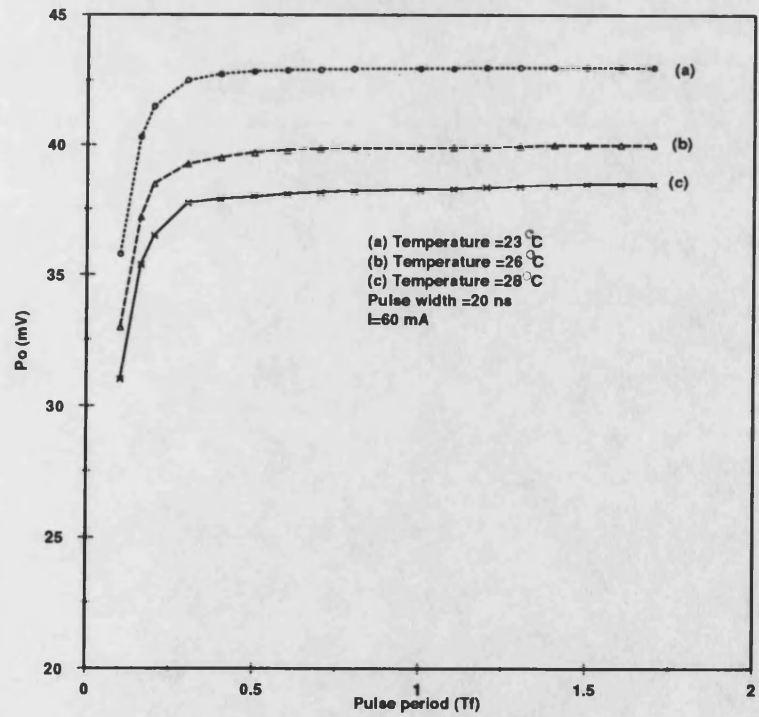


Figure 4.18 The measured received pulse amplitude versus pulse period

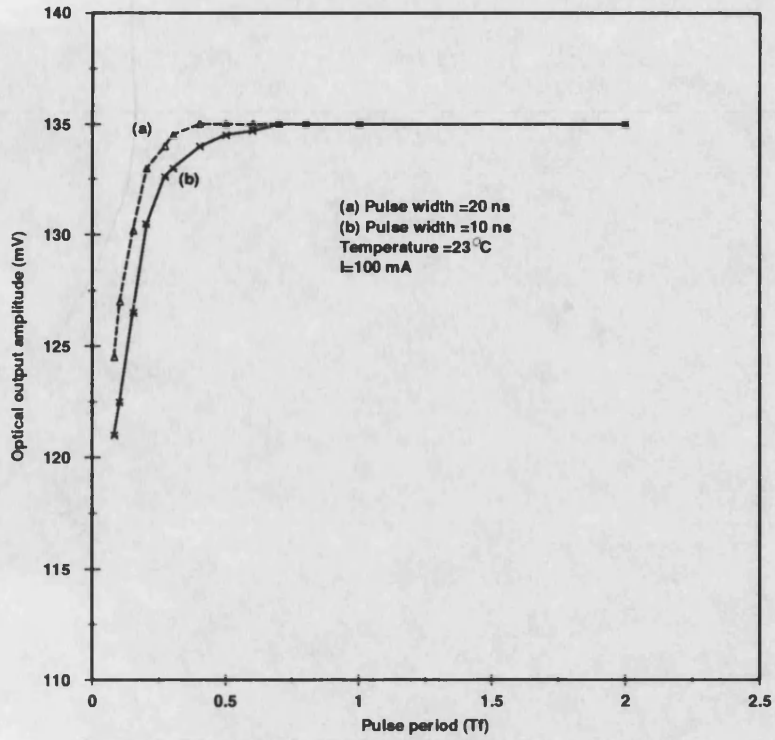


Figure 4.19 Received signal amplitude versus pulse period

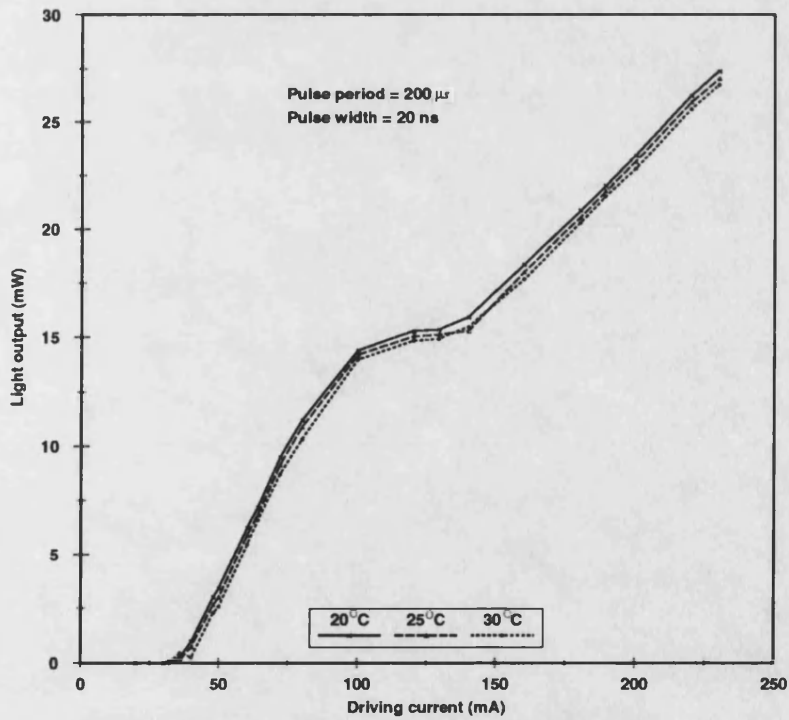


Figure 4.20 Optical output power versus driving current

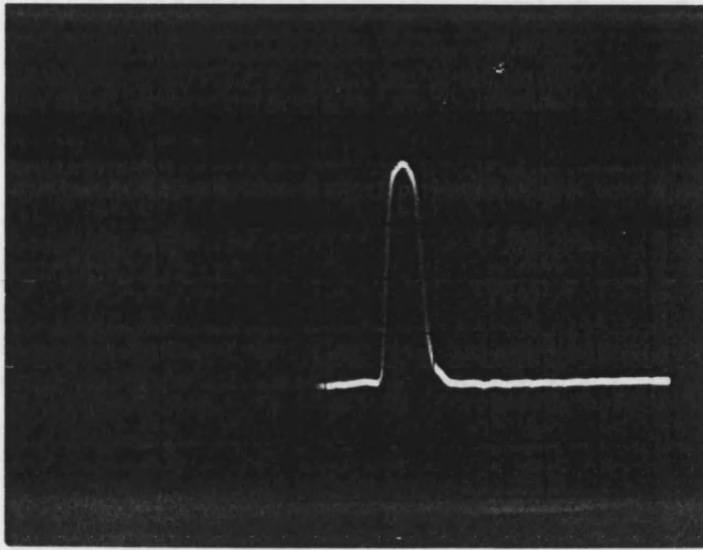


Figure 4.21 Optical output of the laser diode at 150 mA drive current. $T_w=20$ ns, $V_o=50$ mV/cm, $P_o=8.94$ mW

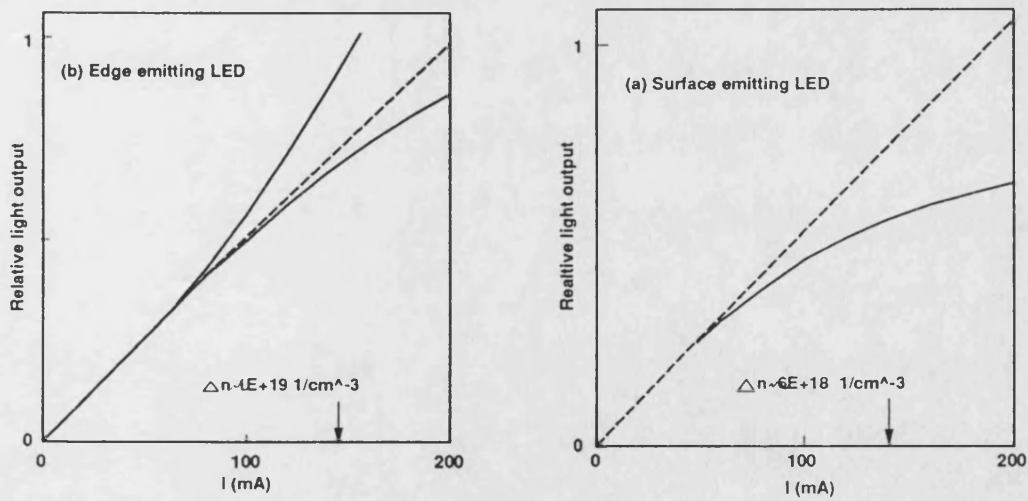


Figure 4.22 Relative output power versus current for typical (a) surface emitters and (b) edge emitters exhibiting various amounts of gain

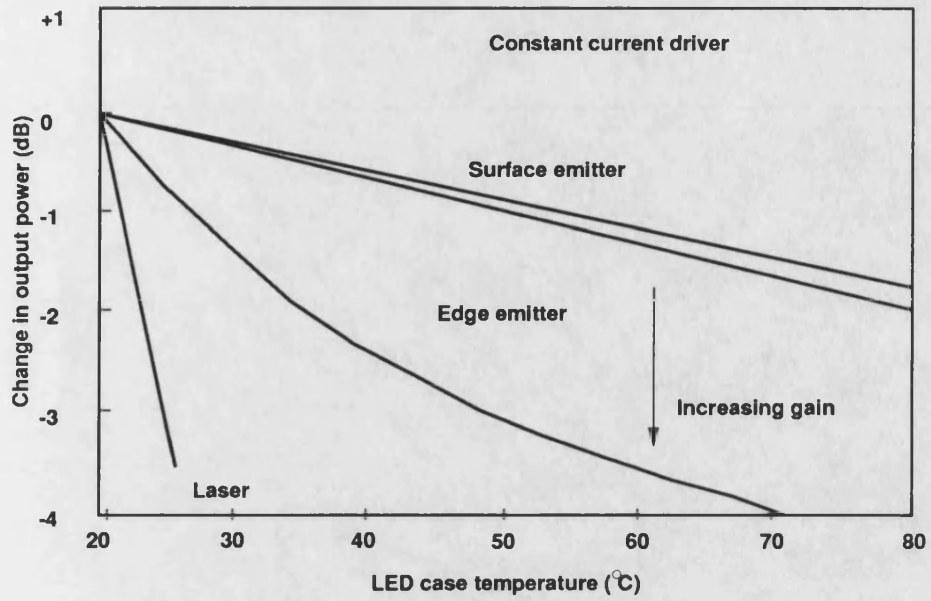


Figure 4.23 Reduction in output power with increased temperature for the devices shown in Fig. 4.22

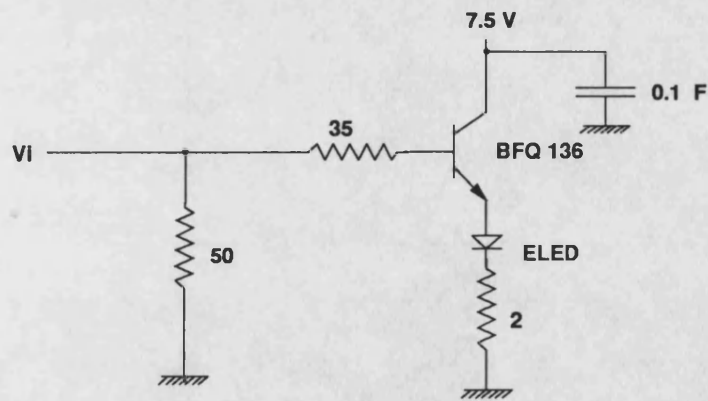


Figure 4.24 ELED driving circuit

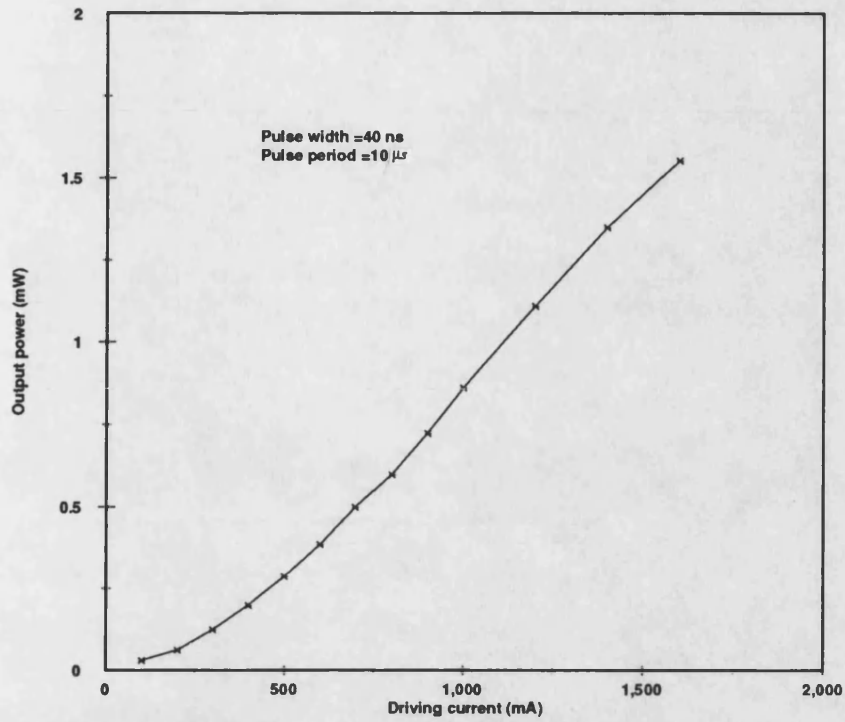


Figure 4.25 L-I characteristic of the ELED 44-62

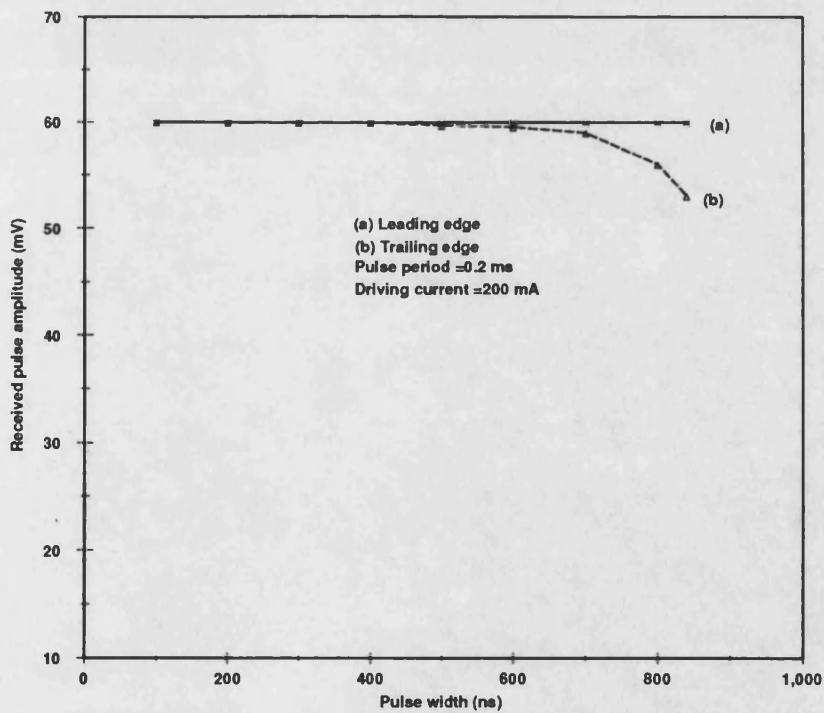


Figure 4.26 Received pulse amplitude versus pulse width

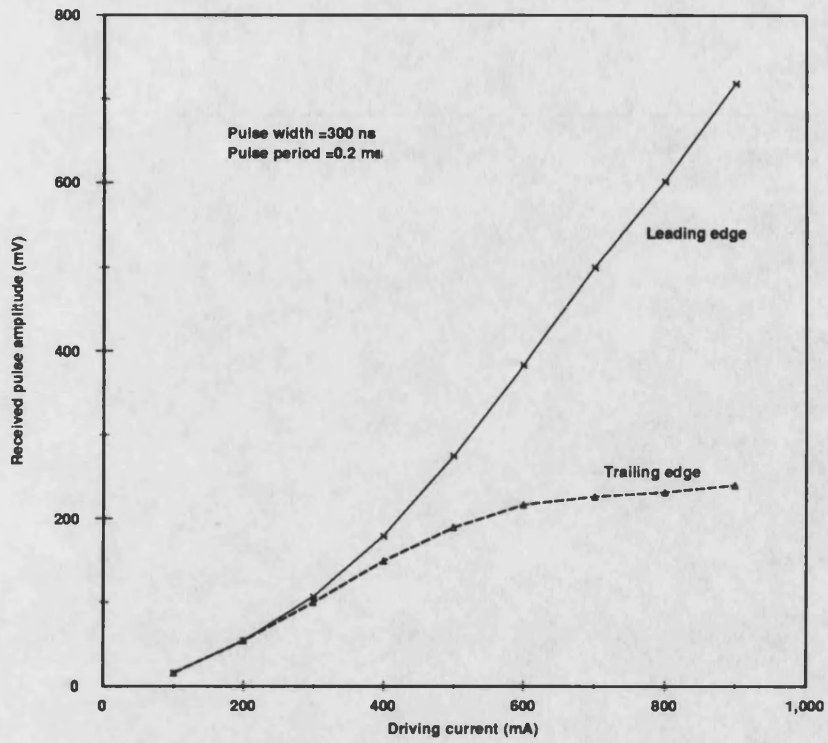


Figure 4.27 Received pulse amplitude versus driving current

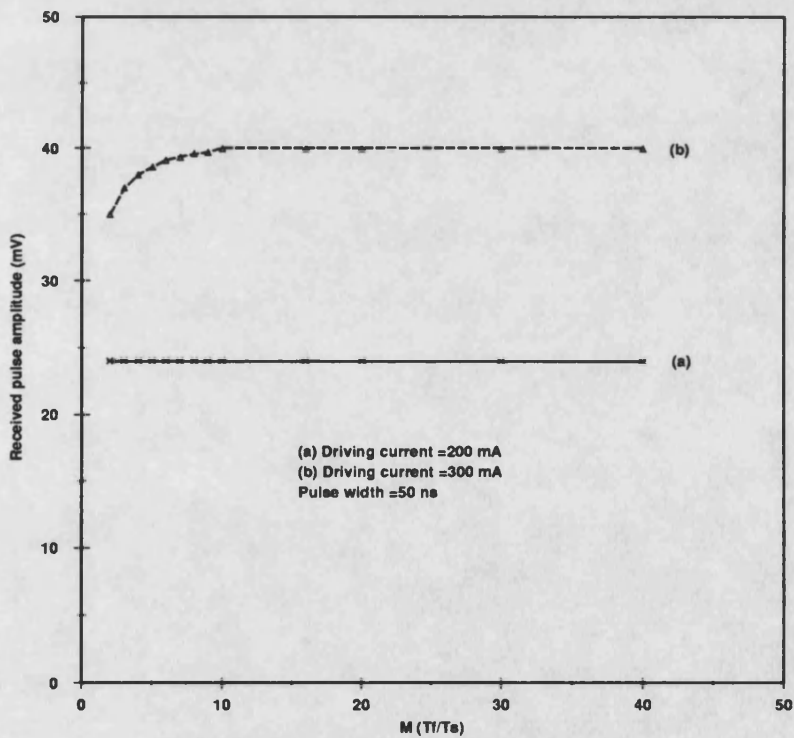


Figure 4.28 Received output power versus pulse duty-cycle

CLOCK SYNCHRONIZATION IN PPM SYSTEM

5.1-INTRODUCTION

Reliable transmission of PPM data in an optical communication system requires that an accurate clock signal be available at the receiver for proper synchronization with the transmitted signal.

Timing recovery is one of the most important receiver functions in synchronous data transmission. Phase and frequency of the clock circuit in the receiver must be adjusted continuously so as to estimate the transition times of the incoming data and to compensate for frequency drifts in the transmitter and receiver oscillators. Failure to do so will cause phase errors between sampling times and optimum sample instances.

Correct decoding of the data requires us to recover from the incoming signal, timing information relating to frame boundaries and time-slot locations, and to determine within which of the M possible time slots a given pulse is located. Timing errors cause energy spillover into adjacent time slots, which decreases the effective signal, increases the effective noise, and increases the probability of error.

In some systems, timing information is sent to the receiver in the form of a special timing signal which is superimposed on the transmitted data waveform, and is identified and separated at the receiver to ensure time synchronization. Alternatively, a receiver may contain a subsystem to extract timing information directly from the data stream and no special timing waveform would be required, resulting in a simpler and more power efficient transmitter.

Frequency and phase synchronization is especially critical in M -ary PPM systems. The received signal is not periodic, pulses are widely-spaced, and vary in position according to the data bit sequence. The effects of timing errors in optical digital systems have been extensively

investigated. Many methods have been proposed and employed for tracking systems including pulse-edge tracking, early-late gate detection, and maximum a posteriori (MAP) estimation. Phase-locked loops have also been studied for use in optical PPM communication system. The choice of a particular method is dependent upon several factors; particularly the data format and coding procedure [GAGLIARDI72, 83].

Receiver timing synchronization of an optical PPM communication system can be achieved using a phase-locked loop (PLL) if the photodetector output is properly processed. In this chapter the theoretical analysis for an optical PPM timing subsystem for the LAN application is given, using a second order PLL. A PLL lock indicator is used to detect when the loop actually runs into lock, so to enable the PPM decoder. Frequency synthesis to generate frame and slot frequencies using a PLL is also discussed. Practical results are given in chapter 7.

5.2-PPM SIGNAL PRE-PROCESSING

A simplified block diagram of the optical PPM receiver is shown in Fig. 5.1. Receiver timing is accomplished in a synchronization subsystem following the photodetector and operating in parallel with the information channel.

In order to give the PLL coherent frequency information sufficient to obtain capture and lock, carrier components must be obtained from the data stream. The time duration of the frequency information fed to the PLL is also important in order to obtain accurate and stable information to update the PLL [GARDNER, YICHAO].

In this simplified analysis, we assume that the PPM system transmits square pulses occupying the entire signal slot. The spectrum of such a PPM signal has a spectral null at the slot frequency, so the received signal at the output of the photodetector, cannot be applied directly

to the PLL. It is possible to generate the required spectral component at the slot frequency from the incoming data stream with non-linear pre-processing of the photodetector output.

5.2.1-SPECTRUM OF FIXED PULSE POSITION

Consider a uniform pulse train, Fig. 5.2a, with pulse width of T_p , pulse period MT_p , and n is a constant. For a rectangular pulse $P(t)=1$ while $|t| < \frac{T_p}{2}$, and this pulse train $x(t)$ can be mathematically represented as a Fourier series with amplitude spectrum of [STREMLER]:

$$C_k = \frac{1}{MT_p} \int_{-\frac{T_p}{2}}^{\frac{T_p}{2}} \exp\left(-j \frac{2\pi k}{MT_p} t\right) dt$$

$$= \frac{1}{M} \text{sinc}\left(\frac{k}{M}\right) \quad (5.1)$$

where k is an integer, and $\text{sinc}(\gamma) = \frac{\sin(\pi\gamma)}{\pi\gamma}$. This amplitude spectrum is drawn in Fig. 5.2b. $C_k=0$, when $k=r.M$, where r is an integer. Hence the spectrum of a uniform pulse train does not show any special components, in fact at $f = \frac{1}{T_p}$, there is a null. We conclude that for a square pulse shape, there is no trackable frequency component at the spectrum of a fixed pulse position.

5.2.2-PROCESSED PULSE

In this section we will follow the analysis done by [LAFAW] and [CHEN85, 86] to preprocess the received PPM signal at the output of the photodetector before applying it to the PLL. First we consider the received signal spectrum at the output of the photodetector without preprocessing. Assume that the output current of a photodetector is $i_D(t)$, and the received optical pulse shape is $x(t)$. The photodetector current consists of a signal current and a noise current, but the noise current is neglected in our case because we assume its amplitude is low

compared with the gaussian noise in the receiver (see chapter 7). Then, without signal preprocessing, the expectation of photodetector output is:

$$E[i_D(t)] = w(t) * \langle x(t) \rangle \quad (5.2)$$

where $w(t)$ is the detector impulse response, and

$$\langle x(t) \rangle = \sum_{k=-\infty}^{\infty} \sum_{j=0}^{M-1} \frac{x_o}{M} P\left(t - kT_f - j\frac{T_f}{M}\right) \quad (5.3)$$

is the signal pulse shape averaged over the M slots in a frame, where x_o is a constant related to the peak optical power of the received pulse, and the brackets $\langle \rangle$ correspond to the time average. Since the received pulse shape, $p(t)$ (Fig. 5.3), is square, Eq. 5.3 is a constant, or:

$$\langle x(t) \rangle = \frac{x_o}{M} \quad (5.4a)$$

and:

$$E[i_D(t)] = D \quad (5.4b)$$

where D is a constant. Eq. 5.4b implies:

$$F\{E[i_D(t)]\} = 2\pi \cdot D \cdot \delta(\omega) \quad (5.5)$$

where $F\{ \}$ denotes Fourier transform. We conclude that, for a square pulse shape, there is no trackable frequency component in the expected detector output signal. Consequently, the phase-locked loop cannot track the output of the photodetector directly. Modeling $P(t)$ as a square pulse represents a worst case situation, for shapes other than square Eq. 5.4a would no longer hold and other frequency components would appear in the output spectrum, so further analysis will be required. Since PPM signals with rectangular pulse shapes do not contain a frequency component at the slot frequency, non-linear preprocessing of the photodetector output is necessary to generate the frequency component. Several possible nonlinearities have been studied, [CHEN85, 86, DATTA, DAVIDSON], and among them are square law, absolute value, $\ln(\cosh)$, and fourth power. [CHEN85, 86, and LAFAW] proposed that filtering and squaring the detected signal generates a slot frequency component, so

PLL can be used to acquire slot synchronization. Fig. 5.4 shows the proposed processing block diagram by [LAFAW], where $h(t)$ is the combined impulse response of the detector and an additional linear filter contained in the preprocessor. Consider the expected value of the square of the detector output current:

$$E[i_D^2(t)] = \langle [h(t)*x(t)]^2 \rangle + h^2(t)*\langle x(t) \rangle \quad (5.6)$$

Again we assume a square, unit-amplitude signal pulse $p(t)$ (Fig. 5.3). Since $p(t)$ is a square pulse, $\langle x(t) \rangle$ is again a constant so the second term of Eq. 5.6 is also a constant. The first term can be written as:

$$h(t)*x(t) = \int_{-\infty}^{\infty} h(t)dt + \sum_{k=-\infty}^{\infty} g\left(t - kT_f - c_k \frac{T_f}{M}\right) \quad (5.7)$$

where $g(t) = h(t)*p(t)$, and $c_k = (0, 1, \dots, M)$ is the random data sequence. Assume $\int_{-\infty}^{\infty} h(t)dt = 1$, and that the pulses occupying the time slots are narrow width no significant overlap, then the solution of Eq. 5.6 will be:

$$E[i_D^2(t)] = \frac{x_o}{M} \int_{-\infty}^{\infty} h^2(t)dt + \left[1 + \frac{2x_o}{M}\right] \left[\int_{-\infty}^{\infty} h(t)dt\right]^2 + \frac{x_o^2}{M} \sum_{k=-\infty}^{\infty} g^2\left(t - \frac{kT_f}{M}\right) \quad (5.8)$$

Since all but the last term are constants, Eq. 5.8 is equivalently expressed as:

$$E[i_D^2(t)] = B + \frac{x_o^2}{M} [h(t)*p(t)]^2 * \sum_{k=-\infty}^{\infty} \delta\left(t - \frac{kT_f}{M}\right) \quad (5.9)$$

where B denotes the sum of the constant terms of Eq. 5.8. Taking the Fourier transform of Eq. 5.9 yields:

$$F\{E[i_D^2(t)]\} = 2\pi B \delta(\omega) + \frac{2\pi x_o^2}{T_f} [H(\omega)P(\omega)] * [H(\omega)P(\omega)] \cdot \sum_{k=-\infty}^{\infty} \delta\left(\omega - k2\pi \frac{M}{T_f}\right) \quad \dots(5.10)$$

where $H(\omega)$ and $P(\omega)$ are the Fourier transforms of $h(t)$ and $p(t)$ respectively. $P(\omega)$ is the transform of the transmitted square pulse and is given by:

$$\begin{aligned} P(\omega) &= \int_0^{T_s} \exp(-j\omega t) dt \\ &= T_s \cdot \text{sinc}(fT_s) \cdot \exp\left(-j\frac{\omega T_s}{2}\right) \end{aligned} \quad (5.11)$$

From Eq. 5.10 it is apparent that we have spectral frequency components at $\omega_n = \frac{2\pi M}{T_s} n$. When $n=1$, ω_1 corresponds to the time slot transmission rate. The transfer function of the preprocessing filter, $H(\omega)$, should be chosen to give maximum signal component at $f_s (= \frac{1}{T_s})$, minimum background noise components, and stationary PLL phase error variance. To satisfy these requirements, the impulse response $h(t)$ of the preprocessing filter can be chosen to be a sinusoidal function and given by:

$$h(t) = \sin\left(\frac{2\pi}{T_s} t\right) \quad , \quad |t| \leq \frac{T_s}{2} \quad (5.12)$$

This is plotted in Fig. 5.5, and the Fourier transform of $h(t)$ is given by:

$$H(\omega) = \frac{\pi T_s}{j} [\text{sinc}\{T_s(f - f_s)\} - \text{sinc}\{T_s(f + f_s)\}] \quad (5.13)$$

and plotted in Fig. 5.6. $g(t)$ can be found by convolving $h(t)$ with $p(t)$, we have:

$$\begin{aligned} g(t) &= -\frac{T_s}{2\pi} \left\{ 1 - \cos\left(\frac{2\pi}{T_s} t\right) \right\} \quad , \quad -T_s \leq t \leq 0 \\ &= \frac{T_s}{2\pi} \left\{ 1 - \cos\left(\frac{2\pi}{T_s} t\right) \right\} \quad , \quad 0 \leq t \leq T_s \end{aligned} \quad (5.14)$$

Fig. 5.7 shows that as a result of the convolution operation, $g(t)$ has duration $2T_s$.

After passing $g(t)$ through the squaring loop, we obtain:

$$g^2(t) = \frac{T_s^2}{2\pi^2} \left\{ \frac{3}{4} - \cos\left(\frac{2\pi}{T_s} t\right) + \frac{1}{4} \cos\left(\frac{4\pi}{T_s} t\right) \right\} \quad , \quad -T_s \leq t \leq T_s \quad (5.15)$$

Which consists of two identical, positive waveforms each of duration T_s , as shown in Fig. 5.8. Thus, the total amplitude of the fundamental frequency component of Eq. 5.15 is:

$$a = 2 \left[\frac{T_s^2}{2\pi^2} \right] \quad (5.16)$$

Preprocessing the detector output as described above will generate a spectral component at the time slot frequency which can be tracked by the PLL.

The preprocessing filter $h(t)$ (Eq. 5.12) can be realized practically by a low-pass Gaussian filter with rms bandwidth $B_o(\approx 1.3\omega_c)$ followed by an ideal differentiator [CHEN85, 86]. The variance of phase error is found to be minimum at this rms bandwidth.

5.3-PHASE LOCKED LOOP

5.3.1-INTRODUCTION

A PLL is a device which enables the phase of a frequency modulated oscillator signal to follow that of the input signal. It contains three basic components; phase detector, low-pass filter, and voltage controlled oscillator (VCO) (Fig. 5.9). The phase detector measures the phase difference between its two inputs and then outputs a voltage proportional to this difference. The output of the phase detector is described by:

$$\begin{aligned} V_d &= k_d \sin(\theta_i - \theta_o) \\ &\cong k_d(\theta_i - \theta_o) \quad \text{if } (\theta_i - \theta_o) \ll \pi \end{aligned} \quad (5.17)$$

where k_d is the gain of the phase detector (in volts/radian), θ_i is the input signal phase, and θ_o is the phase of the VCO output signal [BOYLESTAD, GARDNER]. The phase error voltage, V_d , is filtered by the loop low-pass filter, whose filter transfer function in the frequency domain is given by $F(s)$. The output of the filter is an error voltage, $V_{f,r}$, which is used to control the frequency of the VCO. The VCO has a free-running frequency ω_f and an instantaneous frequency shift proportional to the control voltage input, $\Delta\omega_f = k_o V_{f,r}$, where k_o is the VCO gain constant (in radians/second/volt). The loop is said to be locked when the control voltage applied to the VCO keeps the frequency of the VCO equal to the average frequency of the incoming signal.

The closed loop phase transfer function of the PLL can be written as:

$$H(s) = \frac{\theta_o(s)}{\theta_i(s)} = \frac{k_o k_d F(s)}{s + k_o k_d F(s)} \quad (5.18)$$

And the error transfer function is:

$$\frac{\theta_o(s)}{\theta_i(s)} = \frac{s}{s + k_o k_d F(s)} \quad (5.19)$$

where: $k_o k_d F(s)$ is the forward loop gain.

The transfer function of the loop filter has a considerable influence on the properties of the loop and provides a means of modifying its performance by a judicious choice of parameters. The low pass filter would be chosen to reduce the jitter and noise in the input synchronizing signal, and fundamental characteristics of a PLL, such as capture range, capture time, loop bandwidth, and transient response are controlled primarily by the loop filter. The second order PLL is the most commonly used type. The passive loop filter shown in Fig. 5.10, has the transfer function:

$$F(j\omega) = \frac{j\omega\tau_2 + 1}{j\omega\tau_1 + 1} \quad (5.20)$$

where the time constants $\tau_1 = (R_1 + R_2)C$ and $\tau_2 = R_2C$.

Substituting Eq. 5.20 into Eq. 5.18 and comparing it with the standard form for a second-order system, [GARDNER], yields the following expression for the transfer function:

$$H(j\omega) = \frac{k + j\omega k\tau_2}{k - \omega^2\tau_1 + j\omega(1 + k\tau_2)} \quad (5.21)$$

where $k = k_d k_o$. We can extract useful information from Eq. 5.21: natural frequency $\omega_n = \sqrt{k/\tau_1}$, and damping factor $\eta = \frac{1}{2} \left(\frac{k}{\tau_1} \right)^{\frac{1}{2}} \left(\tau_2 + \frac{1}{k} \right)$. From Eq. 5.21, the lag-lead filter has two time constants, then ω_n and η can be chosen independently, and the loop gain can be made as large as may be necessary for good tracking. With these values defined, the loop filter can readily be designed [GARDNER].

5.3.2-NOISE PROCESSING BY THE PLL

The bandwidth of the noise spectrum at the PLL input is limited by a prefilter, which in this case is a band pass filter, with bandwidth B_i . The input noise signal, which is considered as white noise, is

assumed to have a total power P_n (in watts), and P_s is the input signal power. The spectral density of the input noise is $W_i = \frac{P_n}{B_i}$ in W/Hz. If the noise signal is added to the input signal, the resulting signal is displaced back or forward depending on the instantaneous polarity of the noise signal, and a phase jitter is generated. The SNR at the input of the PLL can be defined as $(SNR)_i = \frac{P_s}{P_n}$, then the square of the rms phase noise (rms value of the phase jitter), of a sinusoidal signal at the input of a PLL is given by the simple relation [BEST]:

$$\begin{aligned} \overline{\theta_{ni}^2} &= \frac{P_n}{2P_s} \\ &= \frac{1}{2(SNR)_i} \quad (rad^2) \end{aligned} \quad (5.22)$$

and the square of the phase spectral density of the phase jitter, Φ , is given by:

$$\Phi = \frac{\overline{\theta_{ni}^2}}{B_i/2} \quad \left(\frac{rad^2}{Hz} \right) \quad (5.23)$$

where the overbar symbolizes the averaging (or mean) operation. We are now looking for the rms value of phase noise at the output of the PLL, which is the input phase, modified by the closed-loop transfer function $H(j\omega)$, or:

$$\overline{\theta_{no}^2} = \int_0^\infty \Phi |H(j\omega)|^2 d\omega \quad (5.24)$$

The integral $\int_0^\infty |H(j2\pi f)|^2 df$ is called the noise bandwidth B_L . Once the PLL is locked, it exhibits a finite bandwidth B_L (Hz) which allows incoming noise to cause jitter on the VCO. The noise bandwidth of the second order PLL is given by:

$$B_L = \int_0^\infty |H(j2\pi f)|^2 df = \frac{\omega_n}{2} \left(\eta + \frac{1}{4\eta} \right) \quad (5.25)$$

Thus B_L is proportional to the natural frequency and the damping factor. Using the lag-lead filter (Eq. 5.20) allows us to control all the loop parameters K , η , and B_L independently. The optimum value of B_L is $\frac{\omega_n}{2}$ and is achieved for a second order loop when the damping factor η is 0.5.

The transient response of the PLL is best at $\eta=0.7$, because the function $B_L(\eta)$ is fairly flat in the neighbourhood of $\eta=0.5$, for this reason $\eta=0.7$ is chosen for most applications [BEST]. From Eqs. 5.22 to 5.24, the phase jitter at the output of the PLL is given by:

$$\overline{\theta_{no}^2} = \frac{P_n}{P_s} \cdot \frac{B_L}{B_i} \quad (5.26)$$

From Eq. 5.26, the SNR at the output of the PLL, $(SNR)_L$ can be defined as:

$$\overline{\theta_{no}^2} = \frac{1}{2(SNR)_L} \quad (5.27)$$

Then the signal to noise ratio at the output of a PLL from Eqs. 5.22, 5.26 and 5.27, is equal to:

$$(SNR)_L = (SNR)_i \frac{B_i}{2B_L} \quad (5.28)$$

It is clear from Eq. 5.28 that the PLL improves the SNR of the input signal by a factor of $\frac{B_i}{2B_L}$. The narrower the noise bandwidth of the PLL, the greater the improvement. For example, if $B_i=4B_L$ then $(SNR)_L=2(SNR)_i$. Stable operation of the PLL is possible if $(SNR)_L$ is greater than 4, or the rms value of phase jitter at the output of the PLL is about 20° [BEST]. A phase detector has only a limited range of operation; and if the phase error exceeds this range, the loop will drop out of lock. The input band-pass filter will determine the input noise to the loop, also, the noise bandwidth can be determined by ω_n and η so these parameters determine the output SNR or the phase jitter.

5.3.3-VCO DRIFT

The lock range of a PLL is the frequency range centered about the VCO free-running frequency over which the loop can acquire lock with the input signal. When the difference between the free running frequency and the average incoming frequency is less than the 3 dB loop bandwidth, the loop will lock up almost immediately without skipping any cycles.

The maximum frequency for which this is possible is the lock-in range and is equivalent to the loop bandwidth [BOYLESTAD]. The lock-in range, $\Delta\omega_L$, for a second order loop is defined as $\Delta\omega_L \approx 2\eta\omega_n$. The range of frequency difference over which a loop will maintain phase lock is the hold-in range and for the second order loop with a passive filter is defined by: $\Delta\omega_H = \pm k_d/k_f$.

Successful PLL design represents a compromise between performance features. A wide loop bandwidth will result in a fast acquisition and lock-up time as well as an extended lock-in range, but will admit more noise, may have a smaller hold-in range, and be more sensitive to small changes in the signal frequency. Alternatively, a narrow bandwidth insures good noise performance and will tolerate a larger amount of input frequency change without losing lock, but will have difficulty acquiring phase-lock. If the value of η is fixed, then changing the value of ω_n will change the lock-in and hold-in ranges, the lock-up time, and the noise bandwidth.

When a PLL's input is random data, as in PPM, this requires the loop bandwidth to be extremely narrow in order to reject input jitter and maintain lock during the frame time. So to design a small loop bandwidth PLL and assure locking of the loop a crystal controlled VCO should be used, i.e. VCXO [GHORBANALI]. If the same type of the crystal is used for the transmitter oscillator and the PLL VCO, then the frequency offset between the transmitter and the receiver will be very small. So the VCO frequency drift can be made to lie within the lock-in range of the PLL.

As discussed before, the PLL operates on phase and frequency information and must have continuous synchronous reinforcement in order to remain in lock. The spacing between the received pulses is critical because we are trying to extract a particular frequency related to clock signals from a received pulse stream. In PPM during the frame time frequency drift can occur, but this drift should be very small, because the oscillator is crystal controlled. In order to select the slot frequency

component from the preprocessed PPM data pattern and suppress other frequency components, an LC resonant circuit is used. The beauty of the tank circuit lies in its ability to store short term phase and frequency coherent information which is easily reinforced by pulses derived from the received PPM pulses. The inductor and the capacitor may be selected to arrive at the desired Q-factor which will sustain the missing clock data harmonic for a given duration of pulse gap before decaying to 1/e of its original amplitude. For example, when the input to a resonant circuit, Fig. 5.11 is a short width pulse of duration T_0 , the output can be written as [MILLMAN]:

$$v_o(t) = \frac{V}{Q} \sin\left(\frac{2\pi}{T_0} t\right) \cdot \exp\left(-\frac{\pi}{QT_0} t\right) \quad Q \gg 1 \quad (5.29)$$

where V is the input pulse amplitude. The higher the Q factor the longer the transient takes to decay. From Eq. 5.29, the time duration of the sustained harmonic output is related by the equation:

$$Q = \pi N \quad (5.30)$$

where N equals the number of cycles in the interval after the original pulse until the harmonic amplitude decays to 1/e of the original amplitude. By setting the period of the resonant frequency equal to the slot period ($\frac{2\pi}{T_0} = \frac{1}{\sqrt{LC}}$) the resonant circuit will oscillate at the accurate slot frequency resulting in a synchronous sinusoidal waveform ideal for driving a PLL. For example, if $Q=63$, then $N = \frac{63}{\pi} \approx 20$, the circuit will ring for 20 cycles before the amplitude of the oscillation decreases to 37 percent of its initial value. If $V=2$ volt, then $v_o=31.7$ mV, and at $N=20$, this value will reduce to 10 mV (assuming $\sin\left(\frac{2\pi}{T_0} t\right)=1$). If the designed PLL is working on the threshold voltage, v_{th} , of 10 mV then the resonant circuit will sustain the missing clock for 20 slots. Higher Q or V is required for wider duration. The maximum distance between PPM pulses could reach to $2(M-1)$, in this case N should go up to 30 for $M=16$, or $Q=94$ and $V=2.5$ volt for the average levels specified in the previous example. The voltage level applied to the resonant circuit

could be amplified to increase the amplitude limit of oscillation. In general, the voltage applied to the PLL should be bigger than or equal to the PLL threshold voltage, or:

$$v_o(2(M-1)T_s) \geq v_{th} \quad (5.31)$$

In the PPM system built in this work, the input signal to the resonant circuit was a double sine wave in each frame (because of differentiation and rectification). This will increase the amplitude of the decayed signal and will keep the resonant circuit oscillating for a longer time compared to the theory discussed above which will keep the PLL locked to the received signal for longer time. Resonant circuit tuning error will pass the unwanted frequency components and cause phase error, and the PLL output may start jittering or the PLL may lock on wrong frequency harmonic.

Once design parameters are fixed, a change in the input signal amplitude can alter the PLL performance. In practice, the limiter at the input of the PLL 564 was used to allow the intended design parameters to remain unchanged over a wide range of signal inputs with a 10 mV minimum, (see chapter 7).

The time constant of the LPF τ_1 (Eq. 5.21) represents the VCO memory with respect to the input frequency. If τ_1 is very high, the VCO losses fewer cycles than with a low τ_1 , this reduces the VCO frequency drift as well, and will ease the requirement for a high Q resonant circuit. From the analysis done in this section it is clear that the maximum value of M for a PPM system depends on an accurate slot synchronization as well, which depends on the bandwidth of a PLL, the characteristics of the LPF filter used, and the quality factor of the resonant circuit before the PLL. Using the theory discussed above, the value of M=32 can be achieved practically easily. .

5.4-PLL LOCK INDICATOR

Many circuits that utilize PLLs need some indication of when the loop actually runs into lock. If the SNR is moderately good and the input signal does not jump around too much, it is not too difficult to detect lock. However, near threshold conditions lock may not be easy to detect. In the PPM case, it is necessary to establish the slot clock before the PPM frame format can be recovered, so it is important to know when this stage of lock has been completed.

A wide variety of lock detection circuits has appeared, some of which work well in particular application but not so well in others [GARDNER, HANISKO, SHARPE]. Noise and glitches, for example, often cause problems; filters or other means must be added to force a makeshift system (i.e. a comparator) to work. Even if the signal is good, the locked condition cannot be detected instantaneously, instead it is necessary to filter the indication for some appropriate length of time to reduce the confusion caused by noise. A method of lock indication employed almost universally is the quadrature phase detector [GARDNER]. A typical arrangement is shown in Fig. 5.12. A further phase detector is included which operates with a quadrature signal from the VCO. A 90° phase shift of the VCO output can be obtained by using a phase shifter or delaying VCO output by $T/4$ (see chapter 7). The output of the in-phase detector is proportional to $\sin(\theta)$, and hence is small for θ , small. The output of the quadrature detector is proportional to $\cos(\theta)$, and hence is large for θ , small, i.e., at lock, so the filtered dc. output of the quadrature detector provides a lock indication signal. This signal is applied to the comparator A to compare it with some threshold set by V_{ref} . When the PLL is out of lock the outputs of both phase detectors are beat notes with small dc components.

5.5-FREQUENCY SYNTHESIS USING PLL

Frequency synthesis is the generation of a frequency or frequencies which are exact multiples of a reference frequency. Usually the reference is very precise and the synthesized frequencies are selectable over some range of wholenumber multiples of a submultiple of the reference. Simply stated, a frequency synthesizer is a crystal-controlled variable-frequency generator.

In DPPM systems we need at least two different synchronized frequencies for the slot and the frame. These frequencies could be easily obtained at the transmitter by dividing the oscillator frequency, but at the receiver these frequencies should be generated from the PLL frequency. The most frequently used technique for frequency synthesis is the indirect method utilizing a VCO in a programmable PLL. The phase-locked synthesizer, in effect multiplies the reference frequency by a variable number. It does so by dividing its output frequency by that variable, and adjusting the output frequency so that after division it is equal to the reference frequency. Fig. 5.13 shows the block diagram for a simple single loop PLL frequency synthesizer. The range of frequencies generated and the resolution are dependent on the divider network and the open-loop gain. The frequency divider is a divide by N circuit, where N is a whole integer number. The simplest form of a divider circuit is a programmable digital up-down counter with an output frequency $f_c = \frac{f_o}{N}$. Once lock has occurred, $f_c = f_{ref}$, and the VCO and synthesizer output frequency $f_o = Nf_{ref}$. Thus the synthesizer is essentially a times -N frequency multiplier. The frequency divider reduces the open-loop gain by a factor of N, so the loop gain for the simple PLL synthesizer of Fig. 5.13 is $k_l = \frac{k_f k_o}{N}$. It is important to realize that the frequency-divider circuit reduces the loop gain so that the other loop components need to have relatively higher gain than for the conventional PLL. The PLL lock range and the capture range will reduce by N.

5.6-SUMMARY

Reliable transmission of PPM data in an optical communication system requires that an accurate clock signal be available at the receiver for proper synchronization with the transmitted signal. With proper nonlinear preprocessing of the detector output signal, a PLL can be used to provide accurate synchronization in a direct detection optical PPM system. For maximum signal component the preprocessing filter can be realized practically by a low-pass Gaussian filter with rms bandwidth 1.3ω , followed by an ideal differentiator.

To design a small loop bandwidth PLL and assume locking of the loop we should use a very stable VCO, i.e. VCXO, and the same type of crystal for both the transmitter and the receiver. We can then be sure that the frequency drift in both the transmitter and the receiver will be very small, and the VCO frequency drift will be within the lock-in range of the PLL. Noise bandwidth and internal jitter of the PLL can be reduced by careful design. A resonant high Q LC circuit tuned to the slot frequency is used before the PLL in order to select and reinforce slot frequency information from PPM data and suppress other harmonics.

5.7-REFERENCES

- BEST, R. E., "Phase-locked loops", McGraw-Hill, 1984, chapter 3.
- BOYLESTAD, R., and NASHELSKY, L., "Electronic devices and circuit theory", Prentice-Hall, 1987, chapter 17.
- CHEN85, C. C., and GARDNER, C. S., "PLL synchronization for direct detection optical PPM communication systems", EOSL publication No. 85-003, University of Illinois, Urban, USA, May 1985.
- CHEN86, C. C., and GARDNER, C. S., "Performance of PLL-synchronized optical PPM communication systems", IEEE Trans. on Commun., Vol. COM-34, Oct. 1986, pp. 988-994.
- DATTA, D., and GANGOPADHYAY, R., "Simulation studies on nonlinear bit

synchronizers in APD-based optical receivers", IEEE Trans. Commun., Vol. COM-35, Sept. 1987, pp. 909-917.

DAVIDSON, F. M., and SUN, X., "Slot clock recovery in optical PPM communication systems with avalanche photodiode photodetectors", IEEE-Trans. on Commun., Vol. COM-37, No. 11, November 1989, pp. 1164-71.

GAGLIARDI⁷², R. M., "The effects of timing errors in optical digital systems", IEEE Trans. Commun., Vol. COM-20, No. 2, April 1972, pp. 87-93.

GAGLIARDI⁸³, R. M., "Time synchronization in optical PPM systems", GLOBECOM 83 IEEE GLOBAL, Telecommunications conference, Conference record San Diego, CA, USA, 28 No.-1 Dec. 1983, pp. 779-83.

GARDNER, F. M., "Phaselock techniques", John-Wiley & Sons, New York, 1966.

GHORBANALI, M., "Clock recovery (timing extraction)", Proc. SPIE, Fiber Optic Networks and Coherent Technology in Fiber Optic Systems II, Vol. 841, August 1987, pp. 80-94.

HANISKO, J. C., "PLL lock indicator uses a single IC", EDN, October 5 1976. pp. 104.

LAFAW, D. A., and GARDNER, G. S., "Timing performance of PLLs in optical PPM communication systems", Technical report, EOSL publication No. 84-001, University of Illinois, USA, August 1984.

MILLMAN, J., and TAUB, H., "Pulse, Digital, and Switching Waveforms", McGraw-Hill Company, USA, 1965, Chapter 2.

SHARPE, C. A., "How can you be sure that your PLL is really locked in?", EDN, February 30 1977, pp. 109-110.

STREMLER, F., "Introduction to communication systems", Addison-Wesley, 1982, chapter 2.

YICHAO, W., "Line-coded PPM for repeatered optical fiber telecommunications", Ph.D. thesis, University of Essex, August 1986.

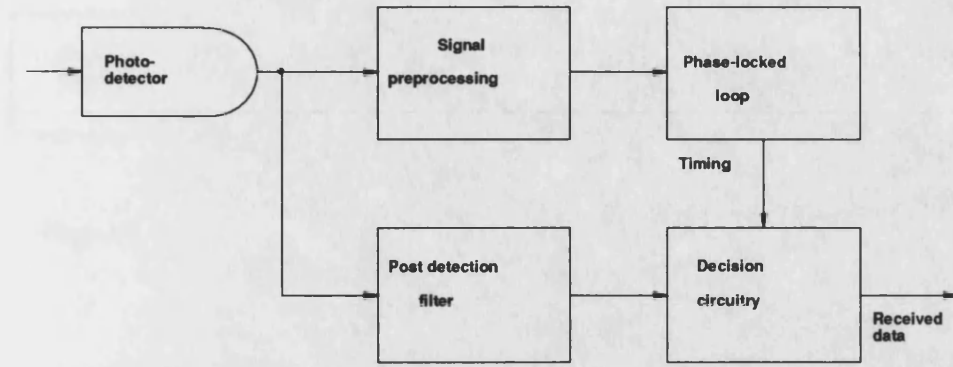


Figure 5.1 Block diagram of the receiver timing subsystem

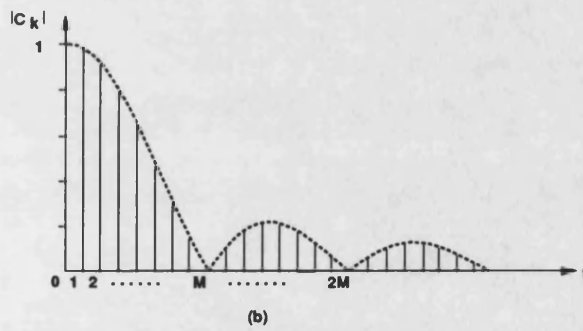
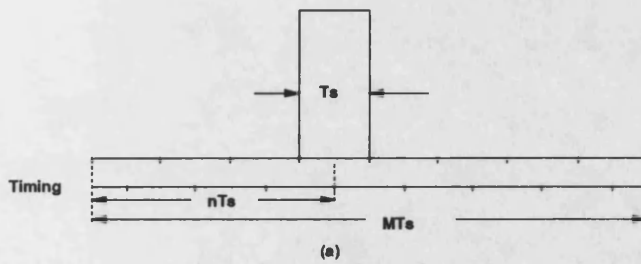


Figure 5.2 Uniform pulse and its amplitude spectrum

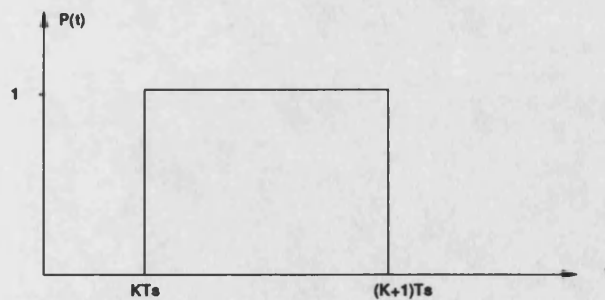


Figure 5.3 Received PPM pulse shape

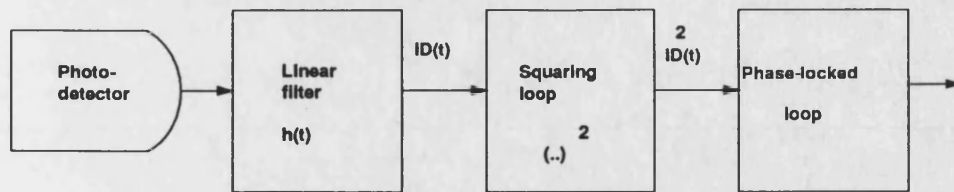


Figure 5.4 Block diagram of the preprocessing circuit

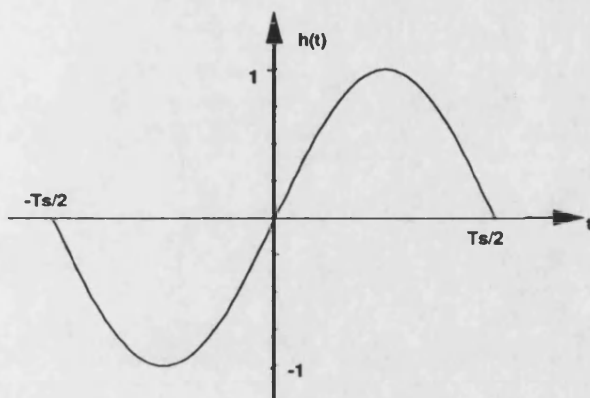


Figure 5.5 The impulse response of the preprocessing filter

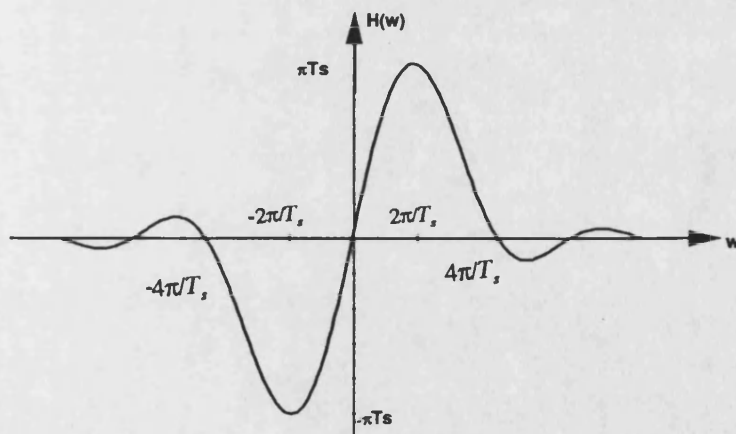


Figure 5.6 The fourier transform of $h(t)$

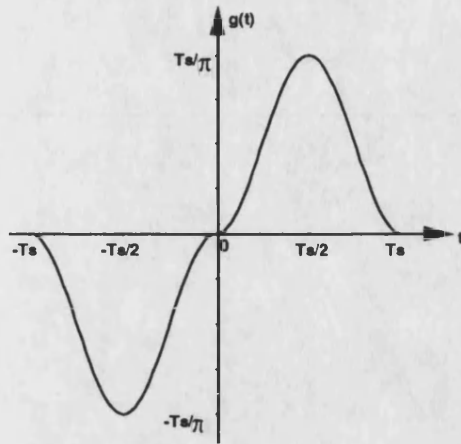


Figure 5.7 The result of convolving $h(t)$ with $p(t)$

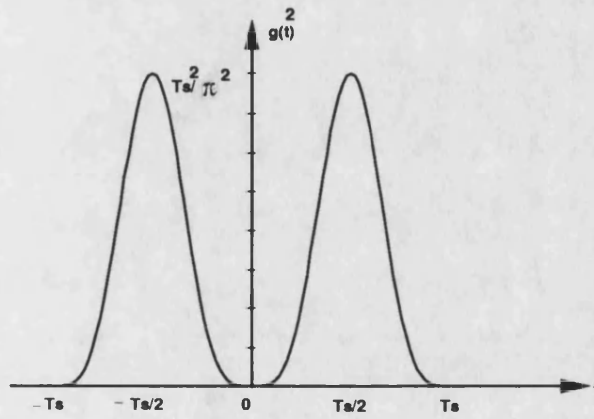


Figure 5.8 The squaring loop output

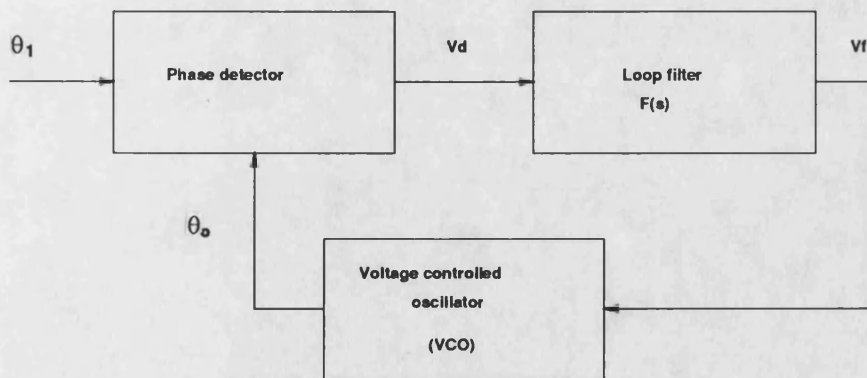


Figure 5.9 PLL block diagram

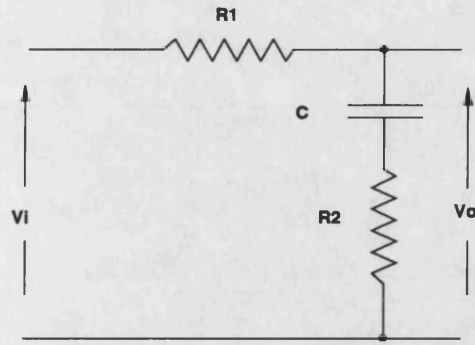


Figure 5.10 Passive loop filter

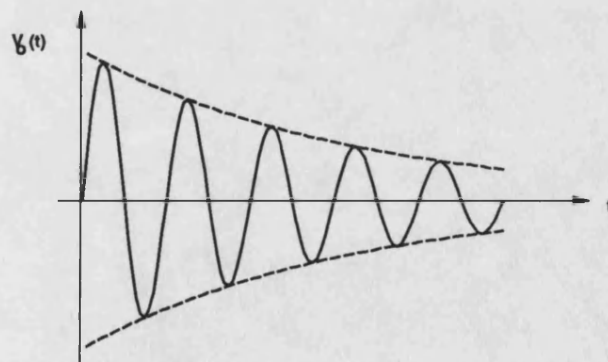
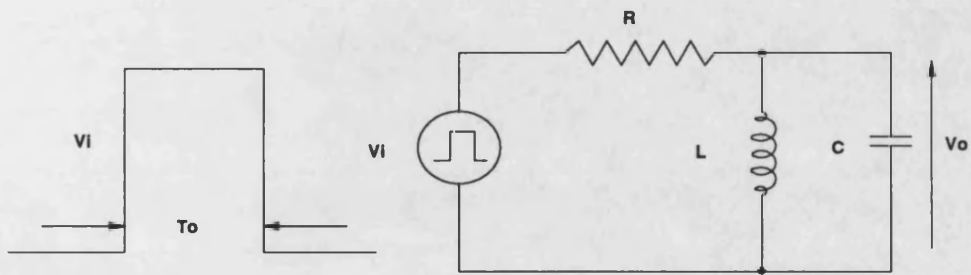


Figure 5.11 The resonant circuit and its input and output

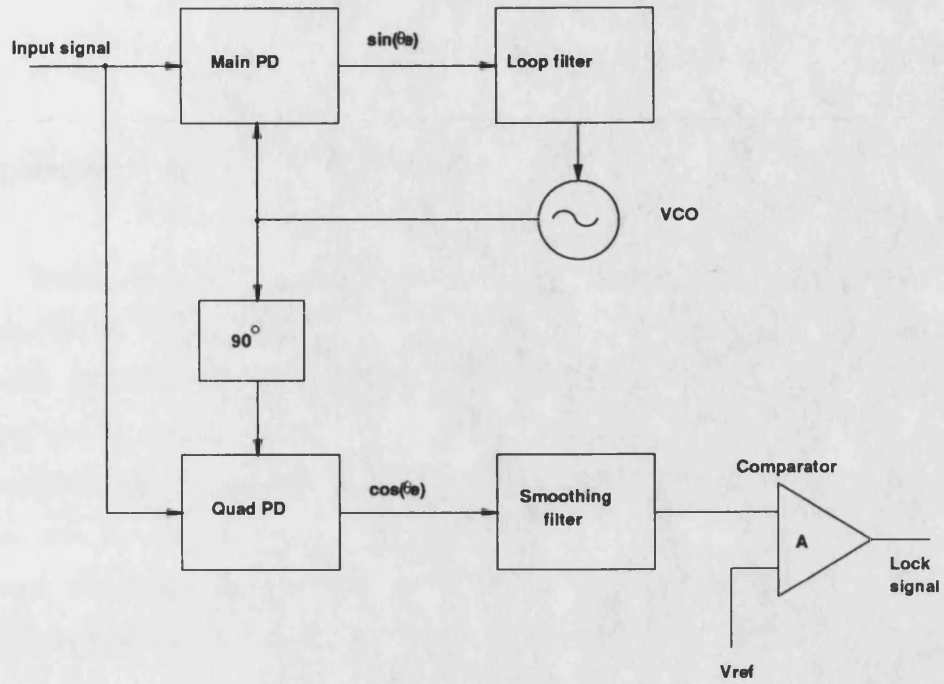


Figure 5.12 Lock Indicator

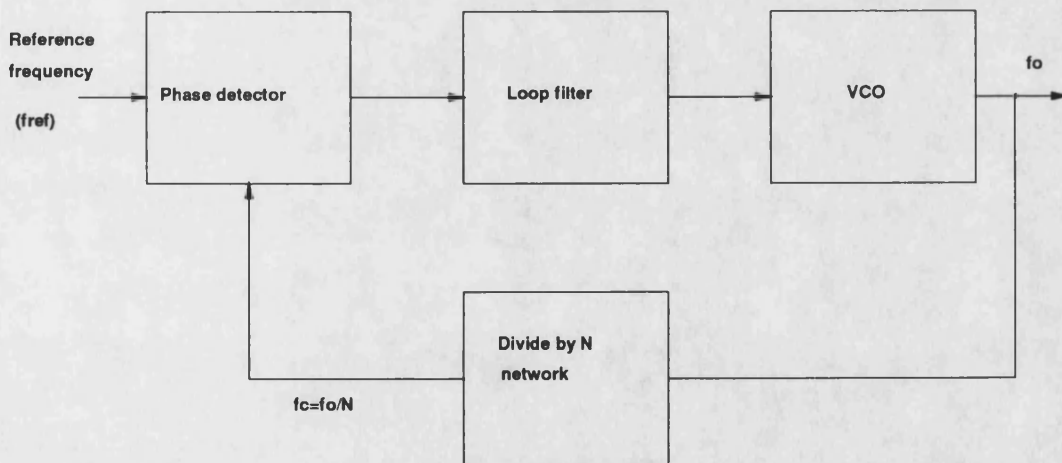


Figure 5.13 PLL synthesizer

CHAPTER -6-
THE OPTICAL PPM TRANSMITTER

6.1-INTRODUCTION

There are many different types of fiber optic transmitter, each designed for a particular use, and although the same LEDs and LDs may be used there are major differences in the modulation scheme and transmission speed. Several factors enter into the performance of a fiber-optic transmitter, including the type of signal being sent, the speed, the operating wavelength, the type of light source and the cost. Digital transmitter circuits must have fast response to produce the fast rise-time pulses needed for digital transmission. The choice among light sources depends primarily upon speed, transmission type, and operating distance. All other things being equal, LEDs may be preferred for analog transmitters because of their more linear response, however, lasers also are used for analog transmission especially over long distance or at high speed. Both LEDs and lasers can be used in digital transmitters, and speed may dictate the choice of a fast LED or an even faster laser diode. Continuous power delivered by the light source can range from tens of milliwatts for a semiconductor laser to tens of microwatts for an LED, although not all of the power is useful. The relevant value is the power that can be coupled into an optical fiber, which depends on the angle over which light is emitted, the size of the light emitting area, the alignment of the source and fiber, and the coupling characteristics of the fiber. The type of the drive circuitry needed for an optical source, depends on application requirements, data format, and the light source [HECHT, SENIOR, PERSONICK, GRUBER, SHUMATE]. This chapter examines an experimental DPPM transmitter and how it and its components work, concentrating on a design for local area network use. The block diagram of the PPM transmitter being built; which includes the coder, the packet generator, and the driving circuit for the optical

source is shown in Fig. 6.1. This transmitter encodes each group of source bits (serial data in PCM form) into a light pulse placed in one of M pulse positions within a time frame of T_f . Each group of data is transmitted over the network as a packet containing data plus slot and frame synchronization pulses. The driving circuit in PPM, should be capable of handling more current than the optical source rated continuous current.

To test the effect of varying M on the system performance, for a given data rate, the system was designed to operate with different values of M and guard space.

6.2-PPM CODER

Serial data in PCM form is shifted with speed f_d (bits/sec) to the PPM coder and converted to PPM form at f_s slots/sec. (n)-bits of binary PCM are coded into one of a set of symbols, which are formed by dividing the frame time into M time-slots, and placing a pulse in one of the M time slots. The PPM coder which is designed and realized practically using transistor-transistor logic (TTL) integrated circuits is shown in Fig. 6.2. The slot frequency, f_s , must be synchronized with data shift frequency, f_d . Serial data clocked by the frequency f_d is converted into parallel form by the shift register (SIPO). This n-bit parallel data is loaded to the shift register (PIPO) by the load pulse (L). The counter is running at a frequency of f_s (which is $\frac{M}{n \log_2 M}$ -times the binary PCM data line rate). The comparator, A, compares the PIPO shift register output with the counter state, and gives a pulse when the two outputs became equal. The comparator B is used to reset the counter at the end of the frame, and has one of its inputs is connected to the counter and the other set to M+1-2. The storage register (PIPO) is loaded at the end of each frame by the load pulse (L) which is derived from the reset pulse. The data-shift frequency f_d prevents the register (PIPO) from clocking while it is loading. D1 and D2 are de-glitching flip-flops.

The designed coder can operate for different values of M and guard space G (M=4, 8, and 16, see section 6.3). For each value of M, the slot frequency f_s , and data shift frequency, f_d , are synthesized from the oscillator clock frequency, f_o . Fig. 6.3 shows the timing diagram for the PPM coder.

6.3-FREQUENCY SYNTHESIS

For a given oscillator clock frequency f_o , it is required to generate the slot clock f_s for the PPM signal and the bit shift clock f_d for the PCM signal (data-shift frequency). f_s and f_d should be synchronized. As discussed in chapter 3, the frame consists of (M) PPM slots plus (i) guard space slots and the input to the frame is $n = \log_2 M$ bit clock periods. The frame time, therefore, will be:

$$\frac{M+i}{f_s} = \frac{\log_2 M}{f_d} \quad (6.1)$$

The parameters M, i, and $\log_2 M$ are integers. If these frequencies are derived by an integer division, (Fig. 6.4), that is:

$$f_s = \frac{f_o}{P} \quad \text{and} \quad f_d = \frac{f_o}{Q} \quad (6.2)$$

Then:

$$\frac{f_s}{f_d} = \frac{Q}{P} = \frac{M+i}{\log_2 M} \quad (6.3)$$

Or $P = \log_2 M$ and $Q = M+i$. Each frame consists of $\log_2 M$ periods of $\frac{f_o}{M+i}$ or $(M+i)$ periods of $\frac{f_o}{\log_2 M}$. But if f_d is to remain fixed as other parameters vary (i.e. M, i, and f_s), then f_o must vary, so f_o must then be synthesized. Let f_o be derived by variable division from crystal frequency f_x . Hence, $f_o = \frac{f_x}{R}$ and:

$$f_d = \frac{f_x}{(M+i)R} \quad (6.4)$$

where R is an integer. $(M+i)R$ is to be constant for all values of M and i , hence this can be done only over a limited range. In an alternative solution, we assume that f_s is a prime source, as shown in Fig. 6.5, then; $f_s = \frac{f_x}{K}$, and $f_d = \frac{f_x \cdot P}{Q}$. Hence:

$$f_d = f_x \cdot \frac{P}{Q \cdot R} \tag{6.5}$$

For constant f_d and f_x : $KP = QR$, where K is a non-integer constant and:

$$R = K \cdot \frac{P}{Q} = K \cdot \frac{\log_2 M}{M+i} \tag{6.6}$$

But R must be an integer, so similar problem arise as above, and f_x must be synthesized.

From the above analysis it can be concluded that exact solutions for generating f_d and f_s from fixed f_o do not exist for range of parameters (M, i) . It can be done only in certain specific cases.

For this reason only certain values for P, M, i , and m were chosen to build the experimental PPM system; which can be realized practically using TTL integrated circuits. The PPM system has been built for $M=4, 8$, and 16 , $m=0.8$, and $f_d=4$ Mbit/s. The block diagram of Fig. 6.6 shows the frequency divider used in the transmitter, where frequency division is done by a programmable divide by n -counter. Table 6.1 shows the slot frequencies and the values of P, R , and Q , for different values of M .

M	f_s (Mbit/s)	T_f (μ s)	M+i	R	P	Q
4	10.00	0.50	5	2	2	5
8	13.33	0.75	10	1	3	10
16	20.00	1.00	20	1	2	10
32	32.00	1.25	40	1	-	-

Table 6.1 Frequency synthesis for different values of M .

6.4-PACKET GENERATION

Local Area Networks (LANs) operate in packet mode [STALLINGS], sending data over the network by packets which are sent through the network one at a time. The information at the source end is divided into a number of packets and transmitted over the network to the destination where it is assembled to retrieve the original information. A typical maximum length of a packet is 1000 to a few thousand bits [STALLINGS]. For the experimental PPM system designed for LAN use, this packet or block consists of clock synchronization pulses, frame synchronization pulses, and a data field (Fig. 6.7). The packet is preceded by the slot synchronization characters, which are used for clock synchronization and their number depends on the time required by the receiver PLL to lock on to the transmitter frequency. Their pattern was identical to an un-modulated PPM, and their pulse width equal to the PPM slot width. This choice will keep the temperature rise inside the optical source emitter, which is depend upon the pulse width and the distance between the pulses, to a minimum (see chapter 4). The number and width of frame synchronization pulses depends on the design, and are used to enable the decoder to determine the beginning of the block of data. The frame synchronization pulses were chosen such that the bit pattern is significantly different from any of the regular characters being transmitted. The receiver thus is alerted to an incoming block of data by the frame synchronization characters and accepts data until the end of the packet. Their pulse width was chosen to be identical to PPM pulse width, and their number were two in the 16 bit frame chosen. The pattern chosen which gives a minimum increase in the temperature of the optical source was 1000000010000000. Fig. 6.8 shows the circuit diagram of the packet generator which has been designed and built using TTL integrated circuits.

The packet generator can transmit successive short packets or transmit one very long packet so that bit error rate tests can be conducted. The

switches S1 and S2 are used for these purposes. The number of clock synchronization pulses can be varied in a packet using the switches S3. Fig. 6.9 shows the timing diagram for the packet generator. Fig. 6.10 shows the photograph of a transmitted packet. To make sure that the operation of the system is reliable and the switching speed is very high, attention has been paid to the design of the printed circuit board (PCB) and the physical arrangement of the components on it. These problems were considered carefully during the design of the system. A ground plane on the component side is provided to minimise the flux linked by the loops formed. The PCB is housed in an earthed metal case, using coaxial sockets for signal connections.

6.5-OPTICAL SOURCE DRIVER

Optical sources used in fiber systems are high-current low-impedance devices. Typical operating currents exceed 100 mA, and typical impedances are a few Ohms. Thus for efficient operation, high-current low-impedance transistors are needed. To attain the highest speed from an LED, one must resort to a low-impedance driver, one that supplies a low-impedance voltage-step, the space charge and diffusion capacitance are thus charged as rapidly as possible. The LED driver must be able to generate enough current to allow the LED to develop its required optical output power, and it must switch this current on and off in response to the input data, implementing rise and fall times consistent with the maximum expected baud rate [PERSONICK, LACY, SENIOR].

Unlike LEDs, lasers are threshold devices. Light output is proportional to the incremental current above threshold. The forward current of the laser diode must be held at a constant value above threshold point to maintain a constant radiant flux output. The operating temperature must be stabilized to prevent output drifts (see chapter 4).

The designed block generator has two outputs; one of them is compatible with a TTL driver circuit and the other is compatible with an ECL driver

circuit. The output of the packet transmitter is applied directly to the optical transmitter driving circuit.

An ELED driving circuit was designed and built as shown in Fig. 4.24; which is an emitter follower and is the simplest low-impedance driver type. The maximum current flow through the ELED is limited by the resistor connected to the emitter of the transistor. The transistor is fixed on a heat sink. The driver circuit can interface a standard TTL source to the ELED. The ELED drive current may be adjusted by resistor R , and should be set for the proper ELED power output level needed for system operation, although it can be increased up to 1.6 A. This circuit gives very high speed, the rise and the fall times of the circuit-LED combination was less than 3 ns. The coder may also used with an ECL compatible laser diode drive circuit. The driving circuit used for the laser diode is discussed in chapter 4 (Fig. 4.7), and used for measuring its characteristics and its suitability for PPM system. The practical results obtained from this PPM transmitter using the ELED discussed in chapter 4, are described in chapters 7 and 8.

6.6-SUMMARY

The design of an experimental optical PPM transmitter is discussed in this chapter. The driver circuit for the PPM system must be designed to work efficiently with a high-current, low-impedance optical source, and low-duty cycle pulse. The rise and the fall time of the driver circuit should be very low. The speed of the coder and the block generator designed can be increased up to 30 Mbit/sec, or the slot width can be decreased down to 33 ns.

An ELED can be used with compatible TTL driver circuits to give a very high peak to average output power, which makes it suitable for PPM system.

6.7-REFERENCES

- HECHT, J., "Understanding fiber optics", Howard W. Sams & Company, USA, 1987, Chapter 6.
- GRUBER, J., MARTEN, P., PETSCHACHER, R., and RUSSEK, P., "Electronic circuits for high bit rate digital fiber optic communication systems", IEEE Trans. on Commun., Vol. COM-26, No. 7, July 1978, pp. 1088-98.
- LACY, E. A., "Fiber optics", Prentice-Hall, 1982, Chapter 3.
- PERSONICK, S. D., "Design of receivers and transmitters for fiber systems", Chapter in fundamentals of optical fiber communications, by BARNOSKI, M. K., Academic-Press, 1981, pp. 295-326.
- SENIOR, J., "Optical fiber communications: principles and practise", Prentice-Hall, London, 1985, Chapter 10.
- SHUMATE, P., and DIDOMENICO, M., "Lightwave Transmitters" Chapter in topics in applied physics: semiconductor devices for optical communication, by KRESSEL, H., Springer-Verlag, 1980, pp. 161-198.
- STALLINGS, W., "Local Networks: An Introduction", Macmillan Publishing Company, New York, 1984, Chapters 2, and 8.

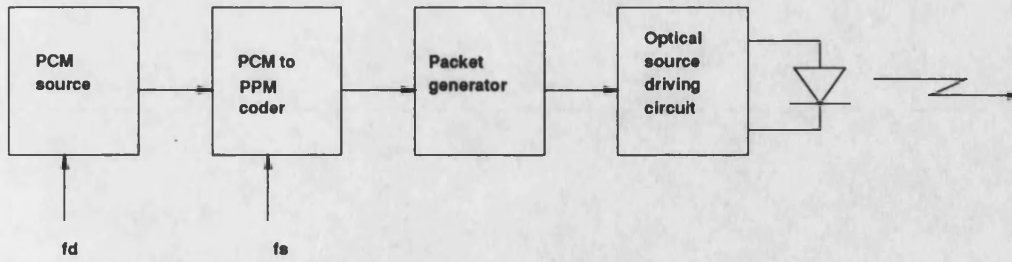


Figure 6.1 The block diagram of the PPM transmitter

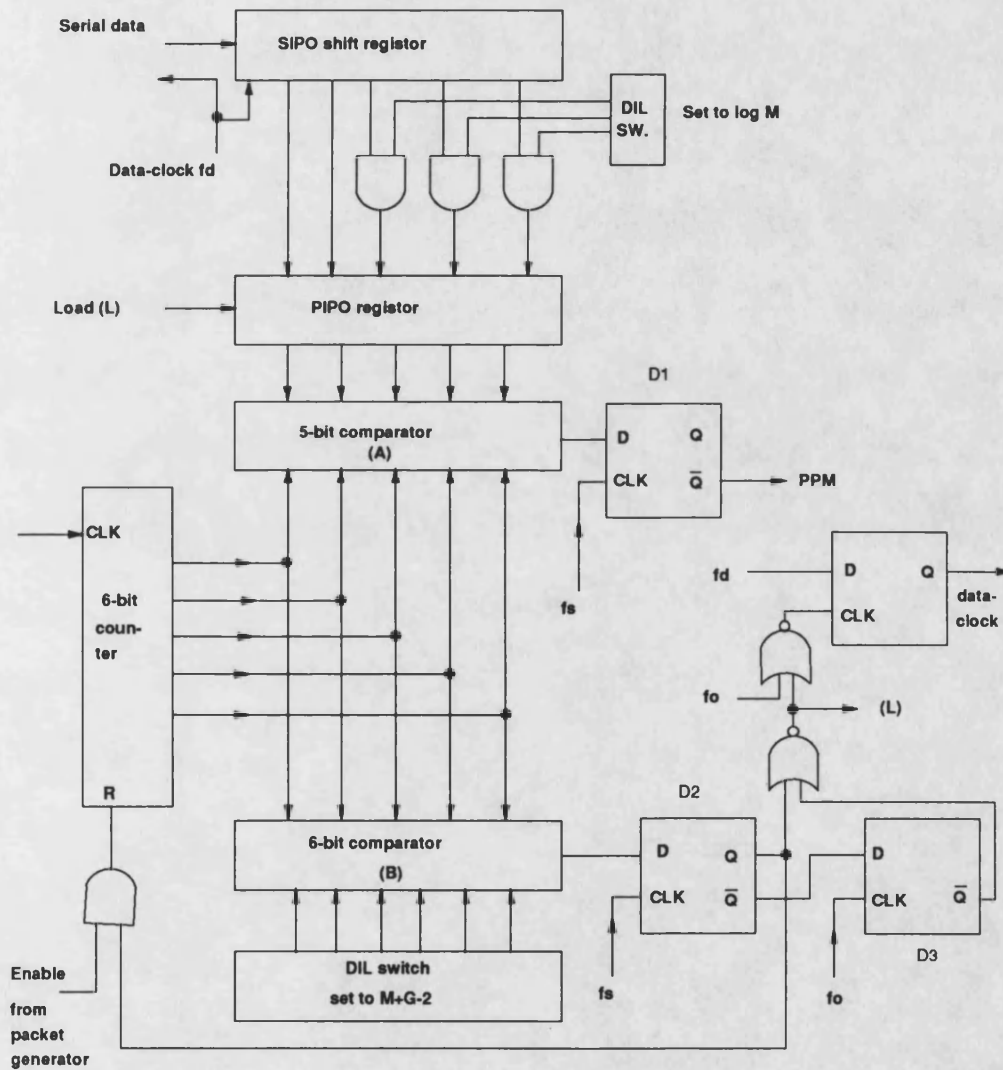


Figure 6.2 The PPM coder

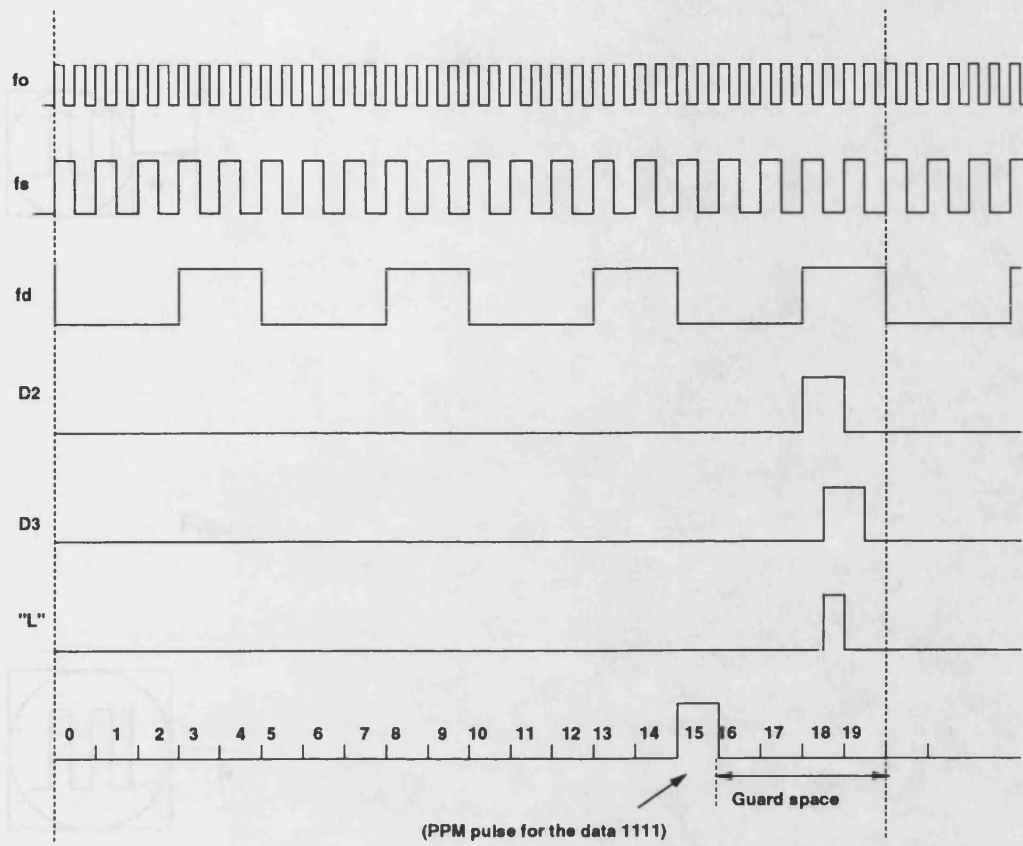


Figure 6.3 The timing diagram of the PPM coder
(for $M=16$, and $m=0.8$)

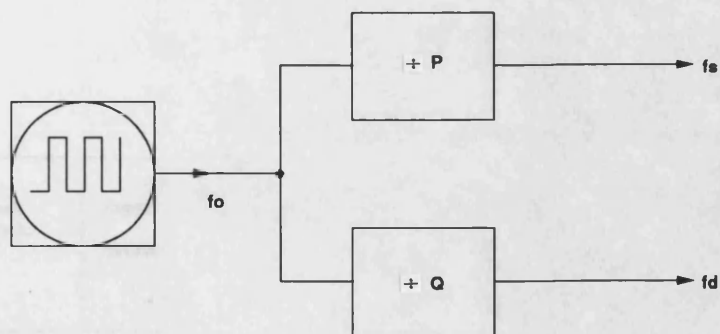


Figure 6.4 Frequency synthesis by an integer division

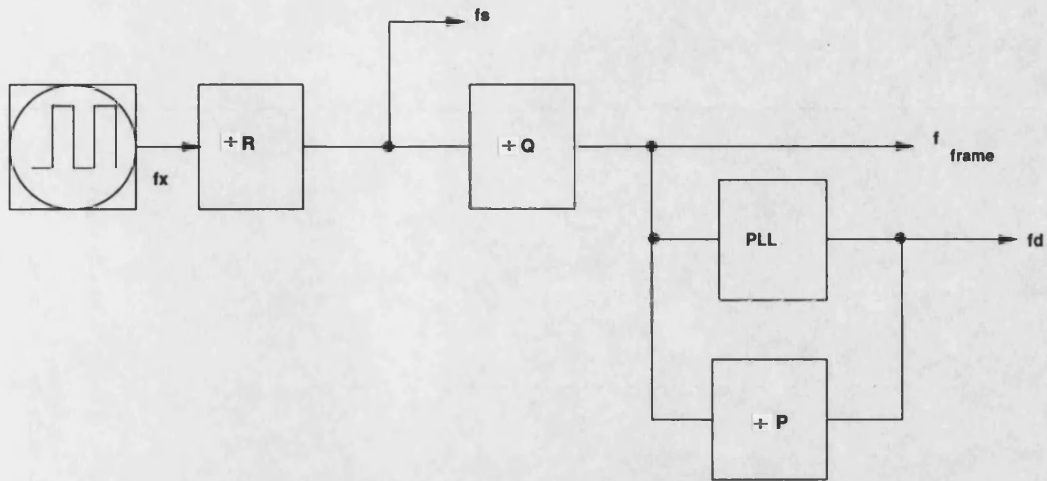


Figure 6.5 Frequency synthesis

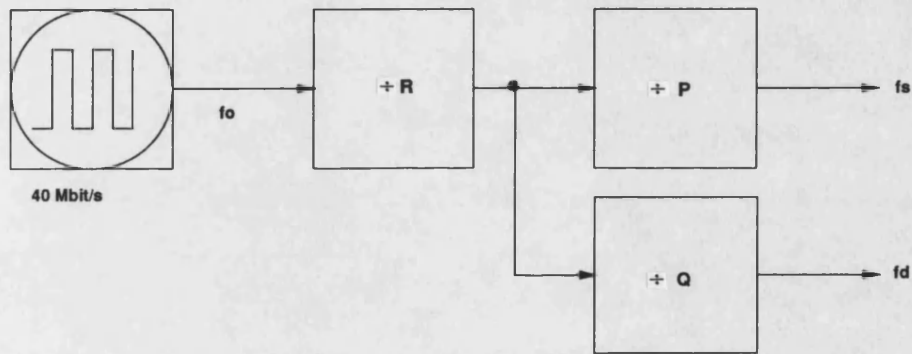


Figure 6.6 The frequency divider used in the transmitter

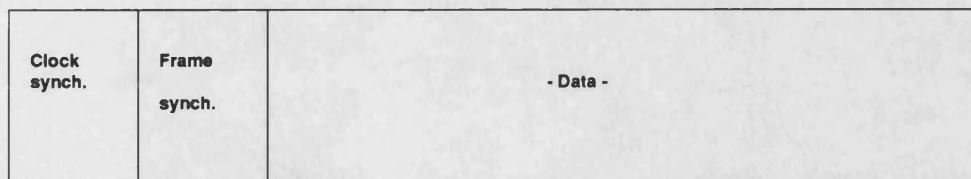


Figure 6.7 The transmitted PPM packet

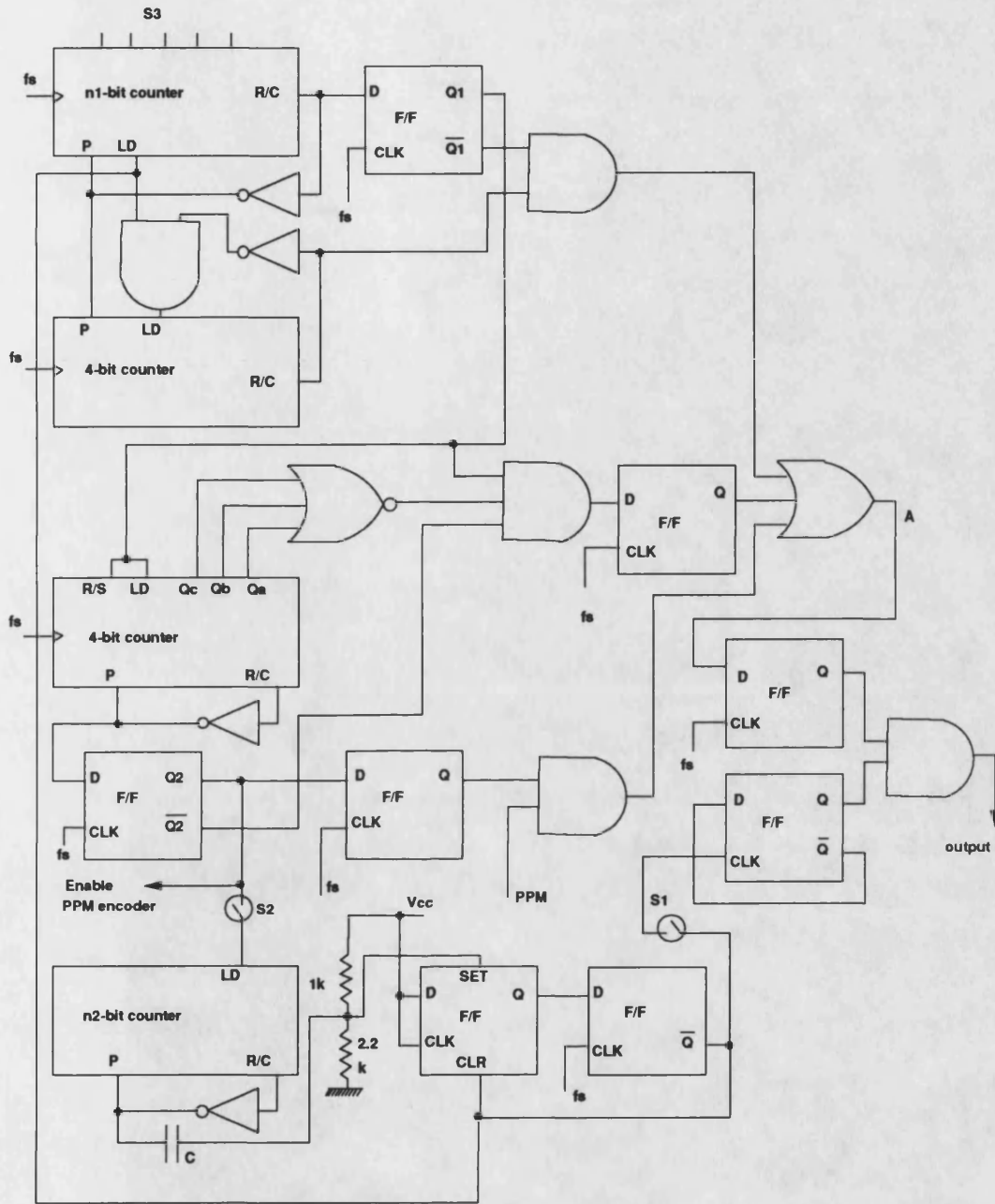


Figure 6.8 The packet generator

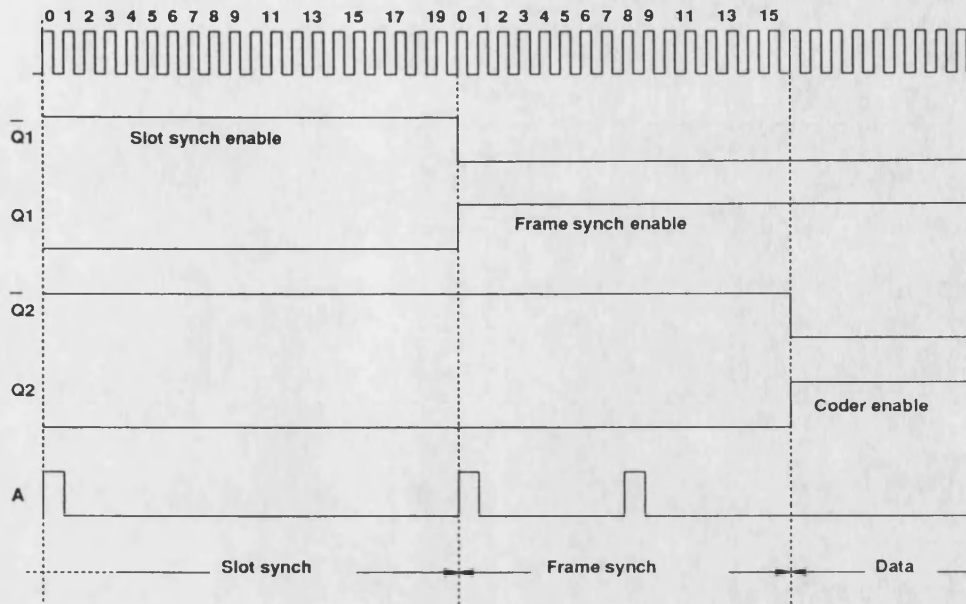


Figure 6.9 The timing diagram of the packet generator

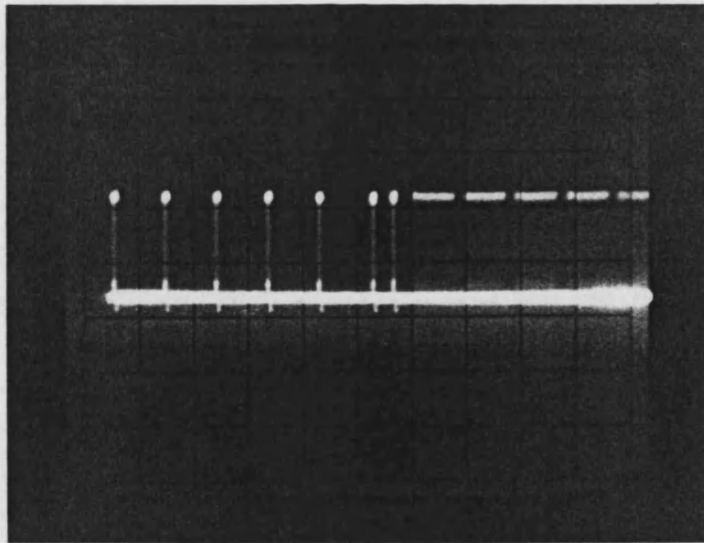


Figure 6.10 A transmitted packet

Horizontal scale = $1\mu\text{S}/\text{div}$.

Vertical scale = $100\text{ mA}/\text{div}$.

CHAPTER -7-
THE OPTICAL PPM RECEIVER

7.1-INTRODUCTION

The purpose of an optical receiver is to detect the light incident upon it and to convert it to an electrical signal containing the information impressed on the light at the transmitted end. A practical PPM receiver consists of a photo-detector, an amplifier, and signal processing circuitry, which first recovers the original PPM format and then decodes it into PCM.

The design of an optical receiver is much more complicated than that of an optical transmitter because the receiver must first detect weak, distorted signals and then make decisions on what type of data was sent based on an amplified version of this distorted signal. An ideal receiver is the one which offers good sensitivity and wide dynamic range at all wavelengths of interest; uses cheap components, is simple to assemble and operate, reliable, readily available, and so on. No practical receiver is considered ideal, but each offers the desired characteristics in different proportion [BRAIN 85].

The optical PPM signal that gets coupled from the light source to the fiber becomes attenuated and distorted as it propagates along the fiber waveguide. Upon reaching the receiver either a PIN or APD converts the optical signal back into an electrical format, which is then amplified and filtered, before a decision circuit compares the signal in each time slot to a certain reference voltage known as the threshold level. Since the sensitivity of a receiver is dominated by the noise sources at the front end, the major emphasis in the literature has been on the design of a low-noise receiver preamplifier. There are three basic approaches to the design of preamplifiers for fiber optic receivers; the voltage amplifier with low input impedance, the high impedance preamplifier, and the transimpedance preamplifier.

An optimum receiver structure for optical PPM systems can be designed by matching the response of the receiver to that of the incident optical pulse [GARRETT, MUOI]

As discussed in chapter 5, for optimum system performance, it is necessary to extract timing information from the received signal in order to synchronize the process of making decisions at the PPM slot rate. For this purpose, a portion of the amplifier output is fed to a timing recovery circuit that generates a clock signal at the baud rate synchronized with the transitions in the received data.

This chapter will be in two parts. The first part will discuss the basic elements of the digital fiber optic receiver; the pre-amplifier, the photodetector, noise sources, and the receiver sensitivity. The second part examines an experimental digital PPM receiver and how it and its components work. The system is designed to work with different values of M , for a given data rate, to test the effect of varying M and guard space on the performance of the system. Provision is made for operating with discrete packets of data.

7.2-OPTICAL RECEIVER THEORY

7.2.1-PHOTO-DETECTORS

Light-wave receivers use high speed photodetectors for conversion of the incoming light pulses to electrical pulses. There are two types of light detector for optical receivers; they are the PIN photodiode and the avalanche photodiode (APD).

The PIN photodiode is the most commonly employed photodetector in long-wavelength optical communication systems. This reverse-biased device is characterized by the relative ease with which it can be fabricated, its extremely high reliability, low noise, and compatibility with low voltage amplifier circuits. In addition, it is an extremely high bandwidth device [FORREST]. PIN photodiodes have a relatively simple structure, having only a pn junction and a depleted region. There

are no gain mechanisms in this device, thus its maximum efficiency is unity and the gain bandwidth is equal to the bandwidth itself. A PIN diode is chosen if thermal-noise limited operation yields sufficient signal quality.

The most outstanding feature of APDs is that they have an internal gain for the induced photo-current. This is caused by avalanche multiplication of electron-hole pairs that takes place in the diode structure. APDs require a circuit for the high reverse bias voltage that ranges from several tens of volts to higher than 100 V. In spite of this, they are dominant in high speed systems with extended transmission distance because of their high sensitivity. APDs are similar to PIN photodiodes in that they are operated under reverse bias, and therefore in the absence of large background dark current.

In choosing a particular photo-detector we mainly need to determine the minimum optical power that must fall on the photodetector to satisfy the BER requirement at the specified data rate. The minimum detectable signal for both PIN photodiodes and APDs is determined by internally generated electrical noise. For PIN photodiodes, the principal source of noise is "shot noise", which arises from small, randomly varying thermally generated currents [DIXON]. For APDs, the principal source of noise is the probabilistic avalanche process, whereby a pair of carriers undergo multiplication, resulting in signal amplification. Because total noise increases with increasing bandwidth, the minimum detectable signal for both PIN photodiodes and APDs will increase with increasing data rate.

The PIN photodiodes are easier to fabricate and operate and are extensively used for low and moderate data rate lightwave transmission systems. Higher sensitivity APDs are advantageous in applications in which extreme regenerator spacing or higher data rates (>1.5 Gbit/sec) in installed systems are desired. In general, APDs cost 5 to 10 times more than PINs, but in exchange they offer higher sensitivity (10 to 20 dB) [LACY]. Fig. 7.1 roughly illustrates the ranges in which these

devices are applied in a bit rate versus distance chart as well as the coverage range of various systems [NAKAGAMI].

One method of comparing the performance of optical receivers with different detectors is to examine the minimum detectable power at a specified error probability for the received pulses. Fig. 7.2 shows an examples of calculations of the minimum detectable power as a function of the bit rate for an error rate of 10^{-9} .

7.2.2-THE PRE-AMPLIFIER

The performance of a receiver (in terms of the sensitivity and the dynamic range) depends not only on the properties of the photodetector but also on the characteristics of the preamplifier. Receivers may include one or more amplification stages. Often the first is called preamplification because it is a special low-noise amplifier designed for weak signals. The choice of circuit configuration for the preamplifier is largely dependent upon the system application. There are a number of significant differences in the performance characteristics between PIN and APD which must be considered within the overall design of the receiver.

Three basic amplifier configurations are frequently used in optical fiber communication receivers. The simplest is the voltage amplifier with low input impedance, but this type of preamplifier allows thermal noise to dominate the receiver which may severely limit its sensitivity. The other two preamplifier configurations, which are preferred for low noise operation, use either a high impedance integrating front end or a transimpedance feedback amplifier. A high input impedance amplifier together with a large detector bias resistor, reduces the effect of thermal noise but also decreases the transmission bandwidth by combining with the input capacitance, including that of the optical detector, and has a limited dynamic range [AIKI].

To overcome the drawbacks of the high input impedance amplifiers we use

a low noise high input impedance amplifier with negative feedback (transimpedance amplifier), which finds wide application for optical fiber applications. This transimpedance preamplifier acts as a current-voltage convertor, gives low noise performance, and has the advantages over a high input impedance design of an improved dynamic range and a high frequency response achieved without the use of a subsequent equalization stage. However, in practice the noise performance of the transimpedance amplifier is not quite as good as that achieved with the high impedance structure due to the noise contribution from the feedback resistor. Nevertheless the transimpedance design incorporating a large value of feedback resistor can achieve a noise performance which approaches that of the high impedance front end. The preamplifier may be integrated with the detector, as in a PIN-FET receiver. In this case the noise in the load resistor can be avoided, and the technique gives a high-impedance design with low noise, but also results in a low dynamic range.

7.2.3-NOISE CONSIDERATIONS IN OPTICAL RECEIVER DESIGN

Noise is the major limiting factor in receiver design. Receiver noise is caused by the spontaneous fluctuations of current or voltage in electronic circuits, and two major types are thermal noise and shot noise. Shot noise arises in electronic devices because of the discrete nature of current flow in the device. Thermal noise arises from the random motion of electrons in a conductor. In a photodiode, shot noise arises from random generation and re-combination of free electrons and holes. The mean-square shot noise current is [PALAIS]:

$$\overline{i_{NS}^2} = 2eI\Delta f \quad (7.1)$$

where e is the magnitude of the charge on an electron, I is the average detector current (which includes both the average current generated by the incident optic wave and the dark current), and Δf is the receiver

bandwidth. The shot noise spectrum is uniform over all modulation frequencies of interest [PALAIS]. According to Eq. 7.1, shot noise increases with current, and hence with an increase in the incident optic power, but the signal power increases with the square of the signal current, so the signal to noise ratio increases. When using an APD an additional shot noise arises from the statistical nature of the multiplication process [PALAIS].

Thermal noise originates within the photodetector load resistor R_L due to thermal interaction between the free electrons and the vibrating ions in a conducting medium. The mean square thermal noise current in a resistor R_L may be written as [PALAIS]:

$$\overline{i_t^2} = \frac{4KT\Delta f}{R_L} \quad (7.2)$$

where T is the absolute temperature, and K is the Boltzmann constant. Since the noise of a PIN photodiode receiver is due mainly to thermal noise sources in the preamplifier, substituting an APD can allow operation with appreciable avalanche gain before the multiplied shot noise on the photo-current becomes significant. There is then an optimum gain for APD at which the SNR of the PCM received signal, is a maximum. For example, in Fig. 7.2 APDs are more sensitive for speeds of 10 Gbit/s and beyond. On the other hand, the combination of a PIN photodiodes with FETs has more superiorities, such as the cost and low operating voltage.

Signal amplification is always accompanied by an equal amount of noise amplification and the amplifier contributes additional noise of its own. The main design criteria to evolve a low-noise optical receiver is to select an appropriate detector and active devices to minimize the total receiver noise for a given bit rate.

7.2.4-RECEIVER SENSITIVITY

The receiver sensitivity, of a PCM system, is defined as the average received optical power in decibels relative to 1 mW which must be fed to the photodiode for achieving a bit error rate of 1 in 10^9 . When using a PPM system the sensitivity of the system improves compared with the definition above. As noise sources within the preamplifier may be dominant, its configuration and design are major factors in determining the receiver sensitivity.

The optical sensitivity of a receiver using an APD as a photodetector is mainly determined by APD shot noise produced in the optical current multiplication process and the optical receivers own noise within the transmission bandwidth. In receivers using PIN photodiodes, since the noise is dominated by thermal noise sources in the preamplifier, the sensitivity can be improved only by reducing the noise of the preamplifier, as in the PIN-FET hybrid [SMITH]. PIN-FET hybrid offers a better sensitivity than other forms of PIN photodiode receiver. A good sensitivity at higher bit rates requires a low input capacitance. For lower bit rates, the dark current can be a dominant source of noise; hence PIN and FET should be designed to have low leakage currents [BRAIN84]

In comparison, a bipolar transistor is a cheaper component than a FET and offers higher values of transconductance, but at the expense of a higher level of noise (arising from the shot noise in the base current) and a higher input capacitance [SMITH].

To provide good sensitivity, the frequency response of a digital optical receiver must be uniform for the range of frequencies over which the transmitted power is distributed. [PERSONICK] has shown that an integrating front-end design can improve the sensitivity of both APD and PIN based receivers, since this allows the spectral density of thermal noise sources at the input to be minimized.

Receiver sensitivity can be calculated from knowledge of detector

responsitivity and noise current output at a given wavelength and receiver front end noise floor. This number varies widely and depend on the exact receiver configuration chosen. For example, the sensitivity of the receiver (P35-6661) used in this work, which has a detector responsitivity of 0.8 and diode dark current of 20 nA, is equal to -40 dBm.

Shot noise and thermal noise currents of this receiver can be calculated using the equations 7.1 and 7.2 respectively. From Eq. 7.2, the rms thermal noise current of this receiver is equal to 5.6 nA, and the thermal noise voltage is equal to 0.28 mV. To calculate the signal current for 10^{-9} PCM error rate to compare it with the thermal and shot noise currents of this receiver, Eq. 3.46 can be used. From Fig. 3.10, for the probability of error 10^{-9} , SNR is equal to 19. When the thermal noise dominates over shot noise, the SNR is given by [PALAIS]:

$$SNR = \frac{R_L(\rho P)^2}{4KT\Delta f} \quad (7.3)$$

where ρ is the responsivity of a detector. From this equation, the signal current is equal to 26.16 nA. The shot noise current which corresponds to this value of signal current can be calculated using Eq. 7.1, which gives $\sqrt{i_{Ns}^2} = 1.16$ nA. It is clear that the shot noise current for this receiver is very small compared with thermal noise and can be ignored. The thermal noise voltage is amplified and at the input of the comparator its rms value is 4.4 mV. The rms noise voltage measured at the input of the comparator is equal to 3.8 mV which is very close to the calculated value.

7.3-THE PRACTICAL DESIGN

The block diagram of the PPM receiver which has been designed and built for local area network use is shown in Fig. 7.3. The system is originally designed to work at a slot rate of 32 MHz, but due to components speed limitations the maximum slot rate achieved practically

MHz. The output of the receiver RX goes into two branches; one branch is for data regeneration, and the other is for clock recovery. In this part of the chapter, the practical results of designing and testing the block diagram parts are discussed. The overall performance of the receiver for PPM signal input and the PPM system is given in chapter 8.

7.3.1-THE OPTICAL RECEIVER

The type of receiver used in this system is the Plessey PIN-FET transimpedance amplifier P35-6661. As discussed in the previous sections, this type of receiver gives low-noise performance, has wide dynamic range, and has wide frequency response compared with other types. This receiver covers data rates up to 140 Mbit/sec, with a sensitivity (for PCM signal) of -40 dBm, and a bandwidth of 95 MHz. The photodiode responsivity at 1300 nm is equal to 0.8 A/W. The receiver is followed by an emitter follower (buffer), which is followed by the amplifier SL 565. The output of the amplifier which goes into two branches is buffered at each branch to match the output impedance of the receiver with the two branches. The circuit diagram of the receiver used is shown in Fig. 7.4. The receiver is pigtailed with the multimode fiber 50/125.

7.3.2-DATA REGENERATION

To extract the transmitted data from the received PPM signal, the signal at the output of the amplifier is bandlimited by a low pass filter then applied to a decision circuit (comparator). In the analysis of the performance of a PPM system in chapter 3, we assumed that the filter is a matched filter, but an ordinary low-pass filter will not effect the performance of the system too much (≈ 1 dB penalty). A Bessel filter type is used in the system, since this type of filter possess a time delay that is maximally flat. Practically after designing this

Bessel filter, using the terminology of [ZVEREV], for a cut off frequency 20 MHz (for $M=16$, $m=0.8$, and $f_d=4$ Mbit/sec), and implementing the hardware for a third order filter (Fig. 7.5), the characteristic of this filter was measured and is shown in Fig. 7.6. The calculated response is shown also in Fig. 7.6 (the responses are normalized to 0 dB gain at zero frequency).

The LPF is followed by the comparator shown in Fig. 7.7, which is used to sense when a varying signal reaches some threshold value. The circuit exhibits hysteresis. The voltage at which the comparator switches state is given by [GAYAKWAD]:

$$e_i = V_{ref} \pm \frac{R_1}{R_1 + R_2} V_o(sat) \quad (7.4)$$

where V_{ref} is the reference voltage, and $V_o(sat)$ is the saturation voltage. The saturation voltage can take on both its positive and negative saturation values and the amount of hysteresis is thus:

$$V_H \equiv [V_o^+(sat) - V_o^-(sat)] \frac{R_1}{R_1 + R_2} \quad (7.5)$$

If the hysteresis voltage is designed to be greater than the peak-to-peak noise voltage, there will be no false output crossing. Thus V_H tells us how much peak-to-peak noise the circuit can withstand. The amount of hysteresis is directly dependent on the magnitude of the positive feedback fraction ($\frac{R_1}{R_1 + R_2}$). The output of the comparator must switch rapidly between saturation levels and also respond instantly to any change of conditions at its inputs.

The hysteresis parameter calculation for the comparator must be related to the rms noise voltage, and the expected signal pulse level at its input. The rms value of the noise voltage calculated in section 7.3 is equal to 4.4 mV at the input of the comparator, and the expected signal level is more than 10 mV for the ranges of the measurements. Then choosing $V_H=10$ mV is reasonable.

The values chosen for the design are; $V_H=10$ mV, $V_o^+(sat)=5$ V, and $V_o^-(sat)=-5$ V, then the value of $R_2=100$ k Ω for $R_1=100$ Ω . The reference voltage is

applied to adjust the switching level to minimize the error rate at the receiver. The integrated circuit used for the comparator was NE 521, which has a propagation delay time of 8 ns. The output of the comparator is applied to a D flip-flop (D1) to synchronize the received data with the recovered slot frequency, and then this data is applied to the frame synchronizer (section 7.3.4).

7.3.3-CLOCK RECOVERY

At the receiver the clock was recovered from the received data in the following two steps: preprocessing and the PLL. Preprocessing for the purpose of clock extraction is indispensable when the transmitted signal has no spectral line at the bit frequency. Thus, the aim of preprocessing, which consists of linear pre-filtering, differentiation and squaring, is to perform an efficient conversion of the density spectrum of the received signal to a spectral line at the bit frequency (see chapter 5). The practical pre-processing circuit used in this work is discussed below.

7.3.3.1-PREPROCESSING

The practical pre-processing circuit used in this work consists of a low pass filter (LPF), amplifier, squarer, and band pass filter (BPF) as discussed in chapter 5 (Fig. 7.8). An extra amplifier stage is added after the BPF. Fig. 7.8 shows the preprocessing circuit diagram. A Gaussian type LPF is used in the preprocessing circuit to band limit the frequency harmonics of the received signal, and the noise. The preprocessing filter, $h(t) = \sin\left(\frac{2\pi}{T_b}t\right)$, discussed in chapter 5, can be realized practically by a low-pass filter with rms bandwidth $B_o (\approx 1.3\omega_o)$, followed by an ideal differentiator. The cut off frequency of the filter is $1.3\omega_o$, (ω_o being slot frequency). The third-order filter is designed using the terminology of [ZVEREV].

The filter is followed by the differentiator. For the square wave input to the differentiator, the output voltage is proportional to the (RC) charging current in response to a square wave input. The circuit transforms the square wave into a series of short pulses if the time constant $\tau=RC$ is small compared to the period of the input wave. Fig. 7.9 shows the signal at the output of the differentiator for a PPM pulse input. In LANs, the assumption that the received pulse shape is rectangular, is acceptable because the dispersion effect is very low (apart from the receiver bandwidth limitation).

The output signal of the differentiator is amplified using the amplifier NE 592. NE 592 is two stage differential output, wide-band video amplifier (120 MHz). It offers an adjustable gain from 400 to 0 with one external resistor. The amplifier designed for a gain of 50 (the first amplifier in Fig. 7.8).

A nonlinear operation is needed to produce a frequency component at the slot rate, and a square-law device was selected to produce the non-linear effect because of its simplicity. An analogue multiplier accepts two input signals, $v_1(t)$ and $v_2(t)$, and produces an output:

$$v_o(t) = k v_1(t) \cdot v_2(t) \quad (7.6)$$

where k is a constant. The balanced modulator-demodulator MC 1496 will operate as a frequency doubler (squarer) by introducing the same frequency at both input ports. Fig. 7.8 shows the circuit diagram of the balanced-modulator demodulator, MC 1496, which used as a squarer [MOTOROLA]. The differential output of the amplifier NE 592 is connected to the inputs of the squarer.

To reject the unwanted harmonics from the spectrum of the multiplier circuit the band pass filter is used, which is simply a series of parallel LC resonant tank circuits. All the resonant circuits are tuned to the desired frequency, f_s , at each node.

Fig. 7.10 shows the frequency response of the resonant circuit, and from the response $Q=45$. The resonant tank circuit filters out unwanted

sub-harmonics, and the output starts ringing with a decay. The signal from the resonant tank is buffered by the emitter follower which provides power gain with virtually no loading on the tank circuit and avoids degrading the Q of the resonant circuit. The output signal of the filter is amplified again by another stage of NE 592 amplifier to apply it to the PLL. The net gain of the preprocessing circuit from the output the receiver to the input of the PLL is about 32.

7.3.3.2-THE PLL

A PLL is used to derive a clock signal of constant amplitude and adequately constant phase from the spectral line of the slot frequency contained in the preprocessed signal. The spectral line generated by the pre-processing circuit at the slot frequency is applied to the PLL 564, and so generates a clock at the slot frequency. The NE 564 is a monolithic PLL designed for operation up to 50 MHz. It consists of a VCO, limiter, phase comparator, and post detection processor. With the chip inputs connected as shown in Fig. 7.11, the free running frequency of VCO is given by the following equation [SIGNETICS]:

$$f_o = \frac{1}{22R_c C_1} \quad (7.7)$$

where $R_c = 100\Omega$, and C_1 is the external setting capacitance in farads (between pins 12 and 13).

The loop filter is explained by the following equation:

$$F(s) = \frac{1}{1 + RC_s} \quad (7.8)$$

where $R = 1.3k\Omega$. By adding capacitors to pins 4 and 5, two poles are added to the loop transfer function at $\omega = \frac{1}{RC}$. The external filtering used at pins 4 and 5 control the dynamic frequency response and stability criteria. The NE 564 is a first order system; therefore the use of single capacitors (at pins 4 and 5) will automatically create a second-order system. An RC series filter combination will cause a

lead-lag condition that will permit dynamic selectivity, along with closed-loop stability (see chapter 5, section 5.3.1).

The phase detector conversion gain (k_d) and the VCO conversion gain (k_o) determine, in large part, the lock range, capture range and linearity characteristics of the NE 564. These device parameters are both dependent upon bias current (I_2 at pin 2) and operating frequency [SIGNETICS].

The frequency of the VCO can be controlled by a crystal instead of the capacitor C_1 (Fig. 7.12). The equivalent circuit of a quartz crystal and its reactance characteristics with frequency is shown in Fig. 7.13 [BONEBREAK]. Its equivalent circuit contains two capacitors, giving a pair of closely spaced series and parallel resonant frequencies. F_R is called the resonant frequency and is where L_1 and C_1 are in series resonance and the crystal looks like a small resistance R_1 . The frequency F_A is the anti-resonant frequency and is the point where L_1-C_1 look inductive and resonate with C_o to form parallel resonant frequency F_A . The crystal's equivalent circuit provides positive feedback and gain at the resonant frequency, leading to sustained oscillations. The crystal which matches the NE 564 VCO drive characteristic is an "AT" cut oscillator crystal which operates near the anti-resonance or parallel mode. The NE 564 tends to operate at a frequency above the specified value when a series mode crystal is used. In Fig. 7.12 the crystal is operated with a series capacitor, and when properly trimmed, this allows the crystal to operate near the series resonant mode. Under certain conditions the circuit may even tend to operate in the third overtone mode unless measures are taken to roll-off the circuit gain. This is the purpose of the capacitor C_1 in Fig. 7.12.

The PLL circuit is designed and built for $f_o=20$, and 40 MHz, the frequency of the VCO being controlled by a crystal for each frequency.

Fig. 7.14 shows the variation of the lock and hold ranges of crystal controlled PLL with the input signal level for $f_o=20$ MHz. The figure shows that the upper limits for the lock and hold ranges are constants, because the crystal will specify the upper limit for VCO frequency while

the lower limit is specified by the series and shunt capacitors. From Fig. 7.14, for a 50 mV sine wave signal applied to the PLL, its lock range is 12 KHz and its hold range is about 25 KHz.

Next is to relate the physical component values of this PLL with the parameters of design discussed in chapter 5. ω_n and η can be calculated as follows: for 50 mV input signal to the PLL the hold range $\Delta\omega_H = k_o k_d = 25$ KHz. Using the equations discussed in chapter 5, $\omega_n = 28.8$ KHz and $\eta = 0.59$ for the lag-lead filter. Then the noise bandwidth B_L can be calculated using Eq. 5.25 which equal 42.4 KHz. The value of the noise bandwidth should be less than the hold range, and this is because of using a crystal to control the VCO frequency. The crystal specifies the upper limit for VCO frequency which reduces the hold and lock ranges. From the values calculated above, signal jittering at the PLL output can be calculated. For the 50 mV signal input to the PLL and the rms noise voltage 3.8 mV (which is measured, see chapter 8), the signal to noise ratio at the input of the PLL is equal to $(SNR)_i = 13$. Then from Eq. 5.26, the phase jitter at the output of the PLL is equal to $\sqrt{\theta_{no}^2} = 3.6^\circ$, and the signal to noise ratio at the output of the PLL is equal to $(SNR)_L = 122.6$ for the band-pass filter bandwidth 800 KHz. This shows that the PLL improves the signal to noise ratio at its output (see chapter 5), and the phase jitter is very small.

The preprocessor circuit is designed to work with a minimum input signal level of 5 mV at the output of the receiver, in this case the input signal level to the PLL will be about 150 mV.

7.3.3.3-THE LOCK INDICATOR

As discussed in chapter 5, the lock indicator designed and built was a quadrature phase detector. When the PLL locks onto the transmitter slot frequency, the lock indicator enables the decoder.

To get a 90 ° phase shifted version of the VCO frequency to apply to the lock indicator, the delay element 74 LS 31 has been used. The PPM

pulse received is delayed by $\frac{T_c}{4}$ (which is equivalent to 90 ° phase shift). The phase shift or the delay is adjusted approximately for each frequency when the value of M is changed. Fig. 7.15 shows the circuit diagram of the lock-indicator, where the PLL NE 564 is used as a quadrature phase detector and a smoothing filter. Loop filter bandwidth is varied till the output of the filter will be smooth enough. The output of the lock indicator is applied to the comparator, NE 521, which compares the lock indicator output with a preset threshold and gives a logic "one" when the PLL frequency is locked onto the transmitted frequency.

7.3.4-FRAME SYNCHRONIZATION

Under burst conditions, when the PLL is locked onto the transmitted signal frequency, the lock-indicator will enable the frame synchronizer. The receiver should recognize the beginning of the transmitted data in the packet, and this is done by the frame synchronizer. Frame synchronization pulses transmitted are recognized by the frame synchroniser which then enables the decoder to start processing the data in the packet.

Fig. 7.16 shows the circuit diagram of the frame synchronizer as designed and built. Serial data is loaded to the frame synchronizer when lock is indicated and the frame synchronizer is enabled. The serial data is loaded to the shift register SIPO. The comparator, C, has one of its inputs connected to the parallel output of the shift register SIPO and the other set to the transmitted frame synchronizer pattern which is (1000000010000000). This pattern was chosen such that it is significantly different from any of the regular characters being transmitted, while maintaining a low duty rates at the transmitter. This pattern is not changed with M, and gives a minimum increase in the temperature of the optical source (see chapter 6, section 6.4). The comparator gives an

output, a pulse, when its two inputs are equal, which is used to enable the passage of the serial data to the decoder (the output of D4 will be "one"), and enable the decoder.

7.3.5-PPM DECODER

The PPM signal received is now decoded to get the data in its original PCM form. The PPM decoder which is designed and realized practically using transistor-transistor logic integrated circuits is shown in Fig. 7.17. The decoder counter is enabled by the frame synchronizer. The counter is running at a frequency of f_s , its output is loaded to the latch PIPO by a PPM pulse, and this data is then loaded into the shift register to represent the PCM data which needs to be converted to serial form. The comparator A is used to reset the counter at the end of the frame, and has one of its inputs connected to the counter and the other set to $(M-2)$. The output of the shift register PIPO is loaded to the shift register PISO at the end of the frame (in the guard space) by the comparator A output. Then the serial data is shifted out of the shift register PISO at the data shift frequency f_d . PPM pulse width is reduced by delaying the pulse and "Anding" it with the original PPM pulse form (see the timing diagram) to prevent loading to the shift register PIPO at the edge of the counter transition time. Also there is no loading to PISO at the time of data transition because the loading pulse width is very much less than the data-shift clock width. Slot frequency, f_s , and data shift frequency f_d should be synchronous because the counter clear pulse (comparator A output) was used to reset the synthesis frequency divider counter (see chapter 5).

Table 7.1 shows the slot and data shift frequencies generated at the receiver for different values of M.

The multiplexer at the output of the decoder is used to select the output of the shift register PISO for different values of M. The value of M is changed in the decoder by changing the setting of the DIL switch

to reset the decoder counter and the frequency synthesis to get f_d . The decoder designed originally to run at slot rate speed of 32 Mbit/s (when $M=32$), but due to components speed limitations a maximum slot rate of 30 Mbit/s is achieved practically. For this reason $M=32$ is not included in the measurements. Fig. 7.18 shows the timing diagram of the decoder.

M	f_o (of VCO) (Mbit/s)	f_s (Mbit/s)	f_d (Mbit/s)
4	20	10	4
8	40	13.33	4
16	20	20	4

Table 7.1 The slot and data shift frequencies generated at the receiver for different values M.

7.4- SUMMARY.

The design of an experimental optical PPM receiver for a LAN is discussed in this chapter. Clock synchronization for a PPM system is an important part of the receiver, which is carried out by preprocessing the received signal and then applying it to a crystal-controlled PLL. Crystal controlled PLL gives stable VCO frequency with very low drift. A high Q LC resonant circuit tuned to the slot frequency, is placed before the PLL circuit in order to select and reinforce slot frequency information from PPM data and suppress other harmonics. Frequency synthesis at the receiver can be done using a PLL or by direct frequency division using a divide by n counter.

7.5-REFERENCES

- AIKI, M., "Low-noise optical receiver for high-speed optical transmission", J. of Lightwave Technology, Vol. LT-3, No. 6, 1985, pp. 1301-6.
- BRAIN85, M., and LEE, T. P., "Optical receivers for lightwave communication systems", J. Lightwave Tech., Vol. LT-3, No. 6, December 1985, pp. 1281-1300.
- BRAIN84, M. C., SYMTH, P. P., SMITH, D. R., WHITE, B. R., and CHIDGEY, P. J., "PIN-FET hybrid receivers for 1.2 Gbit/sec transmission systems operating at 1.3 and 1.55 μm wavelength", Electron. Lett., Vol. 20, No. 21, Oct. 1984, pp. 894-95.
- BONEBREAK, R. L., "Practical techniques of electronic circuit design", Prentice-Hall, 1987, chapter 4.
- DIXON, R. W., and DUTTA, K. N., "Lightwave device technology", AT&T Technical Journal, January/Feb. 1987, Vol. 66, Issue 1, pp. 73-83.
- FORREST, S. R., "Optical detectors for lightwave communication", chapter in "Optical fiber telecommunications II", MILLER, S. E., and KAMINOW, I. P., Editors., Academic Press, London, 1988, pp. 569-99.
- GARRETT, I., "PPM for transmission over optical fibers with direct or heterodyne detection", IEEE-Transactions on Commun., Vol. COM-31, No. 4, April 1983, pp. 518-527.
- GAYAKWAD, R. A., "Op-Amps and linear integrated circuits", Prentice-Hall, USA, 1988, chapter 9.
- HECHT, J., "Understanding fiber optics", Howard W. Sams & Company, USA, 1987, chapter 7.
- KATZMAN, M., "Laser Satellite Communications", Prentice-Hall, USA, 1987, chapter 3.
- KRESSEL, H., "Semiconductor devices for optical communications", Berlin: Springer, 1980, pp. 89-160.
- LACY, E. A., "Fiber optics", Prentice-Hall, USA, 1982, chapter 6.
- MOTOROLA, "Application note AN-531.
- MUOI, T. V., and HULLETT, J. L., "Receiver design for optical PPM

systems", IEEE-Transactions on Commun., Vol. COM-26, No. 2, Feb. 1978, pp. 295-300.

NAKAGAMI, T., and SAKURAI, T., "Optical and opto-electronic devices for optical fiber transmission systems", IEEE-Commun. Magazine, Vol. 26, January 1988, pp. 28-33.

PALAIS, J. C., "Fiber optic communications", Prentice Hall, USA, 1988, chapter 11.

PERSONICK, S. D., "Receiver design for digital fiber optic systems", Bell Syst. Tech. J., Vol. 52, No. 6, July-Aug. 1973, pp. 843-86.

SIGNETICS, "Fiber-optic communication data and applications", 1988.

SMITH, D. R., HOOPER, R. C., and GARRETT, I., "Receivers for optical communications: a comparison of avalanche photodiodes with PIN-FET hybrids", Opt. Quantum Electron., Vol. 10, 1978, pp. 293-300.

ZVEREV, "Handbook of Filter Synthesis", Wiley, 1967.

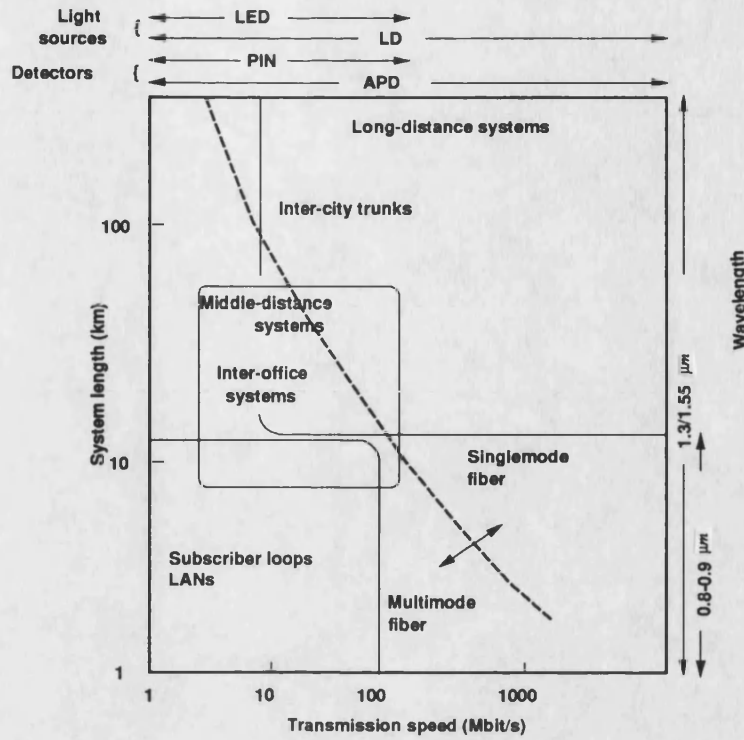


Figure 7.1 Application for optical fiber transmission systems, light sources, and detectors [NAKAGAMI].

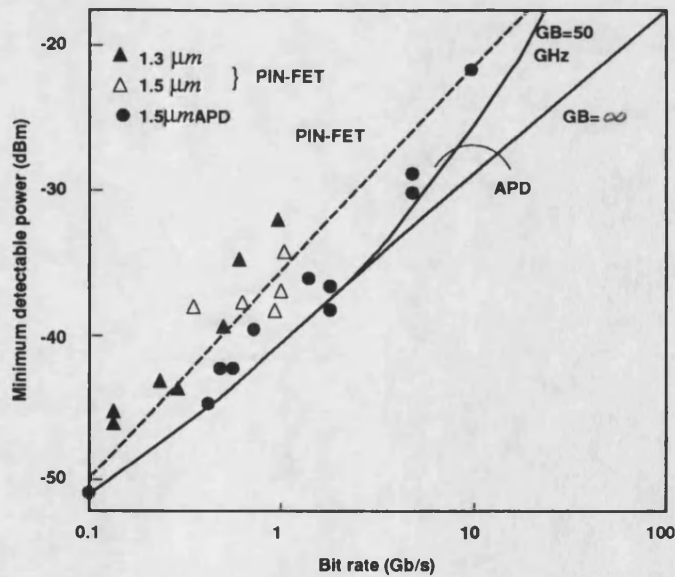


Figure 7.2 Minimum detectable power at an error rate of $1E-9$ as a function of the bit rate [NAKAGAMI]

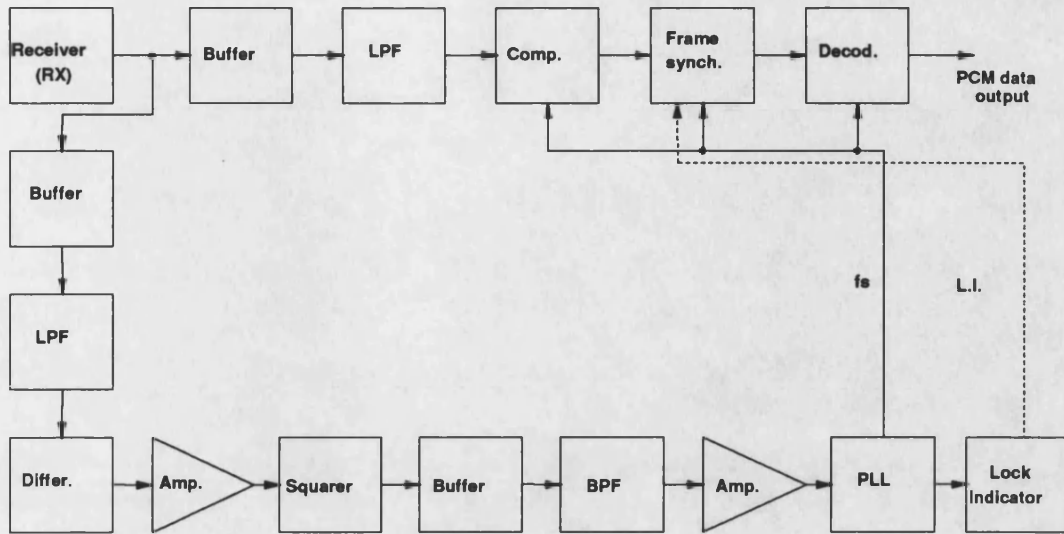


Figure 7.3 The block diagram of the PPM receiver

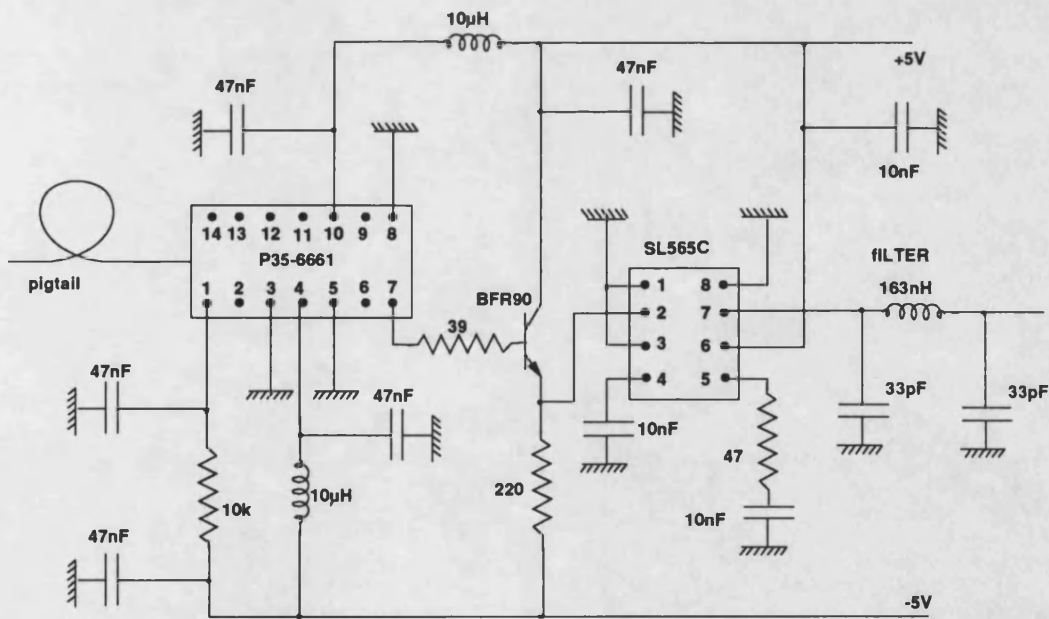


Figure 7.4 P35-6661 140 Mbit/s circuit diagram

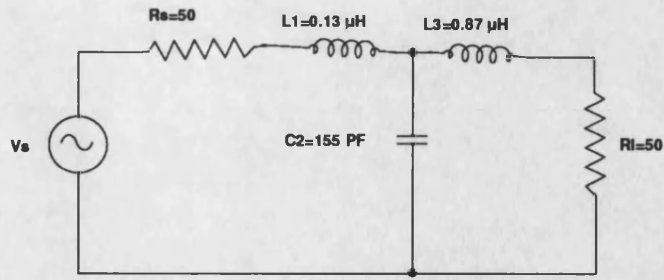


Figure 7.5 The Bessel filter

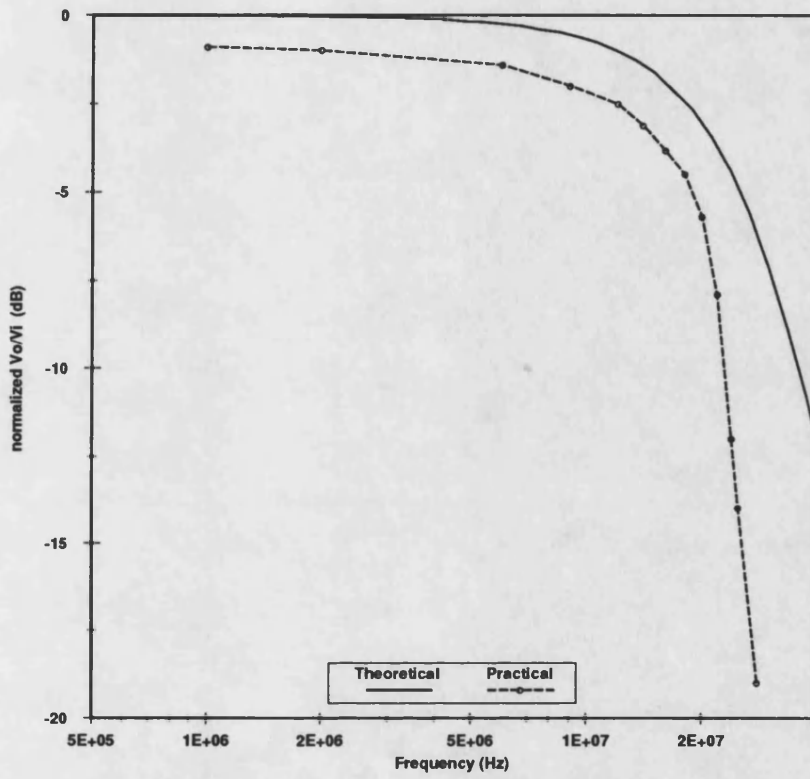


Figure 7.6 The characteristics of the low-pass filter

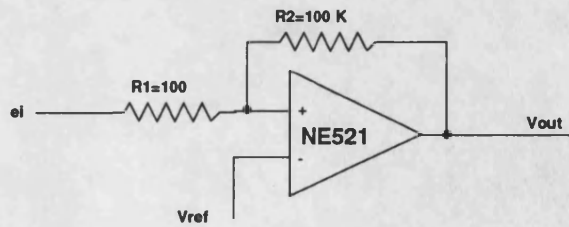


Figure 7.7 The comparator

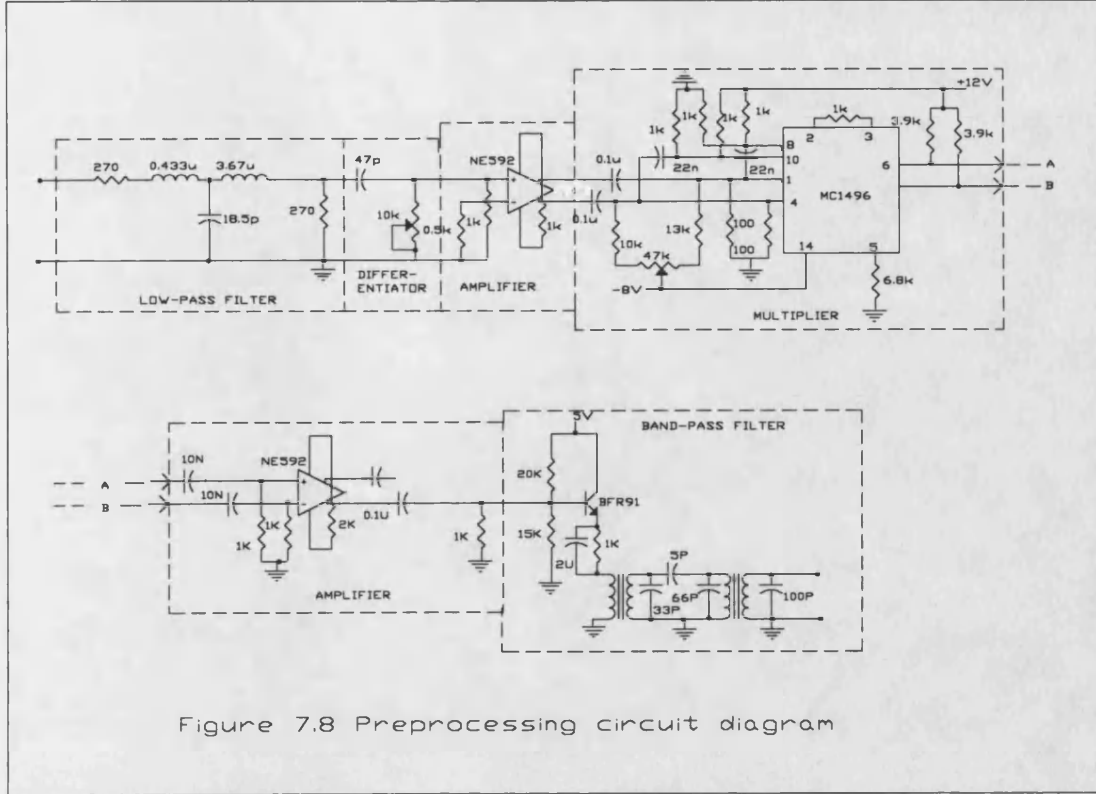


Figure 7.8 Preprocessing circuit diagram

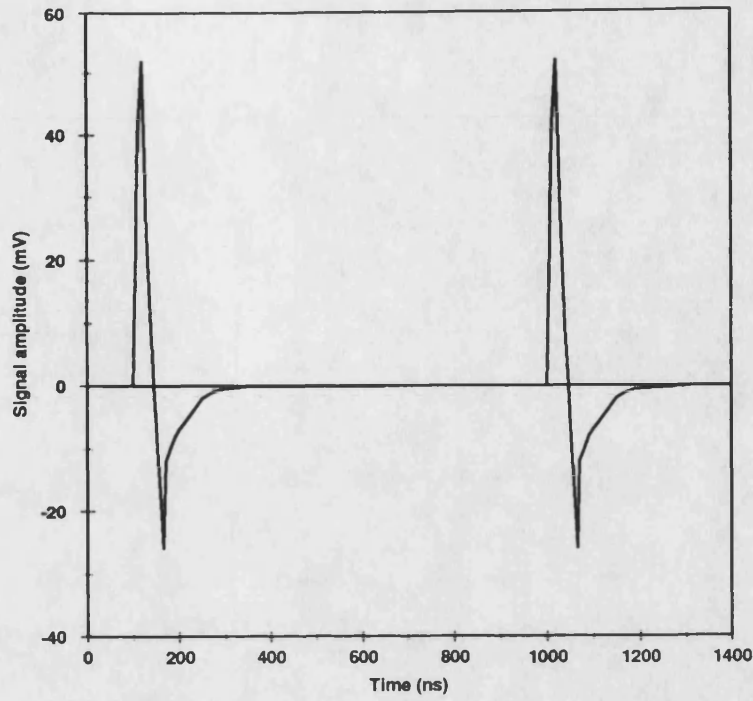


Figure 7.9 Differentiated PPM signal

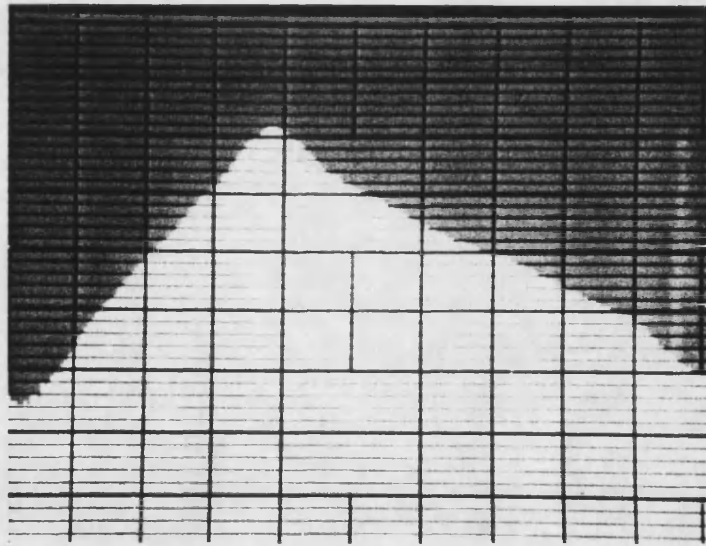


Figure 7.10 Frequency response of the band-pass filter

$f_0 = 20 \text{ MHz}$

Vertical scale : 10 dB/div

Horizontal scale : 1 MHz/div

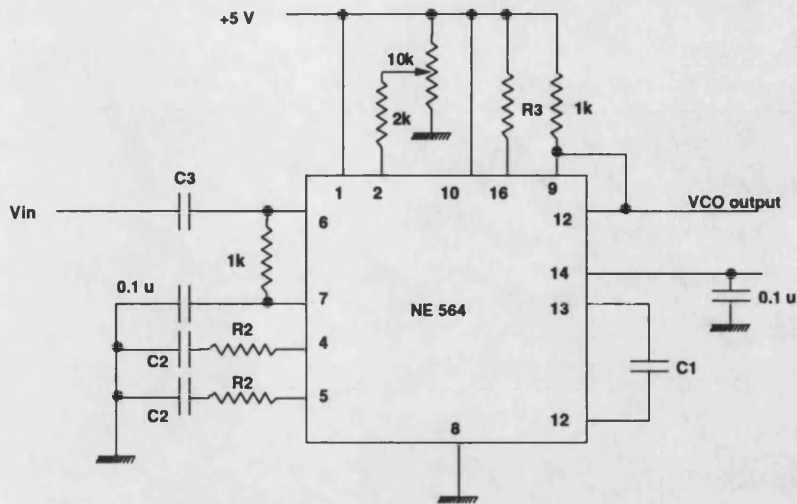


Figure 7.11 The PLL NE 564

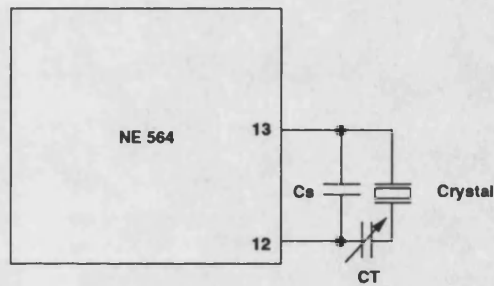


Figure 7.12 Crystal controlled PLL

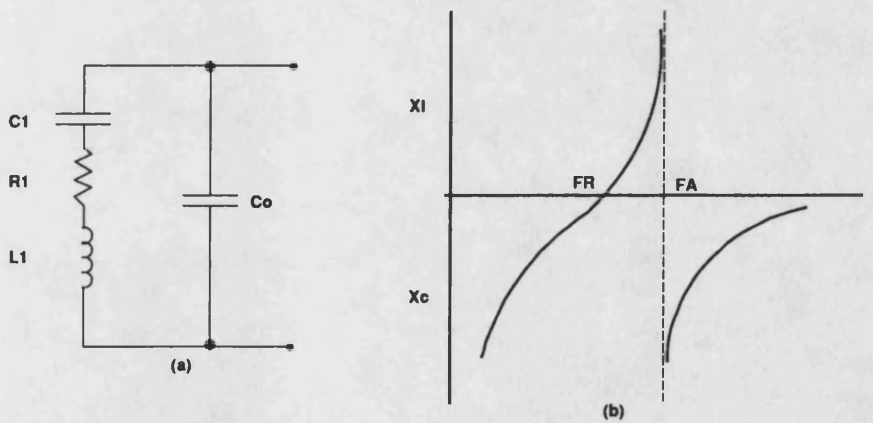


Figure 7.13 (a) Crystal equivalent circuit and (b) Reactance of crystal resonator

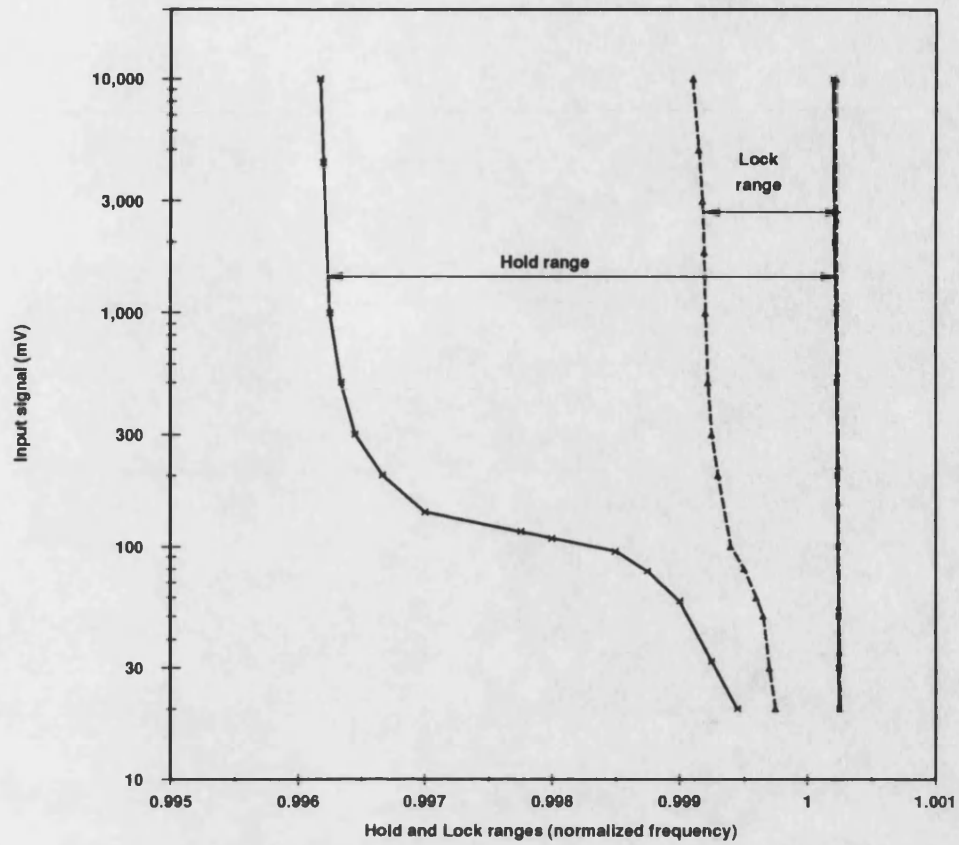


Figure 7.14 Crystal controlled PLL characteristics

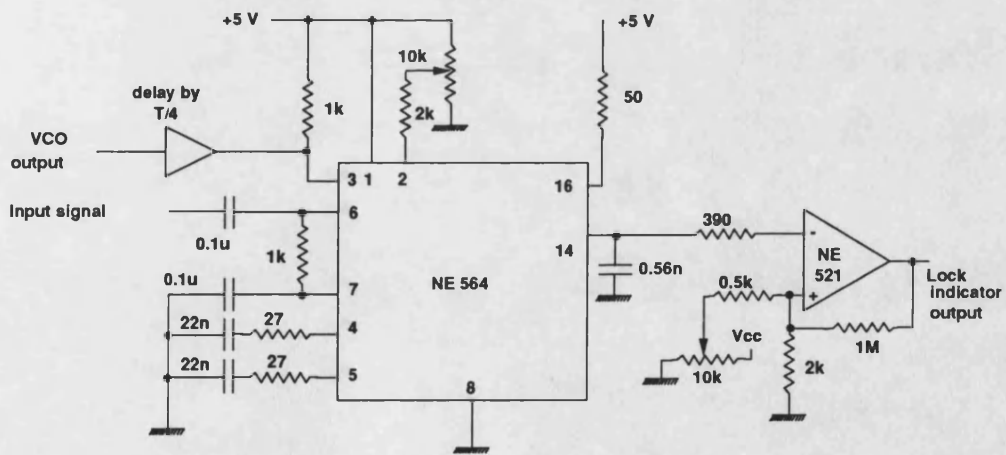


Figure 7.15 The lock indicator

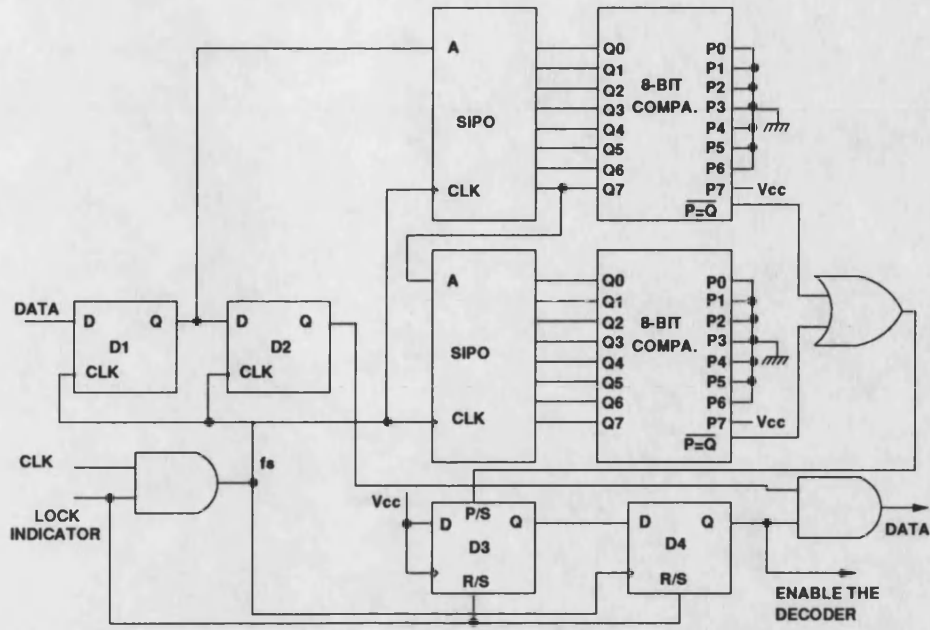


Figure 7.16 The frame synchronizer

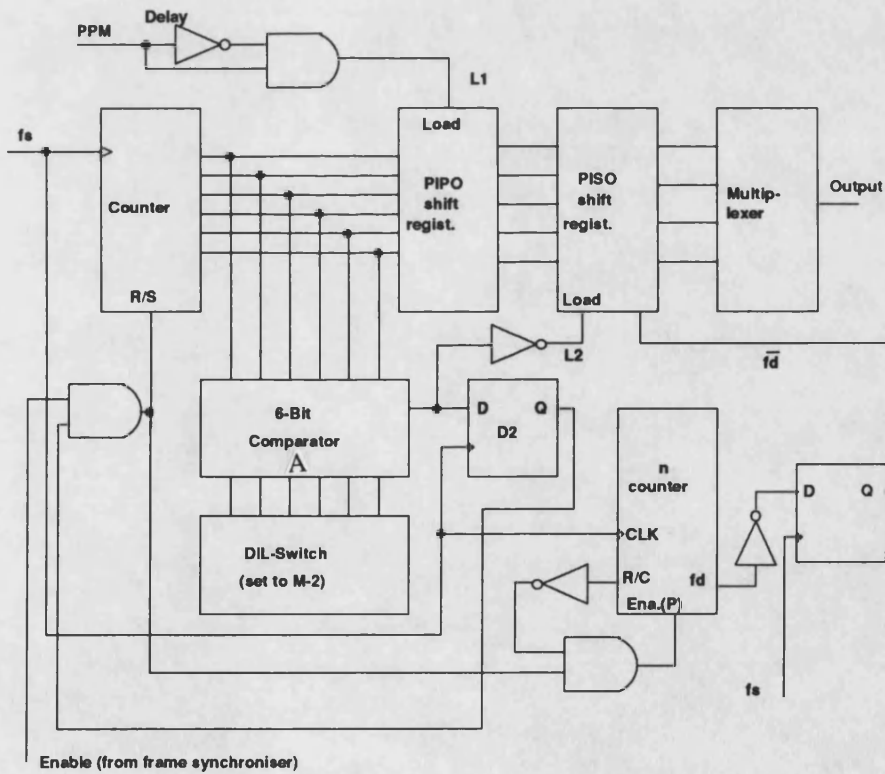


Figure 7.17 The PPM decoder

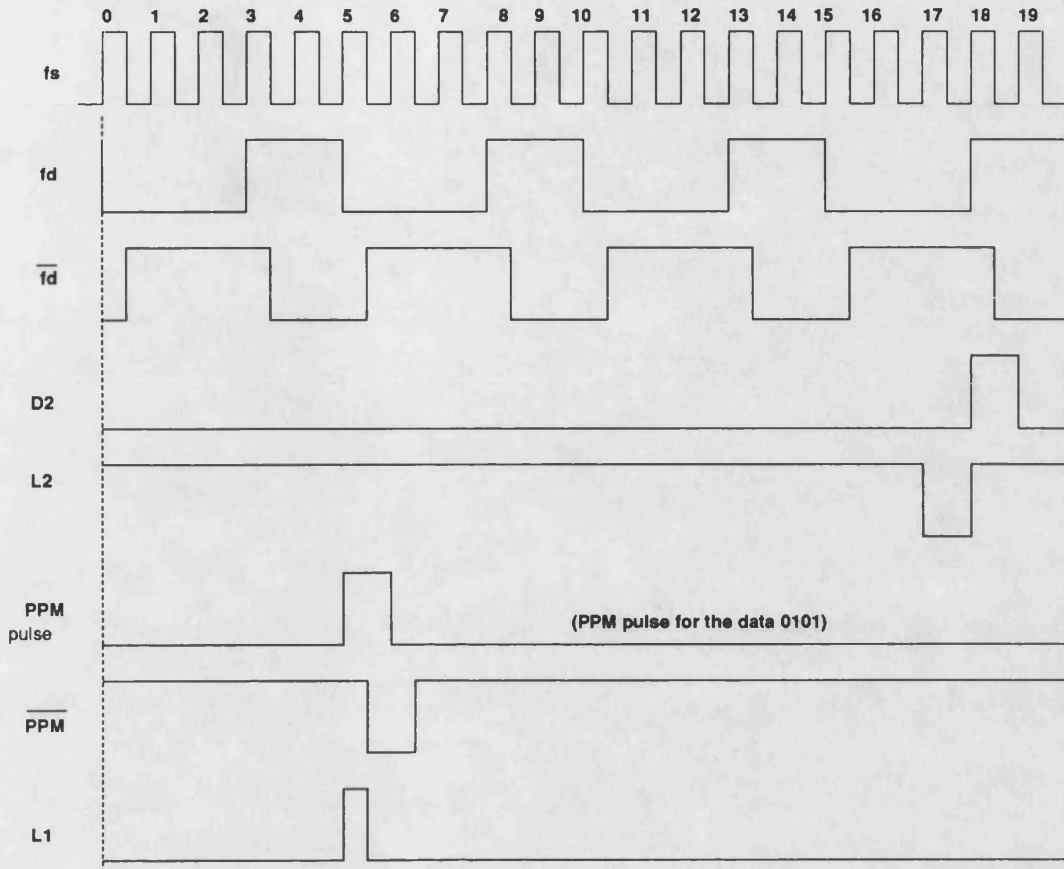


Figure 7.18 Timing diagram of the decoder

CHAPTER -8-
PRACTICAL PPM SYSTEM

8.1-INTRODUCTION

An optical system consists of a transmitter, receiver, and a transmission channel. The block diagram of the experimental optical PPM system which has been designed and built in this work for local area network use is shown in Fig. 8.1. The PPM transmitter designed in chapter 6, and the PPM receiver designed in chapter 7 are used in the system. The transmission channel is an optical fiber arranged as shown in Fig. 8.1. The optical attenuator is used to vary the optical power received by the receiver, and the 3-dB coupler which follows the attenuator, is used to divide the optical power equally between the receiver and the power meter so that the average optical power received by the receiver can be measured.

The bit error rate (BER) is one of the basic measures for the quality of transmission in digital systems, and is usually specified as a target for the design of such systems. This parameter is usually obtained using a test sequence of a fixed period from a PRBS generator. The target value of the BER depends on the practical application areas, for digital telecommunication purposes a design target of $P_e \leq 10^{-9}$ is often assumed. The relation between the BER and the required signal to noise ratio can be calculated from the statistics of signal detection (see chapter 3). In this chapter the measured BER of the PPM system as designed and built, is presented as a set of results for $M=4, 8,$ and 16 . The practical system is also used without the coder and the decoder, as a PCM system, and its performance is measured to compare it with the performance of the PPM system under the same optical conditions.

The clock recovery circuit performance of the PPM system is discussed also in this chapter.

8.2-CLOCK RECOVERY CIRCUIT PERFORMANCE

In this section the performance of the clock recovery circuit for a PPM pulse input, is measured. The circuit parts are discussed in chapter 7 and the complete circuit diagram is shown in Fig. 8.2. The measurements in this section are done for $M=16$, $m=0.8$, $G=4$, $f_s=20$ MHz, and $f_d=4$ MHz.

Fig. 8.3 shows the photographs of the transmitted square optical pulse and the received pulse waveforms. The transmitted pulse is measured using a current probe. The received pulse shape, which is measured at the output of the LPF, is approximately gaussian (as assumed in the theoretical analysis) because of the receiver bandwidth limitation (the fiber has no bandwidth limitation). The received pulses are filtered, differentiated, and squared by the preprocessing circuit before applying them to the PLL. Fig. 8.4 shows the photographs of the waveforms at the differentiator and the rectifier outputs, which are measured at points A and B in Fig. 8.2. This rectified pulse is applied to the band-pass filter to reject the unwanted components from the spectrum of the multiplier. The photograph of the waveform at the output of the band-pass filter, at point C, is shown in Fig. 8.5. The frequency spectrum at the output of the band-pass filter, at point C, for an unmodulated PPM transmitted signal is shown in Fig. 8.6, while Fig. 8.7 shows the photograph of the frequency spectrum of the modulated PPM signal at the output of the band-pass filter. From these spectra it is clear that the unwanted components are attenuated more than 13 dB for an unmodulated and 20 dB for a modulated PPM signal, and that the output frequency component can be tracked by the PLL. The signal at the band-pass filter output is amplified and applied to the PLL.

When the PLL locks on to the transmitted frequency the lock indicator output (at the output of the comparator) will be high, and Fig. 8.8 shows the photograph of the lock indicator output, at point D, for a packet transmitted signal. The figure shows that the PLL needs to about

3-4 PPM pulses (3-4 frames) to lock on to the transmitter frequency under normal operating conditions.

From the measurements done in this section it is shown that for a 22 mV received pulse amplitude at the output of the preamplifier the amplitude of the signal applied to the PLL was about 700 mV peak-to-peak, or the amplification factor of the clock recovery circuit is about 32. For a 50 mV sine wave signal applied to the PLL, its lock range was about 12 kHz and its hold range was about 25 kHz (see chapter 7).

8.3-SETTING-UP THE PPM SYSTEM

The experimental PPM system set-up is shown in Fig. 8.1. Data shift frequency f_d is kept constant (4 MHz) during the measurements, and f_s varies with different values of M (see chapter 5). At the transmitter the frequencies f_s and f_d are synthesized from the source frequency f_o . At the receiver they are synthesized from the PLL clock frequency. For M=8 and m=0.8, the frequency f_s , which is equal to 13.33 MHz, is synthesized using the PLL synthesizer, dividing the 40 MHz VCO frequency by a divide by-3 counter. The frequency f_d is synthesized from the VCO frequency by a divide by-10 counter (Fig. 8.9). For M=4, and m=0.8, the frequency f_s , which is equal to 10 MHz, is synthesized using the PLL synthesizer, dividing the 20 MHz VCO frequency by a divide by-2 counter. The frequency f_d is synthesized from the VCO frequency by a divide by-5 counter (see chapter 5, section 5.5). For M=16 and m=0.8, the frequency f_d is synthesized from f_s , the VCO frequency.

The threshold level, α , at the receiver, for both the PPM and the PCM systems, is adjusted during the measurements to equal half of the received signal amplitude (i.e. $\alpha = 0.5A$, where A is the received PPM pulse amplitude at the input to the comparator).

When the value of M is changed, the band-pass filter frequency is tuned to pass the desired slot frequency in the preprocessing circuit. The bandwidth of the comparator filter is also varied with M.

The system performance is measured using the ELED LH44-62 (discussed in chapter 4) as an optical source at the transmitter. The received optical power is varied using the optical attenuator, and the BER of the PPM system is measured versus the average received optical power. A very long packet (or continuous transmission) is used for the test, which is an unrealistic use of the system, but enables the BER to be measured easily. A PCM data source sends a pseudorandom sequence of NRZ pulses to the PPM transmitter at a rate of 4 Mbit/sec, and the transmitted data are recovered at the PPM receiver. Errors at the receiver are located by an error detector by comparing the transmitted and the received pulses. From the detected number of errors during a period of time, the BER of the system is calculated.

8.4-ERROR-RATE CHARACTERISTICS OF THE PPM SYSTEM

The BER versus average received power of the PPM system is measured for different values of M . Fig. 8.10 shows the measured error-rate characteristics for $M=4, 8, \text{ and } 16$, and $m=0.8$. The measured errors represent all types of errors, including the clock recovery error. It is clear from the figure that for the range of the measurements done in this work the error performance (or the sensitivity) of the PPM system improves when M increases.

To compare the measured results of the BER with the theory, both of these should be carried out under the same conditions. In chapter 3, the error performance of the PPM system in general is analyzed. In this chapter, some of the calculations are repeated at a condition similar to that of the practical system. Fig. 8.11 shows the calculated probability of an undetected error versus SNR for different values of M , when $\frac{T_s}{T_w} = \pi$, and $m=0.8$. The SNR is calculated by dividing the peak signal power by the average noise power. It is clear from the figure that the probability of an undetected error changes slightly with M (about 1 dB when M changes from 4 to 16 for a constant value of the probability of

error) and the curves are very close to the PCM probability of error. In Fig. 8.10, the measured average power can be converted to a peak power by multiplying it by the number of the slots in the frame. Fig. 8.12 shows the measured BER versus the received peak power. In Fig. 8.11, the BER is drawn versus SNR but in Fig. 8.12, the BER is drawn versus the peak power. The measured noise power was approximately equal for different values of M and PCM. For this reason the SNR can be compared to the signal power. Comparing the practical results, Fig. 8.12, with the theoretical results, Fig. 8.11, shows that they are approximately equivalent. The small difference between them (for $M=4$ and 8) may be due to the clock recovery errors, because different methods are used for the frequency synthesis which may effect the gain factor of the PLL. For the same peak power, the performance of the PPM system varies very little with M , and for the same average power, the performance of the system improves with M .

If the same mean power (instead of the peak power) is used in Fig. 8.11 for PCM and PPM, this will give an advantage of $10\log_{10}M$ for PPM compared with PCM if the noise power is assumed constant (even the noise power increases when the system bandwidth increases).

The work presented in the literature shows that the optimum value of M is between 16 and 32 [GARRETT, CALVERT], while in this work $M=16$ is the maximum value achieved. The optimum value in this case is not achieved due to the circuit frequency limitation, since going higher in M depends upon the clock recovery, fiber bandwidth, and the optical source peak to mean power.

Comparing the BER characteristics obtained in this work with the practical results given by [GARRETT] shows that the results are approximately equal with less than 1 dB difference in the receiver sensitivity (see Figs. 8.10 to 8.15).

The bandwidth of the PPM system is limited by the receiver filter, the fiber bandwidth is very large because the fiber length is very short. The filter bandwidth is changed when M is changed.

8.5-EFFECT OF VARYING m ON THE BER

For $M=4$, the modulation index, m , is changed from 0.8 to 0.4 and the BER is measured to see the effect on the system performance of varying the modulation index. Increasing m means increasing the slot time or pulse width and decreasing the guard space time (see chapter 3). When the width of the pulse is decreased, its peak power should be increased to keep the average power constant.

Fig. 8.13 shows the calculated probability of an undetected error versus SNR for $M=4$, and $\frac{T_s}{T_w}=\pi$, when m is changed from 0.8 to 0.4. The calculations are done under a condition similar to that of the practical measurements. It is clear from the figure that the performance of the system improves slightly when m is increased (about 0.5 dB when m is changed from 0.4 to 0.8).

Fig. 8.14 shows the measured BER versus the average received optical power for $m=0.4$ and 0.8. It is clear from the figure that for the same average power, $m=0.4$ gives about 2.8 dB improvement in the sensitivity of the system over $m=0.8$. The measured average power is converted to a peak power, for the purpose of comparison with the theoretical results in Fig. 8.13. Fig. 8.15, shows the measured BER versus the peak power. These two figures (Fig. 8.13, and Fig. 8.15) are in a good correlation with each other. From Fig. 8.15, the increase in the sensitivity of the PPM system is about 0.3 dB, when m is changed from 0.4 to 0.8.

8.6-ERROR-RATE CHARACTERISTICS OF THE PCM SYSTEM

The proposal in this thesis is that PPM can offer better performance than PCM using similar optical components, hence in order to compare the measured error-rate performance of the designed PPM system with the PCM systems, the measurements should be done under the same conditions. The designed PPM system without coder and decoder is used as a PCM system. The low-pass filter bandwidth at the receiver is also changed

to accommodate PCM pulse width received. The BER of the PCM system versus the average received power is measured at 4 Mbit/sec. Fig. 8.16 shows the measured results. The transmitter clock frequency is used directly at the receiver.

The BER versus SNR for the PCM system is calculated in chapter 3 (Fig. 3.10), and is redrawn in Fig. 8.11. From the practical results, the BER calculation is repeated here by measuring the SNR of the received signal and substituting its value in Eq. 3.46:

$$BER = \frac{1}{2} \operatorname{erfc}(0.5\sqrt{SNR}) \quad (8.1)$$

This calculation is for comparing the quality of the measured BER. SNR is calculated by measuring the peak received signal power and the average noise power, and substituting them in Eq. 8.1 to get the probability of error. The received PCM pulse is assumed rectangular and the received power is calculated by squaring the received signal amplitude (the resistance factor drops). The average noise power (which is equal to the square of the noise voltage measured) is measured at the output of the filter using a true rms voltmeter, then the SNR is calculated by dividing the signal power to the average noise power. The noise voltage measured was equal to 3.8 mV. Fig. 8.17 shows the calculated error performance of the PCM system.

The average power in Fig. 8.16 is converted to a peak power, and the BER versus peak power is drawn in Fig. 8.17. The difference between the calculated and the practical measured characteristics is about 1.5 dB. This difference in Fig. 8.17, may be due to the assumptions made during the calculations, that the pulse is rectangular and errors due to adjusting the threshold level (α) because the received signal amplitude is very low.

8.7-PPM VERSUS PCM

Comparing the experimental results between PPM and PCM systems given in the previous sections, shows that using the PPM system gives an improvement in the receiver sensitivity over the equivalent PCM system provided that their mean powers are comparable. This improvement in the receiver sensitivity depends on the number of time slots in the frame and the modulation index. Fig. 8.18 shows the improvements in the receiver sensitivity versus the average received PCM power. The graph shows that the improvement in the receiver sensitivity of the PPM system increases with M .

From these results we conclude that using PPM for optical local area networks can give an advantage over existing PCM systems. As discussed in chapter 5, it is possible to overdrive the optical source and achieve high optical peak power, provided that the transmitted pulse width is short, to achieve high system sensitivity and give improvements over PCM systems.

8.8-SUMMARY

The sensitivity of an experimental PPM system has been measured for different numbers of time slots, M , and modulation depths, m . The practical results are correlated with the theoretical results.

The results show that a digital PPM system can take advantage of available fiber bandwidth to offer a significant improvement in receiver sensitivity over the equivalent PCM system, even though the fiber bandwidth is not included in the measurements because the fiber length was too short.

This improvement is at the expense of a greatly increased peak source power. For the range of the measurements done in this work, it is clear that the improvement in system sensitivity increases with the number

of the slots, M , and the modulation index, m . The limits to this improvement are clock synchronization (which become difficult as M increases), fiber bandwidth, and optical source peak to mean power.

8.9-REFERENCES

GARRETT, I., CALVERT, N. M., SIBLEY, M. J., UNWIN, R. T., and CRYAN, R. A., "Optical fiber digital pulse-position modulation", Br. Telecom. Technol., Vol. 7, No. 3, July 1989, pp. 5-11.

CALVERT, N. M., SIBLEY, M. J., and UNWIN, R. T., "Experimental optical fiber digital pulse position modulation system", Electronics Letters, Vol. 24, January 1988, pp. 129-131.

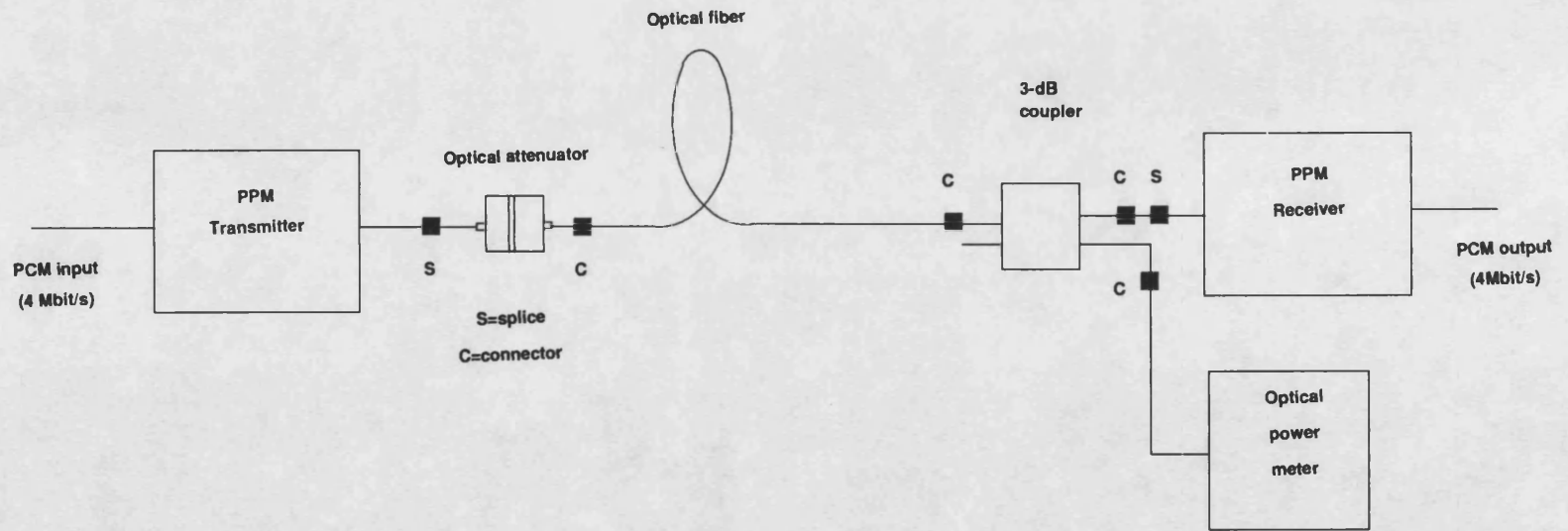


Figure 8.1 Optical PPM system

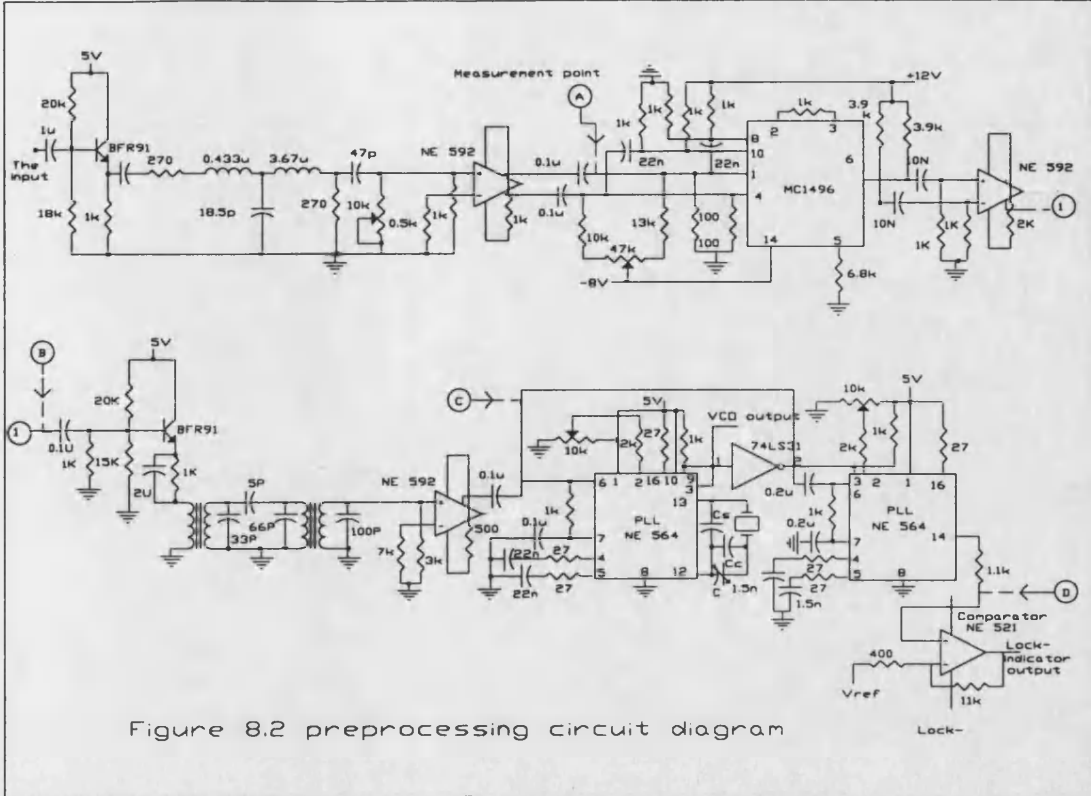


Figure 8.2 preprocessing circuit diagram

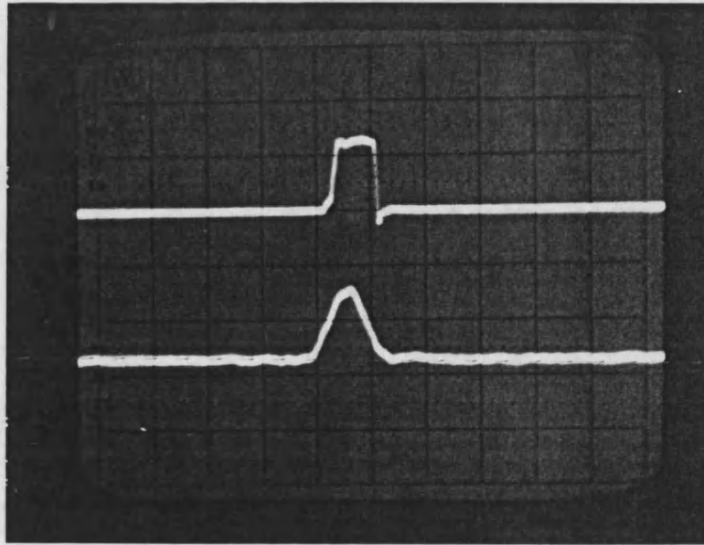


Figure 8.3

Upper: The transmitted pulse 100 mA/div.

Lower: received pulse 100 mV/div.

Horizontal scale 50 nS/div.

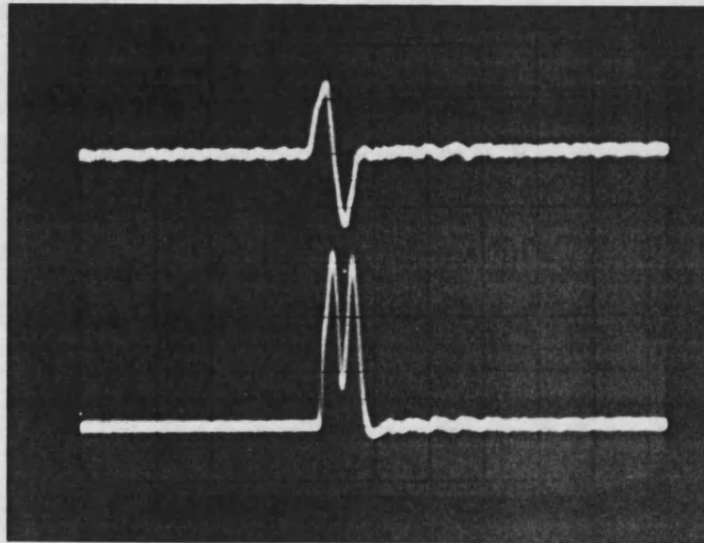


Figure 8.4

Upper: the differentiator output 50 mV/div.

Lower: multiplier output 100 mV/div.

Horizontal scale 100 nS/div.

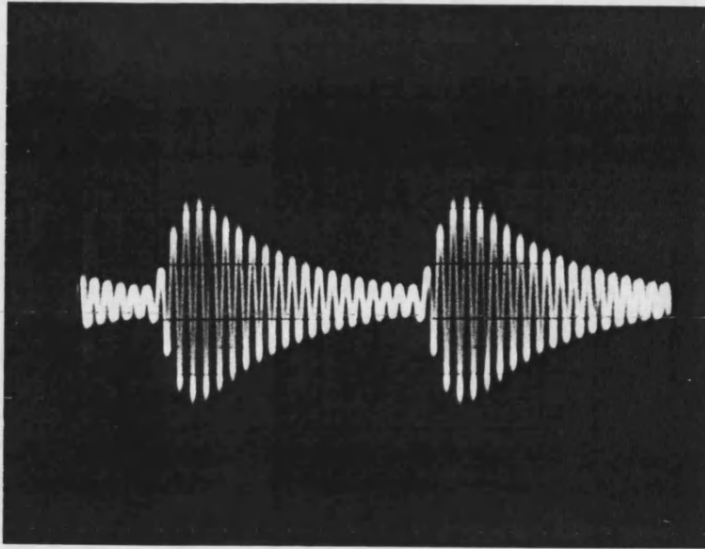


Figure 8.5 The signal at the output of the band-pass filter
Vertical scale 0.5 V/div.
Horizontal scale 200 nS/div.

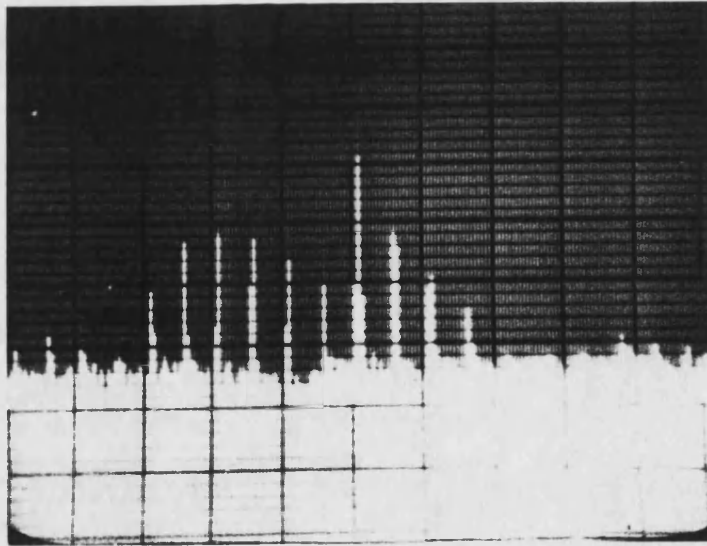


Figure 8.6 Frequency spectrum at the output of the band-pass filter for unmodulated PPM input
Vertical scale 10 dB/div.
Horizontal scale 2 MHz/div.

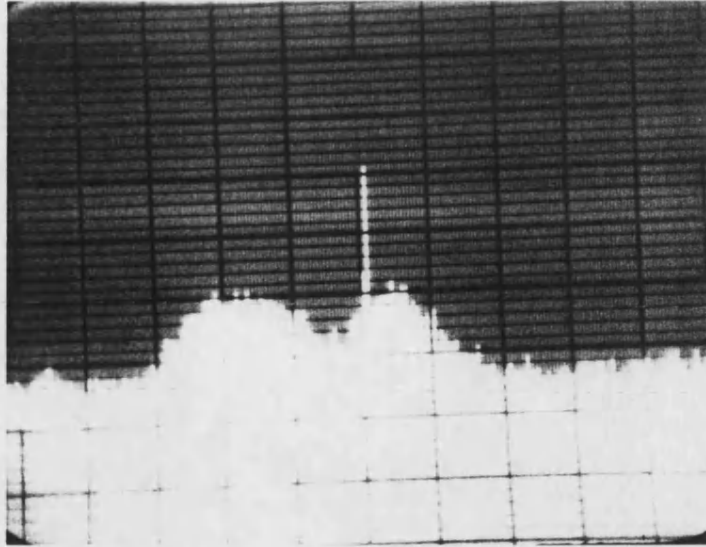


Figure 8.7 Frequency spectrum at the output of the band-pass filter for modulated PPM input
Vertical scale 10 dB/div.
Horizontal scale 2 MHz/div.

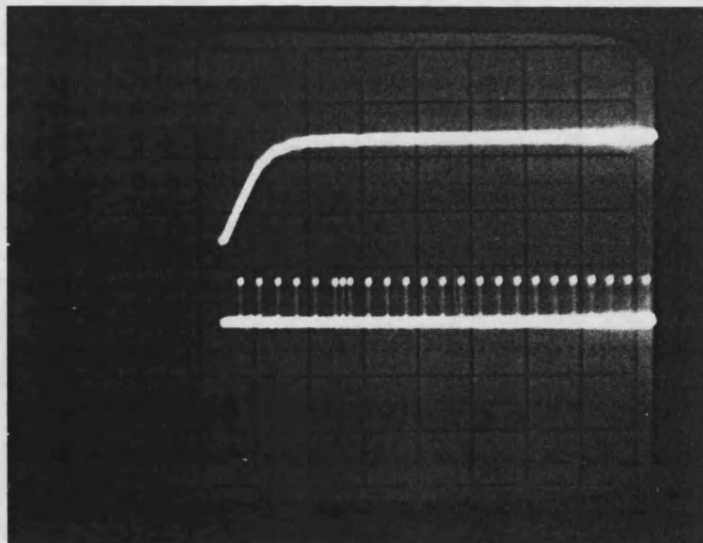


Figure 8.8 Lock indicator output
Horizontal scale 1 μ s/div.

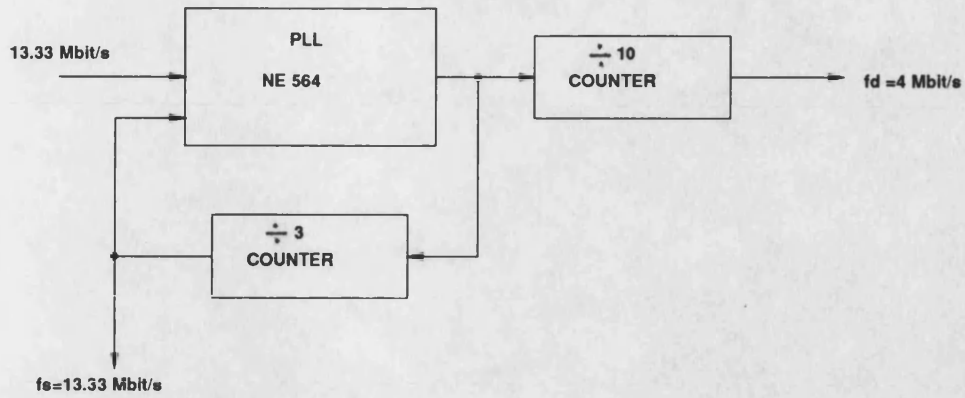


Figure 8.9 Frequency synthesis using PLL

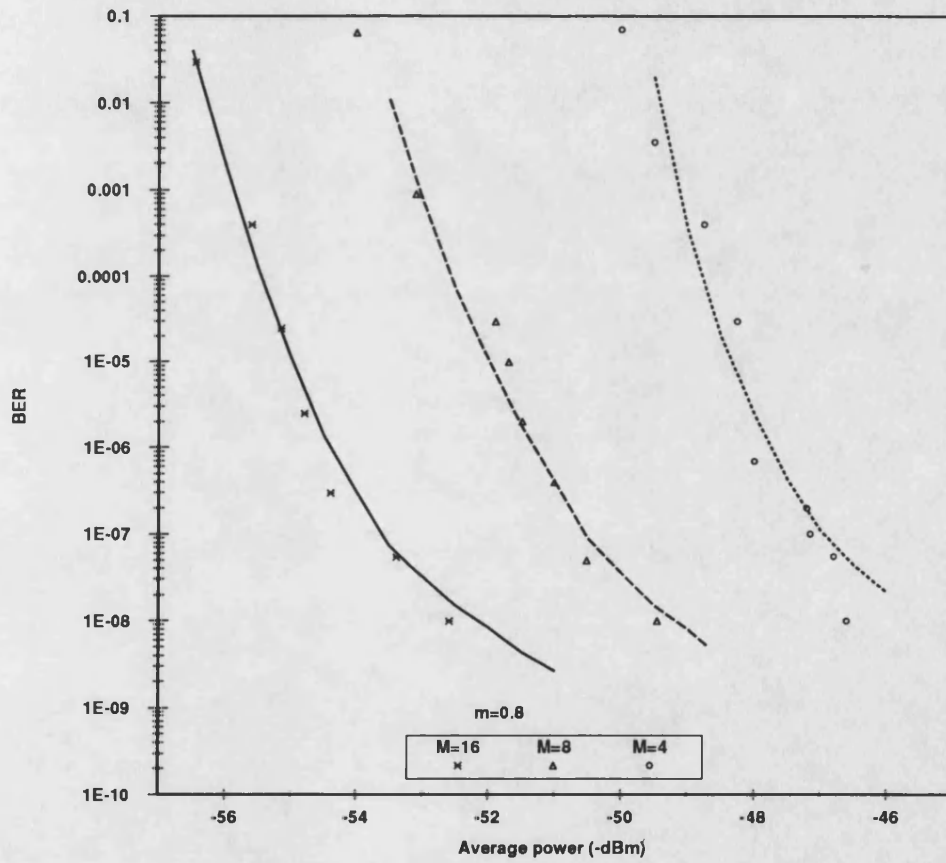


Figure 8.10 The BER versus average received power of the PPM system

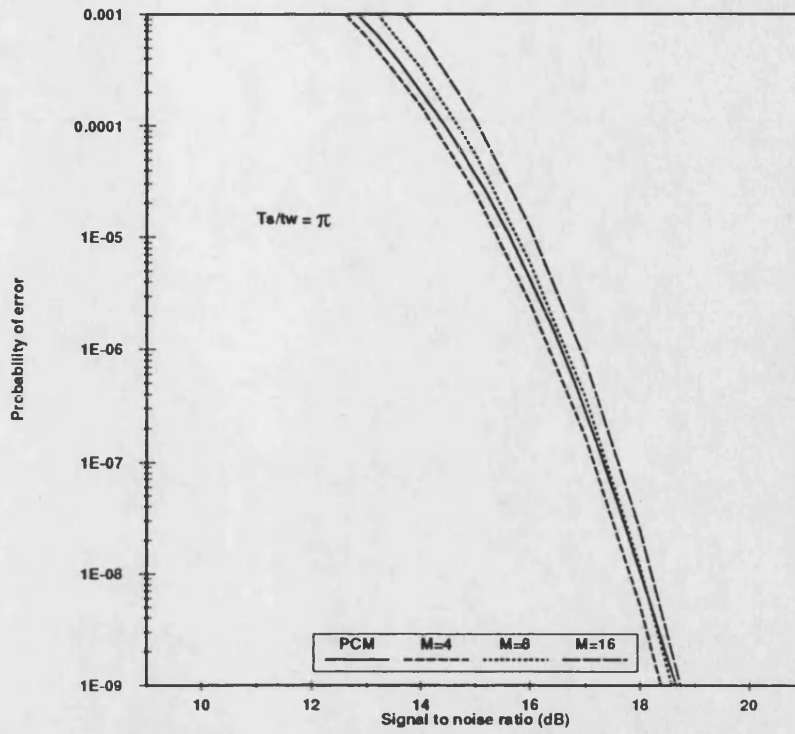


Figure 8.11 Calculated probability of an undetected error versus SNR

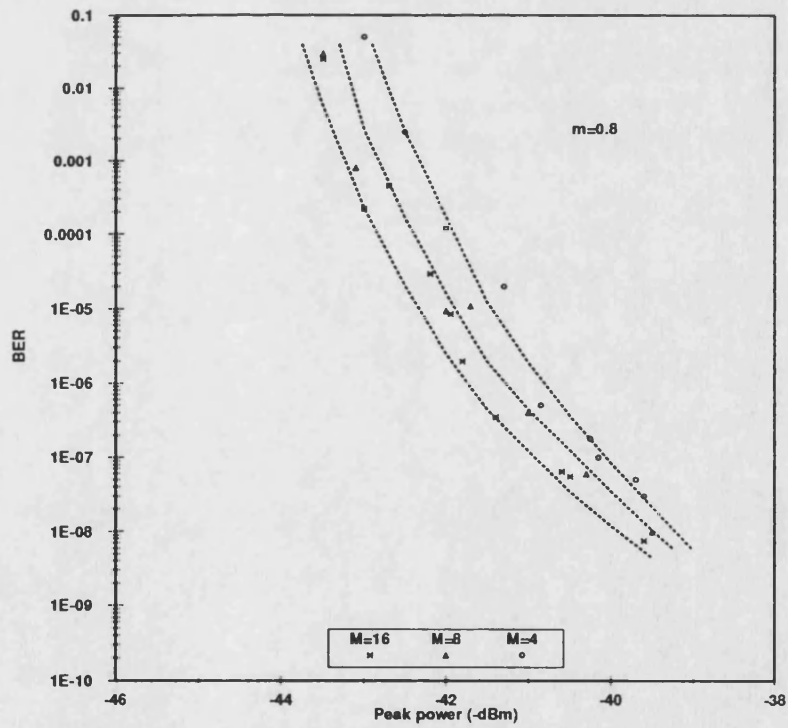


Figure 8.12 BER versus received peak power

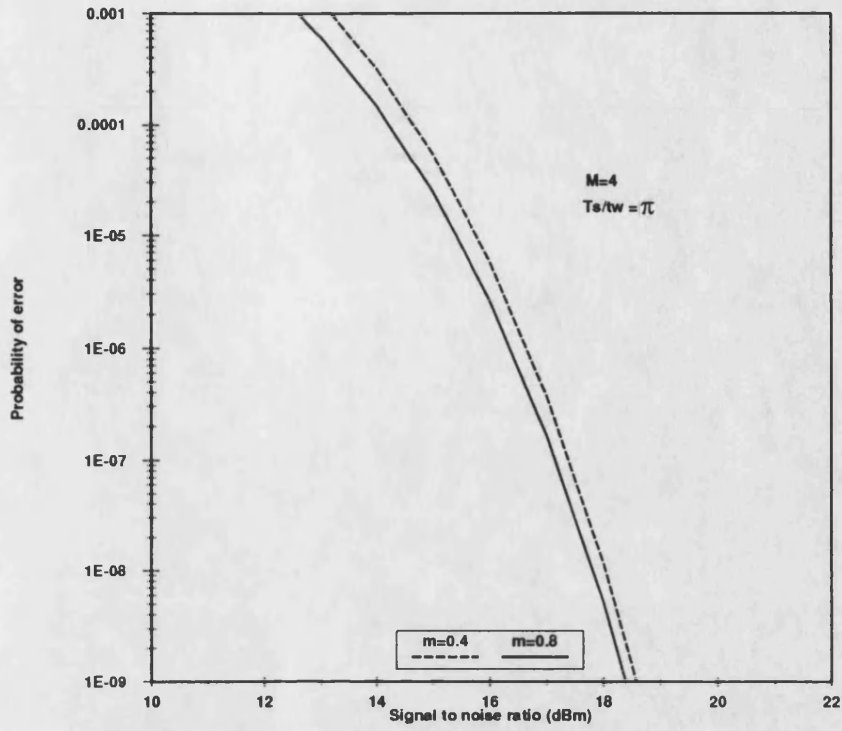


Figure 8.13 Probability of an undetected error versus SNR

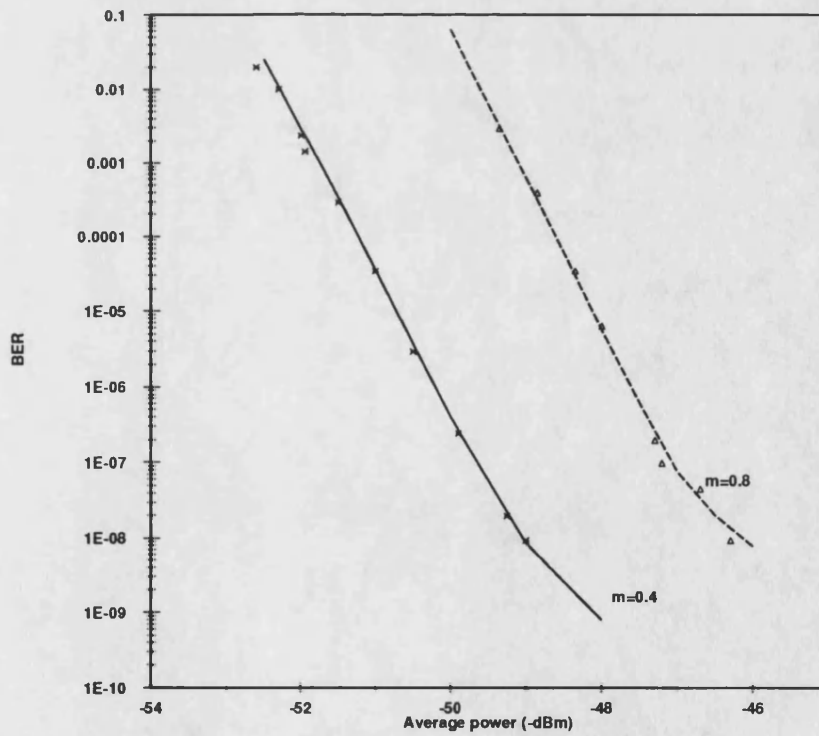


Figure 8.14 Measured BER versus the average received power

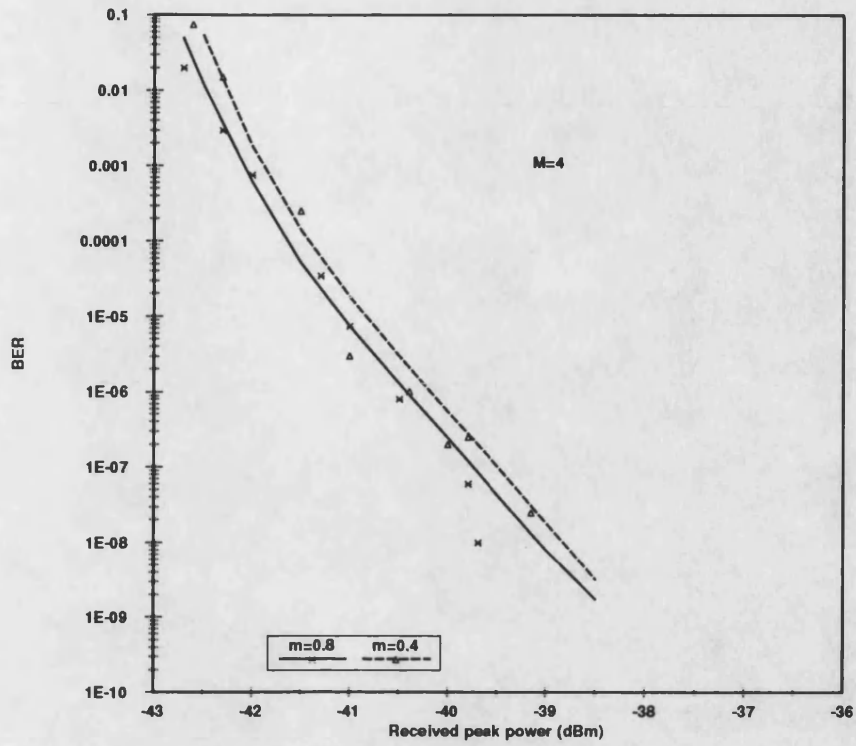


Figure 8.15 BER versus peak power

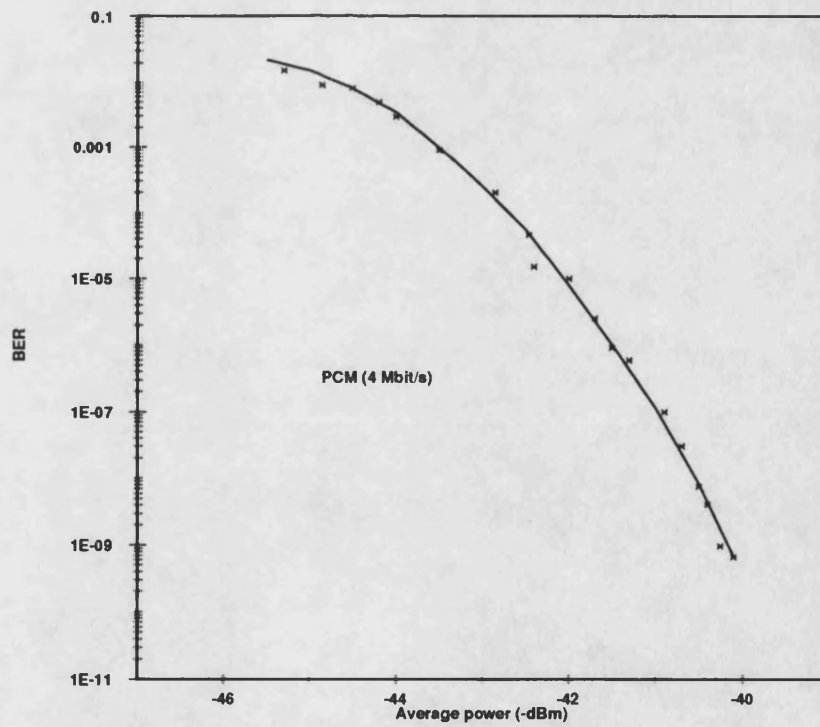


Figure 8.16 The BER of the PCM system

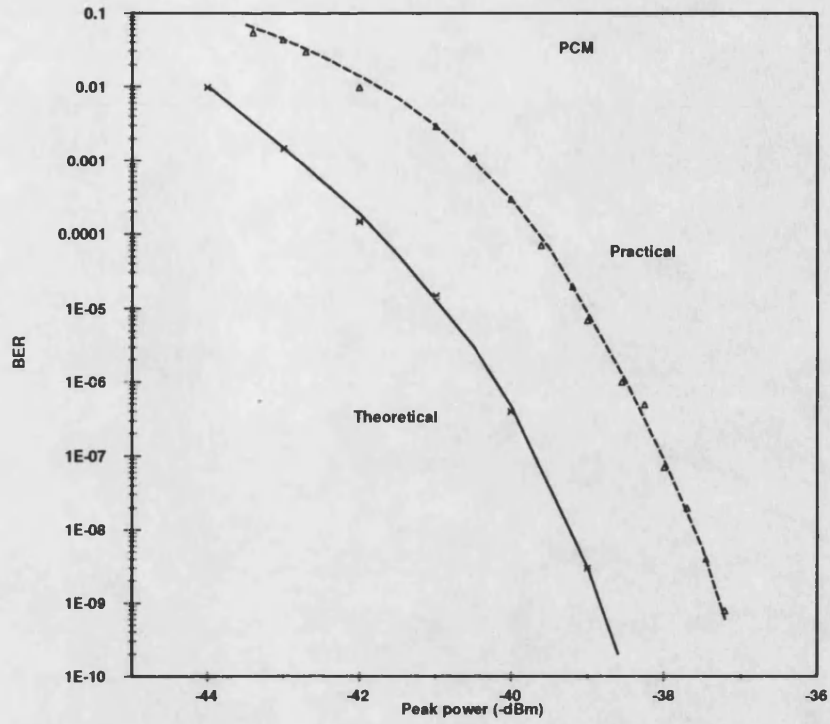


Figure 8.17 The calculated error performance of the PCM system

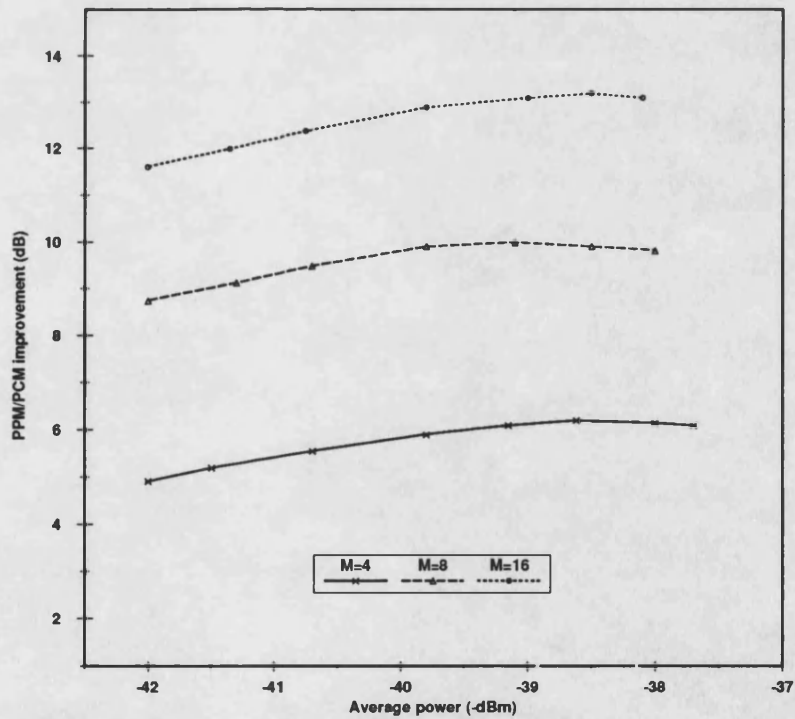


Figure 8.18 The improvement in the receiver sensitivity

CHAPTER -9-

APPLICATION OF PPM TO LANs

9.1-INTRODUCTION

We proposed in this work, that PPM signal coding could be a better choice for a LAN than PCM. Working from the theoretical and experimental results given in previous chapters, the application of digital PPM to a passive LAN is discussed and analyzed in this chapter, in terms of the advantages when compared with an existing PCM system working over a given fibre network.

LAN system performance depends upon the optical power budget, and the system rise time budget. The losses in the optical part of the system are added up, and an assessment made of the receiver sensitivity and transmitter output power needed to get the necessary performance. A very high peak power can be obtained from a LD or an ELED when a short width low duty-cycle pulse is used, but the improvement in receiver sensitivity of a PPM system depends upon the optical source peak/mean power ratio.

Any improvement in receiver sensitivity due to the use of PPM, is used to increase the number of tapping points or nodes connected to a passive LAN. Two types of passive local area network are discussed in this chapter; the bus and the star network.

PPM pulses need a higher bandwidth system than the corresponding PCM system, so during the design the speed of the system or the rise time budget should be checked. System speed is typically limited by the transmitter rise time, fiber response time, and the receiver rise time. The transmitter rise time is attributable primarily to the light source and its circuitry, while the receiver rise time results from the photodetector response and the 3-dB electrical bandwidth of the receiver front end.

The two types of fiber optic waveguide which generally are used for LAN

applications are single-mode fiber and graded-index multimode fiber. With either of these two types of fiber an ELED or a LD can be used as a transmitter, and this depends on the application and the data rate of the system. A surface emitting LED cannot be used for a LAN because of its broader line-width which causes dispersion, and because of its smaller modulation bandwidth.

9.2-PPM VERSUS PCM

Assume a binary PCM system, operating at an information rate of B bits/s. A corresponding PPM system operates with an M slot frame, and a modulation index m , and carries $\log_2 M$ bits of information at an information rate of $(\frac{m \cdot \log_2 M}{MT_s})$ bits/s. For the two systems to have the same information throughput, then for an error-free transmission:

$$BT_s = \frac{(m \cdot \log_2 M)}{M} \quad (9.1)$$

where T_s is the slot width. For $B=4$ Mbit/s, $M=16$, and $m=0.8$; then $f_s=20$ MHz. As the slot rate, f_s , increases, the fiber bandwidth necessary for transmission increases. For a bandlimited PPM system, if PCM and PPM systems are to have the same signal to noise ratio at the detector, then the ratio of their peak powers, for $\frac{T_s}{t_w} > 2$, can be written as (chapter 3):

$$\left(\frac{A_p}{A_c}\right)^2 \cong \frac{W}{B} 2\sqrt{2\pi} \quad (9.2)$$

where A_p and A_c are the peak optical power amplitudes in the receiver input of PPM and PCM respectively, W is the system bandwidth, and t_w is the rms full width of the received pulse. For a LAN using a wideband fiber network, the ratio of the peak optical powers at the transmitter in order to achieve similar performance in PPM as for PCM, can be written as [MARTIN]:

$$\frac{A_p}{A_c} = \left(\frac{M}{m \cdot \log_2 M} \right)^{\frac{1}{2}} \quad (9.3)$$

Any increase in the peak power above this value will give an advantage for the PPM system. As discussed in chapter 4, LD and ELED can give a very high peak powers provided that the pulse duty-cycle is very low. If the two systems operates at the same mean power, then PPM gives an advantage relative to PCM, which makes it efficient from an information point of view.

Choosing the threshold level is important in a bandlimited system because of pulse dispersion, since the probability of missing a pulse increases as the threshold level increases. In a wideband system the threshold level variation has very little effect on the probability of an undetected error because the dispersion in the pulse is very low, and the PPM pulse received is almost rectangular.

9.3-PPM SYSTEM DESIGN

The design of a PPM system for a LAN requires a broad view of the overall parameters of such a network. In this section the parameters required for a PPM system design, and the parameters which effect received signal quality in general are discussed and analysed. In PPM transmitter design for a LAN, the most important factors are the transmitted peak power, the wavelength and the line-width of the source. As discussed in chapter 4, the maximum available optical power from a semiconductor laser at wavelengths around 850 nm, is limited by catastrophic optical damage, and is a function of the optical power density and of the pulse length. The allowable peak power at which catastrophic damage occurs vary inversely with the square-root of pulse width, for pulse lengths under about 1 μ s. Experimental and theoretical studies have shown that powers which are up to two orders of magnitude greater than the PCM power can be achieved for pulses of the order of 10 ns

(see chapter 4). It is clear from the analysis and the experimental work done that it is possible to overdrive the LD or the ELED and achieve high peak output power provided that the transmitted pulse width is short compared with the thermal time constant of the device. Also the literature shows that a 850 nm laser can give up to 20 times of the diode rated mean power and a 1300 nm laser can give up to 50 times its rated mean power (see chapter 4). However the mean power rating must not be exceeded.

In practical tests (chapter 4), an LD gave about 10 dB increase in the peak power over the device rated power, and an ELED gave about 17.9 dB increase in the device peak power over its rated power. From these results it is clear that optical sources can easily give a higher peak power to get an advantage of using PPM over PCM.

The maximum data rate of the system is determined mostly by the type of transmitting optical source in use.

Take an example, based on a PCM system of 4 Mbit/s. Not only is this a LAN standard rate [STROLE], but it also corresponds with the experimental system in chapter 8. Table 9.1 summarizes the required PPM data rate, slot width, frame length T_f , peak power penalty and limiting peak to mean power. Clock idle interval represents the number of slots and guard spaces in a frame, and gives an idea as how stable the clocks must be as M is taken to larger values. The modulation index is assumed 0.8. The limiting peak/mean power represents the limit to the excess power which is available to overcome transmission loss.

A large receiver bandwidth is required to receive a rectangular pulse with minimum spillover so as to avoid the onset of wrong-slot errors. Reliable transmission of PPM data in an optical communication system requires that an accurate clock signal be available at the receiver for proper synchronization with the transmitted signal. This could be carried out by the method discussed in the chapters 4 and 7.

M	f_s (MHz)	T_s (ns)	T_r (μ s)	peak power penalty (dB)	clock idle interval (M/m)	Limiting peak/mean power
4	10	100	0.5	2	5	7
8	13.33	75	0.75	2.6	10	10
16	20	50	1.0	3.5	20	13
32	32	31.25	1.25	4.5	40	16
64	53.33	18.75	1.5	5.6	80	19
128	91.42	10.94	1.75	6.8	160	22

Table 9.1 PPM parameters for 4 Mbit/s system

The type of light source used depends on the type of fiber, the amount of dispersion that can be tolerated, and the desired transmission distance. The maximum data rate is constrained by the fiber, but determined mostly by the type of transmitting device (optical source) in use. The information capacity of an optical fiber is usually specified by the bandwidth-distance product in MHz.km (see chapter 2). In many cases, the capacity of fiber optic media can be upgraded by simply changing the emitters and the detectors of the fiber optic links.

The impulse response of the optical fiber is assumed gaussian with an rms full-width of $\frac{1}{\pi W}$. When the gaussian impulse response of the fiber is convolved with a rectangular pulse of width T_s , this gives [MARTIN]:

$$x(t) = Q[2\pi W T_s (f_s t - 1/2)] - Q[2\pi W T_s (f_s t + 1/2)] \quad (9.4)$$

where $\sqrt{(2\pi)} \cdot Q[u] = \int_{-\infty}^{\infty} \exp\left(-\frac{v^2}{2}\right) dv$, which is a smeared pulse with normalized form. In Eq. 9.4, the signal overspill into an adjacent slot is small if $W T_s > 2$. Table 9.2 shows the bandwidths required by a PPM system for the information rate 4 Mbit/s. The parameters in table 9.2 can be scaled up or down as required. Single-mode and Graded-index fiber can easily achieve the limits specified in table 9.2 (see chapter 2). Operation

Operation at higher rates, for example 100 Mbit/sec (which is used in FDDI), is possible for certain values of M, fiber type, and optical source type.

The choice between the single-mode and graded-index fibers for LAN use is discussed in the following subsections.

M	4	8	16	32	64
$2f_s$	20	26.6	40	64	106.66

Table 9.2 Estimated bandwidths for 4 Mbit/sec.

9.3.1-SINGLE-MODE FIBER

When a single-mode fiber is used in a LAN there will be no bandlimiting for reasonable data rates, so the transmitter and the receiver will be the major bandwidth limits.

Fig. 9.1 shows the relation between f_s and B for different values of M (Eq. 9.1). Assume that ELED limits f_s to about 150 Mbit/sec and LD limits f_s to about 1 Gbit/sec, then from Fig. 9.1, for a given value of B, the maximum value of M can be selected according to the limits specified above. For instance, suppose that B=10 Mbit/sec, which is a common LAN speed particularly for Ethernet, then M can take any value up to 256 if a LD is used. If an ELED is used then M can be increased up to 64. Fig. 9.2 shows the relation between parity $\frac{A_p}{A_c}$ versus M for different values of modulation index m. The figure defines the increase in peak optical power which is necessary for a given system to operate in PPM rather than in PCM. Any system advantage in transmission loss can be gained only by increasing the peak optical power still further.

Fig. 9.3 shows the relation between peak/mean power ratio and M. The mean power of the device is limited to the CW rating, while maximum

peak/mean power is limited by the dissipation of the device (LD or ELED). The maximum peak/mean power ratio is given by the clock idle interval (see table 9.1). From the figure the excess power available for a PPM network can be obtained for a given value of M (the curve c shown in the figure). When the conditions discussed above are met, the receiver bandwidth (W) should be chosen such that $W > 2f_r$, then the signal overspill into an adjacent slot will be very small and gives negligible wrong-slot errors.

For example, if the LD ML 4102 (which has 10 dB peak/mean power ratio), the single-mode fiber MS8 [GEC] (which has a bandwidth of 30 GHz.km), and the Plessy PIN-FET transimpedance P35-6661 receiver (which has a bandwidth of 95 MHz) is used in a network then the receiver will be the main source of bandwidth limit. The values of M and B can be found from Fig. 9.1. If the ELED LH44-62 (which has 17.9 dB peak/mean power ratio) is used with the single-mode fiber and the receiver then the ELED and the receiver will limit the bandwidth.

9.3.2-GRADED-INDEX FIBER

If a graded-index fiber is used in the system then the medium is bandlimited to W Hz. If a LD is used, then W is the laser-bandwidth of the fiber, but if an ELED is used, then W is the compromised bandwidth of source plus fiber [REFI]. From Fig. 9.1, for $W > 2f_r$, the value of M can be selected, which gives minimum signal overspill into an adjacent slot.

The relation between $\frac{A_p}{A_c}$ for parity and W/B, which is calculated using Eq. 9.2, is shown in Fig. 9.4. The figure shows that the peak power required by the system increases with M at low W/B ratios because of pulse dispersion.

The maximum limit of peak/mean power ratio can be calculated using Fig. 9.3. Receiver bandwidth should be larger than $2f_r$ for negligible wrong-slot errors.

For example, if the graded-index fiber MG50 [GEC] (which has a bandwidth of 800 MHz.km) is used with the LD ML4102 and the receiver Plessey P35-6661, then the system bandwidth will be limited by the fiber and the receiver. The values of M and B can be found from Fig. 9.1. If the ELED LH44-62 is used instead of the laser diode then the ELED and the receiver will limit the bandwidth of the system.

Table 9.3 shows the PPM slot frequency (f_s) variation with M for some PCM data rates which are already in use in LANs.

B (Mbit/s)	4	10	16	50	100
M	f_s (MHz)	f_s (MHz)	f_s (MHz)	f_s (MHz)	f_s (MHz)
4	10	25	40	125	250
8	13.3	33.3	53.3	166.6	333.3
16	20	50	80	250	500
32	32	80	128	400	800
64	53.3	133.3	213.3	666.6	1333.3
128	91.4	228.6	365.7	1142.8	2285.7
256	182.	400	640	2000	4000

Table 9.3 Slot frequency variation with M for a given values of B

Assume that ELED limits f_s to about 150 Mbit/s and LD limits f_s to about 1 Gbit/s, then from the table the value of M can be found for a given value of B and optical source type. From the table the fiber type to use can also be found (fiber bandwidth > $2f_s$).

9.4-PASSIVE BUS LAN

In a passive bus network, each station is attached directly to the transmission medium (optical fiber) through a passive tee coupler (see chapter 2). The tee coupler may have a large tap ratio to take only a small amount of optical power from the main path, but passive tapping of an optical fiber can have a high insertion loss (see chapter 2). Fiber attenuation is not significant in a network with a diameter of less than 1 km. The number of stations that can be put on an optical fiber data bus is usually limited by the total allowable attenuation between transmitter and receiver which is a linear function of the number of stations. The total distribution loss in the bus network can be calculated using [PALAIS]:

$$L = (N - 1)L_{THP} + L_{TAP} + 2NL_c \quad (9.5)$$

where N is the number of stations connected to the bus, L_{THP} is the coupler throughput loss, L_{TAP} is the tap loss, and L_c is the connector loss (see chapter 2). Adding more stations to the network will effect the throughput loss and the connector loss. When a PPM system is used instead of PCM, the receiver sensitivity is improved, and this can be translated into an increase in the number of stations connected to the network. Eq. 9.5 can be used to calculate the number of stations connected to the network. The added loss for an extra station connected to the network is equal to $L_{THP} + 2L_c$. For example, assume that N_1 stations are connected to a bus network when PCM signalling is used, and the stations are connected to the bus by a 10 dB coupler, which has a throughput loss of 0.46 dB. Assume that the connector loss is equal to 1 dB. When a PPM system is used instead of PCM, the increase in the receiver sensitivity is say 13 dB, which has been obtained practically for $M=16$ (see chapter 8). Using Eq. 9.5, the number of extra stations, N_2 , which could be added to the bus is $N_2=5$. The number N_2 is a function of the connector loss L_c . Connectors produce between 0.5 and 1 dB of loss.

Splices are sometimes used in place of connectors because they have lower loss (0.1 to 0.05 dB). Table 9.4 shows variation of N_2 with the connector loss L_c , for this example.

L_c (dB)	2	1	0.5	0.2	0.1	0.05
N_2	2	5	8	15	19	23

Table 9.4 Number of extra stations versus connector loss

9.5-PASSIVE STAR LAN

In a star network, each station is connected by a point-to-point link to a common central star coupler, which distributes power equally to each of the receiver ports from any one transmitter port (see chapter 2). When PPM instead of PCM is used, the number of extra stations or ports which could be added to the network due to an improvement in receiver sensitivity can be calculated using (chapter 2, Eq. 2.19):

$$L = -10 \log\left(\frac{1}{N}\right) + L_E + 2L_c \quad (9.6)$$

where L is the total distribution loss associated with the star coupler, L_E is the star excess loss, and L_c is the connector loss. If the number of ports when PCM is used equal to N_1 , then using PPM the number will be N_2 . For example, using the 13 dB increase in receiver sensitivity, which obtained practically for PPM $M=16$, will increase the number of output ports about 20 times. This figure is calculated as follows: assume that L_1 is the loss when PCM is used, or:

$$L_1 = -10 \log\left(\frac{1}{N_1}\right) + L_E + 2L_c \quad (9.7)$$

Then L_1+13 , represents the loss when PPM is used, or:

$$L_1 + 13 = -10 \log \left(\frac{1}{N_2} \right) + L_E + 2L_c \quad (9.8)$$

Solving the equations above we get $N_2 = 19.95N_1$, assuming that the star excess loss L_E is constant for both cases, although the excess loss of a practical device does increase with the number of ports. The excess loss may vary from about 1 dB for 16 ports to 3 dB for 128 ports [PALAIS]. This shows that the number of extra ports due to the improvement in receiver sensitivity is very high compared with the bus network. Splices may be substituted for connectors to improve the loss budget.

9.6-SUMMARY

The application of PPM to a passive local area network in place of PCM, results in an improvement in receiver sensitivity, and hence an increase in the number of stations which may be connected to the network. The improvement in receiver sensitivity of the PPM system is a function of the optical source peak/mean power and the number of the time slots of the PPM frame (M).

Fiber attenuation and dispersion are not significant for the information rate 4 Mbit/sec, and M up to 256. For higher values of information rate or data throughput the dispersion should be checked to avoid the onset of the wrong-slot errors. Using a wide-band fiber and receiver will avoid the onset of wrong-slot errors.

Transmitting devices (optical sources) can be either laser diodes or edge-emitting light-emitting diodes. Peak/mean power of the optical source should be very high to give an advantage over PCM. More than 10 dB has been obtained practically when a LD is used, and about 17.9 dB when an ELED is used, but greater improvements are possible.

The type of an optical source used depend on the type of fiber, the amount of dispersion that can be tolerated and the desired transmission distance. When a single-mode fiber is used in a LAN using PPM then there will be no bandlimiting for reasonable data rates, so the transmitter

and the receiver will be the major bandwidth limits. If a graded-index fiber is used in the system then the medium is bandlimited which depends on the type of the optical source in use. With a single-mode fiber and a laser diode M can be increased up to 256 or more and the data rate can be increased up to 100 Mbit/sec. If a graded-index fiber is used then the value of M is determined by the bandwidth of the optical source and the PCM data rate (B) limit.

Coding and decoding circuits are realized with TTL logic, which can be used up to $M=32$, and $m=1$ (for the information rate $B=4$ Mbit/sec). For higher values of B and M , ECL logic must be used.

Slot or clock synchronization of a PPM system, which is an important part of the receiver, can be carried out using a crystal-controlled PLL (see chapters 4 and 7).

In the passive bus LAN the number of extra stations possible with PPM depends strongly on the connector loss, and the excess loss of the coupler. Worthwhile improvements can be obtained.

In the passive star LAN, using PPM will increase number of ports dramatically.

9.7-REFERENCES

GEC Optical fiber data sheet 1986.

MARTIN, J. D., "PPM for local area networks", Proceedings "Fiber-Optics 89", SPIE, Vol. 1120, London, Apr. 1989, pp. 14-24.

PALAIS, J. C., "Fiber optic communications", Prentice-Hall, 1988, chapter 8.

REFI, J. J., "Fiber-bandwidth and its relation to system design", J. of Optical Sensors, Vol. 2, 1987, pp. 89-105.

STROLE, N. C., "The IBM token-ring network-a functional overview", IEEE network magazine, Vol. 1, January 1987, pp. 23-30.

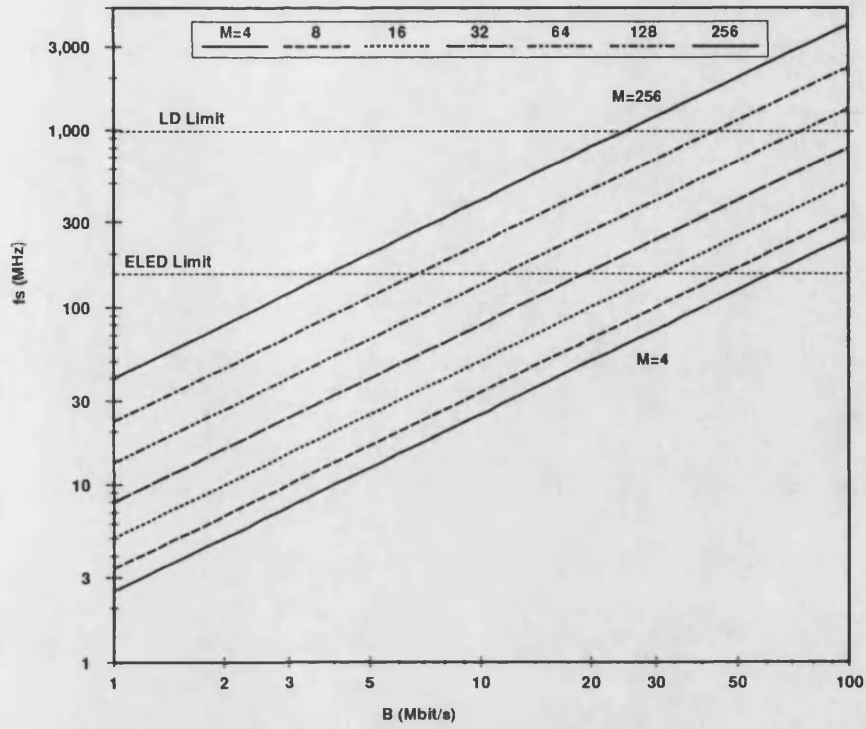


Figure 9.1 Slot frequency variation with PCM data rate

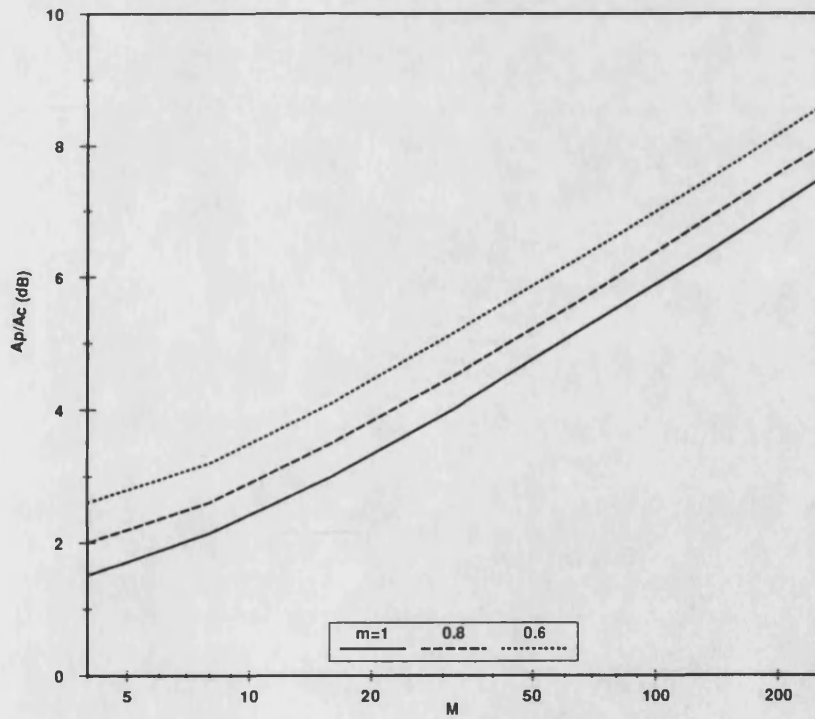


Figure 9.2 Peak power increase with M

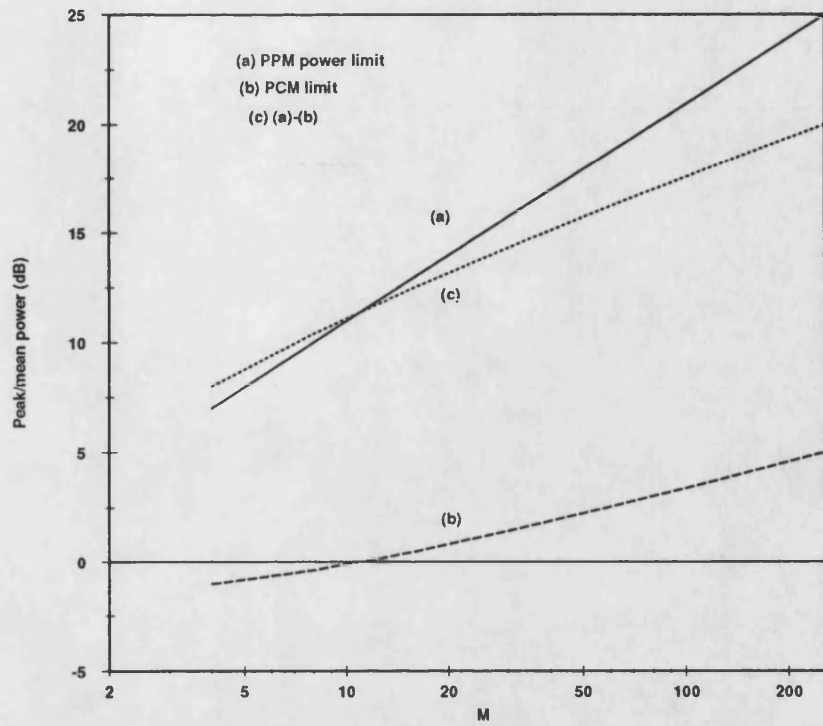


Figure 9.3 Transmitter power limitation

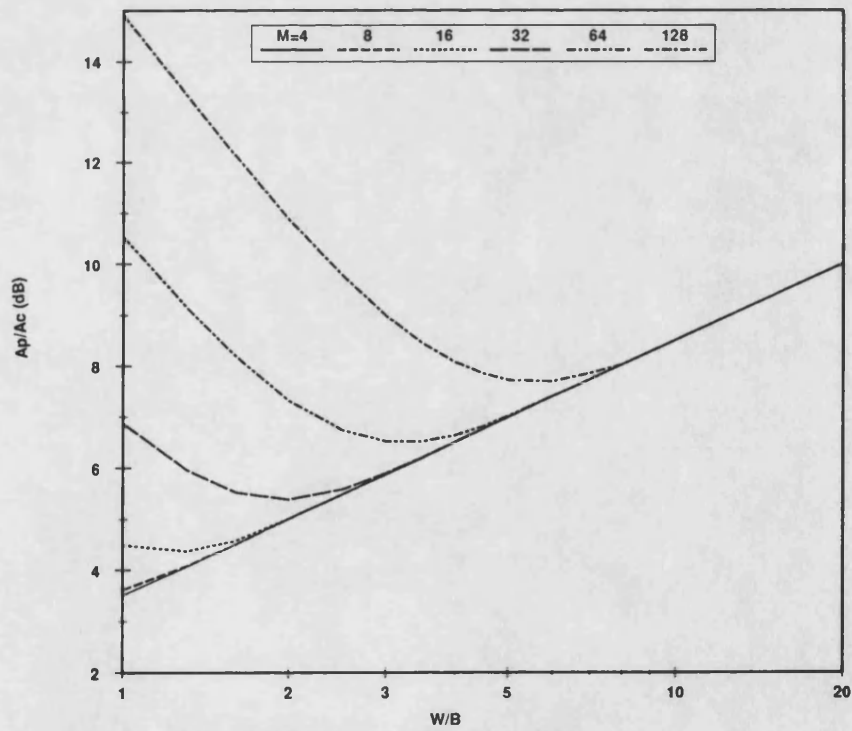


Figure 9.4 A_p/A_c for parity versus W/B

CHAPTER -10-

CONCLUSIONS AND FUTURE WORK

10.1-CONCLUSIONS

The transmission loss of an optical link must be accommodated between the two boundaries of available transmitted power and achievable receiver sensitivity. In an installed passive fiber-optic local area network the limited power budget of each optical fiber link, including unavoidable branching and tapping losses, sharply limits the number of stations in the network. In such passive networks, any improvement in receiver sensitivity means that the number of stations or tap points can be increased, and this was the aim of the investigation presented in this thesis. Digital pulse position modulation (PPM) can in principle be used to effect a trade-off between the large transmission bandwidth provided by optical fiber and an increased transmission distance (or number of stations or tapping points) in a passive LAN (see chapter 2, references [LESH, GAGLIARDI, GARRETT, CALVERT, PIERS]). Application of the PPM principle to LAN parameters is studied in the thesis, and design criteria confirmed by construction of a model system. The number of extra tapping points or stations is calculated for a certain value of improvement in receiver sensitivity, for passive bus and star networks. The analysis in this work assumes that PCM signalling exists in a given LAN, and then seeks to discover the conditions under which a conversion to PPM will give similar performance, and the conditions under which PPM gives an advantage over PCM. In order to get an improvement in receiver sensitivity the PPM transmitted mean power should be comparable to that produced by a "CW" laser or LED in a binary PCM system. In other words, the predicted advantage of a PPM depends very much on peak/mean power characteristic of the optical source.

The characteristics of a PPM system are analysed and compared with those

of a comparable PCM system, to check the improvement obtained in sensitivity. Although many detailed analysis have been made (see chapter 2, references [GARRETT, PIERS]), a simplified analysis has been made here to calculate the error performance of a PPM system compared with the performance of a PCM system (chapter 3). Thus we can see if the idea of using PPM in a LAN is worthwhile, on the basis of broad systems calculations. If the results are satisfactory, then a particular detailed analysis can be made to optimise the actual operating conditions.

When a single-mode fiber is used in a LAN there will be no bandlimiting for reasonable data rates, so the transmitter and the receiver will be the major bandwidth limits. If a graded-index fiber is used in the system then the medium is bandlimited to W Hz. Different analysis apply to each of these cases (see chapter 2, reference [REFI]).

A PPM pulse in a frame is subjected to two types of error, they are: erasure error and false-alarm error. The effective-error performance of the PPM is calculated on the frame basis. It is calculated and analysed for the following three cases; error free, undetected error, and detected error. Choosing the threshold level (α), at the receiver, is important in the bandlimited system because of pulse dispersion. As the threshold level increases the probability of an undetected error increases because the probability of missing the pulses increases. In the wideband system the threshold level variation has very little effect on the probability of an undetected error because the dispersion in the pulse is very low.

The optimum value of threshold level for a given $\frac{W}{B}$ (where W is the fiber or the receiver bandwidth, and B is the information rate) is determined by the probability of an undetected error and the throughput of the system. The threshold level $\alpha=0.5$ is the approximately optimum value for the bandlimited and the wideband systems analysed. When a wideband fiber is used and the received pulse shape is rectangular, under these conditions the adjacent-slot errors have no special preference.

From the analysis done in chapter 3, it is clear that the modulation index variation has a little effect on the error performance of the PPM system (~ 0.8 dB for $\Delta m=0.2$), for a constant value of signal to noise ratio.

It is clear from the theoretical analysis that a significant improvement in receiver sensitivity is only possible if the PPM transmitter can work with a similar mean power as for PCM (see chapter 1, reference [GARRETT]). Real improvements are therefore possible, only if the optical transmitter can deliver a significantly greater peak power than in the PCM case.

The maximum available optical power from a semiconductor laser (AlGaAs diodes) is limited by catastrophic optical damage of the end mirror facets. The power level at which catastrophic damage occurs in a given laser has been found to decrease with the square root of the pulse length for pulse lengths under about 1 μ s. The maximum output power of an ELED is also limited by junction temperature and the nonradiative components increased at high current density (see chapter 4, reference [SAUL]). In order to verify the theory above, the practical characteristics of some LDs and ELEDs were measured to see if they are suitable for PPM.

The characteristics of the LD ML 4102 (which is AlGaAs laser) have been measured under conditions of short high current low duty-cycle pulses, showing that it is possible to overdrive the device and achieve high output peak power provided that the transmitted pulse width is short compared with the thermal time constant of the device. With drive currents of approximately 247 mA (compared with maximum continuous current of 100 mA), more than 10 dB increase in the peak power over the device rated power was observed. The temperature rise was negligible for $M>15$ (where M represents the duty-cycle of the pulse), and about 8.2 dB increase in the diode peak power over the diode rated power. Several other devices were tested and gave similar results. These practical results show that this LD can be used for PPM and offer a

worthwhile advantage over PCM. If for example it used for $B=4$ Mbit/s, then M can be increased up to 8. The maximum limit for data rate and the value of M can be found from table 9.1 and the Figs. 9.2 and 9.3. From the practical results obtained by measuring the characteristics of the ELED LH44-62, it is clear that this ELED device can be overdriven and can achieve high peak power provided that the current pulses are short (50 ns) and at low duty cycle ($M>8$). With a drive current of approximately 1.6 A, a 17.9 dB increase over the 100 mA CW output power has been observed. The temperature effect on the device is very low provided that the pulse width is kept short (20-50 ns) up to about 900 mA. This diode seems ideal for use in an optical LAN operating in a PPM mode; for example with a slot width of 30 ns and a frame of 16 slots, the diode can be over-driven by a drive current of 500-700 mA and produce a 12 dB enhancement of the system sensitivity. Several other ELEDs with different powers were tested and they show similar results. The maximum limit of B and M for this ELED can be obtained from table 9.1 and the figures 9.2 and 9.3. For example for $B=4$ Mbit/s, M can be increased up to 64.

The type of optical source used depends on the type of fiber, the amount of dispersion that can be tolerated and the desired transmission distance. When a single-mode fiber is used in a LAN using PPM then there will be no bandlimiting for reasonable data rates, so the transmitter and the receiver will be the major bandwidth limits. With a single-mode fiber and a laser diode, M can be increased theoretically up to 256 or more and the data rate can be increased up to 100 Mbit/s. In wideband fibers the values of M and B are limited by power considerations. If a graded-index fiber is used then the medium is bandlimited and the value of M is determined by this bandwidth and the PCM data rate (B). An ELED can now be used, taking advantage of its simple operation.

Practical PPM and PCM systems were built (transmitter, optical channel, and receiver) and their characteristics measured to verify the theory discussed and analysed in this work. A data rate of 4 Mbit/s was chosen

for convenience.

The design of an experimental optical PPM transmitter is discussed in chapter 6. The coder and the block generator for the PPM transmitter were built using TTL integrated circuits which can be used up to $M=32$ ($m=1$) for $B=4$ Mbit/s. For $B=4$ Mbit/s and $m=0.8$, the value of M could be set to 4, 8, and 16, and the modulation index m was variable from 0.8 to 0.4 for $M=4$. The ELED discussed above was used with the transmitter circuit designed, but a LD could also be used.

Reliable transmission of PPM data in an optical communication system requires that an accurate clock signal be available at the receiver for proper synchronization with the transmitted signal. A digital PPM signal carries information by the time location of its pulses, so it follows that systems using this signalling format will require more accurate synchronization than for PCM. It is required to recover from the incoming signal timing information relating to frame boundaries and time slot locations. The design of an experimental timing subsystem for the receiver is not so easy, especially for high values of M . The received signal is not periodic, pulses are widely spaced, and vary in position according to the data bit sequence. With proper nonlinear preprocessing of the detector output signal, a PLL can be used to provide accurate synchronization of the slot clock in a direct detection optical PPM system. For maximum signal component at the preprocessing circuit output the preprocessing filter can be realized practically by a low-pass Gaussian filter with rms bandwidth 1.3ω , followed by an ideal differentiator (chapter 5, section 5.2.2).

To design a small loop bandwidth PLL (a narrow bandwidth insures good noise performance and will tolerate a larger amount of input frequency change without losing lock) and assume locking of the loop a very stable VCO, i.e. VCXO (crystal-controlled VCO) should be used, and the same type of crystal should be used for both the transmitter and the receiver. We can then be sure that the frequency drift in both the transmitter and the receiver will be very small, and that the VCO frequency drift

will be within the lock-in range of the PLL. Noise bandwidth and internal jitter of the PLL can be reduced by careful design. A resonant high Q LC circuit tuned to the slot frequency is placed before the PLL in order to select and reinforce slot frequency information from the preprocessed PPM data received and suppress other harmonics. The design of an experimental optical PPM receiver using the method mentioned above, is discussed in chapter 8. It is not easy to filter, differentiate, square, filter again a very weak signal, then amplify it about 32 times (see chapter 8) in order to apply it to the PLL to get a very stable clock signal. A very stable system needs careful design.

The frame synchroniser enables the receiver to recognize the beginning of the transmitted data in a packet. Decoding and frame synchronisation circuits are realized in this experimental model with TTL logic elements, which can be used up to $M=32$ ($m=1$), for $B=4$ Mbit/s; for higher values of B or M , ECL logic must be used. Due to these limits the system is used up to $M=16$ and $m=0.8$. The parameters shown in table 9.1 for this data rate can be scaled up or down as required. Lower rates can be realised easily so far as the bandwidth is concerned, although the source peak/mean power will reduce (because the pulse duty-cycle will increase). Higher values of M are possible up to $M=16$ with conventional TTL components (for $B=4$ Mbit/s), but for higher values of M more complex components, like ECL, must be used to build a PPM system.

The sensitivity and error rate characteristics of an experimental PPM system have been measured for different numbers of time slots M , and modulation depth m . The practical results are correlated with the theoretical results, showing that the simplified analytical model developed in chapter 3 is adequate.

The results show that a digital PPM system can take advantage of available fiber bandwidth to offer a significant improvement in receiver sensitivity over the equivalent PCM system, even though the fiber bandwidth is not included in these measurements because its length was too short. For the range of the measurements done in this work, it is clear that

the improvement in PPM system sensitivity increases with the number of the time slots in the PPM frame (M) and the modulation index (m). The limits to this improvement are the clock synchronization which becomes more difficult as M increases, fiber bandwidth limit, and optical source peak/mean power (as M increase peak/mean power should increase).

The application of PPM to passive LANs is discussed and compared with PCM in chapter 9. The extra number of stations or nodes connected to a passive bus or star network due to the improvement in receiver sensitivity is calculated. For example, 5 extra stations could be added to the bus for a 13 dB increase in receiver sensitivity (which obtained practically for $M=16$ and $m=0.8$) when the connector loss is 1 dB, and 23 extra stations when the connector loss is 0.05 dB. In a passive bus network, the number of stations connected to the network, or the number of extra stations, depends strongly on the connector loss, and the excess loss of the optical coupler. In a passive star network, using PPM will increase the number of output ports dramatically. For example, using the 13 dB increase in receiver sensitivity will increase the number of output ports about 20 times.

The data rate of 4 Mbit/s was chosen for the experimental study because it is used in token-bus networks, but table 9.3 shows the PPM slot frequency variation with M for other PCM data rates which are already in use in some LANs.

10.2-FUTURE WORK

The aim of this work was to show that PPM can overcome a greater transmission loss than PCM given similar transmitting and receiving devices. This increase in the transmission loss could be translated to an increase in the number of branching and tapping points in a passive local area network. The aim has been achieved in this work, but there are some points which need further investigation during future work, to reduce the limitations and to improve the sensitivity of the system further.

1- The received PPM signal contains jitter introduced by the position modulation process, which gets into the timing system, and can cause transition errors. If a large number of successive PPM pulses appear at a similar position in each frame, the PLL output will drift in its phase and tend to lock onto the average position of these pulses. Jitter occurs when this average is different from the unmodulated position. Line coding to suppress this type of jitter has been studied theoretically (see chapter 5, reference [YICHAO]) and needs to be applied to any practical PPM system.

2- In LANs, the data are transmitted as packets. As discussed in chapter 6, when the PLL locks onto the transmitter slot clock, the lock indicator is used to enable the frame synchroniser and the decoder, so that the transmitted data enters the decoder from the beginning of the data field (after the frame synchronising pulses) until the end of the packet. However, in the experimental system, the lock indicator, the frame synchroniser and the decoder will stay on for a while at the end of the packet (see chapter 6). It is required to disable them at the end of each packet to prevent the data contained in other packets from entering the decoder

before the frame synchronisation for the new packet. This area needs further investigation. During the system performance measurement an infinitely long packet was used, which is unrealistic but enables the BER to be measured easily. Measuring the performance of the system during packet transmission needs further work. The data from the PRBS generator can be sent as packets and recovered at the receiver to measure the probability of error of the system during packet transmission.

3- The design of the practical PPM system for different values of M and m is not covered the whole required range of M and m due to speed limitations in the components. The whole range of M and m is required to measure the system performance and to find the optimum value of M and m . The optimum value of M which is found by [GARRETT] is 32, so it is desirable to build a PPM system which covers these values of M and m , in order to verify the optimum value of M and m as found by [GARRETT].

4- In a passive LAN, the dynamic range of the received signal can be large, and the performance of the PLL preprocessing circuit and the pulse detection will vary with the amplitude of the received signal. The lock and capture range of the PLL vary with the applied signal amplitude. The threshold level of the pulse detection circuit should be adjusted each time when the received signal amplitude vary. An automatic gain control circuit (AGC) must be used before the preprocessing and pulse detection circuits to fix these parameters. AC coupling in the receiver may also cause some problems for low duty-cycle PPM signals; the PPM pulse may be differentiated because of the coupling capacitor, and the average level of the PPM pulses will vary according to the presence of the PPM pulses. The problem of the average level could be eased by using line coding as mentioned above.

5- Having shown that PPM is potentially a good technique to use in order to enhance the performance of an existing LAN, the design and production of a new PPM system to use instead of an old PCM system should be considered from an economical point of view. The benefits of applying PPM in terms of how many existing systems might benefit, and how much engineering work is required to produce an add-on unit need further investigation.